Scattering and ACTH Regulation

A thesis submitted for the degree of
Doctor of Philosophy
in Electrical and Electronic Engineering
from the
University of Canterbury
Christchurch, New Zealand

by

Vaughan Allan Smith
B.E. (Hons I)

July, 1992

Abstract

The work reported in this thesis is concerned with two completely separate topics — scattering and adrenocorticotropic hormone (ACTH) regulation.

The accuracies of two approximate scattering formulations, the Born approximation and geometrical optics, are investigated and compared. The distortion associated with multiple scattering in Born inversion is shown to be severe in situations where the refractive indices of object components are only slightly (<5%) different from the background. Second and higher order multiple scattering is found to contribute negligible distortion to the reconstruction. Backpropagation is explicitly formulated and implemented for receivers in the far-field, but Fourier interpolation is found to be a preferable method for performing Born inversion in the simulation situation. Shift-and-add, a form of frequency diversity processing which has been previously proposed to reduce distortion in Born inversion, is comprehensively tested. Although the anticipated reduction in distortion is not achieved, some improvement is demonstrated. Furthermore, this work shows the need for iterative solutions to realistic inverse scattering problems.

A new solution to the two-dimensional bent-ray computed tomography problem is developed. It is based on a novel ray description which does not require the ray paths to be known. The refractive index distribution is therefore found by solving linear equations, rather than through the conventional process of ray tracing. Reconstructions of circularly symmetric refractive index distributions demonstrate the feasibility of this approach and encourage further development.

The information available from a recently developed method for sampling pituitary effluent (PES) in the horse is examined. The current sampling interval of $30s$ is found to be appropriate for measuring ACTH and arginine vasopressin (AVP), but not necessarily corticotropin-releasing hormone (CRH). Blood flow variations are found to have essentially negligible effect on measurement of hormone concentrations at the corticotropes.

A recently proposed model of ACTH regulation, derived from static cell culture results, is tested on PES data and found to be inappropriate for the *in vivo* situation.

The relationships between AVP, CRH, cortisol and ACTH are examined using cross-correlation, pulse analysis and models of ACTH regulation. The pulse analysis indicates that the delay between AVP or CRH and ACTH is 0-$30s$. Results from all three techniques indicate that AVP is the important physiological ACTH secretagogue in the horse. Results from the modeling analysis suggest that the relative potency of AVP and CRH depends on the cortisol concentration, and that when this is low, CRH is the dominant secretagogue. Modeling results also reveal that the principal effects of cortisol on ACTH

secretion occur in the pituitary, and not in the brain as is currently believed. In addition, they show that in some situations AVP, CRH and cortisol are sufficient to explain almost all ACTH secretion, although the pulse analysis indicates that additional secretagogues do have physiological effects. Furthermore, this work demonstrates the need for rapid sampling and makes some suggestions regarding important mechanisms operating in the corticotrope *in vivo*.

Acknowledgements

My research and this thesis could not have come about without the support of many people. I am deeply grateful to my original supervisor, Professor Richard Bates[1], for convincing me to undertake this research, and for contributing so many ideas to it. His enthusiasm for new ideas was unbounded, and he provided me with a shining example of how research should be done. My sincerest thanks go also to my current supervisor, Dr Alan McKinnon, for his guidance and insight. I have the greatest respect for him on both a professional and personal level, and have thoroughly enjoyed our interaction. I am also indebted to Professor Cliff Irvine who was responsible for my introduction to endocrinology, and much of my tutelage in the subject. His depth of knowledge and desire to learn have been a constant source of amazement.

I would also like to thank Dr Susanne Dale, Tony Enright and Dr Ross Murch for their parts in solving the problems in Part I, and Dr Sue Alexander, Professor Rick Donald, Dr Jane Ellis, Dr Marg Evans, Dr John Livesey and Dr Drusilla Mason for discussions on the analyses in Part II. The quality of my research has been considerably enhanced by their various inputs; indeed, the research in Part II would not have been possible without the data supplied by Cliff Irvine and Sue Alexander. I further thank many of the above people, along with Dr Phil Bones, Dr Kathy Garden, Dr Mike Hayes, Andrew Le Beau, Rachel Mulligan, Brenda Satherley, Craig Tuffnell and Amanda Woods, for commenting on drafts of this thesis. Their suggestions have greatly improved its content and readability.

In addition, I thank Alison Dingle and Dr Alan Murch for their assistance with my research on Chaos. Special thanks also go to Dr David Wall for our many discussions on reconstructing susceptability kernals, and on over-relaxation extensions to Born inversion. While our ideas remain unimplemented, these discussions certainly broadened my understanding of Inverse problems. My appreciation goes to Dr Pete Gough for acting as my departmental supervisor following Professor Bates' death. I would also like to express my thanks to all the unmentioned students and staff of the Electrical Engineering Department for discussions, support and entertainment provided over the course of this research.

I gratefully acknowledge receipt of New Zealand University Grants Committee, Edward and Isabel Kidson, and William Georgetti Postgraduate Scholarships.

Finally, I wish to thank my parents for providing me with the opportunities that have lead to the writing of this thesis.

[1] Died November 1990

Preface

The work reported in this thesis is concerned with two completely separate topics — scattering and adrenocorticotropic hormone (ACTH) regulation — which are covered in Parts I and II respectively, since any attempt to connect them could only be confusing. I also spent some time investigating Chaos, but the results of this research are presented elsewhere [Smith *et al.*, 1988]. Since a thesis should emphasize original contributions, in writing this thesis I have attempted to review only work related to my own subsequent research. This restriction is relaxed slightly in Part II to allow for the expected reader background, but seems particularly appropriate in Part I since I have coauthored an extensive review of inverse scattering [Bates *et al.*, 1991]. The aim of the following paragraphs is to identify the original aspects of my research. This research has been performed by myself, either alone or in collaboration with others. Collaboration is made clear by references in particular chapters.

Part I of this thesis deals with scattering, which is the interaction of wave motion with inhomogeneous media. My aim in Part I has been to investigate manageable new methods to allow indirect observation of objects. Two such methods are presented in Chapter 3.

Chapter 1 provides an introduction to scattering in refracting media. It establishes the partial differential equation and notation used in this thesis to describe wave motion, before formally defining the direct and inverse scattering problems. It contains no original material.

Chapter 2 presents a comparison of the Born and geometrical optics (GO) approximations (the two approximate formulations of scattering on which the new inverse solutions in Chapter 3 are based) with the exact solution. A major motivation for this work was to assess the approximations underlying the two new inverse solutions considered in Chapter 3. Although a comparison of these approximations does not appear to have been made previously, basic knowledge of their validity is widespread. The most important new results in this chapter therefore relate to the effect of multiple scattering on the Born approximation. The effect of first order multiple scattering on the scattered field measured along a line has been shown previously [Azimi and Kak, 1983]. However, this study compares the exact scattered field in the far-field with that calculated using the Born approximation.

Chapter 3 contains investigations of Born inversion and two new solutions to the inverse scattering problem. In section 3.1.2 backpropagation is explicitly formulated for receivers in the far-field for the first time. The comparison of backpropagation and Fourier interpolation in section 3.1.4 has been made previously for receivers along a

line [Pan and Kak, 1983; Slaney and Kak, 1985]. However, having the receivers in the far-field is found to reduce the relative accuracy and resolution of backpropagation. Section 3.1.5 presents what appear to be the first exact reconstructions of multi-component objects using Born inversion. Previous reconstructions have considered only first order multiple scattering in solving the associated direct problem [Azimi and Kak, 1983]. My investigation of the distortion in Born inversion due to multiple scattering therefore extends the work of Azimi and Kak [1983], who demonstrated the distortion, but used approximate Born inversion. Section 3.1.5 also provides the first illustration of the distortion caused by multiple scattering when cylinder refractive indices and/or sizes are not all equal. The first new inverse scattering solution investigated uses a form of frequency diversity processing called 'Shift-and-add' (SAA) which has been developed at Canterbury by the Bates[2] group [Bates and Cady, 1980]. SAA has been previously proposed to reduce the distortion in Born inversion [Bates and Robinson, 1981; Minard *et al.*, 1985; Minard, 1985], and Professor Bates had been awaiting the simulation study reported in section 3.1.7 for a number of years. Section 3.1.7 also presents the first realistic implementation of an extension to SAA, termed differential SAA, which has been proposed as more suitable for extended objects [Minard, 1985]. The second new inverse solution, proposed in section 3.2, is a novel bent-ray computed tomography (CT) solution. It is the first such solution where refraction is appreciable, yet ray tracing is not required. Results presented in section 3.2.5 indicate that it compares well with conventional bent-ray CT solutions which require ray tracing.

Chapter 4 presents conclusions on the original results presented in Chapters 2 and 3, and suggests lines of further research.

ACTH is the principal hormone released from the pituitary in response to stress. My aim in Part II of this thesis has been to use data from the novel technique of Pituitary Effluent Sampling (PES), pioneered by Irvine and Alexander [1987] at Lincoln University, New Zealand, to investigate ACTH regulation. In doing this it became apparent that an investigation of the information available from PES was also required.

Chapter 5 serves to introduce and review ACTH regulation. In particular, it presents current knowledge on the intracellular mechanisms behind ACTH secretion, since these form the basis for a mechanistic model of ACTH regulation in Chapter 7. It contains no original material.

Chapter 6 contains investigations of the information available from PES, the problems with the technique, and how it compares with alternative methods for investigating ACTH regulation. My comments, in section 6.1.3, on the suitability of deconvolving circulating adrenal axis hormone concentrations, result from engineering experience combined with interpretation of results from the many applications of deconvolution to the endocrine system. The analysis, in section 6.3.4, of the effects of sampling and of the sampling rate is entirely new, although the techniques used are well established. Hopefully this work will be used to provide guidelines for PES sampling rates in the future. My comments accompanying this analysis regarding the periodicity of adrenal axis hormones are in mild defiance of current thinking; however, this thinking appears to be changing. The work, contained in section 6.3.5, is the first formal analysis of the size and effects of blood flow variations in the data afforded by PES. I derived all

[2]Professor R.H.T. Bates, along with his students and associates

three methods used to produce limits for the coefficient of variation of blood flow. The accompanying analysis of the effect of these variations on PES data is also original.

Chapter 7 presents my analysis of ACTH regulation using crosscorrelation, pulse analysis and modeling. The crosscorrelation results in section 7.1.1 are hardly revolutionary, but they extend those presented elsewhere [Alexander *et al.*, 1991; Alexander *et al.*, 1988] by their completeness and use of helpful transformations. Likewise, the pulse analysis in section 7.1.2 has been performed elsewhere [Engler *et al.*, 1989; Guardabasso *et al.*, 1991], but the quality of PES data makes this work more useful. The pulse analysis is extended in section 7.2 to provide the first examination of the delay between AVP or CRH and ACTH, either *in vivo* or *in vitro*. Wishing to also pursue a modeling based analysis, I set about finding a useful model of ACTH regulation. The interpretation in section 7.3 of the qualitative model recently proposed by Schwartz *et al.* [1989] is my own, as is the analysis of its suitability. Its failure to explain PES data then led me to summarize important recent findings on ACTH regulation in section 7.4, which I used to formulate my own mechanistic model of ACTH regulation in section 7.5.1. This model, the results obtained from it, and the conclusions drawn from them are all original. The accuracy with which the model is able to replicate ACTH secretion is perhaps all the more surprising when one considers that my work appears to be the first quantitative attempt to model ACTH regulation.

Finally, Chapter 8 presents conclusions regarding the original results presented in Chapters 6 and 7, and suggests lines of further research.

I wrote all of the software needed for the above research, apart from that to solve the inverse bent-ray CT problem in Chapter 3. During the course of my studies the following papers have been prepared:

Enright S.A., Dale S.M., Smith V.A., Murch R.D. and Bates R.H.T. (1992), 'Towards solving the bent-ray tomographic problem', *Inverse Problems* **8** (1), February, pp. 83–94.

Bates R.H.T., Smith V.A. and Murch R.D. (1991), 'Manageable multidimensional inverse scattering theory', *Physics Reports* **201** (4), April, pp. 185–277, invited paper.

Smith V.A. and McKinnon A.E. (1990), 'Modelling ACTH regulation' *New Zealand Branch Meeting of the Australasian College of Physical Scientists and Engineers in Medicine*, Christchurch, November.

Smith V.A., Murch A.R. and Dingle A.A. (1988), 'Non-random noise mechanisms', *Proceedings of the National Electronics Conference* **25**, September, pp. 188–193.

Smith V.A., Mason D.R., McKinnon A.E., Irvine C.H.G., and Alexander S.L. (1992), 'A modeling investigation of the role of AVP, CRH and cortisol in ACTH regulation', in preparation.

Smith V.A., McKinnon A.E. and Irvine C.H.G. (1992), 'The effect of sampling rate on investigations of the adrenal axis', in preparation.

Smith V.A., McKinnon A.E. and Irvine C.H.G. (1992), 'The delay between AVP or CRH and ACTH', in preparation.

Contents

Glossary

Unless indicated otherwise, abbreviations and symbols used in this thesis have the meanings given below.

ACTH	adrenocorticotropic hormone, also known as *adrenocorticotropin* and *corticotropin*
AVP	arginine vasopressin, also known as *antidiuretic hormone* (ADH)
cAMP	cyclic adenosine 3,5-monophosphate
COV	coefficient of variation
CPU	central processor unit
CRH	corticotropin releasing hormone
CT	computed tomography
dB	decibel
F	cortisol
FFT	fast Fourier transform
$\mathcal{F}(\cdot)$	temporal Fourier transform

$$\mathcal{F}[f(t)] = F(\mathrm{f}) = \int_{-\infty}^{\infty} f(t) e^{-j2\pi \mathrm{f} t} dt$$

$\mathcal{F}(\cdot)$	spatial Fourier transform

$$\mathcal{F}[f(\mathbf{x})] = F(\mathbf{u}) = \int\!(K) \int_{-\infty}^{\infty} f(\mathbf{x}) e^{-j\mathbf{u}\cdot\mathbf{x}} dV(\mathbf{x})$$

where $\mathbf{x}$ and $\mathbf{u}$ are K-dimensional position vectors in image and Fourier space respectively, $\int\!(K)\int$ is a K-dimensional integral, and dV is a volume element in K-dimensional space.

$\mathcal{F}^{-1}(\cdot)$	inverse spatial Fourier transform

$$\mathcal{F}^{-1}[F(\mathbf{u})] = f(\mathbf{x}) = \frac{1}{(2\pi)^K} \int\!(K) \int_{-\infty}^{\infty} F(\mathbf{u}) e^{j\mathbf{u}\cdot\mathbf{x}} dV(\mathbf{u})$$

GnRH	gonadotropin releasing hormone
GO	geometrical optics

ICS	intercavernous sinus
IFFT	inverse fast Fourier transform
IP_3	inositol 1,4,5-trisphosphate
j	$\sqrt{-1}$
$\mathcal{L}$	relative path length
LH	luteinizing hormone
LVZ	low velocity zone
ME	median eminence
ν	refractive index
OXT	oxytocin
PES	pituitary effluent sampling
PKA	protein kinase A
PKC	protein kinase C
POMC	pro-opio-melanocortin
PVN	paraventricular nuclei
ψ	field
SAA	shift-and-add
SON	supraoptic nuclei
SNR	signal-to-noise ratio
$S(\mathbf{x})$	electrical path length
Υ	space

Part I

Scattering

CHAPTER 1

Background to Scattering

As humans we have an insatiable desire to discover more about the physical world in which we live; indeed many of our discoveries are of immense practical use to us. Our senses of sight and hearing allow us to guess at the nature of objects beyond our physical reach. These senses can be greatly enhanced by use of the many different types of telescope, microscope, and amplifier available today. However, there are still many objects which even our enhanced senses cannot gather sufficient information about to satisfy our needs. Examples of such objects are minerals, oil, or water in the ground, internal body organs, and fish in the deep sea. Our aided or unaided senses then fail because there is no light, sound, smell, taste, or contact to perceive these objects by. Our only recourse in these situations is to excite the object with some form of emanation, of which electromagnetic and acoustic radiations are the most common. Interpretation of radiations that have passed through, or been deflected from the object then provides us with information about it.

Virtually all such radiations satisfy wave equations and are therefore referred to from now on as *wave motions*. It is theoretically (and physically) acceptable to regard any perturbation of wave motion as *scattering* [Newton, 1966], which gives rise to the title of this thesis. Furthermore, it is appropriate to employ the generic term *scatterers* to encompass objects and inhomogeneous media, and to call the part of space occupied by them the *scattering region*.

Research into scattering is conventionally partitioned into a *direct problem* and an *inverse problem*. The goal of any inverse scattering algorithm is, as indicated above, to estimate the distribution throughout the scattering region of the scatterers' *constitutive parameters*, i.e. their physical properties (see section 1.2). Conversely, the goal of any direct scattering algorithm is to estimate the scattering which results from the interaction of wave motion with the scatterers. While the ultimate aim of scattering research is to develop new or improved inverse scattering solutions, the inverse problem cannot be considered in isolation. The direct problem is usually fundamental to both the inverse solution and the understanding of scattering that allowed the solution to be developed.

This chapter formalizes the direct and inverse scattering problems in anticipation of the research presented in Chapters 2 and 3. Some real-world applications of inverse scattering serve to further introduce the subject in section 1.1. Section 1.2 sets out the differential equations used in this thesis to describe wave motion in various media. After the necessary establishment of the scattering geometry in section 1.3, the direct and inverse scattering problems are formally defined in sections 1.4 and 1.5 respectively.

1.1 Applications of Inverse Scattering

Inverse problems are of great actual or potential practical use because one can acquire so much information about the physical world, in both a general scientific sense and for specific technical and commercial applications, by probing objects with wave motions. To illustrate this, table 1.1 lists the major scientific and technological applications of inverse scattering. The types of wave motion and the inversion techniques invoked in practice are also listed. Even though conservative fields cannot really be classed as wave motions, they are included because of their practical importance, and because of theoretical similarities between some of the inversion techniques invoked for conservative and wave fields. For details about applications and inversion principles listed, the interested reader is referred to the associated references which are intended to be illustrative rather than comprehensive.

1.2 Mathematical Models of Scattering

Wave motion in various media can be modeled by differential equations which can be formulated in either the time or frequency domain. This section describes the differential equations appropriate in the context of this thesis and their underlying assumptions. The relative merits of time and frequency domain formulations are also discussed (in section 1.2.3).

1.2.1 Time domain formulations

For the purposes of this thesis, macroscopic electromagnetic phenomena are adequately described by Maxwell's equations [Jones, 1964]. When the medium is source free, linear, time invariant, and isotropic, and there is negligible coupling between orthogonal polarizations, Maxwell's equations can be written as the partial differential time domain equation

$$\nabla^2\Psi(\mathbf{x},t) - \beta(\mathbf{x})\dot{\Psi}(\mathbf{x},t) - (\nu(\mathbf{x})/c)^2\ddot{\Psi}(\mathbf{x},t) + \mu(\mathbf{x})\Psi(\mathbf{x},t) = 0 \qquad (1.1)$$

where c is the free-space wave speed, $\beta(\mathbf{x})$, $\mu(\mathbf{x})$ and $\nu(\mathbf{x})$ are constitutive parameters which are related in table 1.2 to the properties of the medium, and $\Psi(\mathbf{x},t)$ is a complex valued scalar wave function representing a single component of the electric or magnetic field [Felsen and Marcuvitz, 1973]. $\Psi(\mathbf{x},t)$ exists at all points $\mathbf{x} \in \Upsilon$, a space of arbitrary dimension, and all instants t in time. The Cartesian coordinate in the direction of the chosen component of the vector field is denoted by ξ.

Acoustic radiation can also be described by (1.1) with $\Psi(\mathbf{x},t)$ representing the velocity potential of the particles in the medium [Wilcox, 1984]. Table 1.2 relates the constitutive parameters to properties of the acoustic medium. Note that, while not discussed in this thesis, (1.1) is also able to describe all of the other types of wave motion listed in table 1.1 [Spencer, 1980; Truesdell, 1977].

Application area	Type(s) of wave motion	Inversion principle(s)
Antenna reflector synthesis [Keller, 1959; Westcott, 1983]	Electromagnetic (radio frequency waves) or acoustic	Geometrical optics inversion
Astronomical interferometry [Bates, 1982]	Electromagnetic (radio frequency or optical)	Fourier inversion or CT
Crystallography [Cowley, 1975; Ramachandran and Srinivasan, 1970]	Electromagnetic (X-rays) or non-relativistic quantum mechanical (beams of neutrons or electrons)	Fourier inversion based on Born inversion
Baggage inspection	Electromagnetic (X-rays)	Conventional radiology
Medical imaging [Berntsen *et al.*, 1990; Brown and Barber, 1988; Seagar and Bates, 1985]	Conservative electric field (audio-frequency currents)	Impedance tomography
[Morris, 1986; Webb, 1988]	Conservative magnetic field (1-100 MHz)	Fourier inversion or CT
[Garden *et al.*, 1989; Herman, 1983; Jackson, 1988; Wells, 1987]	Electromagnetic (X-rays)	Conventional radiology or CT
[Dallas and Wagner, 1987]	Electromagnetic (gamma rays)	Gamma camera, SPECT and PET
[Sieber, 1983; Wells, 1977]	Ultrasonic (MHz frequencies)	Echolocation (B-scan) based on Born inversion
Microscopy [Misell, 1978]	Electromagnetic (optical) and non-relativistic quantum mechanical (electron beams)	Conventional radiology or CT or scatter imaging
[Shimizu *et al.*, 1989]	Acoustic (50 MHz - 2 GHz)	
Non-destructive testing	Acoustic (100 kHz - 50 MHz)	Echolocation
[Bond and Reynolds, 1987; Thomson and Chimenti, 1986]	Electromagnetic (X-rays)	Conventional radiology or CT or scatter imaging
Oceanography [Bleistein *et al.*, 1984; Spiesberger, 1985]	Acoustic (100-500 Hz)	Profile inversion
Particle scattering [Newton, 1980; Newton, 1981c]	Non-relativistic quantum mechanical	Born approximation and series
Plasma probing [Ahn and Jordan, 1976]	Electromagnetic	Born approximation and series or CT
Prospecting by remote probing	Conservative electric fields (audio frequency currents)	Impedance imaging
[Parasnis, 1979; Rea, 1984; Sieber, 1983]	Conservative field (gravitational or magnetic)	Exact iterative
	Electromagnetic (< 20 kHz)	
Radar [Fritsch, 1965; Gjessing, 1978; Skolnik, 1970]	Electromagnetic (low MHz to hundreds of GHz)	Echolocation
Seismology [Daily, 1986; Lines, 1986; Schoenberger, 1984; Sengbush, 1983]	Acoustic and Elastic	Multistatic echolocation supplemented by migration
Sonar [Kinsler *et al.*, 1982; Urick, 1975]	Acoustic (100Hz - 500kHz)	Echolocation

Table 1.1 Application areas together with types of wave motion and inversion principles on which they rely. Abbreviations have their conventional meanings, i.e. CT, computed tomography; SPECT, single photon emission CT; and PET, positron emission CT.

Emanation	$\beta(\mathbf{x})$	$\mu(\mathbf{x})$	$\nu(\mathbf{x})$
Electromagnetic	$\mu_m\sigma$	$\nabla(\frac{\partial}{\partial\xi}\log_e\epsilon)$	$\sqrt{\frac{\epsilon\mu_m}{\epsilon_0\mu_0}}$
Acoustic	k^2q/ρ	$\frac{2\rho\nabla^2\rho-3\nabla\rho\cdot\nabla\rho}{4\rho^2}$	$\sqrt{\frac{\rho}{\kappa}}$

Table 1.2 Constitutive parameters $\beta(\mathbf{x})$, $\mu(\mathbf{x})$ and $\nu(\mathbf{x})$ related to the properties of propagating media for electromagnetic and acoustic wave motion. The symbols used, and the properties of the media they represent are: μ_m, magnetic permeability; μ_0, free-space permeability; σ, electrical conductivity; ϵ, electrical permittivity; ϵ_0, free-space permittivity; k, angular frequency 2πf; q, coefficient of expansive friction + $\frac{4}{3}$ coefficient of viscosity; ρ, mass density; and κ, adiabatic bulk compression modulus [Born and Wolf, 1980; Morse and Feshbach, 1953].

1.2.2 Frequency domain formulations

Because (1.1) is linear in $\Psi(\mathbf{x},t)$ and the medium is assumed to be temporally invariant, an equivalent description of the model can be formulated in the temporal frequency domain. Wave motion can then be described by $\psi(\mathbf{x},k)$, which is the (temporal) Fourier transform [Bracewell, 1978] of $\Psi(\mathbf{x},t)$. The differential equation for $\psi(\mathbf{x},k)$ is obtained by Fourier transforming (1.1), thereby producing the frequency dependent, or Helmholtz wave equation [Morse and Feshbach, 1953]

$$\left(\nabla^2 + k^2\nu^2(\mathbf{x}) + \mu(\mathbf{x}) - jck\beta(\mathbf{x})\right)\psi(\mathbf{x},k) = 0 \tag{1.2}$$

Although the wave equations (1.1) and (1.2) are exactly equivalent, the latter is (in an important sense) more versatile because the three constitutive parameters appearing in (1.1) can be combined in the frequency domain as a single generalized constitutive parameter, written here as $\chi = \chi(\mathbf{x},k)$. Thus (1.2) can be simplified, and simultaneously generalized, to

$$\left(\nabla^2 + k^2\chi^2(\mathbf{x},k)\right)\psi(\mathbf{x},k) = 0 \tag{1.3}$$

where

$$\chi^2(\mathbf{x},k) = \nu^2(\mathbf{x}) - jc\beta(\mathbf{x})/k + \mu(\mathbf{x})/k^2 \tag{1.4}$$

The first term on the right hand side of (1.4), which is independent of k, determines the (non-dispersive) speed of the wave motion at each point in the medium. The square root of this term is known historically as the refractive index.

In free-space $\mu(\mathbf{x}) = \beta(\mathbf{x}) = 0$ and $\nu(\mathbf{x}) = 1$. The wave equation then becomes

$$\nabla^2\psi(\mathbf{x},k) + k^2\psi(\mathbf{x},k) = 0 \tag{1.5}$$

which is known as the free-space wave equation.

Because scattering is such a vast technical science [Bates *et al.*, 1983], it is not possible, or desirable, to cover all of its aspects here. Consequently, this thesis is confined to the case where the refractive index is not constant, but varies, generally in more than one dimension. Such multidimensional variation causes *refraction*, or bending of the wavefronts. Furthermore, for the purposes of this thesis, (1.1) and (1.4) are further simplified by setting $\beta(\mathbf{x}) = \mu(\mathbf{x}) = 0$ throughout Υ. Because the great

majority of media are non-magnetic, the permeability of the medium can be assumed to be equal to its free-space value μ_0, and so negligible error results in general from the assumption $\beta(\mathbf{x}) = 0$. Setting $\mu(\mathbf{x}) = 0$ poses a more significant limitation since the permittivity, ϵ, cannot be allowed to exhibit appreciable spatial variations in the ξ-direction. The implication here is that $\nabla(\Psi(\mathbf{x},t)\frac{\partial}{\partial\xi}\log_e\epsilon)$ must be everywhere small compared with both $\nabla^2\Psi(\mathbf{x},t)$ and $\frac{1}{c^2}\ddot{\Psi}(\mathbf{x},t)$ [Born and Wolf, 1980; Jones, 1964]. While the class of media that satisfies this limitation is restricted, it is wide enough to be of considerable practical interest. The advantage of the approximation is that

$$\chi(\mathbf{x},k) = \nu(\mathbf{x}) \tag{1.6}$$

and so is real and frequency independent.

Acoustic wave motion occurs in two forms, known as primary or pressure p-waves and secondary or shear s-waves [Sengbush, 1983]. When $\Psi(\mathbf{x},t)$ represents the acoustic field, assuming $\mu(\mathbf{x}) = \beta(\mathbf{x}) = 0$ requires that the viscosity of the medium be effectively zero so that there is negligible transformation of energy between p- and s-waves [Wilcox, 1984]. Setting $\mu(\mathbf{x}) = 0$ also requires that changes in the density of the medium are small. Experimental results demonstrate that these conditions can be realistic [Robinson and Greenleaf, 1986].

1.2.3 Comparison of time and frequency domain formulations

Time domain formulations are hyperbolic partial differential equations, whereas frequency domain formulations are elliptic partial differential equations [Morse and Feshbach, 1953]. Because hyperbolic equations admit solutions that are discontinuous, the notion of causality, as exemplified by the propagation of pulses, can be incorporated into time domain formulations [Garabedian, 1964]. This represents a powerful argument in favour of time domain formulations. However, a disadvantage which often outweighs this is that discontinuous solutions can be highly unstable numerically. On the other hand, frequency domain formulations can allow several different characteristics of a medium to be combined into a single constitutive parameter, as in (1.4). For example, dispersion and attenuation, characterised by $\mu(\mathbf{x})$ and $\beta(\mathbf{x})$ respectively, which have to be inserted separately into time domain formulations, can be combined in the frequency domain by permitting $\chi(\mathbf{x},k)$ to be complex and frequency dependent.

From a theoretical point of view, time domain and frequency domain formulations are equivalent. However, the numerical and practical difficulties associated with time domain approaches can be daunting. Consequently, in accordance with the majority of the current literature on inverse problems, the rest of this thesis concentrates exclusively on frequency domain formulations.

1.3 Scattering Geometry and Notation

Space is denoted by Υ, an arbitrary point P in which is labelled by the position vector $\mathbf{x}$ with respect to an arbitrarily chosen coordinate origin O. In three dimensions $\mathbf{x}$ has Cartesian, cylindrical polar and spherical polar components $(x,y,z),(\rho;\phi,z)$ and

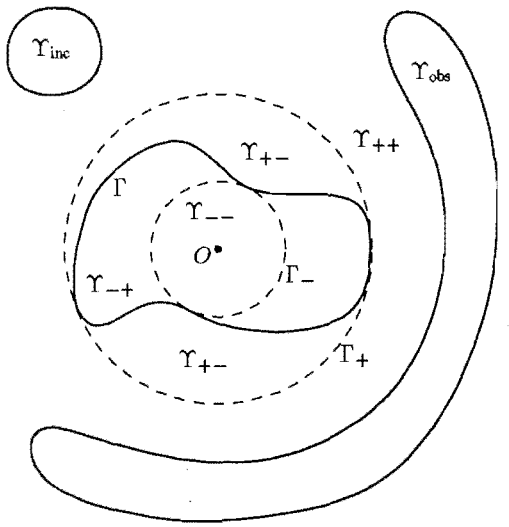

Figure 1.1 Notation for different regions of space displayed for the two dimensional case.

$(r; \theta; \phi)$ respectively. Note that angular coordinates are identified by prefacing them with semi-colons rather than commas.

The scattering region, which can be two or three dimensional (Υ^2 or Υ^3), is taken to be finite and denoted by Υ_-, which is enclosed by the surface Γ. The sphere or cylinder Γ_-, centered on O and inscribing Υ_-, partitions Υ_- into Υ_{--} and Υ_{-+} which are interior and exterior, respectively, to Γ_-. The part of Υ exterior to Γ is denoted by Υ_+. The sphere, or cylinder Γ_+ centered on O, circumscribing Υ_-, partitions Υ_+ into Υ_{+-} and Υ_{++} which are interior and exterior, respectively, to Γ_+. The regions Υ_{inc} and Υ_{obs} are where, respectively, the sources of the incident wave motion reside and the scattered wave motion is observed. It is also useful to define $\bar{\Upsilon}_{inc}$ to include all Υ except that in Υ_{inc}. Figure 1.1 illustrates the above notation. Thus

$$\Upsilon = \Upsilon_- \cup \Gamma \cup \Upsilon_+ = \Upsilon_{inc} \cup \bar{\Upsilon}_{inc} \quad \text{and} \quad \Upsilon_- \cap \Gamma = \Upsilon_+ \cap \Gamma = \emptyset \tag{1.7}$$

where $\emptyset$ is the empty set, with

$$\Upsilon_- = \Upsilon_{--} \cup \Gamma_- \cup \Upsilon_{-+} \quad \text{and} \quad \Upsilon_{--} \cap \Gamma_- = \Upsilon_{-+} \cap \Gamma_- = \emptyset \tag{1.8}$$

$$\Upsilon_+ = \Upsilon_{+-} \cup \Gamma_+ \cup \Upsilon_{++} \quad \text{and} \quad \Upsilon_{+-} \cap \Gamma_+ = \Upsilon_{++} \cap \Gamma_+ = \emptyset \tag{1.9}$$

and

$$\Upsilon_{inc} \subset \Upsilon_{++} \quad \text{and} \quad \Upsilon_{obs} \subset \Upsilon_{++} \tag{1.10}$$

In accord with the assumptions and notation in section 1.2, space is taken to be homogeneous and isotropic, having a refractive index of unity, throughout Υ_+, which is taken to be free (of impressed sources) everywhere except in Υ_{inc}. Within Υ_- the refractive index can vary arbitrarily.

The wave motion's sources, of density $\sigma(\mathbf{x}, k)$, are confined to Υ_{inc}, from which issues the incident field $\psi_{inc}(\mathbf{x}, k)$. The interaction of the wave motion with the scatterers within Υ_- generates the scattered field $\psi_{scat}(\mathbf{x}, k)$, so the total field is

$$\psi(\mathbf{x}, k) = \psi_{\text{inc}}(\mathbf{x}, k) + \psi_{\text{scat}}(\mathbf{x}, k) \tag{1.11}$$

Since the incident and scattered fields can be defined arbitrarily provided they sum to the total field [Bates *et al.*, 1983], the incident field is here defined to have free-space form, i.e. it is a solution to (1.5) in $\bar{\Upsilon}_{\text{inc}}$. This means that the incident field is understood to everywhere possess the same form as it would actually have if the the refractive index was unity throughout the entire scattering region. The scattered field is then defined by (1.11). Substitution of (1.11) into the frequency dependent wave equation (1.3) allows (1.3) to be written as two wave equations

$$(\nabla^2 + k^2)\psi_{\text{inc}}(\mathbf{x}, k) =. \begin{cases} 0 & \mathbf{x} \in \bar{\Upsilon}_{\text{inc}} \\ -\sigma(\mathbf{x}, k) & \mathbf{x} \in \Upsilon_{\text{inc}} \end{cases} \tag{1.12}$$

and

$$\left(\nabla^2 + k^2\right) \psi_{\text{scat}}(\mathbf{x}, k) = -k^2[\nu^2(\mathbf{x}) - 1][\psi_{\text{inc}}(\mathbf{x}, k) + \psi_{\text{scat}}(\mathbf{x}, k)] \tag{1.13}$$

Because the left hand side of (1.13) has the same form as the free-space equation (1.5), the right hand side can be considered to be a density of equivalent sources embedded in free-space. The field emanating from these sources constitutes the scattered field.

1.4 The Direct Scattering Problem

In terms of the notation introduced in sections 1.2 and 1.3, the general direct scattering problem can be defined as: given $\psi_{\text{inc}}(\mathbf{x} \in \Upsilon, k)$, or equivalently $\sigma(\mathbf{x} \in \Upsilon_{\text{inc}}, k)$, and the refractive index, $\nu(\mathbf{x} \in \Upsilon_{-})$, determine $\psi_{\text{scat}}(\mathbf{x} \in \Upsilon_{\text{obs}}, k)$.

This general problem is well posed and relatively well understood, although it continues to generate a large amount of active research. Manageable exact solutions to the direct problem exist for special cases, but cannot be expected in general because although $\psi_{\text{scat}}(\mathbf{x} \in \Upsilon_{\text{obs}}, k)$ in (1.13) depends linearly on $\psi_{\text{inc}}(\mathbf{x} \in \Upsilon_{-}, k)$, it depends non-linearly on $\nu(\mathbf{x} \in \Upsilon_{-})$. In a particular application, where exact solutions are not available or not computationally feasible, one of the many approximate solutions will usually yield satisfactory results. Chapter 2 compares two such approximate solutions with an exact solution.

1.5 The Inverse Scattering Problem

In terms of the notation introduced in sections 1.2 and 1.3, the general inverse scattering problem can be defined as: given $\sigma(\mathbf{x} \in \Upsilon_{\text{inc}}, k)$ and $\psi_{\text{scat}}(\mathbf{x} \in \Upsilon_{\text{obs}}, k)$, reconstruct the refractive index, $\nu(\mathbf{x} \in \Upsilon_{-})$.

No computationally direct and efficient approach to solving this general problem has so far been found, even when the choice of Υ_{inc} and Υ_{obs} is unrestricted. The reasons for this are explained in section 1.5.1, while the rest of this section elaborates on some of the more interesting (and frustrating) aspects of the inverse scattering problem.

1.5.1 Dimensionality difficulty

By construction $\Upsilon_{++} \cap (\Upsilon_{-} \cup \Upsilon_{+-}) = \emptyset$, and so $\psi_{\text{scat}}(\mathbf{x} \in \Upsilon_{++}, k)$ is outgoing (i.e. consists entirely of outward travelling waves). This means that all of the information in $\psi_{\text{scat}}(\mathbf{x} \in \Upsilon_{++}, k)$ is available from measurements taken on a single surface within Υ_{++} that surrounds Υ_{-} (although using more surfaces will improve the signal-to-noise ratio). Now, although $\psi_{\text{scat}}(\mathbf{x} \in \Upsilon_{++}, k)$ does not effectively vary in the radial direction, $\nu(\mathbf{x} \in \Upsilon_{-})$, and hence $\psi(\mathbf{x} \in \Upsilon_{-}, k)$, will in general. To solve the general inverse scattering problem it is necessary, at least implicitly, to reconstruct $\psi(\mathbf{x} \in \Upsilon_{-}, k)$. Consequently, one is required to infer a quantity from data which is of one less dimension. It is conceptually possible that an extra dimension could be added to $\psi_{\text{scat}}(\mathbf{x} \in \Upsilon_{++}, k)$ by varying the direction and/or frequency of ψ_{inc}, because $\psi_{\text{scat}}(\mathbf{x} \in \Upsilon_{++}, k)$ depends on the direction and frequency of ψ_{inc} in general, but $\nu(\mathbf{x})$ does not. Unfortunately a suitable algorithm to do this has not been found.

In general, therefore, one must contrive means of either reducing the dimensionality of what needs to be reconstructed, or consistently continuing $\psi_{\text{scat}}(\mathbf{x} \in \Upsilon_{++}, k)$ back into Υ_{-}. The first possibility has so far been realized only by introducing approximations, which cannot always be valid of course. Such techniques, termed *approximate non-iterative*, presently form the basis for virtually all practical solutions to scientific, medical and technological multidimensional inverse scattering problems [Bates *et al.*, 1983]. The second possibility has been implemented, in principle, but its practical manifestations seem too complicated to be manageable (at least in the near future) [Budreck and Rose, 1990; Weston, 1989], except perhaps in special circumstances [Murch *et al.*, 1988]. The problem with these *exact* approaches is that the mapping between the scattering data and the constitutive parameter to be identified is non-linear. Except in special cases, the only way to solve such equations is iteratively and at enormous computational expense. It is, therefore, difficult to believe that exact approaches could be applied effectively to real-world data in the absence of quite detailed *a priori* information about the scatterers. However, such information just might be obtained from the approximate non-iterative solution which is most appropriate in any particular instance. This could eventually prove to be the main justification for developing approximate approaches.

Note that the dimensionality difficulty evaporates when Υ_{-} collapses to the surface Γ, because $\psi(\mathbf{x}, k)$ can then vary arbitrarily in only two directions on Γ.

1.5.2 Dimensionality of space

One dimensional inverse scattering theory is comparatively complete and very well understood [Bednor *et al.*, 1983; Bruckstein and Kailath, 1987; Habashy, 1991; Habashy and Mittra, 1987; Kristensson and Krueger, 1987; Newton, 1981b; Tijhus, 1987], which contrasts spectacularly with the state of the general theory for more than one spatial dimension. There are two major reasons for the relative simplicity of one dimensional inverse scattering problems. The first is that one knows *a priori* the directions of all rays. There is only one direction! The second reason is that it is always possible to transform a wave equation involving a spatially variable refractive index, but depending upon only a single spatial Cartesian coordinate, into a Schrödinger (or plasma wave) equation for which the refractive index is everywhere unity [Habashy and Mittra, 1987].

It can be immediately appreciated that the technical (due to not being able to transform to the equivalent of the Schrödinger equation) and conceptual (associated with being unclear *a priori* as to the actual ray paths) difficulties experienced with three dimensional inverse scattering problems are undiminished to any significant degree in two dimensions. On the other hand, the computational effort required to simulate two dimensional inverse scattering scenarios is much less than for their three dimensional manifestations. For this reason, the studies presented in this thesis are for two dimensions.

Note that there is a central aspect of wave motion that cannot be modeled in two space dimensions. This is the coupling between orthogonal polarizations in spatially inhomogeneous media [Budden, 1985; Silver, 1949; Stratton, 1941], which was assumed negligible in section 1.2, as in almost all standard formulations of wave motion.

1.5.3 Contamination

Real-world measurements are always contaminated with additive noise and other imperfections which place irreducible limits on the faithfulness with which the constitutive parameters of scatterers can be reconstructed. However, errors inherent in the assumptions underlying all manageable multidimensional inverse scattering algorithms often represent the most significant source of contamination. The effects of such contamination can usually be considerably reduced by incorporating *a priori* information about the scatterers into the inversion algorithm using various standard, well established statistical [Craig and Brown, 1986; Sabatier, 1987] and regularization techniques [Bertero *et al.*, 1988b; Bertero *et al.*, 1988a; Dubovikova and Dubovikov, 1987; Scales and Gersztenkorn, 1988; Sneidman and Vogel, 1989].

1.5.4 Uniqueness considerations

Having found a solution to a particular inverse scattering problem, it is important to know if the solution is the only reasonable one, or whether a multiplicity of different solutions is likely to exist. In a practical situation, contamination means that the best that can be hoped for is a multiplicity of similar solutions, the range of which accords with the signal-to-noise ratio of the data. The well known ill-posedness of many inverse problems [Baltes, 1980; Bertero and de Mol, 1981; Bertero *et al.*, 1988b; Nashed, 1981; Sabatier, 1983] warns that such accord cannot be expected in general.

All data must necessarily be sampled in space and time. Since the volume of Υ_- is finite, the sampling theorem for Fourier transforms [Bates and McDonnell, 1989] confirms that uniqueness need not be adversely affected by the data being sampled. However, if the sampling is so *coarse* that it fails to satisfy the constraints set by the sampling theorem (with regard to the size of Υ_-), then the solution cannot be other than non-unique, independent of the contamination level.

CHAPTER 2

Direct Scattering Solutions

The direct scattering problem has been defined as (see section 1.4): determine the scattered field resulting from interaction of a known incident field with an object of known refractive index. There are two very good reasons why the direct problem is important. Firstly, in order to solve the inverse problem one must solve the direct problem to obtain the scattered field. Secondly, study of solutions to the direct problem enhances one's understanding of scattering, and so may suggest new methods for solving the inverse problem. This chapter therefore describes how the direct problem is solved to provide the data used in Chapter 3, and also compares the approximations on which the new inverse solutions in Chapter 3 are based.

In Chapter 1 it was established that the scattered field, $\psi_{\text{scat}}(\mathbf{x}, k)$, the refractive index, $\nu(\mathbf{x})$, and the incident field, $\psi_{\text{inc}}(\mathbf{x}, k)$, are not related in a simple manner, and so a general explicit expression for $\psi_{\text{scat}}(\mathbf{x}, k)$ in terms of $\nu(\mathbf{x})$ and $\psi_{\text{inc}}(\mathbf{x}, k)$ cannot be stated. However, if very specialized objects are chosen then it is possible to determine ψ_{scat} analytically and exactly (exact, that is, to within the approximations implicit in the Helmholtz equation). Section 2.2 develops such a solution for ψ_{scat}, which is used both to provide data for inversion in section 3.1, and in this chapter to assess the accuracy of the approximations employed in Chapter 3. Since exact analytical relationships between $\psi_{\text{scat}}(\mathbf{x}, k)$, $\nu(\mathbf{x})$, and $\psi_{\text{inc}}(\mathbf{x}, k)$ are unavailable in general, $\psi_{\text{scat}}(\mathbf{x}, k)$ could be calculated numerically. However, it is much more practical to introduce approximations which enable a general (approximate) analytic relationship between $\psi_{\text{scat}}(\mathbf{x}, k)$, $\nu(\mathbf{x})$, and $\psi_{\text{inc}}(\mathbf{x}, k)$ to be obtained. Sections 2.3 and 2.4 introduce the Born and Geometrical Optics (GO) approximations (the two approximations used in Chapter 3), and demonstrate how they allow the direct problem to be solved analytically. Furthermore, subsections 2.4.2 and 2.4.3 describe the manner in which the direct problem in section 3.2 is solved. The validity of the Born and GO approximations is then assessed in section 2.5. This assessment is original in that it uses a multi-component object. Important results deriving from the assessment therefore relate to the effect of interactions between individual components of the object.

2.1 A Suitable Test Object

As mentioned above, the direct problem must be solved (by measurement or simulation) in order to provide data with which solution of the inverse problem can be attempted. In addition, the accuracy of approximate solutions to the direct problem can be most readily

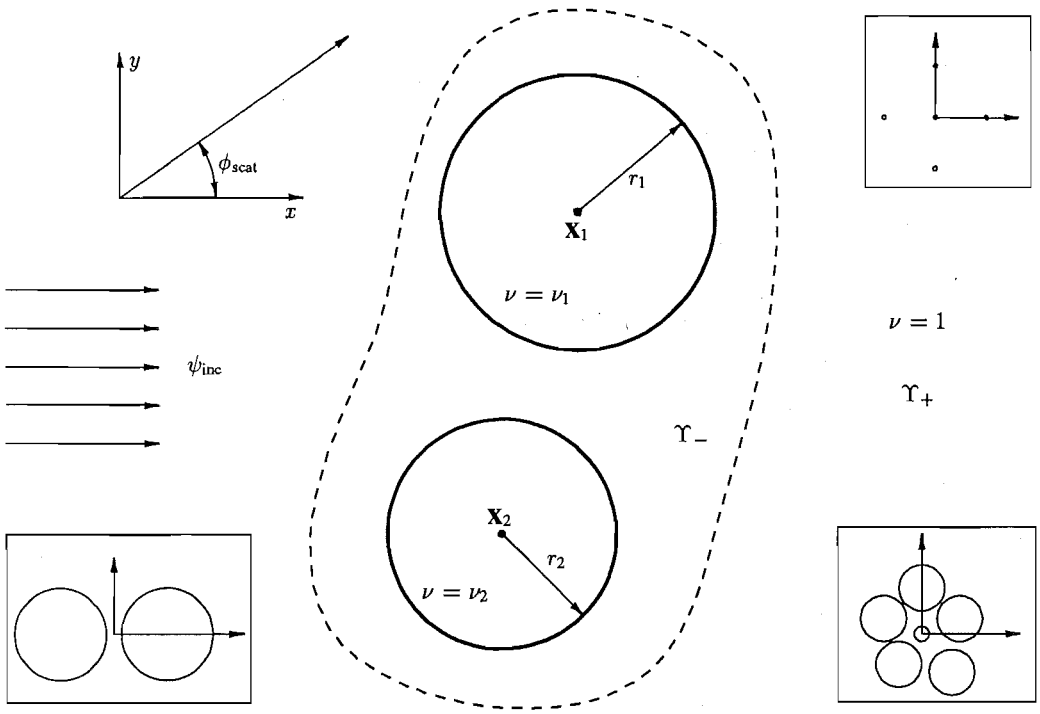

Figure 2.1 The prototypical scattering object which consists of a number of circular cylinders. Cylinder number i has radius r_i, constant refractive index ν_i, and center at coordinates $\mathbf{x}_i$. The incident radiation is planar and propagates in the direction of the positive x-axis, i.e. $\phi_{inc} = 0$. The scattered field is calculated for a range of scattering angles ϕ_{scat}. Inserts at the lower left, lower right, and upper right show the actual scattering objects corresponding to figures 2.9-2.10, 2.11-2.12, and 2.13 respectively.

determined by comparing them to the exact solution for the same object. However, exact analytic solutions to the direct scattering problem exist only for a very limited class of objects. These objects consist of homogeneous regions whose boundaries correspond to surfaces on which coordinates, belonging to any of the eleven separable coordinate systems, are constant [Morse and Feshbach, 1953]. The simplest finite objects with separable coordinates are circular cylinders in Υ^2, and spheres in Υ^3. Therefore, the test object used in this chapter consists of a set of circular cylinders of variable size and position, each with a constant refractive index. This test object is illustrated in figure 2.1. Note that a number of different object configurations are used.

2.2 An Exact Formulation

The test object used in this chapter (and in section 3.1) is chosen so that the exact solution to the direct problem can be determined analytically. One method for obtaining this solution uses eigenfunction expansions [Morse and Feshbach, 1953]. The foundation of this method is to find solutions to the Helmholtz equation (1.3), in each homogeneous region, of the form

$$\psi(\mathbf{x}, k) = F_1(x_1, k\nu)F_2(x_2, k\nu)F_3(x_3, k\nu) \tag{2.1}$$

where x_1, x_2, x_3 represent a general right-handed, curvilinear coordinate system, and ν is the constant refractive index of the homogeneous region. Each of the terms in the expansion is known as a mode or partial wave. In any of the eleven separable coordinate systems, the Helmholtz equation has an infinite number of individual solutions of the form (2.1). The most general solution in a homogeneous region is then a linear combination of all the individual solutions. Since the three factors on the right hand side of (2.1) are together referred to as an eigenfunction, the expression

$$\psi(\mathbf{x}, k) = \sum_{l,m,n=-\infty}^{\infty} A_{l,m,n} F_{1,l}(x_1, k\nu) F_{2,m}(x_2, k\nu) F_{3,n}(x_3, k\nu) \tag{2.2}$$

is called an eigenfunction expansion. Note that the $A_{l,m,n}$, which are constant expansion coefficients, are in general complex. Expansions in other regions of the object have the same general form. The eigenfunctions are orthogonal [Morse and Feshbach, 1953], so that

$$\int_L F_{i,m}(x_i) F_{i,n}(x_i) dx_i = \begin{cases} C_n^{F_i} & m = n \\ 0 & m \neq n \end{cases} \tag{2.3}$$

where L represents the interval of the coordinate axis on which the eigenfunction $F_{i,m}(x_i)$ is defined and $C_n^{F_i}$ is a constant.

2.2.1 Single-cylinder objects

To find the solution to a particular scattering problem it is necessary to invoke supplementary conditions; in particular the boundary, radiation, and finiteness conditions [Jones, 1964]. As an example, consider the two dimensional case where the object, Υ_-, is a circular cylinder of radius R and refractive index ν^-, centered on the origin. Since, in cylindrical coordinates, a separated solution to the Helmholtz equation must be a combination of Bessel functions and exponentials [Morse and Feshbach, 1953], an incident plane wave is expressed as [Jones, 1964]

$$\psi_{\text{inc}}(\rho; \phi, k) = \sum_{m=-\infty}^{\infty} a_m J_m(k\rho) e^{jm\phi} \tag{2.4}$$

where $J_m(\cdot)$ is the Bessel function of the first kind of order m, and the a_m depend on the direction of propagation, ϕ_{inc}, according to $a_m = (-j)^m e^{-jm\phi_{\text{inc}}}$ [Jones, 1964]. In choosing a representation for the scattered field it is essential to consider that eigenfunctions of the Helmholtz equation can exhibit infinities at points of the interval on which they are defined [Abramowitz and Stegun, 1965]. Therefore, the finiteness condition can be satisfied only if Hankel functions of the second kind ($H_m^{(2)}(\cdot)$ where m is the order) are chosen to represent ψ_{scat} because $\lim_{\rho\to\infty} J_m(\rho) = \infty$. Since the $H_m^{(2)}(\cdot)$ are outgoing, this choice also satisfies the radiation condition which requires the field to be entirely outgoing in Υ_+. Thus, the scattered field in Υ_+ must be written as

$$\psi_{\text{scat}}(\rho; \phi, k) = \sum_{m=-\infty}^{\infty} A_m^+ H_m^{(2)}(k\rho) e^{jm\phi} \tag{2.5}$$

where the A_m^+ are constant expansion coefficients. When choosing an expansion for the field in Υ_-, the finiteness condition can be satisfied only if Bessel functions of the

first kind are used because $\lim_{\rho\to 0} H_m^{(2)}(\rho) = \infty$. The expansion for the field in Υ_- is therefore

$$\psi(\rho;\phi) = \sum_{m=-\infty}^{\infty} A_m^- J_m(k\nu^-\rho)e^{jm\phi} \tag{2.6}$$

where the A_m^- are constant expansion coefficients.

Finally, the boundary conditions are satisfied by matching the actual values and first derivatives of the general solutions from Υ_- and Υ_+ across their boundary surface, i.e.

$$\begin{aligned} \psi(R^-;\phi,k) &= \psi_{\text{inc}}(R^+;\phi,k) + \psi_{\text{scat}}(R^+;\phi,k) \\ \tfrac{\partial}{\partial\rho}\psi(R^-;\phi,k) &= \tfrac{\partial}{\partial\rho}[\psi_{\text{inc}}(R^+;\phi,k) + \psi_{\text{scat}}(R^+;\phi,k)] \end{aligned} \tag{2.7}$$

where R is the radius of the cylinder, and $^\pm$ superscripts refer to infinitesimal increments and decrements respectively. Since the boundary of the cylinder spans the full range of ϕ (so the representations are orthogonal), (2.7) can be solved straightforwardly because each partial wave is orthogonal. For this example, when $\phi_{\text{inc}} = 0$, (2.7) becomes

$$\begin{aligned} A_m^- J_m(k\nu^- R) &= (-j)^m J_m(kR) + A_m^+ H_m^{(2)}(kR) \\ \nu^- A_m^- J_m'(k\nu^- R) &= (-j)^m J_m'(kR) + A_m^+ H_m'^{(2)}(kR) \end{aligned} \tag{2.8}$$

These two equations allow each of the constants $A_m^\pm$ to be determined for all m. Hence, when the object is a single circular cylinder, a solution for $\psi_{\text{scat}}(\mathbf{x} \in \Upsilon, k)$ can be obtained knowing the incident field $\psi_{\text{inc}}(\mathbf{x}, k)$. Note that when the cylinder is perfectly reflecting, i.e. the field in Υ_- is zero, the boundary conditions (2.7) are simplified to

$$\psi_{\text{inc}} = -\psi_{\text{scat}} \tag{2.9}$$

and (2.8) becomes

$$(-j)^m J_m(kR) = -A_m^+ H_m^{(2)}(kR) \tag{2.10}$$

2.2.2 Multi-cylinder objects

The number of objects for which exact analytic solutions can be obtained using eigenfunction expansions is increased by the addition theorems for eigenfunctions [Watson, 1966], which allow translation of the coordinate origin. This permits the incident field on one object due to scattering from another to be calculated, and thus the total scattered field from a composite object can be determined iteratively. To calculate $\psi_{\text{scat}}(\rho;\phi)$ for the object in figure 2.1, the scattered field $\psi_{\text{scat}}^1(\rho;\phi)$ from the cylinder closest to Υ_{inc}, and due to $\psi_{\text{inc}}(\rho;\phi)$, is first calculated as described in section 2.2.1. The field incident on the next cylinder $\psi_{\text{inc}}^2(\rho;\phi)$ is then estimated as the sum of $\psi_{\text{inc}}(\rho;\phi)$ and the incident field due to scattering from the first cylinder $\psi_{\text{inc}}^{1\to 2}(\rho;\phi)$, where

$$\psi_{\text{inc}}^{1\to 2}(\rho;\phi) = \mathcal{A}^{1\to 2}(\psi_{\text{scat}}^1(\rho;\phi)) \tag{2.11}$$

$\mathcal{A}$ indicates that an addition theorem has been invoked to transfer $\psi_{\text{inc}}^{1\to 2}(\rho;\phi)$ from coordinates centered on the first cylinder to coordinates centered on the second cylinder. Using this notation, the field incident on the n^{th} cylinder is

$$\psi_{\text{inc}}^n(\rho;\phi) = \psi_{\text{inc}}(\rho;\phi) + \sum_{l=1, l\neq n}^{N} \psi_{\text{inc}}^{l\to n}(\rho;\phi) \tag{2.12}$$

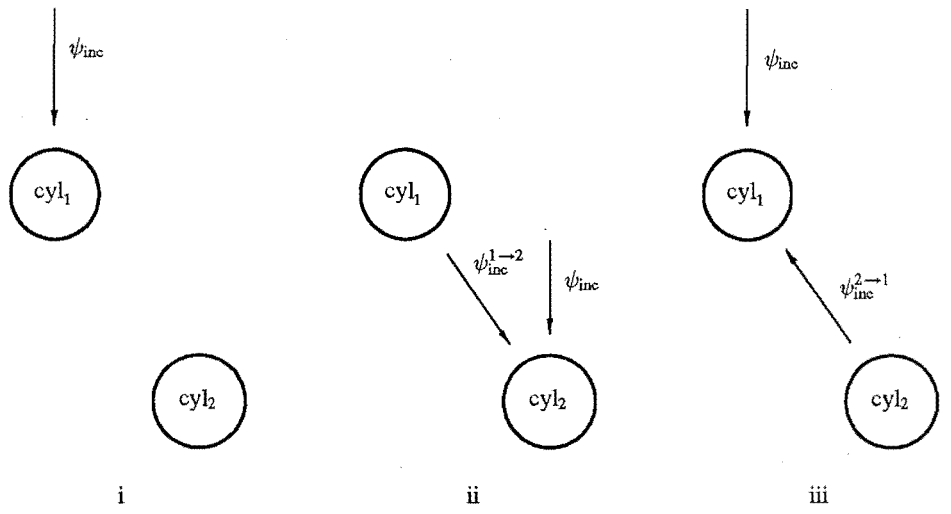

Figure 2.2 The first three steps in the calculation of the field scattered from a two cylinder object.

where N is the number of cylinders in the object. Once the field on the N^{th} cylinder has been estimated using (2.12), the $\psi_{\text{inc}}^n(\rho;\phi)$ for $n \in [1, N]$ are recalculated until they are sufficiently accurate. The first three steps in the process for a two cylinder object are depicted in figure 2.2. Note that (2.12) necessarily converges because it accurately represents the actual multiple scattering process, and

$$\psi_{\text{scat}}(\rho;\phi) = \sum_{n=1}^{N} \psi_{\text{scat}}^n(\rho;\phi) \tag{2.13}$$

then produces the total scattered field. Alternatively, the whole problem could be solved without iteration by simultaneously solving the boundary conditions for all cylinders. While this approach is more complicated, it could require less computation. However, the scheme described by (2.12) and (2.13) was used in preference because it allows the effects of multiple scattering to be investigated.

2.2.3 Implementation

In calculating ψ_{inc}^n iteration was stopped when the relative change in the largest of the $|A_m|$ for cylinder n was less than 10^{-5}. M, the number of A_m coefficients required for each cylinder, was chosen so that $|A_{M-2}|$, $|A_{M-1}|$, and $|A_M|$ were all less than 10^{-5} times the largest $|A_m|$ because of the oscillatory nature of Bessel functions. The accuracy of the resultant scattered field can be confirmed by the forward scattering theorem [Bowman *et al.*, 1969] which requires that

$$\sum A_m^2 = -\sum \mathcal{R}(A_m (j)^m e^{jm\phi_{\text{inc}}}) \tag{2.14}$$

where the A_m are the A_m^+ from (2.5) when ψ_{scat} is the total scattered field, and $\mathcal{R}(z)$ is the real part of z. This equality was always satisfied to within $10^{-3}\%$, and usually to within $10^{-6}\%$. Note that for the trivial case of one cylinder no iteration is necessary and only one set of $A_m^{\pm}$ is required.

The exact solution described above can be determined only for a very restricted and completely unrealistic class of objects. In practice, when relating ψ_{inc}, ν and ψ_{scat}, it is therefore common to introduce whatever approximation is deemed most appropriate for a given application. The two approximations employed in Chapter 3 to solve the inverse problem are now set out (in sections 2.3 and 2.4), and their validity examined by using them to solve the direct problem.

2.3 The Born approximation

An exact solution for the scattered field is given by (1.13), which can be alternatively written as the volume source formulation [Bates and Ng, 1972], i.e.

$$\psi_{\text{scat}}(\mathbf{x}, k) = \int_{\Upsilon_-} k^2[\nu^2(\mathbf{x}_1) - 1]\psi(\mathbf{x}_1, k)g(\mathbf{x}, \mathbf{x}_1, k)d\Upsilon(\mathbf{x}_1) \tag{2.15}$$

where $g(\mathbf{x}, \mathbf{x}_1, k)$ is the Green's function which gives the field at the point $\mathbf{x}$ due to a point source at $\mathbf{x}_1$. The Born approximation is that

$$\psi_{\text{scat}} \ll \psi_{\text{inc}} \tag{2.16}$$

or equivalently, that the actual field in the object is the same as if the object were not present. While this assumption may be entirely reasonable in some scattering contexts [Newton, 1981c], this thesis only considers objects with spatially varying refractive index where the assumption is highly questionable. The advantage of the Born approximation is that replacing $\psi(\mathbf{x}_1, k)$ in (2.15) by $\psi_{\text{inc}}(\mathbf{x}_1, k)$ makes the resultant expression analytically solvable. This expression can be further simplified by choosing $\psi_{\text{inc}}(\mathbf{x}, k)$ to be a plane wave, i.e.

$$\psi_{\text{inc}}(\mathbf{x}, k) = e^{-j\mathbf{k}\cdot\mathbf{x}} \tag{2.17}$$

where the direction of propagation is specified by the unit vector $\hat{\mathbf{k}} = \mathbf{k}/k$, and evaluating $\psi_{\text{scat}}(\mathbf{x}, k)$ in the far-field to simplify the Green's function. Equation (2.15) then becomes [Jones, 1964]

$$\psi_{\text{b}_{\text{ff}}}(\hat{\mathbf{x}}, k) = \int_{\Upsilon_-} k^2[\nu^2(\mathbf{x}_1) - 1]e^{-jk(\hat{\mathbf{k}}-\hat{\mathbf{x}})\cdot\mathbf{x}_1}d\Upsilon(\mathbf{x}_1) \tag{2.18}$$

where $\psi_{\text{b}_{\text{ff}}}(\hat{\mathbf{x}}, k)$ is the Born approximation to $\psi_{\text{scat}}(\mathbf{x}, k)$ evaluated in the far-field, and in the direction specified by $\hat{\mathbf{x}} = \mathbf{x}/|\mathbf{x}|$. Note that the constant coefficient $e^{-jk|\hat{\mathbf{x}}|}/4\pi|\hat{\mathbf{x}}|$ has been ignored to clarify the important mathematical argument. Now recognize that (2.18) is simply the Fourier transform of $k^2[\nu^2(\mathbf{x}, k) - 1]$ [Jones, 1964]. On defining $\mathbf{k}' = k(\hat{\mathbf{k}} - \hat{\mathbf{x}})$ and writing the Fourier transform operator as $\mathcal{F}$, (2.18) can be written as

$$\psi_{\text{b}_{\text{ff}}}(\hat{\mathbf{x}}, k) = k^2\mathcal{F}[\nu^2(\mathbf{x}) - 1](\mathbf{k}') \tag{2.19}$$

If the scattered field is observed for all $\hat{\mathbf{x}}$ and the incident field is a plane wave with direction of incidence $\hat{\mathbf{k}}$, then the vector $\mathbf{k}' = k(\hat{\mathbf{k}} - \hat{\mathbf{x}})$ traces out a circle (sphere in Υ^3) as illustrated in figure 2.3. The radius of this circle is k and its center is located at $\mathbf{k}$. Consequently, the Fourier transform of $k^2[\nu^2(\mathbf{x}) - 1]$ on this circle represents the far-field scattering due to an incident plane wave $e^{-j\mathbf{k}\cdot\mathbf{x}}$.

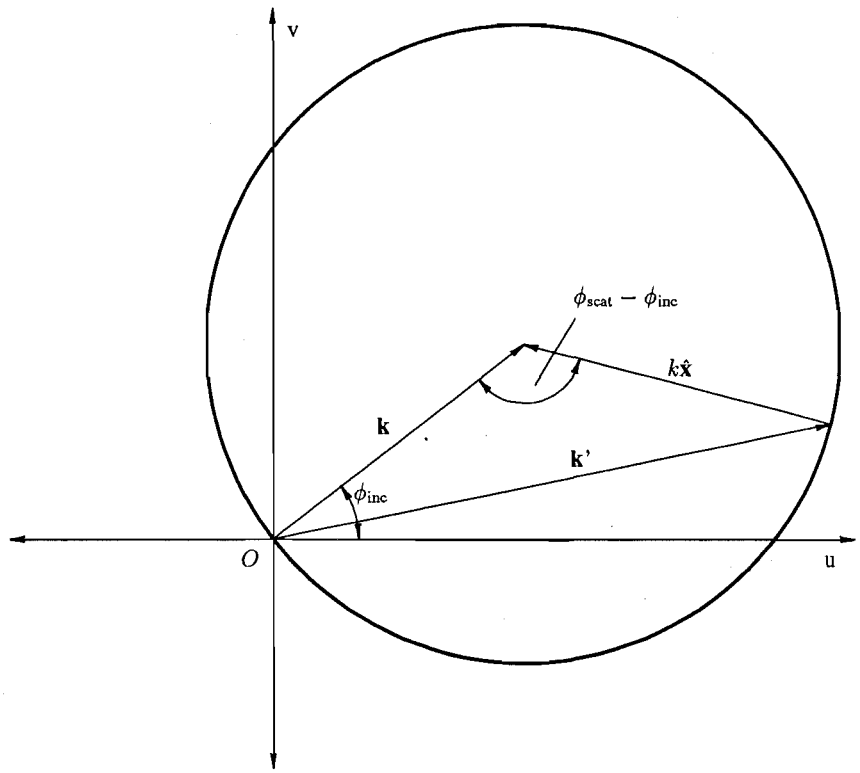

Figure 2.3 Locus in Fourier space corresponding to observable scattered field. The scattered field is related to the Fourier transform of $k^2[\nu^2(\mathbf{x}) - 1]$ on a circle (sphere in Υ^3) in Fourier space. The center of the circle lies at the extremity of the vector $\mathbf{k}$, where $\mathbf{k}$ defines the direction, ϕ_{inc}, in which the incident field travels. The unit vector $\hat{\mathbf{x}}$ defines the direction, ϕ_{scat}, in which the scattered field is measured. Note that the point O corresponds to scattering in the direction ϕ_{inc}, i.e. $\phi_{scat} = \phi_{inc}$.

In spite (or perhaps because!) of constituting the simplest of the recognized approaches to diffraction, the Born approximation is invoked more widely in practice than any other formulation (see section 1.1). It is, nevertheless, important to recognize that the assumption on which the approximation is based can be invalid, even when there is very little scattering. As mentioned above, this assumption allows $\psi(\mathbf{x} \in \Upsilon_-, k)$ to be replaced by $\psi_{inc}(\mathbf{x} \in \Upsilon_-, k)$. However, the incident field can be expected to be a useful approximation to the total field only if the latter's wavefronts do not deviate appreciably from the incident wavefronts. This deviation can be simply expressed as $\mathcal{L}$, the difference between electrical and actual path lengths of a ray passing through Υ_-. The electrical path length, S, of the actual ray corresponding most closely to the incident ray is approximately [Born and Wolf, 1980]

$$S = \int_{l_1(\mathbf{x})}^{l_2(\mathbf{x})} \nu(\mathbf{x}) dl(\mathbf{x}) \tag{2.20}$$

where l_1 and l_2 identify the points where the incident ray enters and leaves Υ_-, and dl is the element of path length along the ray. Consequently, the Born approximation can

be expected to be valid only if the refractive index satisfies

$$\mathcal{L} = |\int_{l_1(\mathbf{x})}^{l_2(\mathbf{x})} [\nu(\mathbf{x}) - 1] dl(\mathbf{x})| \ll \lambda \tag{2.21}$$

for all rays traversing Υ_-, where λ is the wavelength. A more useful measure of deviation is therefore $\mathcal{L}_{\max}$, the maximum distance between wavefronts of ψ_{inc} and ψ.

2.3.1 Implementation

To calculate $\psi_{\text{bf}}(\hat{\mathbf{x}}, k)$, an image of $k^2[\nu(\mathbf{x})^2 - 1]$ was Fourier transformed and equispaced values on the circle $|k[(1,0) - \hat{\mathbf{x}}]| = k$ determined by linear interpolation. Note that $\hat{\mathbf{k}} = (1,0)$ corresponds to $\phi_{\text{inc}} = 0$.

The validity of calculating the scattered field using the Born approximation is assessed in figures 2.4 and 2.5 for the simple case of an object consisting of a single circular cylinder of constant refractive index. These results show that when $\mathcal{L}_{\max}$ is very small, i.e. $< \lambda/4$, the Born approximation is quite accurate.

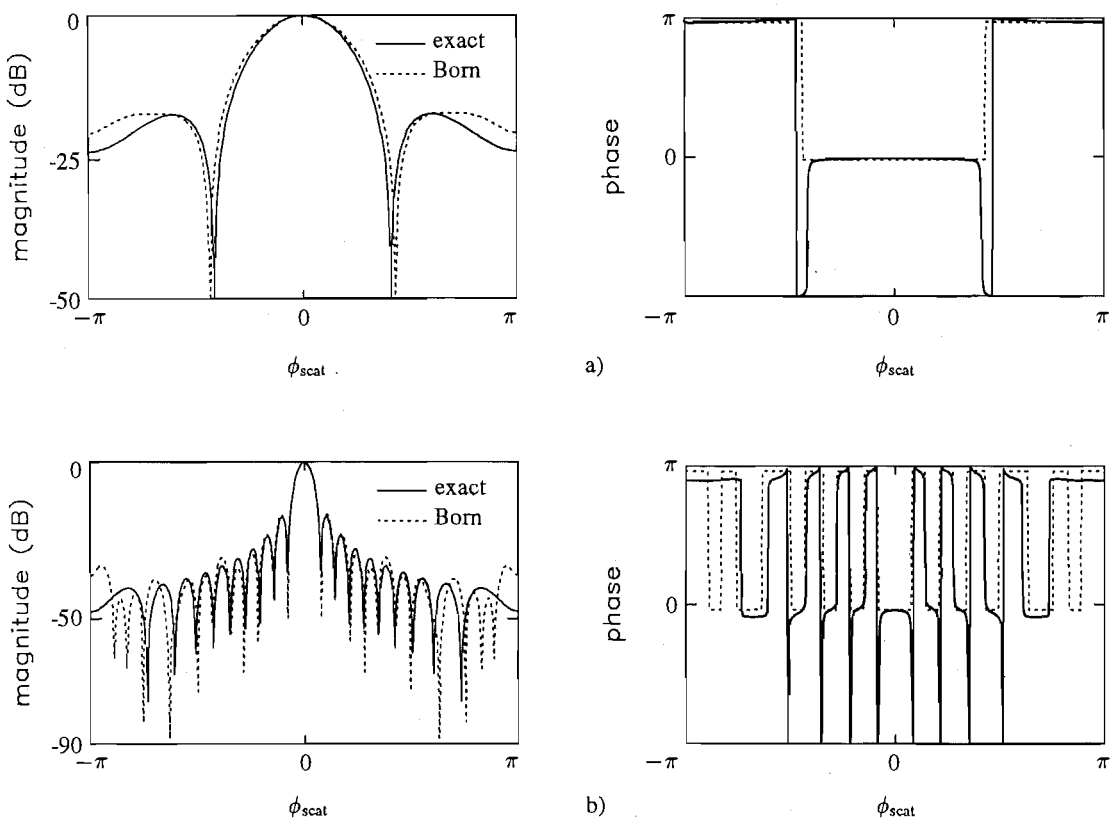

Figure 2.4 Far-field radiation patterns of ψ_{scat} showing the accuracy of the Born approximation within its range of validity. The object is a single cylinder with $\nu = 1.01$, i.e. the refractive index (or speed of propagation) is 1% higher in Υ_- than in Υ_+. (a) and (b) correspond, respectively, to the diameter of the cylinder being 1λ and 10λ, and $\mathcal{L}_{\max}$ being 0.01λ and 0.10λ. Other objects are considered in subsequent figures.

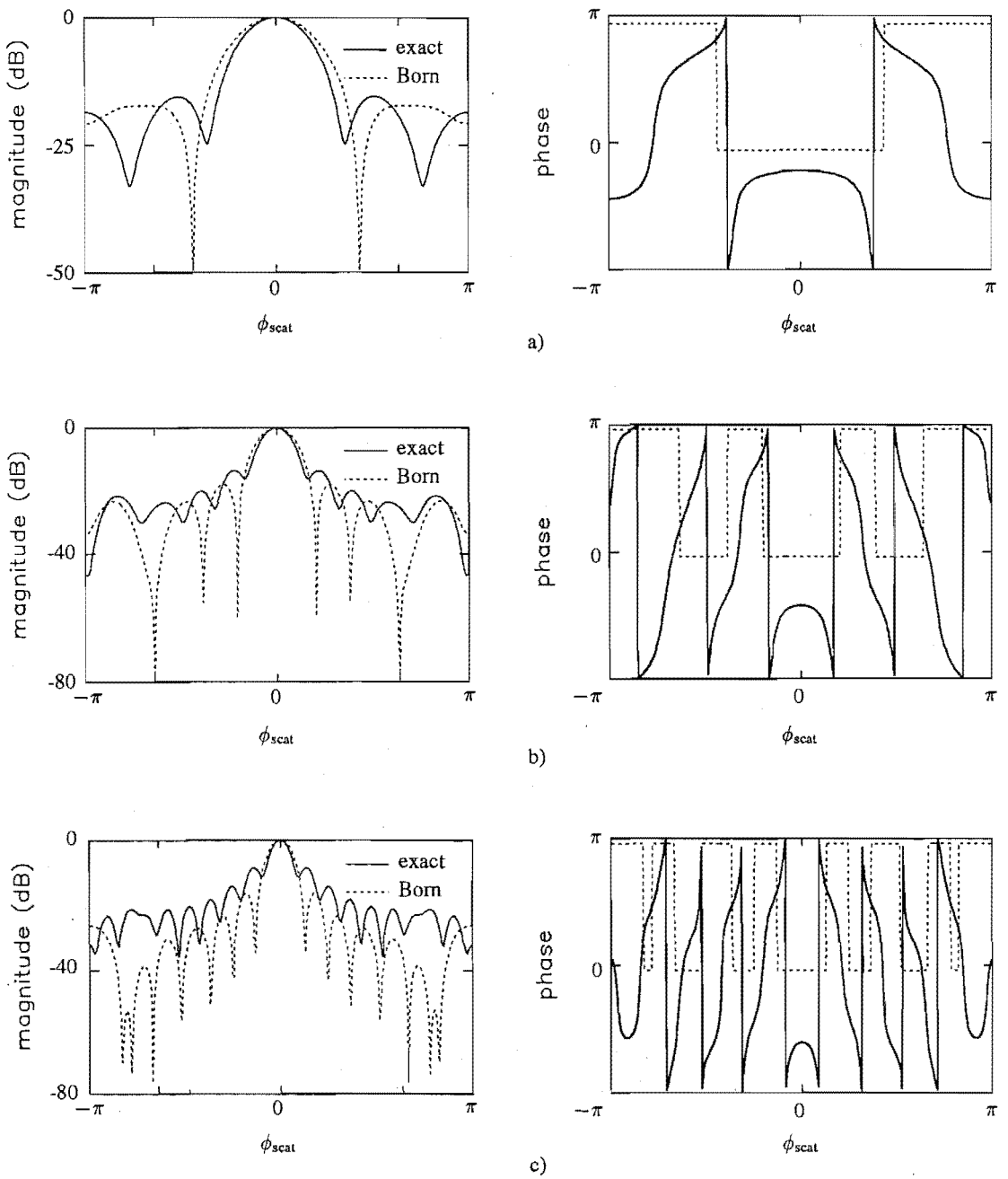

Figure 2.5 Far-field radiation patterns of ψ_{scat} showing the accuracy of the Born approximation around its range of validity. The object is a single cylinder with $\nu = 1.25$. (a), (b), and (c) correspond, respectively, to the diameter of the cylinder being 1λ, 2λ, and 3λ, and $\mathcal{L}_{max}$ being 0.25λ, 0.50λ and 0.75λ.

2.4 Geometrical optics (GO)

In many situations of practical interest, the refractive index of the medium varies appreciably only over distances which are large compared to the wavelength of the radiation. This is, of course, true for all media if the frequency of the radiation is high enough. Under this approximation the Helmholtz equation (1.3) reduces to [Jones, 1964]

$$\nabla S(\mathbf{x}) \cdot \nabla S(\mathbf{x}) = \nu^2(\mathbf{x}) \tag{2.22}$$

which is known as the eikonal equation. $S(\mathbf{x})$ is defined by expressing the field in the form

$$\psi = \psi(\mathbf{x}, k) = A(\mathbf{x}) e^{-jkS(\mathbf{x})} \tag{2.23}$$

where $A(\mathbf{x})$ and $S(\mathbf{x})$ are real, so that $kS(\mathbf{x})$ is the phase of the field and $A(\mathbf{x})$ is its amplitude.

A formal solution to (2.22) is [Born and Wolf, 1980]

$$S(\mathbf{x}) = \int_0^{l(\mathbf{x})} \nu(\mathbf{x}_1)\, dl(\mathbf{x}_1) \tag{2.24}$$

where $dl(\mathbf{x})$ is the element of arc along a continuous (but not necessarily everywhere analytic) curve $l(\mathbf{x})$, beginning at a point in Υ_{inc} and of length $l(\mathbf{x})$ at the point P having position vector $\mathbf{x}$. It transpires $l(\mathbf{x})$ is such that [Born and Wolf, 1980]

$$\delta \int_0^{l(\mathbf{x})} \nu(\mathbf{x}_1)\, dl(\mathbf{x}_1) = 0 \tag{2.25}$$

This is Fermat's principle, which states that energy propagates along the path for which the travel-time is a local minimum. Equation (2.25) leads to Snell's laws of reflection and refraction [Jones, 1986].

One can think of each curve $l(\mathbf{x})$ as a *ray*, with $S(\mathbf{x})$ being its electrical path length [Born and Wolf, 1980]. A wavefront of ψ is, by definition, any surface on which the phase, and therefore S, is constant. It follows from (2.25) that rays always intersect wavefronts perpendicularly and therefore represent the direction in which energy propagates. This is the essence of *geometrical optics* (GO) [Born and Wolf, 1980; Deschamps, 1972; Fradkin, 1989; Kline and Kay, 1965; Sleeman, 1982].

Given a particular refractive index distribution and a set of initial conditions, (2.22) is sufficient to determine $S(\mathbf{x})$. Conversely, in general there is no explicitly solvable expression for the field amplitude, $A(\mathbf{x})$, although it can be determined analytically by invoking conservation of energy flow once the rays have been traced through the medium. Consider the elemental tube of rays shown in figure 2.6. Because the energy propagates along the rays no energy is lost across the sides of the tube. Consequently

$$|A_1|^2 d\Sigma_1 = |A_2|^2 d\Sigma_2 \tag{2.26}$$

where $d\Sigma_1$ and $d\Sigma_2$ are the elemental areas of the tube at two positions along the tube, and A_1 and A_2 are the amplitudes of the wavefront at $d\Sigma_1$ and $d\Sigma_2$, respectively. This means that the amplitude of the field at all positions along the tube can be calculated if the amplitude is known at any one position. Generally, the radiation pattern of the source of the rays is known, so its amplitude can be used as a reference amplitude. Thus $S(\mathbf{x})$ and $A(\mathbf{x})$ can be calculated and the field determined.

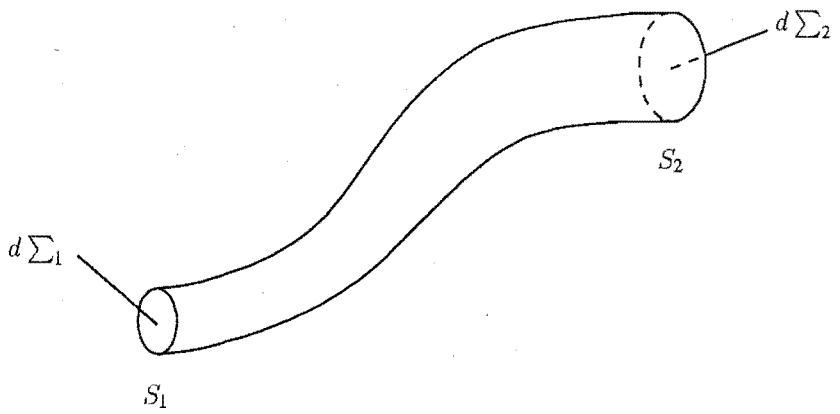

Figure 2.6 An elemental tube of rays of area $d\Sigma_1$ and $d\Sigma_2$ at the wavefront positions S_1 and S_2 respectively.

2.4.1 Implementation

When a medium has a piecewise constant refractive index, as for the objects used in this chapter (see figure 2.1), GO is particularly convenient to apply because rays within each piecewise constant region are straight. Once a ray reaches a discontinuity, refracted and reflected rays are generated, according to Snell's laws of refraction and reflection [James, 1986]. The amplitudes of these rays are proportional to the refraction and reflection coefficients for plane waves incident upon planar interfaces, which are determined by matching amplitudes and first derivatives across the interface (as for (2.7)) [Jones, 1964; James, 1986]. The reflected and refracted rays are then individually traced until they intersect another discontinuous boundary where the process is repeated. The number of multiple interactions to be calculated for each ray depends on the particular problem and the degree of accuracy required. To produce the results in this chapter all rays were traced until their magnitudes were less than 10^{-5} (initial magnitude was unity), or they entered Υ_{++}. The total field at a point is then simply the superposition of all incident, reflected and refracted rays. The field in figures 2.7 and 2.9-2.12 was determined by using 10^5 initial rays and summing all rays entering Υ_{++} within half-degree intervals. This discrete approach was used because caustics (i.e. ray crossings) in piecewise homogeneous objects make (2.26) difficult to apply.

The accuracy of the GO approximation (i.e. the above method) in solving the direct problem is assessed in figure 2.7 for the simple case of an object consisting of a single cylinder of constant refractive index. These results indicate that the GO, or high frequency approximation is quite inaccurate for homogeneous objects with dimensions as small as 20λ. Because GO is a high frequency approximation, it will become more accurate as the dimensions of the object increase.

2.4.2 Geometrical Optics for inhomogeneous media

When the refractive index is inhomogeneous and continuous (discontinuities are handled as above), as it is for the objects considered in section 3.2, a suitable differential

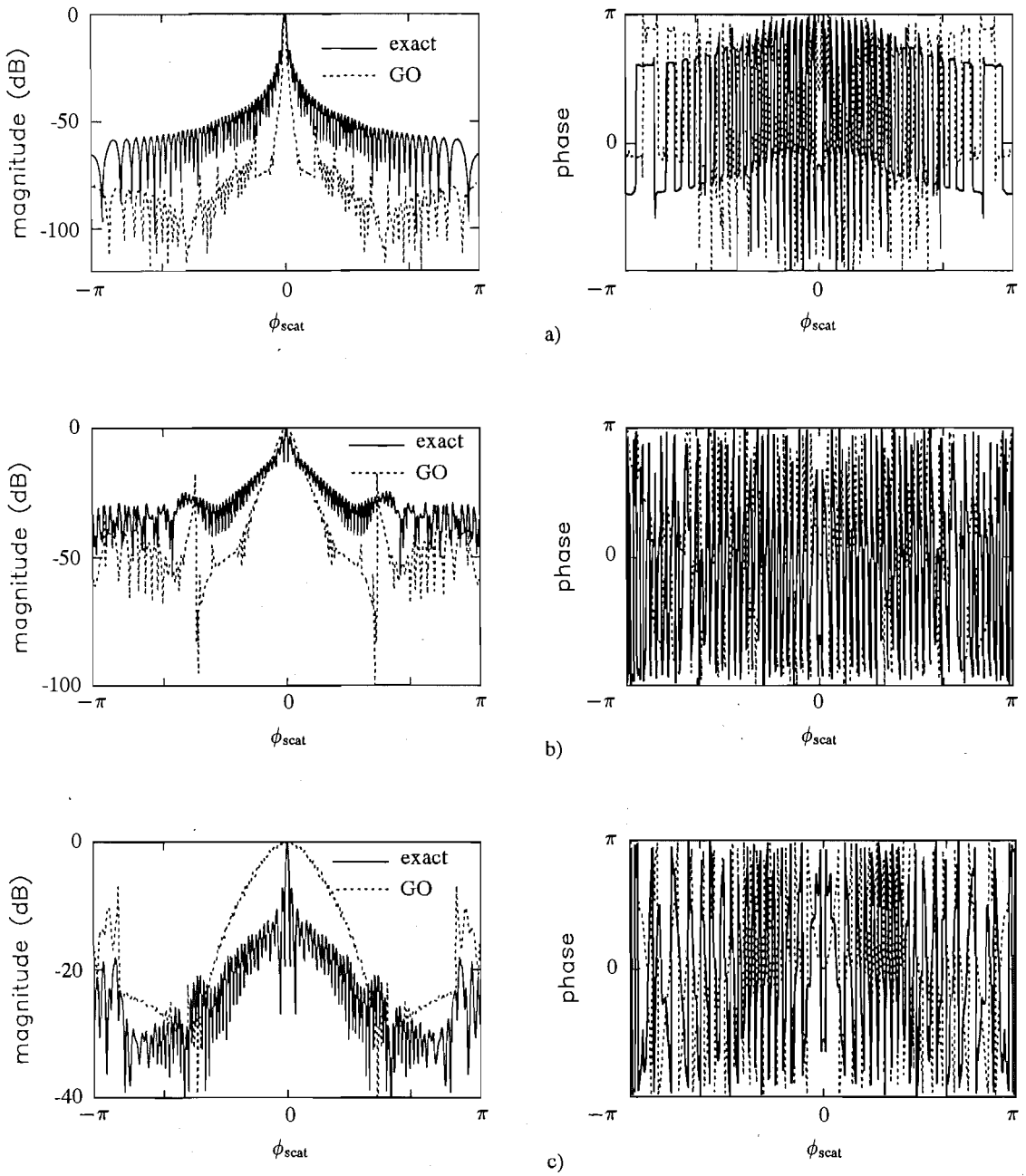

Figure 2.7 Far-field radiation patterns of ψ_{scat} showing the accuracy of the GO approximation when the object is a single cylinder of diameter 20λ. (a), (b) and (c) correspond, respectively, to the refractive index of the cylinder being 1.01, 1.10, and 1.50. Note that GO is relatively insensitive to the size of the cylinder, i.e. these results would be very similar even if different sized cylinders were used.

equation for the ray path is required. Because any surface $S(\mathbf{x}) = constant$ represents a wavefront, $\nabla S(\mathbf{x})$ must be normal to the wavefront. Thus, $\nabla S(\mathbf{x})$ determines the direction of each ray. Inspection of (2.22) reveals that the magnitude of $\nabla S(\mathbf{x})$ is $\nu(\mathbf{x})$. Therefore, the differential equation for a ray is

$$\frac{d\mathbf{x}(l)}{dl} = \frac{\nabla S(\mathbf{x})}{\nu(\mathbf{x})} \tag{2.27}$$

where $\mathbf{x}(l)$ is the position vector of an arbitrary point on a ray and l is arc length along the ray. The algorithm used to solve the direct problem arising in Chapter 3 is based on expanding $\mathbf{x}(l)$ as a second order Taylor series. With the inclusion of (2.27) and the Euler equations [Arfken, 1985], which constitute a necessary condition for the existence of a minimum value for (2.24), the algorithm is [Andersen and Kak, 1982]

$$\mathbf{x}(l+\Delta l) = \mathbf{x}(l) + \frac{d\mathbf{x}(l)}{dl}\Delta l + \frac{1}{2\nu(\mathbf{x})}\left[\nabla\nu(\mathbf{x}) - \left(\nabla\nu(\mathbf{x}) \cdot \frac{d\mathbf{x}(l)}{dl}\right)\frac{d\mathbf{x}(l)}{dl}\right](\Delta l)^2 \tag{2.28}$$

2.4.3 Implementation

Given a starting point $\mathbf{x}(l_0)$ and an initial direction $\frac{d\mathbf{x}(l_0)}{dl}$ for the ray, (2.28) enables a ray to be traced recursively at discrete points, each separated along the ray by arcs of length Δl. Note that $\nu(\mathbf{x})$, $\nabla\nu(\mathbf{x})$ and $\frac{d\mathbf{x}(l)}{dl}$ also need to be known at each point $\mathbf{x}(l)$. Since $\nu(\mathbf{x})$ is given in the direct problem, $\nabla\nu(\mathbf{x})$ can be calculated everywhere in the medium. On the other hand, there is no explicit formula for $\frac{d\mathbf{x}(l)}{dl}$, which must be evaluated with the aid of some appropriate numerical procedure for calculating derivatives. Since Andersen and Kak [1982] offer no suggestion as to which procedure might be most effective, an iterative algorithm suggested by Murch [1990] was adopted. It comprises the following steps:

1. A first estimate of $\frac{d\mathbf{x}(l)}{dl}$ is obtained as

$$\frac{d\mathbf{x}(l)}{dl} = \frac{\mathbf{x}(l) - \mathbf{x}(l-\Delta l)}{\Delta l} \tag{2.29}$$

   which is then used to calculate $\mathbf{x}(l+\Delta l)$ using (2.28).

2. From the above value of $\mathbf{x}(l+\Delta l)$ a mid-point estimate of $\frac{d\mathbf{x}(l)}{dl}$ is calculated:

$$\frac{d\mathbf{x}}{dl} = \frac{\mathbf{x}(l+\Delta l) - \mathbf{x}(l-\Delta l)}{2\Delta l} \tag{2.30}$$

3. This new estimate of $\frac{d\mathbf{x}(l)}{dl}$ is then used to calculate a new $\mathbf{x}(l+\Delta l)$

4. Steps 2-3 are repeated until the difference between successive estimates of $\frac{d\mathbf{x}(l)}{dl}$ is less than 10^{-5}.

The accuracy of this ray tracing algorithm is conveniently assessed by applying it to 'Maxwell's fish-eye' [Barnes and Solomon, 1973], which is the circularly symmetrical refractive index distribution

$$\nu(\mathbf{x}) = \nu_o(1 + \frac{|\mathbf{x}|}{a})^2 \tag{2.31}$$

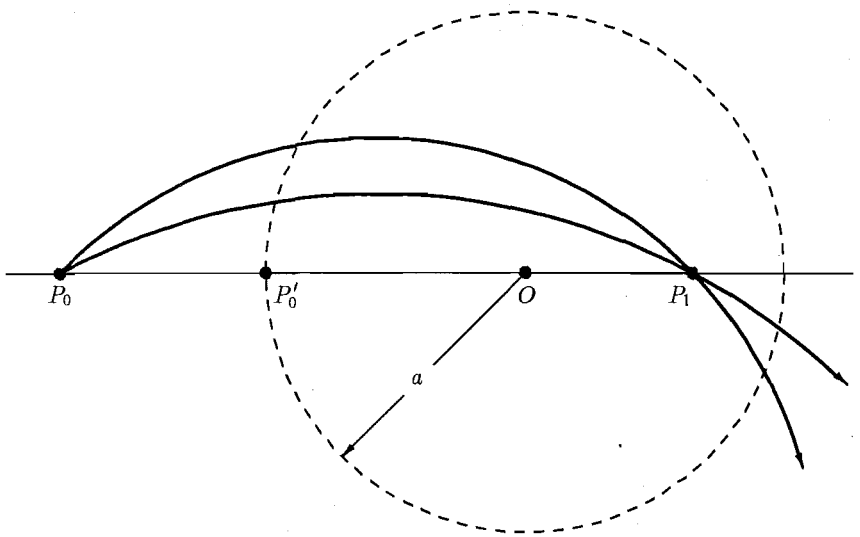

Figure 2.8 Diagram showing rays in Maxwell's 'fish-eye'. All rays from an arbitrary point P_0 meet at an image point P_1. If a ray is released from P_0', at a distance a from O in a direction perpendicular to the line P_0O, then the ray traces a circle of radius a centred at O.

where $\mathbf{x}$ is the position vector of an arbitrary point, and ν_0 and a are constants. A characteristic property of this distribution is shown in figure 2.8. All rays from an arbitrary point P_0 meet at an image point P_1 such that the line P_0P_1 intersects O. The distances $|P_0O|$ and $|OP_1|$ are related through $|P_0O| \cdot |OP_1| = a^2$. Therefore, if a ray is released from P_0', at a distance a from O in a direction perpendicular to the line P_0O, the ray traces a circle of radius a centred at O. As Andersen and Kak [1982] imply, a severe test for a ray tracing algorithm is to require it to trace such a circle. It is also desirable for the algorithm to do this as efficiently as possible, which is equivalent to employing a minimum number of recursions. The algorithm outlined above requires 250 recursions to close, to within 1%, a circle having a diameter of 40 Δl. This performance appears identical to that achieved by Andersen and Kak [1982], but superior to that of other published algorithms [Smith *et al.*, 1980; Fawcett and Keller, 1985].

There are two distinct problems in this thesis which are solved by ray tracing. The first, described in this chapter, is to determine wave motion at one point if it is known at another, i.e. determine ψ_{scat} knowing ψ_{inc}. The second, which arises in section 3.2, is to find the ray linking two points. The simplest method (and the one implemented here) to achieve the latter, is to send off rays toward the point one wishes to link with. A Newton method can then be used to converge to the correct initial angle of the required ray.

2.5 Comparison of Direct Solutions

This section assesses the range of validity of the Born and GO approximations in solving the direct scattering problem. To this end, some more solutions to the direct problem are shown in figures 2.9-2.13 for objects consisting of multiple cylinders. Exact or accurate solutions for the scattering from one cylinder [Leviatan and Boag, 1987; Murch, 1990;

Robinson and Greenleaf, 1986], and even multiple cylinders [Jin and Liepa, 1989; Yokota *et al.*, 1986], have been calculated before for a wide range of object variations. However, almost all of this work has had the solution of the direct problem as its sole (and worthy) aim. The goal in this section is to use the exact result to assess the accuracy of approximate solutions in order to determine the applicability of the inverse solutions in Chapter 3. It appears that a comparison between solutions to the direct problem using the Born or GO approximations and the exact solution has not been made previously for multi-component objects. The results here serve to illustrate the different domains of applicability of the two approximations and the effect of multiple scattering on the Born approximation.

The Born approximation is the simplest of the approximations which explicitly account for diffraction. What does not seem to have been fully appreciated until recently is that the approximation is exact only when scattering is negligible [Coates and Chapman, 1990; Ramm, 1990]. It assumes that $\psi_{\text{inc}}(\mathbf{x} \in \Upsilon_-, k)$ approximates $\psi(\mathbf{x} \in \Upsilon_-, k)$, but this can be true only if $\nu \approx 1$, or if the object's largest dimension is only a few wavelengths. However, the widespread use of the Born approximation (see section 1.1) indicates that it can be useful even when scattering is appreciable. Many extensions to the approximation attempt to widen its range of validity, in particular by partially accounting for the difference in wavefront positions of ψ_{inc} and ψ [Bates, 1988; Devaney and Oristaglio, 1983; Levy and Esmersoy, 1988]. The Rytov approximation, which is computationally similar, has also been argued to have wider validity in some situations [Soumekh and Kaveh, 1986]. Furthermore, the Born approximation can be thought of as the first term of a series which converges to the exact solution for $\psi_{\text{scat}}(\mathbf{x}, k)$ under appropriate conditions [Arfken, 1985; Kleinman *et al.*, 1990].

The results in this chapter illustrate the comment in the previous paragraph that the Born approximation is never truly accurate when $\nu \not\approx 1$. For this reason it is pointless to suggest a range of relative path lengths, $\mathcal{L}_{\max}$, for which the Born approximation is accurate. Whether it is accurate enough to be useful can be determined only by solution of the corresponding inverse problem. In figure 2.4, where the refractive index deviation and the object are small, the Born approximation is obviously appropriate because it predicts ψ_{scat} well. In figures 2.5 and 2.9-2.13 a range of situations where the approximation is less appropriate are shown. The decrease in accuracy with increasing $\mathcal{L}$ is well known [Jones, 1964] and is considered only briefly here in figure 2.5. It is more interesting to consider the effect of multiple scattering on the approximation. In figures 2.9 and 2.11, $\mathcal{L}_{\max}$ is 0.24λ and $\approx 0.12\lambda$ respectively, yet the Born field is less accurate than could be expected from results in figures 2.4 and 2.5 (note the phase in the forward direction). The error due to multiple scattering is better illustrated by comparing figures 2.11(a) and (b) with figure 2.13(c) where $\mathcal{L}_{\max}$ is ten times greater. Note that the accuracy of the Born approximation has decreased markedly. In contrast, $\mathcal{L}_{\max}$ also increases by a factor of ten between figures 2.13(a) and (b), yet the accuracy of the Born approximation hardly changes. The difference is that multiple scattering has appreciable effects in the first instance, but not in the second. Also note that in figure 2.13(c), where $\mathcal{L}_{\max} \approx 1.2$, the Born approximation is very much worse at predicting ψ_{scat} than in figure 2.13(b) where $\mathcal{L}_{\max} = 1.5$. All of these results indicate that the distance, $\mathcal{L}$, between wavefronts of ψ and ψ_{inc} is not necessarily an accurate predictor of the validity of the Born approximation. In particular, even when $\nu \approx 1$, multiple scattering can

be an important source of error if individual components of a multi-component object are large and fairly close together. It is important to distinguish this case from that in figures 2.13(a) and (b) where the scatterers are small, strong and close together. While multiple scattering occurs with this geometry, its effects on the Born approximation are less important. This comparison shows that the validity of the Born approximation is dependent, to perhaps a previously unappreciated extent, on object geometry. The effects of multiple scattering on the Born approximation are discussed again in section 3.1.5.

GO is a conceptually simple method for determining the field when variations in refractive index occur slowly. It explicitly accounts for refraction and multiple scattering, but not diffraction. This deficiency is overcome by an extension to GO called the Geometrical Theory of Diffraction (GTD) [Herrmann, 1987; James, 1986]. However, GTD is of less interest here because it has not been incorporated into inverse scattering algorithms. One of the principal advantages of GO is that it is not affected by the size of the object, provided a high frequency approximation is appropriate. This suggests that GO would be a good basis for a reconstruction algorithm capable of handling appreciable refraction in large objects (see section 3.2).

It is well known that when object inhomogeneities are comparable in size to the wavelength, diffraction is appreciable and the GO (or high frequency) approximation is not valid. The results in this chapter suggest that the GO approximation is still unsuitable for homogeneous objects with dimensions of 20λ. Although not shown here, it is appropriate for inhomogeneous objects of this size, provided that spatial variations of the refractive index are sufficiently smooth that a high frequency approximation is justified. While it would have been interesting to assess the accuracy of GO for larger cylinders, the Bessel functions in the eigenfunction expansion become too large to allow the exact solution to be determined. The investigation in this chapter of the accuracy of the GO approximation is therefore of limited use. However, it does show that, while perhaps not appropriate for the size of object in figures 2.10 and 2.12, GO is still more accurate than the Born approximation in these situations.

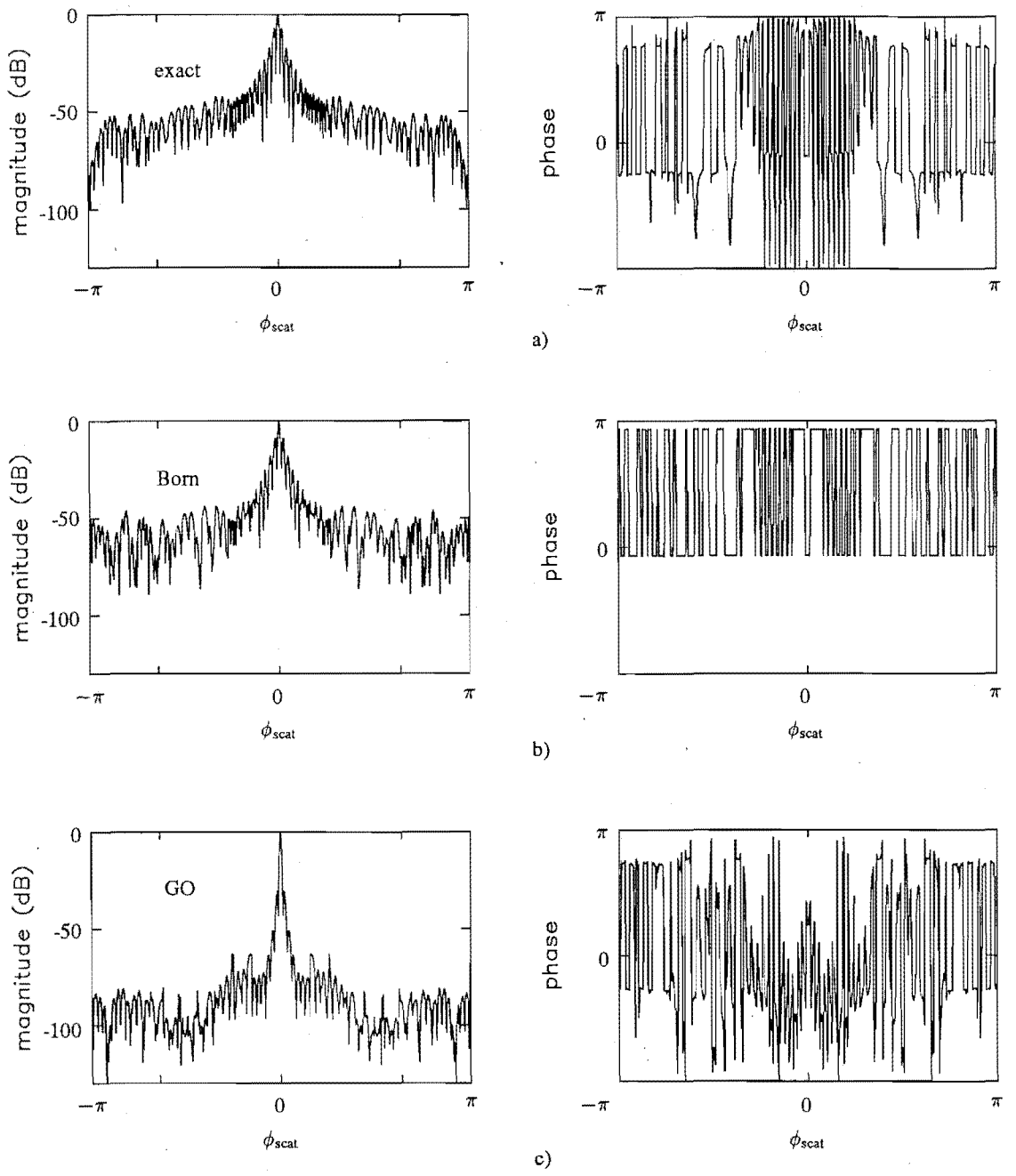

Figure 2.9 Far-field radiation patterns of ψ_{scat} to compare the Born and GO approximations. The object is the two cylinder object shown in figure 2.1 where the cylinders have diameter 12λ, centers at $(-7\lambda, 0)$ and $(7\lambda, 0)$ and refractive index 1.01. $\mathcal{L}_{max} = 0.24\lambda$.

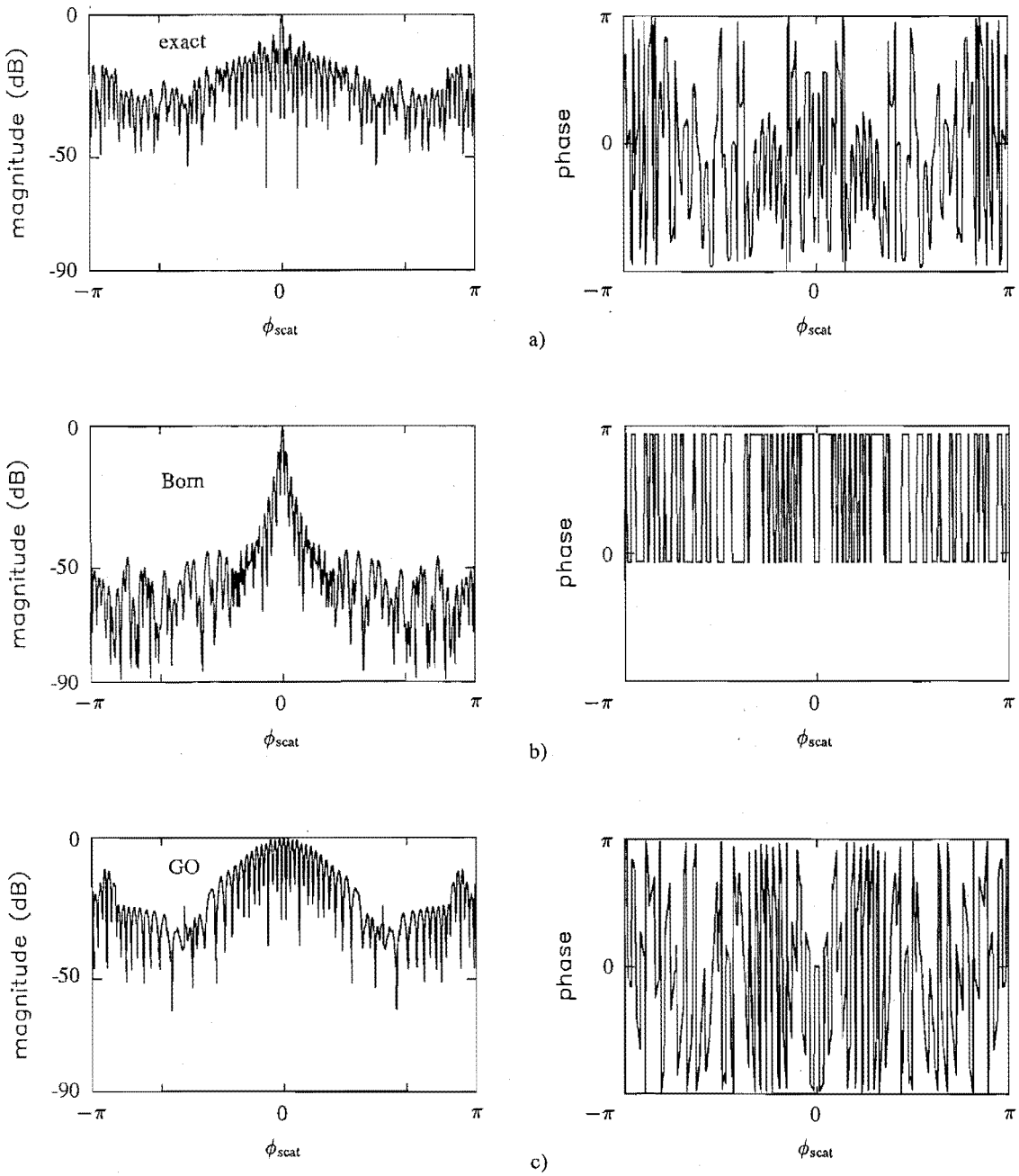

Figure 2.10 Far-field radiation patterns of ψ_{scat} to compare the Born and GO approximations. The object is the two cylinder object shown in figure 2.1 where the two cylinders have diameter 12λ, centers at $(-7\lambda, 0)$ and $(7\lambda, 0)$ and refractive index 1.5. Note that the Born solution in (b) is the same as that in figure 2.9. $\mathcal{L}_{max} = 12\lambda$.

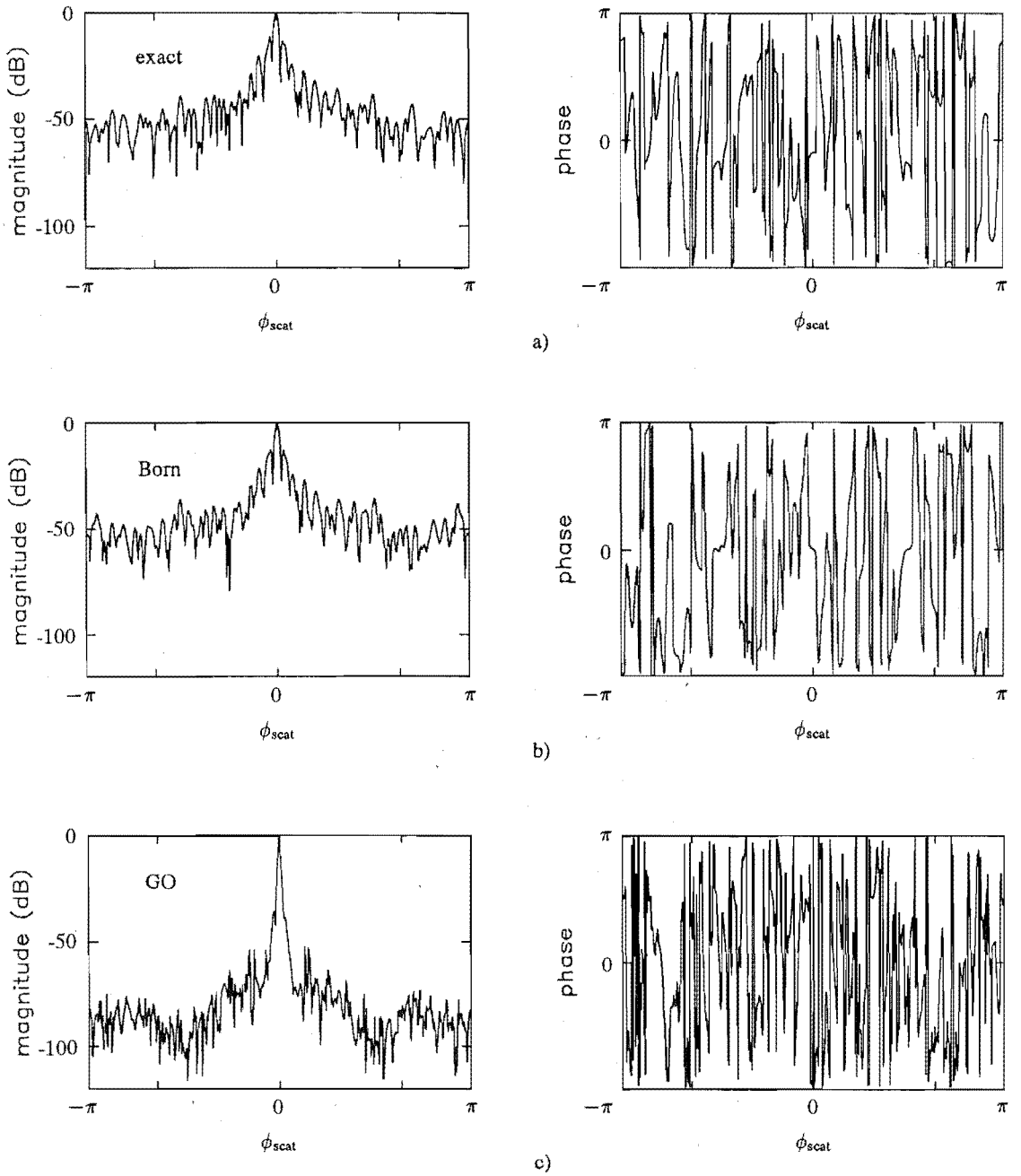

Figure 2.11 Far-field radiation patterns of ψ_{scat} to compare the Born and GO approximations. The object is the six cylinder object shown in figure 2.1. Using notation from this figure $\mathbf{x}_1 = (-5, 2)$, $\mathbf{x}_2 = (-3, -4)$, $\mathbf{x}_3 = (0, 6)$, $\mathbf{x}_4 = (4, -5)$, $\mathbf{x}_5 = (5, 2)$, $\mathbf{x}_6 = (0, 0)$, $2r_{1,2,3,4,5} = 6\lambda$, $2r_6 = 2\lambda$, and $\nu_{1,2,3,4,5,6} = 1.01$. $\mathcal{L}_{max} \approx 0.12\lambda$.

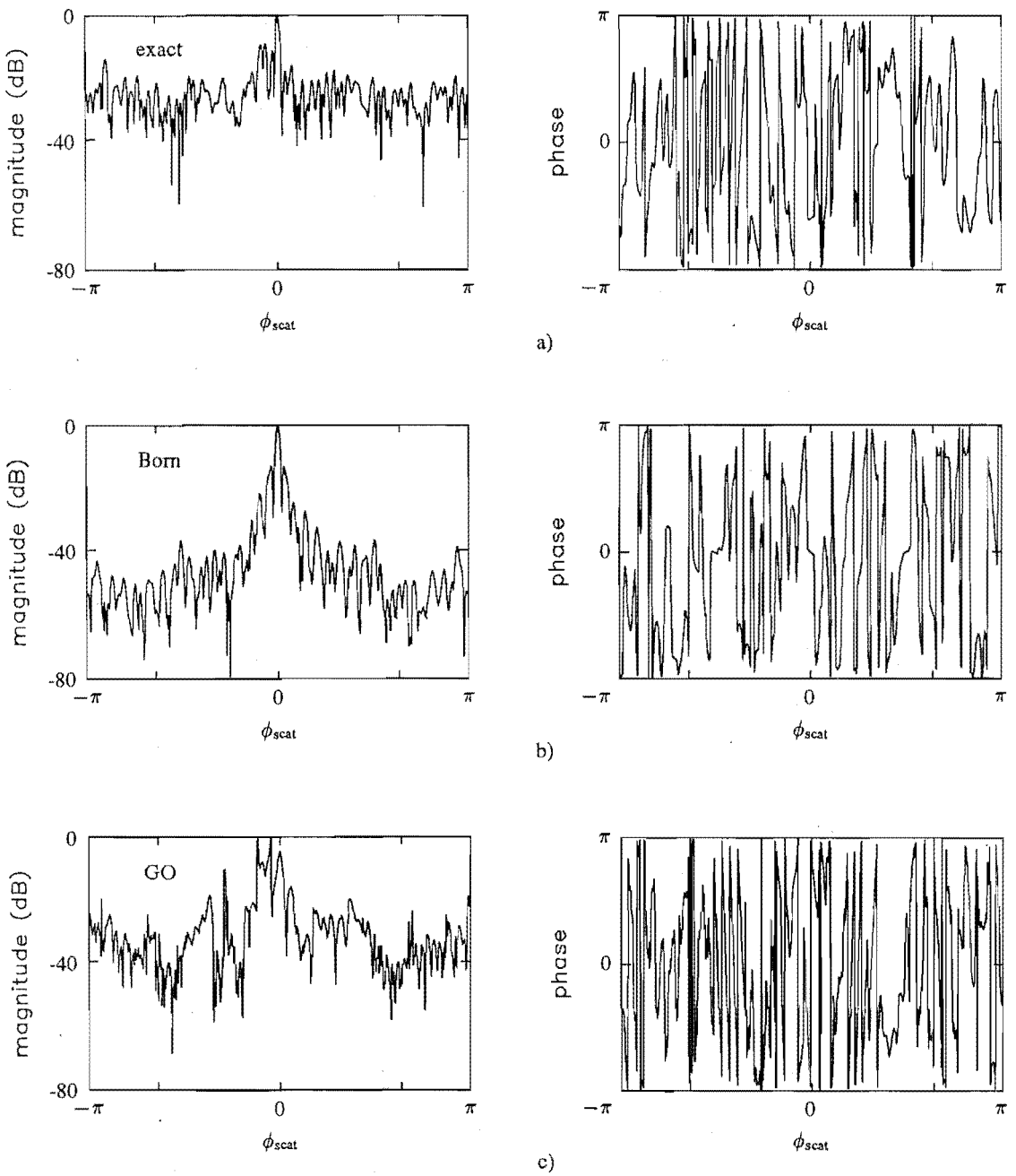

Figure 2.12 Far-field radiation patterns of ψ_{scat} to compare the Born and GO approximations. The object is the six cylinder object shown in figure 2.1. Using notation from this figure $\mathbf{x}_1 = (-5,2)$, $\mathbf{x}_2 = (-3,-4)$, $\mathbf{x}_3 = (0,6)$, $\mathbf{x}_4 = (4,-5)$, $\mathbf{x}_5 = (5,2)$, $\mathbf{x}_6 = (0,0)$, $2r_{1,2,3,4,5} = 6\lambda$, $2r_6 = 2\lambda$, and $\nu_{1,2,3,4,5,6} = 1.5$. Note that the Born solution in (b) is the same as that in figure 2.11. $\mathcal{L}_{max} \approx 6\lambda$.

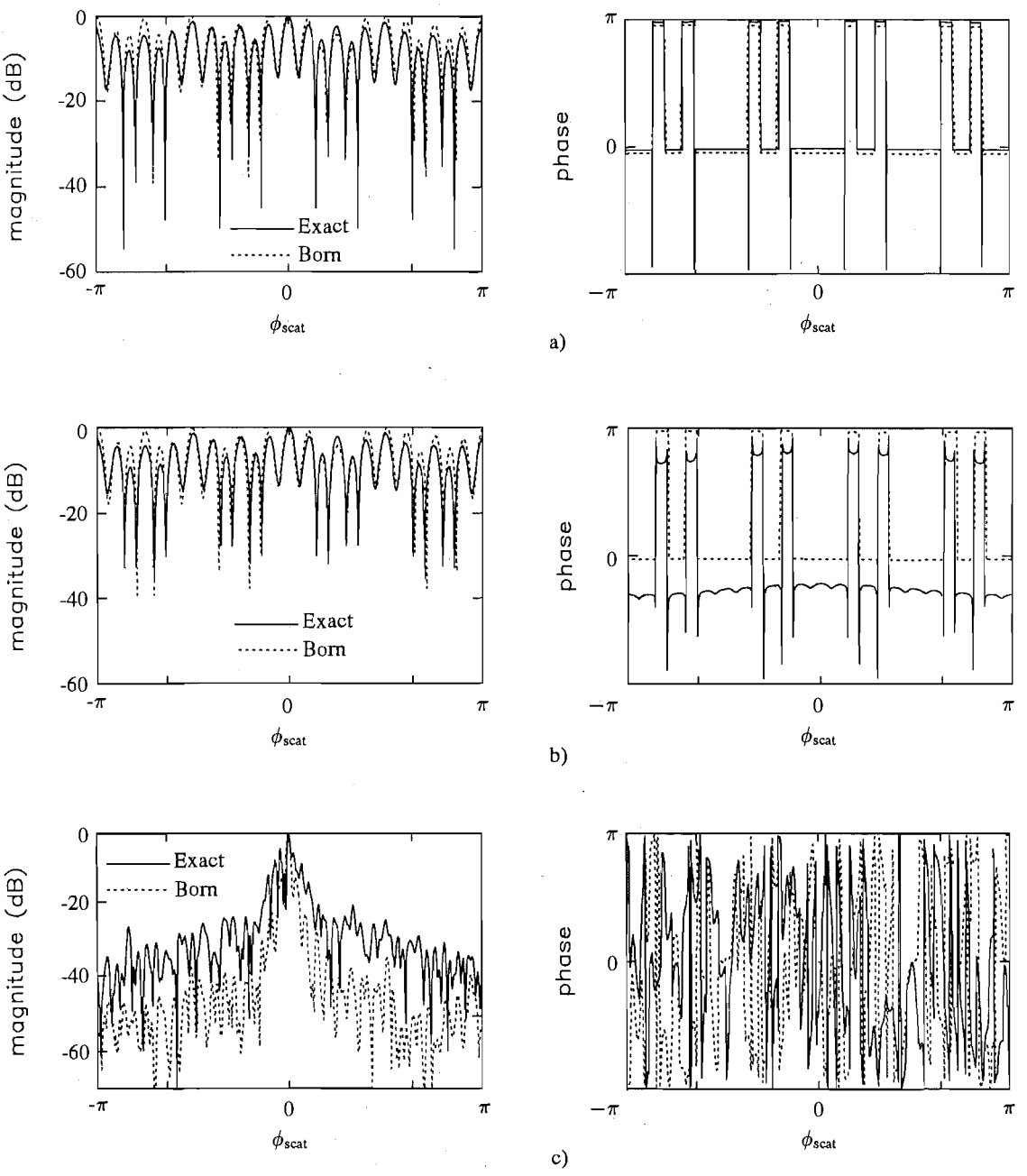

Figure 2.13 Far-field radiation patterns of ψ_{scat} showing the effects of multiple scattering on the accuracy of the Born approximation. The object used for (a) and (b) is the five cylinder object shown in figure 2.1. Using notation from this figure $\mathbf{x}_1 = (-3,0)$, $\mathbf{x}_2 = (0,-3)$, $\mathbf{x}_3 = (0,0)$, $\mathbf{x}_4 = (0,3)$, $\mathbf{x}_5 = (3,0)$, $2r_{1,2,3,4,5} = 0.25\lambda$. (a) and (b) correspond to $\nu_{1,2,3,4,5,6} = 1.05$ and $\nu_{1,2,3,4,5,6} = 1.5$ respectively. The object used for (c) is described in figures 2.11 and 2.12, but here has $\nu_{1,2,3,4,5,6} = 1.1$. $\mathcal{L}_{max}$ is 0.15λ, 1.5λ, and $\approx 1.2\lambda$ in (a), (b) and (c) respectively. Note that for these three examples, $\mathcal{L}_{max}$ is a very bad predictor of the validity of the Born approximation.

CHAPTER 3

New Inverse Scattering Solutions

Scattering research is really about investigating new inverse scattering algorithms capable of revealing more information about objects being imaged. This chapter details two such investigations.

As implied in Chapter 2, exact solutions to the inverse scattering problem posed in this thesis are possible, although not presently practical due to the excessive computation involved. Therefore, practical solutions are unavoidably approximate. Approximate inverse scattering approaches, where detailed *a priori* information about the scatterers is unavailable, can be partitioned according to the type of approximation made. The two important groups are *diffraction tomography*, where a wave equation is used as the descriptor of wave motion, and *computed tomography* (CT), where wave motion is described by rays (which are almost always assumed to be straight). As suggested in Chapter 2, diffraction tomography is the more sophisticated method [Robinson and Greenleaf, 1986], but is limited by the appropriateness of the wave equation. With regard to diffraction tomography, section 3.1 investigates a method for reducing distortion by using an image processing technique called Shift-and-add (SAA), which has been developed at Canterbury University by the Bates[1] group. With regard to CT, a significant improvement results if wave motion can be described by bent rays. This improvement has been demonstrated previously, but has required ray tracing. The approach reported in section 3.2 is a bent-ray CT solution which does not require ray tracing.

3.1 Born Inversion

The Born approximation is one of the most commonly invoked approximations in inverse scattering applications [Boyse and Keller, 1986; Blackledge *et al.*, 1987; Pratt and Worthington, 1988; Wu and Toksöz, 1987] (see also section 1.1) due to the ease with which its inverse can be formed. Despite this relative ease, some uncertainty exists as to whether Fourier interpolation or backpropagation is the most effective method for performing Born inversion [Pan and Kak, 1983]. The backpropagation algorithm for receivers in the far-field is derived in section 3.1.2, and implementation details for both methods are given in section 3.1.3. Section 3.1.4 then compares the two methods and finds a greater difference in effectiveness when the receivers are in the far-field, than in the 'standard' CT configuration.

[1] Professor R.H.T. Bates, along with his students and associates

In the context of this thesis, the assumptions on which the Born approximation is based are often invalid [Johnson and Tracy, 1983]. It is therefore important to seek ways to extend the basic approximation's validity. In particular, and as illustrated in Chapter 2, the Born approximation can be invalid due to excessive relative path length, $\mathcal{L}$, through the object, and/or multiple scattering. The path length problem is clearly the more important of the two effects and research to compensate for it has been prolific [Bates, 1988; Beylkin, 1985a; Beylkin, 1985b; Caorsi *et al.*, 1990; Chew and Wang, 1990; Clayton and Stolt, 1981; Devaney and Oristaglio, 1983; Esmersoy *et al.*, 1985; Esmersoy and Levy, 1986; Howard *et al.*, 1990; Levy and Esmersoy, 1988; Murch, 1992; Schultz and Jaggard, 1987; Slaney *et al.*, 1984; Soumekh and Kaveh, 1986; Wang and Chew, 1989; Wombell and Fiddy, 1988]. Investigations of even the effect of multiple scattering have been limited [Azimi and Kak, 1983]. Section 3.1.5 presents the first Born reconstructions of multi-cylinder objects where ψ_{scat} has been determined exactly and goes on to thoroughly investigate the distortion caused by multiple scattering.

No attempt appears to have been made to reduce distortion caused by multiple scattering. Presumably this is because of the difficulty of the problem, along with the complication of the associated direct problem. The Shift-and-add (SAA) algorithm has previously been proposed to reduce distortion due to both multiple scattering and excessive relative path length [Bates and Minard, 1984; Bates and Minard, 1983; Minard, 1985; Minard *et al.*, 1985; Bates and Robinson, 1981]. A suitable SAA extension to Born inversion is formulated in section 3.1.6 and implemented in section 3.1.7. The resultant reduction in distortion is then discussed in section 3.1.8.

3.1.1 Formulation of Born inversion

Equation (2.19) states that the Born approximation relates the scattered field in the far-field, $\psi_{\text{scat}_\mathbf{f}}(\hat{\mathbf{x}}, k)$, to the refractive index, $\nu(\mathbf{x})$, through the Fourier transform, i.e.

$$\psi_{\text{scat}_\mathbf{f}}(\hat{\mathbf{x}}, k) = k^2 \mathcal{F}\left[\nu_b^2(\mathbf{x}) - 1\right](\mathbf{k}') \tag{3.1}$$

where $\mathbf{k}' = k(\hat{\mathbf{k}} - \hat{\mathbf{x}})$, $\hat{\mathbf{x}}$ is the unit vector in the direction in which $\psi_{\text{scat}_\mathbf{f}}(\hat{\mathbf{x}}, k)$ is measured, $\hat{\mathbf{k}}$ is the unit vector in the direction of incidence of $\psi_{\text{inc}}(\mathbf{x}, k)$, and $\nu_b(\mathbf{x})$ is the Born reconstruction of $\nu(\mathbf{x})$. Since the Born approximation, and therefore inversion based on the Born approximation, is only accurate when the refractive index is known *a priori* to be identically unity [Coates and Chapman, 1990; Ramm, 1990], it must produce distorted images for all objects. However, its wide use demonstrates that such images can still contain useful information. Chapter 2 has shown that the Born approximation can be expected to be a useful approximation if the refractive index is such that $\mathcal{L}_{\max} < 0.25\lambda$ (so that $\psi_{\text{inc}} \approx \psi$) and object components are well spaced relative to their individual sizes (so that multiple scattering does not cause significant distortion).

Inspection of (3.1) might suggest that, where the Born approximation is appropriate, the refractive index could be immediately and straightforwardly estimated from the scattered field by invoking the inverse Fourier transform of $\psi_{\text{scat}_\mathbf{f}}(\hat{\mathbf{x}}, k)$. However, it is apparent from section 2.3 and figure 2.3 that $\psi_{\text{scat}_\mathbf{f}}(\hat{\mathbf{x}}, k)$, for all $\hat{\mathbf{x}}$, provides information about $\mathcal{F}[\nu_b^2(\mathbf{x}) - 1]$ only on a circle. Consequently, in order to cover as much of Fourier space as possible, observations of $\psi_{\text{scat}_\mathbf{f}}(\hat{\mathbf{x}}, k)$ must be made for all directions $\hat{\mathbf{k}}$

of $\psi_{\text{inc}}(\mathbf{x}, k)$ as well. The coverage of Fourier space then corresponds to the interior of a circle of diameter $2k$ (see figure 2.3). Thus the spatial resolution, Δx, of the image is

$$\Delta x \leq \frac{2\pi}{2k} = \frac{\lambda}{2} \tag{3.2}$$

which accords with the intuitive notion that any spatial variations in refractive index that are significantly smaller than a wavelength cannot be discerned. The inverse Fourier transform of the scattering data is then a band limited approximation to the true distribution of $\nu(\mathbf{x})$.

For computational reasons, any Born inversion scheme must be implemented using the inverse fast Fourier tansform (IFFT). However, numerical techniques for inverting (3.1) using the IFFT require that the scattering data be sampled on a rectangular grid [Bracewell, 1978]. This can be realized by making observations of the field at specified $\hat{\mathbf{x}}$ and $\hat{\mathbf{k}}$, so that each sample lies at a point on the desired grid. However, this exact method is tedious because a different $\hat{\mathbf{x}}$ and $\hat{\mathbf{k}}$ must be employed for each grid point. Moreover, it is unnecessary since interpolation methods can produce equivalent reconstructions. Interpolation methods involve recording $\psi_{\text{scat}_\mathbf{f}}(\hat{\mathbf{x}}, k)$ for a number of directions $\hat{\mathbf{k}}$ of $\psi_{\text{inc}}(\mathbf{x}, k)$. This data can then be transferred on to the desired rectangular grid in either the frequency or space domains. Performing the interpolation in the frequency domain involves interpolating from the curves, $\mathbf{k}'$, on to a rectangular grid. Performing the interpolation in the space domain is known as backpropagation and was developed by Devaney [1982] and Kaveh *et al.* [1982].

3.1.2 Backpropagation

Backpropagation is one method for performing Born (or Rytov) inversion. The method avoids Fourier domain interpolation by using two coordinate transformations which allow the scattering data to be directly placed on to a rectangular grid in Fourier space. A number of extensions to the original backpropagation algorithm have been made [Devaney, 1983; Devaney, 1984; Devaney, 1985b; Devaney, 1985a; Devaney, 1986; Devaney, 1987; Devaney, 1989; Xue and Wei, 1987], but none of these explicitly uses the receiver geometry in Chapter 2 where ψ_{scat} is measured in the far-field at all angles around the object. Hence, a derivation of the backpropagation algorithm for receivers in the far-field follows.

Consider the inverse (2D) Fourier transform of (3.1)

$$\nu_b^2(\mathbf{x}) - 1 = \frac{1}{k^2(2\pi)^2} \iint_{\infty}^{\infty} \psi_{\text{scat}_\mathbf{f}}(\hat{\mathbf{x}}, k) e^{j\mathbf{u}\cdot\mathbf{x}} d^2\mathbf{u} \tag{3.3}$$

As already discussed, a diffraction tomography experiment measures the Fourier transform of the object on circles in Fourier space. These circles are mapped on to rectangular coordinates by introducing a change of variables:

$$\mathbf{u} = \mathbf{k}' = k(\hat{\mathbf{k}} - \hat{\mathbf{x}}) = k \begin{bmatrix} (\cos\phi_{\text{inc}} - \cos\phi_{\text{scat}}) \\ (\sin\phi_{\text{inc}} - \sin\phi_{\text{scat}}) \end{bmatrix} \tag{3.4}$$

so that

$$d^2\mathbf{u} = k^2 |\sin(\phi_{\text{inc}} - \phi_{\text{scat}})| d\phi_{\text{inc}} d\phi_{\text{scat}} \tag{3.5}$$

Before writing (3.3) in a new form, it is also necessary to introduce a rotated (ξ, η) coordinate system in image space, where

$$\mathbf{x} = \begin{bmatrix} -\xi \sin\phi_{\text{inc}} - \eta\cos\phi_{\text{inc}} \\ \xi\cos\phi_{\text{inc}} - \eta\sin\phi_{\text{inc}} \end{bmatrix} \tag{3.6}$$

This enables the dot product $\mathbf{u}\cdot\mathbf{x}$ to be written as

$$\sin(\phi_{\text{inc}} - \phi_{\text{scat}})\xi + [\cos(\phi_{\text{inc}} - \phi_{\text{scat}}) - 1]\eta \tag{3.7}$$

Now substituting (3.5) and (3.7) into (3.3) gives

$$\begin{aligned} \nu_b^2(\mathbf{x}) - 1 \;=\; & \frac{1}{2(2\pi)^2}\int_{-\pi}^{\pi} d\phi_{\text{inc}} \int_{-\pi}^{\pi} d\phi_{\text{scat}} |\sin(\phi_{\text{inc}} - \phi_{\text{scat}})| \psi_{\text{scat}_{\mathbf{f}}}(\phi_{\text{inc}} - \phi_{\text{scat}}, k)\cdot \\ & e^{jk[\sin(\phi_{\text{inc}}-\phi_{\text{scat}})\xi + [\cos(\phi_{\text{inc}}-\phi_{\text{scat}})-1]\eta]} \end{aligned} \tag{3.8}$$

where the extra $\frac{1}{2}$ comes from the double coverage of Fourier space by the ϕ_{inc}, ϕ_{scat} coordinate system. The remaining impediment to using the FFT is the integral with respect to ϕ_{scat}. This is overcome by introducing the (κ, γ) coordinate system, which is related to the $\mathbf{u} = (u, v)$ system by a rotation through $\phi_{\text{inc}} + \frac{\pi}{2}$ as illustrated in figure 3.1. The substitution is described by

$$\begin{aligned} \sin(\phi_{\text{inc}} - \phi_{\text{scat}}) &= \kappa/k \\ \Rightarrow \cos(\phi_{\text{inc}} - \phi_{\text{scat}}) &= \sqrt{k^2 - \kappa^2}/k \end{aligned} \tag{3.9}$$

where $-k \le \kappa \le k$, so that

$$d\phi_{\text{scat}} = d\kappa/\sqrt{k^2 - \kappa^2} \tag{3.10}$$

Note that for (3.9) to be a valid single valued substitution, $\phi_{\text{inc}} - \phi_{\text{scat}}$ must lie in the interval $[-\frac{\pi}{2}, \frac{\pi}{2}]$.

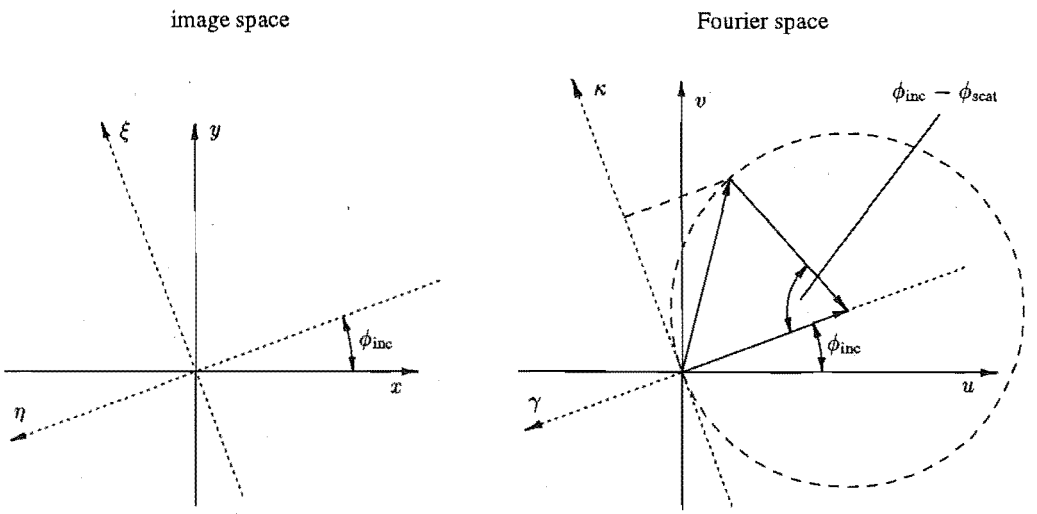

Figure 3.1 Geometry for backpropagation.

The relationship between the object and the scattering data can therefore be written as

$$\nu_b^2(\mathbf{x}) - 1 = \frac{1}{8k\pi^2} \int_{-\pi}^{\pi} d\phi_{\text{inc}} \int_{-k}^{k} d\kappa \frac{|\kappa|}{\sqrt{k^2 - \kappa^2}} \psi_{\phi_{\text{inc}}}(\kappa, k) e^{j[\kappa\xi + (\sqrt{k^2-\kappa^2} - k)\eta]} \tag{3.11}$$

where $\psi_{\phi_{\text{inc}}}(\kappa, k)$ denotes the scattered field, $\psi_{\text{scat}_\mathbf{f}}(\hat{\mathbf{x}}, k)$, due to a planar incident field in the ϕ_{inc} direction, with κ and $\hat{\mathbf{x}}$ being related by (3.4) and (3.9). Finally, the implementation of (3.11) is more apparent if it is written as

$$\nu_b^2(x, y) - 1 = \frac{1}{8k\pi^2} \int_{-\pi}^{\pi} d\phi_{\text{inc}} \Pi_{\phi_{\text{inc}}}(x \sin\phi_{\text{inc}} - y \cos\phi_{\text{inc}}, x \cos\phi_{\text{inc}} + y \sin\phi_{\text{inc}}) \tag{3.12}$$

where

$$\Pi_{\phi_{\text{inc}}}(\xi, \eta) = \int_{-k}^{k} d\kappa \frac{|\kappa|}{\sqrt{k^2 - \kappa^2}} \psi_{\phi_{\text{inc}}}(\kappa, k) e^{j(\sqrt{k^2-\kappa^2} - k)\eta} e^{j\kappa\xi} \tag{3.13}$$

Before considering the implementation of (3.11) further, it is important to mention a significant difference between (3.3) and (3.11). Any value of κ corresponds to two points on the circle in Fourier space, and so, to avoid ambiguity, only scattering data in the forward direction can be used, i.e. $|\phi_{\text{inc}} - \phi_{\text{scat}}| \leq \frac{\pi}{2}$. Following (3.2), because $|\kappa| \leq k$, the spatial resolution of the backpropagated image is

$$\Delta x \leq \frac{2\pi}{k} = \lambda \tag{3.14}$$

or half that of the Fourier interpolated image. This difference in resolution does not occur with the 'standard' CT configuration where receivers are placed along a line, because scattering data is available in only the forward direction and so the potential resolution of all reconstruction algorithms is λ.

3.1.3 Implementation

Fourier interpolation, backpropagation and the exact method for performing Born inversion were all implemented to ensure that the most efficient method was chosen for the analysis in subsection 3.1.7. The exact and Fourier domain interpolation methods are similar and begin by determining ϕ_{inc} and ϕ_{scat} for each pixel in the image. Any pixel can actually fall on two circles so, to avoid ambiguity, $\phi_{\text{inc}} - \phi_{\text{scat}}$ was limited to the range [0,π]. When using the exact method, given ϕ_{inc} and ϕ_{scat}, $\psi_{\text{scat}_\mathbf{f}}(\phi_{\text{inc}} - \phi_{\text{scat}}, k)$ was calculated for each pixel. Alternatively, when using Fourier interpolation, $\psi_{\text{scat}_\mathbf{f}}(\phi_{\text{inc}} - \phi_{\text{scat}}, k)$ was calculated for a number of values of ϕ_{inc} and ϕ_{scat}. The correct $\psi_{\text{scat}_\mathbf{f}}$ for each pixel was then estimated by bilinear interpolation between the closest known values of $\psi_{\text{scat}_\mathbf{f}}(\phi_{\text{inc}} - \phi_{\text{scat}}, k)$. Having determined the field corresponding to each pixel in the image, the refractive index distribution was obtained by taking the IFFT of the image, dividing by k^2, adding unity and taking the magnitude of the square root (see (3.1)). Since $\nu_b(\mathbf{x})$ is real, it can be argued that one should take the real part of the square root. However, most of the reconstructions shown in this chapter have significant detail in their imaginary parts, so that their magnitudes were found to be closer to the true object.

The computational procedure used to reconstruct an $N \times N$ image using backpropagation, i.e. (3.13) and (3.12), can be presented in the form of the following steps.

1. For a given ϕ_{inc}, $\psi_{\text{scat}_{\text{ff}}}(\sin(\phi_{\text{inc}} - \phi_{\text{scat}}), k)$ was determined at N equi-spaced values of $\sin(\phi_{\text{inc}} - \phi_{\text{scat}})$ with $\phi_{\text{inc}} - \phi_{\text{scat}}$ in the range $[-\frac{\pi}{2}, \frac{\pi}{2}]$.

2. In accordance with (3.13), the data, $\psi_{\text{scat}_{\text{ff}}}(\kappa, k)$, were multiplied by a separate filter
$$\frac{|\kappa|}{\sqrt{k^2 - \kappa^2}} e^{j(\sqrt{k^2-\kappa^2}-k)\eta}$$
for each depth, η, in the image. $\sqrt{2}N$ depths were required to avoid loss of spatial resolution [Crawford and Kak, 1979].

3. Each one dimensional filtered projection was then windowed, zero-padded and Fourier transformed. A Hamming window [Harris, 1978] was found to be adequate to reduce 'ringing' at cylinder edges. Zero-padding the projection data to be $2N$ samples long was required to allow the filter in step 2 to be implemented in Fourier space. This is because using the IFFT makes the filtering efficient, but multiplication in Fourier space corresponds to circular convolution [Slaney and Kak, 1985]. Zero-padding ensures that circular convolution is equivalent to the desired aperiodic convolution. It also reduces the interpolation error.

4. The bilinearly interpolated value of the Fourier transformed filtered projection was allocated to each pixel, (x, y), in the image in accordance with (3.12).

5. Steps 1-4 were repeated for 100 equi-spaced ϕ_{inc}. As a new projection was taken up, its contribution was added to the current sum at pixel (x, y).

For the reconstructions shown in this chapter, both interpolation methods used 100 equi-spaced intervals of ϕ_{inc} in the range [0,2π]. When comparing Fourier interpolation to backpropagation, 64 receivers (or equivalently, values of ϕ_{scat}) were used. For subsequent reconstructions, however, 360 receivers were used. This improved the reconstruction accuracy for a negligible increase in computation. All reconstructions were normalized, and unless otherwise indicated, cover the range of x and y from -8λ to 8λ.

3.1.4 Backpropagation vs frequency domain interpolation

Three different Born inversion methods have been described. Expending the computational effort associated with the exact method is unnecessary because, as illustrated in table 3.1 and in figures 3.2(a), (b) and (c), when a sufficient number of view angles and

Born inversion method	N_{Rx}	RMS error
backpropagation	64	0.3%
Fourier interpolation	64	0.1%
Fourier interpolation	360	$< 5 \times 10^{-4}$%

Table 3.1 Root mean square (RMS) error in reconstructing a cylinder using three interpolation schemes. Error is relative to the exact reconstruction. The second column gives the number of receivers used.

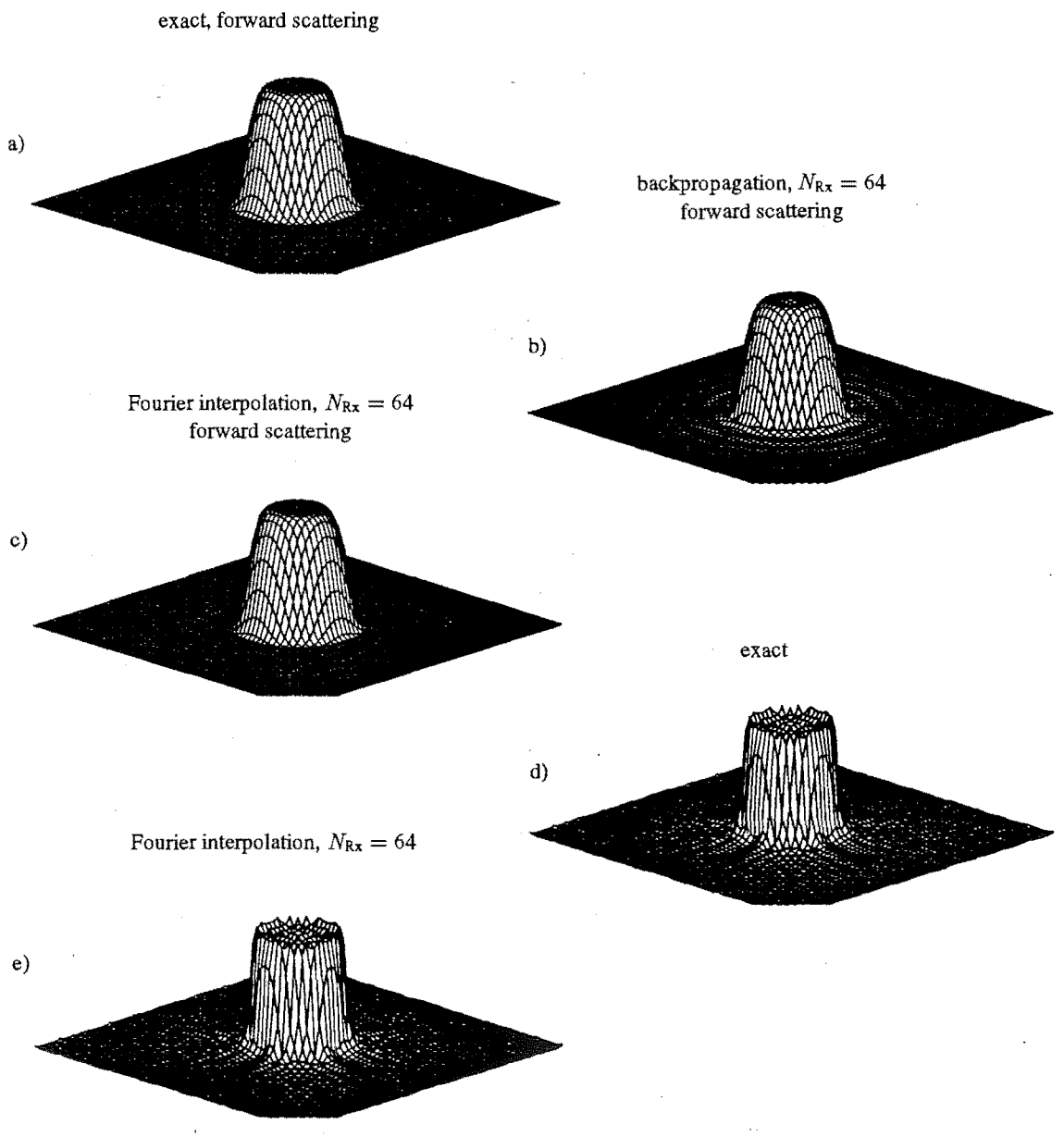

Figure 3.2 Reconstruction accuracy of various methods of Born inversion. The object is a single cylinder of diameter 4λ, refractive index 1.005, and centered on the origin. The reconstructions in (a), (b) and (c) use ψ_{scat} in the forward direction, a Hamming window and respectively, exact, backpropagation, and Fourier interpolation reconstructions. (d) and (e) show unfiltered exact and Fourier interpolation reconstructions respectively. N_{Rx} is the number of receivers used.

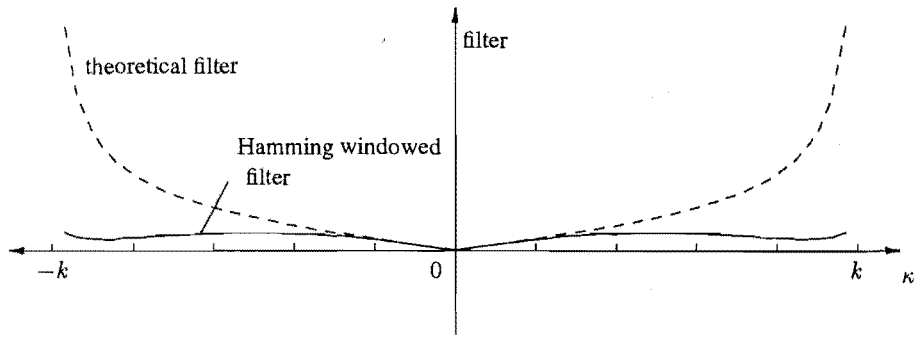

Figure 3.3 Ideal and practical backpropagation filters for receivers in the far-field.

receivers are used, all three methods give essentially the same result. Note that the data has been Hamming windowed in all of these subfigures to reduce the interpolation errors in (b). As already mentioned, when ψ_{scat} is available in only the forward direction, backpropagation and Fourier interpolation are theoretically identical. Previous researchers, who used receivers on a line, concluded that although reconstruction accuracies were similar, Fourier interpolation was preferable because it involved less computation [Pan and Kak, 1983; Slaney and Kak, 1985; Soumekh *et al.*, 1983]. The situation considered here, where complete far-field scattering data is available, is different because Fourier interpolation has twice the potential resolution of backpropagation. This difference in resolution is illustrated in figure 3.2. In practice, the potential resolution of Fourier interpolation is more than double that of backpropagation because the high frequency emphasis of the backpropagation filter

$$|\kappa|/\sqrt{k^2-\kappa^2} \tag{3.15}$$

serves to magnify any interpolation errors close to cylinder edges. Thus, the data must be windowed (i.e. low pass filtered), which further reduces the resolution of the backpropagated image. The windowing can also be thought of as introducing the less noisy version of the ideal backpropagation filter shown in figure 3.3.

As already mentioned, a significant limitation of backpropagation is the computation involved. For the 64×64 pixel reconstructions shown in figure 3.2, 64 receivers were used, but the projection data was zero-padded to 128 samples. As 91 depths, η, were also used, the processing for each of the 100 view angles involved 91 128-point IFFTs. In contrast, Fourier domain interpolation required 128 64-point IFFTs. Given the $N \log_2 N$ computational cost of an IFFT, backpropagation was 166 times more computationally expensive than Fourier interpolation. However, remember that this is only the cost of the solution to the inverse problem. Calculation of the direct problem is also a major cost in the overall problem considered here, and this cost could affect the choice of reconstruction procedure. For instance, if backpropagation could obtain the same accuracy as Fourier interpolation with fewer view angles (i.e. fewer solutions of the direct problem), then this would offset the higher cost of the inverse procedure. However, table 3.1 indicates that for high quality reconstructions with the receivers in the far-field, Fourier interpolation is slightly more accurate than backpropagation for a given number of receivers. To compound the differences between the two methods,

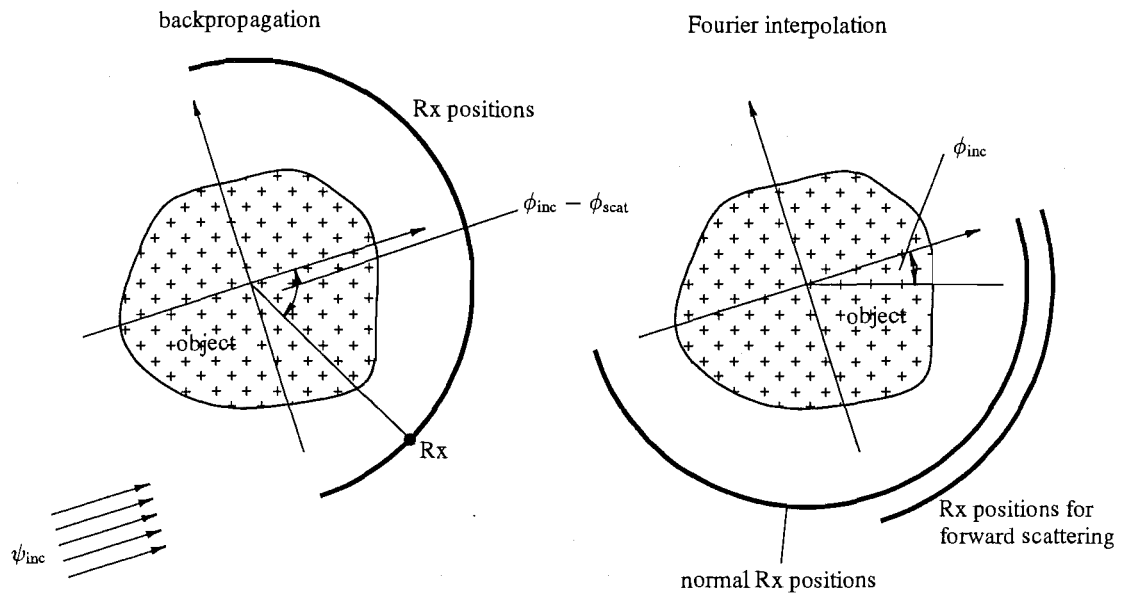

Figure 3.4 Receiver (Rx) array positions for backpropagation and Fourier interpolation.

the backpropagation reconstruction in figure 3.2(b) required more CPU time than the equivalent exact reconstruction in the same figure.

Note that the comparison is made using ψ_{scat} in only the forward direction and after windowing. This ensures that the resolution of Fourier interpolation is reduced to that of backpropagation, but results in greater angular density of receivers for Fourier interpolation. The effect is illustated in figure 3.4 where receivers are equi-spaced in the intervals $\phi_{inc} - \phi_{scat} \in [0, \frac{\pi}{2}]$ and $\phi_{inc} - \phi_{scat} \in [-\frac{\pi}{2}, \frac{\pi}{2}]$, respectively, for Fourier interpolation and backpropagation. The difference in receiver spacing will contribute to the slight difference in accuracy of the two methods. Part of the reduced accuracy of backpropagation can also be attributed to the high frequency emphasis of the backpropagation filter (3.15) associated with receivers in the far-field. This emphasis has resulted in greater interpolation errors than those that occur in the 'standard' CT geometry where receivers are placed along a line [Slaney and Kak, 1985].

The above comments apply to high quality reconstructions in the simulation situation with receivers in the far-field. Fewer receivers, noisy data and alternative receiver geometries were not considered. It is worth remarking that when data are limited, the interpolation error of both methods can be reduced by zero-padding, although this process is much more expensive in the backpropagation context [Slaney and Kak, 1985]. On the other hand, the degradation caused by limited data is much more severe when using Fourier interpolation, particularly when using multi-component objects, since (as shown in Chapter 2) the angular variation of ψ_{scat} is greater. Fortunately, in the simulation situation, Fourier interpolation can be improved for negligible additional computational cost by using more receivers.

Given the prohibitive computational cost and reduced resolution of backpropagation, all further reconstructions were obtained using Fourier interpolation with 100 view angles and 360 receivers. This strategy appeared to give accurate reconstructions in all cases.

3.1.5 Multiple scattering in Born inversion

Having selected a method for Born inversion, attention is now directed towards the effects of multiple scattering. Some examples of Born inversion are provided in figure 3.5 for multi-cylinder objects. In (a) the two cylinders in the object are clearly visible. However, more importantly, multiple scattering is causing appreciable distortion even though the cylinders have refractive indices only 1% higher than the background refractive index. (b) and (c) illustrate the well known increase in distortion with increase in refractive index. Note that a similar increase in distortion occurs when increasing the frequency of ψ_{inc} or the size of the cylinders. While the effects of multiple scattering are perhaps better illustrated in figures 3.6 and 3.7, figures 3.5(d) and (e) consider non-uniform cylinder sizes and refractive indices. In both instances multiple scattering results in irregularly raised cylinder boundaries. This form of distortion does not appear to have been demonstrated before. Finally, (f) illustrates that recognizable reconstructions are still possible even when the Born approximation is markedly invalid. For instance, the Born approximation replaces $\psi(\mathbf{x} \in \Upsilon_-, k)$ by $\psi_{\text{inc}}(\mathbf{x} \in \Upsilon_-, k)$, yet the maximum distance between wavefronts of ψ and ψ_{inc}, $\mathcal{L}_{\text{max}}$, is 1.75λ, implying that in some parts of the object ψ_{inc} is a very bad approximation to ψ. Certainly, the object is harder to recognize in (c) where the cylinders are still centered on a line and $\mathcal{L}_{\text{max}}$ is only 1.2. It is therefore apparent, as predicted in Chapter 2, that the accuracy of the Born approximation is highly dependent on the object geometry. Much of this dependence is due to the effects of multiple scattering.

Born inversion of single cylinder objects has been extensively investigated [Duchêne *et al.*, 1985; Paoloni, 1986; Slaney *et al.*, 1984]. However, accurate reconstructions of multi-cylinder objects, such as those in figure 3.5, do not appear to have been published before. This is probably due to the practical, if not analytical complication of the associated direct problem (see section 2.2). Instead, workers have ignored multiple scattering effects completely in determining $\psi_{\text{scat}_{\mathbf{f}}}(\mathbf{x}, k)$, or have considered only first order effects [Azimi and Kak, 1983]. The effect that this has on the reconstruction is illustrated in figures 3.6 and 3.7, where multiple scattering is neglected in (a) and (d), only first order effects are considered in (b) and (e), and (c) and (f) show exact reconstructions (exact, that is, to the accuracy of the Born approximation). It is clear that multiple scattering causes significant distortion although the refractive indices of the cylinders are only 3% higher than the background refractive index. Having identified (from figure 3.6) the form of the distortion due to multiple scattering, reference to figures 3.5(a), (b) and (c) reveals the rapid increase in the severity of this distortion with increasing refractive index. In addition, comparison of figures 3.6 and 3.7 shows that, although multiple scattering definitely still occurs when cylinders are small relative to their separation, it causes less distortion in Born inversion. This is the reason that the exact reconstruction in figure 3.7 is better than those in figure 3.6 although, for the three subfigures, $\mathcal{L}_{\text{max}}$ is greatest in figure 3.7.

While some of the effects of object geometry on multiple scattering have been set out in section 2.5, it is appropriate to make some points in the light of results from figures 3.5-3.7.

1. Multiple scattering causes very marked degradation of Born inversion if the object components are large relative to their separation. What is not well known is that

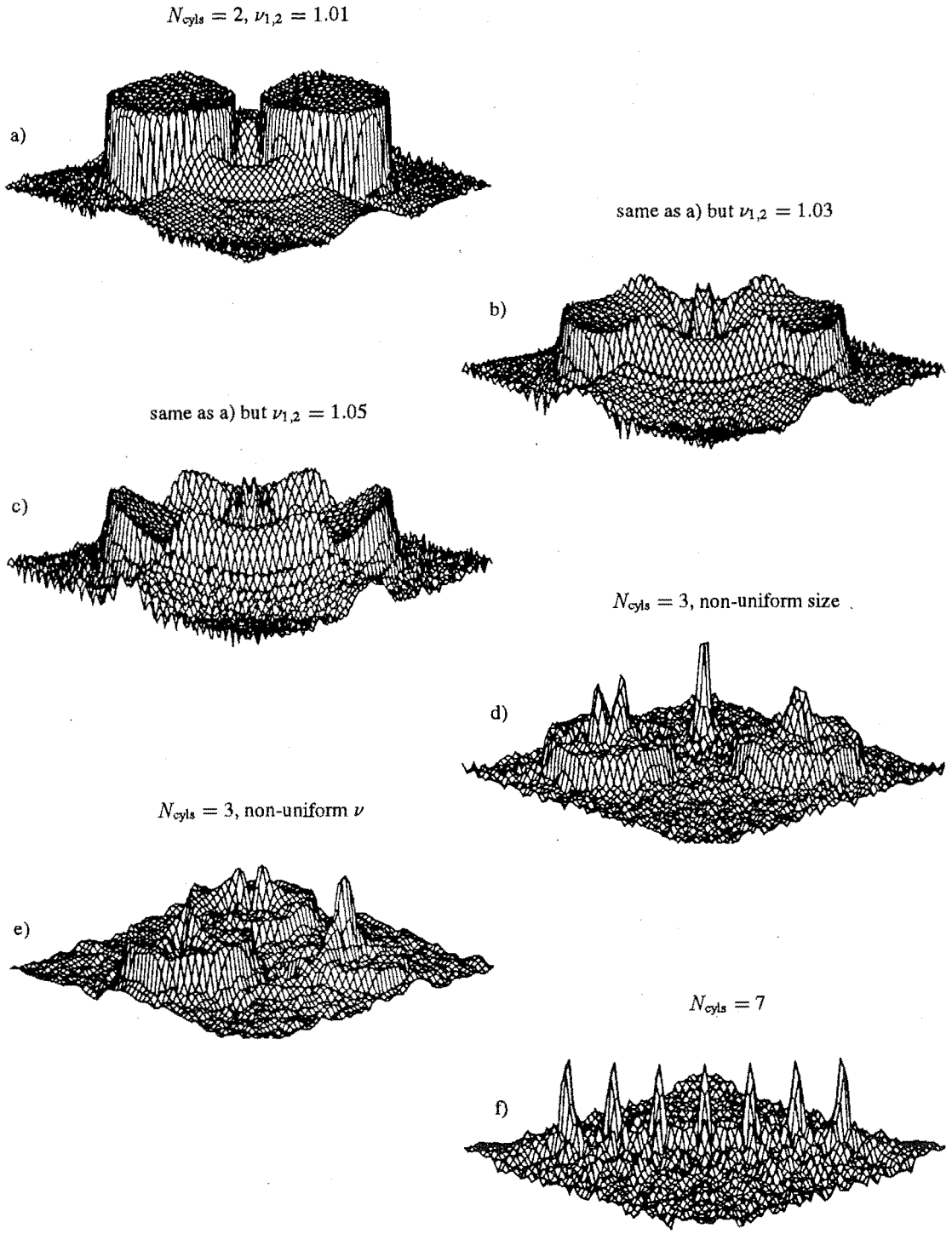

Figure 3.5 Illustration of Born inversion for multi-cylinder objects. Using notation from figure 2.1, (a), (b) and (c) all have $\mathbf{x}_1 = (-5\lambda, -5\lambda)$, $\mathbf{x}_2 = (5\lambda, 5\lambda)$, $2r_{1,2} = 12\lambda$, and $\nu_{1,2} = 1.01$, 1.03 and 1.05 respectively. (d) is described by $\mathbf{x}_1 = (-3\lambda, 3\lambda)$, $\mathbf{x}_2 = (-3\lambda, -3\lambda)$, $\mathbf{x}_3 = (3\lambda, 3\lambda)$, $2r_1 = 0.5\lambda$, $2r_{2,3} = 6\lambda$, $\nu_1 = 1.015$, and $\nu_{2,3} = 1.01$. (e) is described by $\mathbf{x}_1 = (-3\lambda, 3\lambda)$, $\mathbf{x}_2 = (0, -4\lambda)$, $\mathbf{x}_3 = (4\lambda, 2\lambda)$, $2r_{1,2,3} = 6\lambda$, $\nu_1 = 1.02$, $\nu_2 = 1.03$, and $\nu_3 = 1.01$. Finally, (f) is described by $\mathbf{x}_{1,2} = (\pm 4.5\lambda, \pm 4.5\lambda)$, $\mathbf{x}_{3,4} = (\pm 3\lambda, \pm 3\lambda)$, $\mathbf{x}_{5,6} = (\pm 1.5\lambda, \pm 1.5\lambda)$, $\mathbf{x}_7 = (0, 0)$, $2r_{1,2,3,4,5,6,7} = 0.5\lambda$, and $\nu_{1,2,3,4,5,6,7} = 1.5$. $\mathcal{L}_{max}$ is respectively 0.24λ, 0.72λ, 1.2λ, 0.12λ, 0.3λ, and 1.75λ. (a), (b) and (c) have range $\pm 16\lambda$. All reconstructions use Fourier interpolation, 100 views, and 360 receivers.

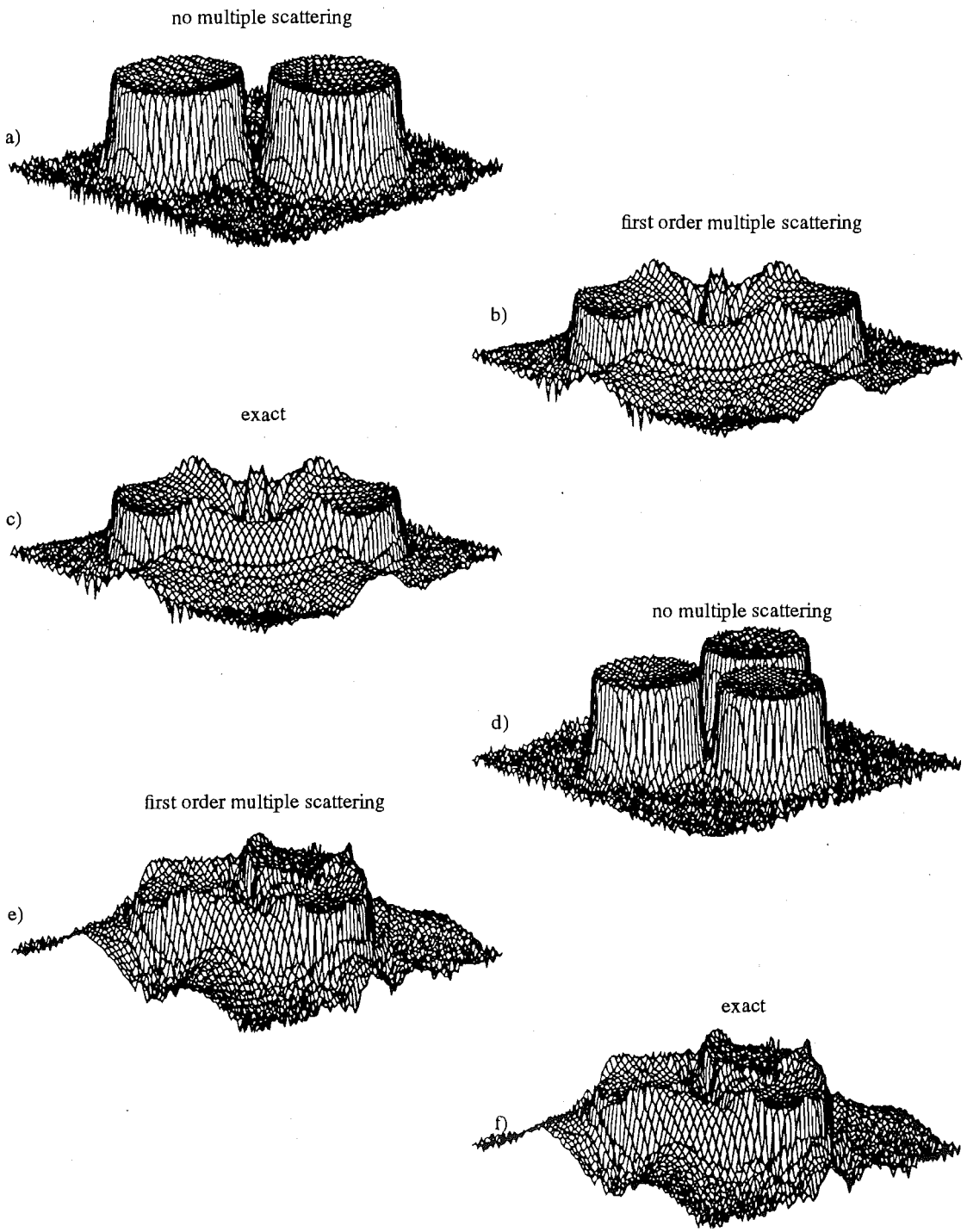

Figure 3.6 Illustration of the effects of multiple scattering on Born inversion. Reconstructions in (a) and (d) have no multiple scattering included in the calculation of $\psi_{\text{scat}_\mathbf{f}}(\mathbf{x}, k)$, those in (b) and (e) include only first order effects, and those in (c) and (f) are exact. (a), (b) and (c) all have $\mathbf{x}_1 = (-5\lambda, -5\lambda)$, $\mathbf{x}_2 = (5\lambda, 5\lambda), 2r_{1,2} = 12\lambda$, and $\nu_{1,2} = 1.03$. (d), (e) and (f) all have $\mathbf{x}_1 = (-2\lambda, 7\lambda), \mathbf{x}_2 = (-3\lambda, -6\lambda)$, $\mathbf{x}_3 = (7\lambda, 0), 2r_{1,2,3} = 12\lambda$, and $\nu_{1,2,3} = 1.03$. All subfigures have range $\pm 16\lambda$ and $\mathcal{L}_{\max} = 0.72\lambda$.

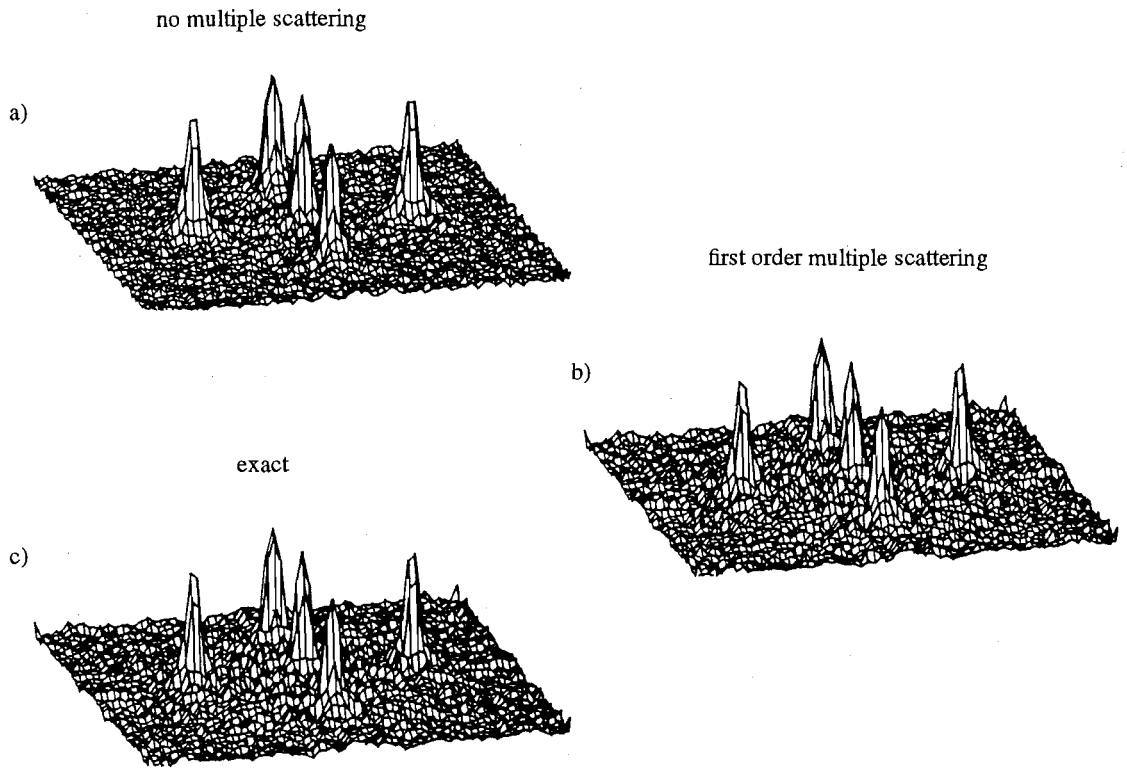

Figure 3.7 Illustration of the effects of multiple scattering on Born inversion. (a) has no multiple scattering included in the calculation of $\psi_{\text{scat}_\mathbf{f}}(\mathbf{x}, k)$, (b) includes only first order effects, and (c) is exact. Using notation from figure 2.1, (a), (b) and (c) all have $\mathbf{x}_1 = (-4\lambda, 0)$, $\mathbf{x}_2 = (0, -4\lambda)$, $\mathbf{x}_3 = (0, 0)$, $\mathbf{x}_4 = (0, 4\lambda)$, $\mathbf{x}_5 = (4\lambda, 0)$, $2r_{1,2,3,4,5} = 0.5\lambda$, and $\nu_{1,2,3,4,5} = 1.5$. $\mathcal{L}_{\max}$=0.75λ.

this degradation occurs even if the objects have refractive indices that are only slightly different (i.e. <5%) from that of the background and $\mathcal{L}_{\max}$ is small enough that Born inversion could be expected to give good results.

2. Although multiple scattering still occurs, it causes less distortion in Born inversion if the object components are small relative to the distance between them. This is true even if the components are strongly scattering, although the opposite is commonly believed [Minard, 1985].

3. The form of distortion caused by multiple scattering depends on the size, shape, location and refractive index of the object components.

Remember that the difference between the subfigures within figures 3.6 and 3.7 is in how the direct problem is solved, and not in the Born inversion process. For instance, in the two cylinder object where first order multiple scattering is considered, the field incident on each cylinder is the sum of ψ_{inc} and the scattered field from the other cylinder due to ψ_{inc} (see figure 2.2). This does not give the true scattered field, but the similarity of figures 3.6(b) and (e) to (c) and (f), and figure 3.7(b) to (c), demonstrates that including first order scattering gives a good approximation to the true field. The marked change in reconstructions where multiple scattering is ignored demonstrates that at least first

order effects must be considered in solving the direct problem, if results are to be at all realistic. For the same reason, it is apparent that if the effects of multiple scattering could be reduced, then a significant improvement in the reconstruction of $\nu(\mathbf{x})$ would result.

One method proposed to both reject the effects of multiple scattering and to reduce the distortion inherent in Born inversion, is Shift-and-add (SAA), as developed at Canterbury by the Bates group [Bates and Minard, 1984; Bates and Minard, 1983; Bates and Robinson, 1981; Minard, 1985; Minard *et al.*, 1985; Robinson, 1982; Tan, 1988].

3.1.6 Compensating for distortion in Born inversion

Shift-and-add is a method of deconvolution applicable when an ensemble of differently distorted images are available [Bates and Cady, 1980; Davey, 1989]. The technique was first used to remove the distorting effects of the atmosphere on astronomical images produced by large telescopes [Bates and Cady, 1980; Bates, 1982]. Apart from its very successful application to astronomical speckle imaging, SAA has also been successfully applied to speech processing [Brieseman *et al.*, 1987], ultrasonic CT imaging [Minard *et al.*, 1985] and ultrasonic B-scan imaging [Bates and Robinson, 1981; Bates and Robinson, 1982]. It is the promising results obtained in the ultrasonic imaging applications of SAA which suggested the approach investigated here.

The essential idea of SAA is that the distortion of an image is likely to be least where the image is 'brightest', i.e. the magnitude is greatest. Therefore, if all pixels in an image are referenced to the brightest pixel and a number of independently distorted images superimposed, then the image detail can be expected to sum coherently. Of course, the distortion in each image is also superimposed, but since the images are complex and assuming that these distortions are statistically independent, then they will sum incoherently. Thus, SAA processing can be expected to increase the contrast between desired and unwanted image detail (where the above assumptions are justified). Alternative processing strategies which also use ensembles of images are available, but SAA has the distinction of being the simplest and least noise sensitive [Minard, 1985].

It seems appropriate to base the SAA processing scheme used here on the one found to be successful in previous ultrasonic applications where SAA processing has involved: (a) forming a number of different images of the object using conventional B-scan, but with different frequencies of ψ_{inc}; (b) finding the pixel with largest magnitude and shifting the image (without rotation) so that this pixel is in the center of the SAA image; (c) adjusting the phase of each image so that the phase of the pixel with largest magnitude is zero; and (d) coherently adding the images together and taking the magnitude of the result [Robinson and Bates, 1980; Robinson, 1982]. Ultrasonic images formed at different frequencies have been found to be sufficiently independent that this processing scheme gives significantly improved images of one and two dimensional wire targets [Minard *et al.*, 1985]. It is, of course, important that the refractive index does not vary with frequency, and although this was assumed in section 1.2, it has been demonstrated in the medical imaging context [Paoloni, 1987].

The mathematical justification for SAA processing, in the context of multiple scattering (including reflection) and diffraction tomography, is not considered in detail here for reasons that will become apparent in section 3.1.8. The interested reader is referred

to Bates and Minard [1984] and Minard [1985]. The more intuitive reasoning can be (and has been) thought of as described below.

SAA has been experimentally demonstrated to reduce the effects of multiple scattering [Bates and Minard, 1984]. The reason for this is that rays describing multiple scattering typically have longer path lengths than those describing single scattering. The longer path lengths are more frequency dependent and so are more likely to destructively interfere when different frequencies are used. Since this argument can be expected to apply in the diffraction tomography context, SAA processing should reduce distortion caused by multiple scattering.

With regard to compensating for other forms of distortion in Born inversion, SAA has been demonstrated to perform ensemble deconvolution [Davey, 1989]. The image reconstructed by Born inversion can be expressed in the form

$$s_m(\mathbf{x}) = f(\mathbf{x}) \odot h_m(\mathbf{x}) + c_m(\mathbf{x}) \tag{3.16}$$

where $\odot$ denotes convolution; $f(\mathbf{x}) \odot h_m(\mathbf{x})$ is that part of the reconstructed image which can be represented by convolution of the ideal image, $f(\mathbf{x})$, with a distorting function, $h_m(\mathbf{x})$; $c_m(\mathbf{x})$ is called the contamination and represents the remaining image distortion. The subscript m denotes the member of the ensemble of images being considered. Provided that a reasonable part of the distortion associated with Born inversion can be modeled as a convolution of the ideal image with some unknown distorting function then, because SAA performs deconvolution, the image will be improved by SAA processing. While the validity of this assumption is critical to the success of SAA processing [Minard *et al.*, 1985; Davey, 1989], it has been virtually ignored by previous analyses showing that SAA and Born inversion may be capable of diffraction limited imaging. Considering the reconstruction differences shown in figure 3.6, where different frequencies are used but multiple scattering is ignored, the assumption is certainly highly questionable. The same conclusion can be drawn from the ultrasonic CT images of Minard *et al.* [1985] who consider a distorting medium placed between the object and the receivers. As the medium moves closer to the object, SAA processing becomes less effective due to the distortion becoming less well described by a convolution. The receiver and object geometry considered in section 3.1 can be considered an extreme case of a distorting medium close to the object, which suggests that SAA may be ineffective.

Thus, while no previous attempt appears to have been made to use SAA in the diffraction tomography context, the technique has certainly been proposed and theoretically justified as a worthwhile extension to diffraction tomography [Bates and Minard, 1984; Bates and Minard, 1983; Bates and Robinson, 1981; Minard, 1985; Minard *et al.*, 1985; Robinson, 1982; Tan, 1988].

3.1.7 Implementation

As mentioned in section 3.1.6, SAA requires an ensemble of independently distorted images. In previous ultrasonic CT and B-scan applications, reconstructed images with sufficiently independent distortion have been obtained by using different frequencies [Minard *et al.*, 1985; Bates and Robinson, 1981]. The same approach is adopted here with reconstructions of (complex) refractive index being made at a number of different frequencies. The SAA processing algorithm used in the ultrasonic CT and B-scan

applications has been described in section 3.1.6. However, the approach used here differs in that the reconstructed image is not translated to position the pixel with the largest magnitude in the center of the SAA image. This is because distortion in Born inversion can be seen (in figure 3.6) to reduce the quality of the reconstruction, but not to introduce translation as could be expected if the object was viewed through a distorting medium. Thus, the SAA processing used here involved: (a) adjusting the phase of each image so that the phase of a reference pixel was zero; (b) adding the ensemble of images together; and (c) taking the magnitude of the sum as the SAA image. It is also worth noting that the degree of distortion evident in reconstructions obtained using Born inversion, along with the apparent lack of a translation component to this distortion, makes it seem unlikely that the distortion can be predominantly described by a convolution.

SAA has been previously found to work well when there is a single 'bright' pixel in the image, which is presumably accurately reconstructed and to which all other pixels can be referred. Performing SAA on images without a suitable dominant reference will generate artefacts which result from using the wrong reference, although these can be reduced by subsequent processing. Unfortunately, in the diffraction tomography context, the brightest pixel in the image is not necessarily related to the highest refractive index because of the distortion introduced by multiple scattering. This point is clearly illustrated in figure 3.5(e), where the largest magnitude occurs on the boundary of the cylinder with the smallest refractive index. Distortion of this type is cause for some concern, as SAA relies on the brightest pixel being more accurately reconstructed than the rest of the image. This suggests that SAA is less than ideally suited for use with diffraction tomography, and in particular Born inversion, due to the type of error introduced by multiple scattering.

In an attempt to provide a more suitable reference, two alternative processing strategies were used to augment the investigation using 'standard' SAA. Previous investigations of SAA have used much more 'impulse-like' objects than those of interest here. For larger piecewise continuous objects, differential SAA, where the reference is located as the largest change in magnitude of each image, has been proposed to be more effective [Minard, 1985]. Thus, differential SAA was implemented here for the first time. Simple averaging was also tested, for although such a simple-minded processing scheme was unlikely to remove the effects of multiple scattering, it provided an idea of the noise suppression achievable by frequency diversity processing. So three processing schemes were investigated:

1. Averaging, which does not rely on finding a relatively undistorted reference. This most basic form of frequency diversity processing has been previously demonstrated to reduce background noise levels and improve object localization [Gehlbach and Sommer, 1987; Magnin *et al.*, 1982]. It can also be thought of as incoherent SAA in this instance.

2. SAA, where the phase of each individual image was adjusted to zero the phase of the brighest pixel.

3. Differential SAA, where the phase of each individual image was adjusted to zero the phase of the pixel where the largest magnitude change occured.

It is also necessary to consider the type of objects which might be more accurately reconstructed by SAA processing. SAA can be expected to cause destructive interference of unwanted image detail only if the difference in maximum path lengths, at the minimum and maximum frequencies used, is greater than $\lambda/2$, i.e.

$$\Delta\mathcal{L}_{\max} = \mathcal{L}_{\max}(k_{\max}) - \mathcal{L}_{\max}(k_{\min}) > \lambda/2$$

Since $\mathcal{L}$ is linearly related to frequency, if an octave bandwidth is used, i.e.

$$k_{\max} = 2k_{\min}$$

then $\mathcal{L}_{\max}$ must be greater than $\lambda/2$ when $k = k_{\min} = 1$. However, remember that a small $\mathcal{L}_{\max}$ is one of the best indicators of the suitability of the Born approximation. Thus, SAA processing is likely to be useful only where the Born approximation is either invalid, or becoming invalid. In this context, it is worth commenting that if the Born approximation was accurate, then varying the frequency would provide no extra information. It is the frequency dependent distortion in Born inversion that allows SAA processing to be used. The frequency dependence of this distortion is illustrated by figures 3.8-3.11, (b) and (c). As mentioned previously, if a significant part of this distortion cannot be modeled as a convolution, then SAA processing may not improve the reconstruction.

The SAA frequency range used was an octave (i.e. $k_{\max} = 2k_{\min}$) which has previously been found to be wide enough to give good results, while allowing transducers to operate reasonably efficiently [Robinson and Bates, 1980]. The number of different frequencies used is a compromise between extra computation and potential improvement in image quality, but is required to be sufficiently large. There is, however, no point in using too many frequencies, because images formed at adjacent frequencies will no longer be sufficiently independent. One hundred different frequencies were used here as this number has been found to be adequate [Robinson and Bates, 1980]. Results of applying SAA processing to 100 reconstructions obtained by Born inversion at equi-spaced intervals of k in the range [1,2] are shown in figures 3.8-3.11. Images are labeled to describe the processing involved in their formation. Figure 3.8 shows reconstructions of an object containing two cylinders which are apparent in all figures. This simple object was chosen to give a clear example of the effects of SAA processing. The lack of improvement in the reconstruction could be attributed to the lack of a 'bright' reference pixel which has been available in most previous successful applications of SAA. Hence, the object reconstructed in figure 3.9 is the same as that in figure 3.8, but with the addition of a small cylinder of high refractive index to act as a SAA reference. Given the lack of success of SAA processing for the larger diameter cylinders in figures 3.8 and 3.9, figures 3.10 and 3.11 respectively show the application of SAA processing to smaller diameter cylinders with higher refractive index, and to small perfectly reflecting cylinders as have been used in previous successful SAA investigations [Minard *et al.*, 1985].

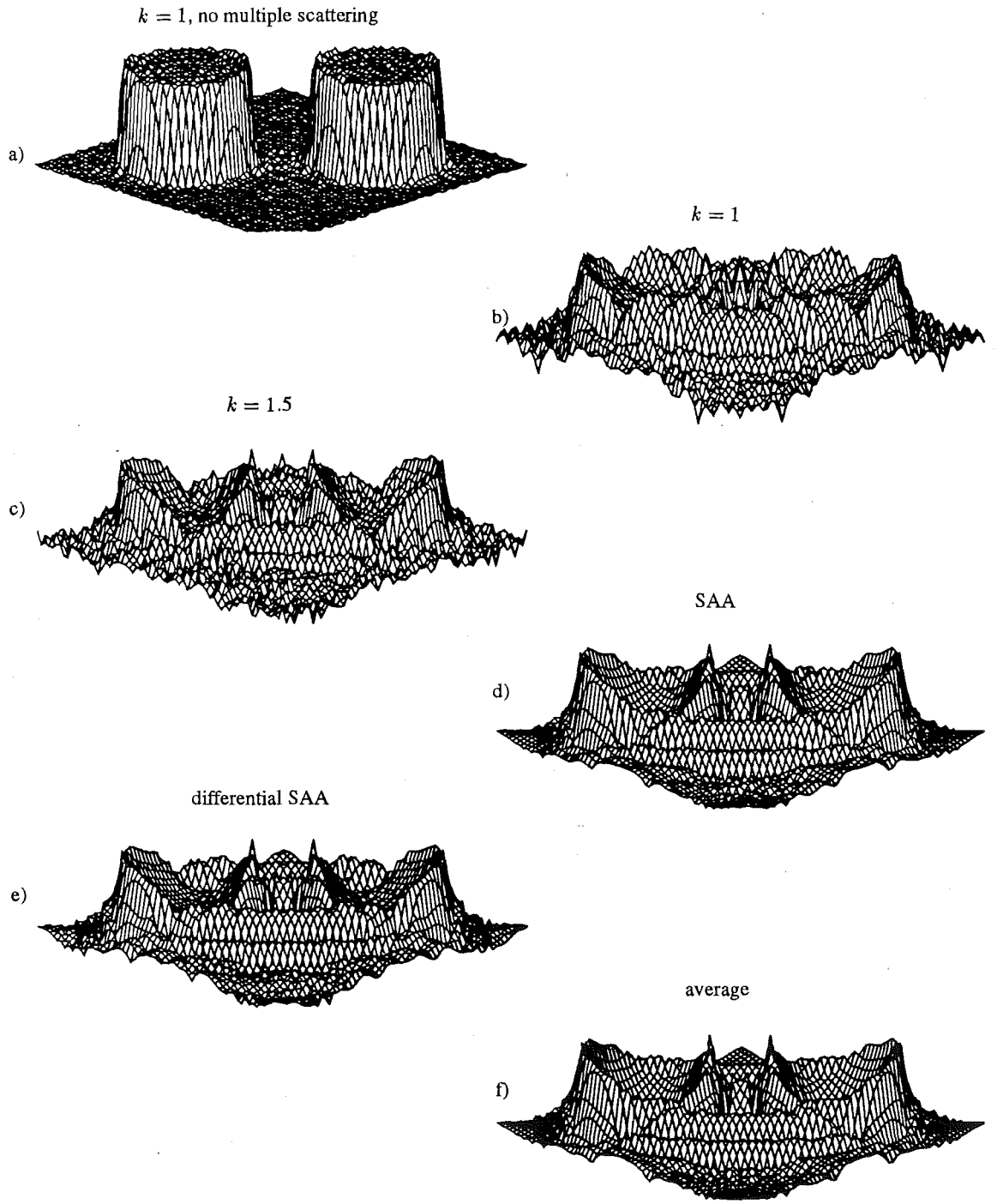

Figure 3.8 The effect of SAA processing on the reconstruction of ν by Born inversion. The object is described by $\mathbf{x}_1 = (-3, -3)$, $\mathbf{x}_2 = (3, 3)$, $2r_{1,2} = 6\lambda$, and $\nu_{1,2} = 1.1$. (a) shows an ideal reconstruction obtained when $\nu_{1,2} \approx 1$. Reconstructions in (b) and (c) were obtained by Born inversion at $k = 1$ and $k = 1.5$ respectively. Those in (d)-(f) were obtained by combining 100 images obtained for k equi-spaced in the range [1,2], as described in the text.

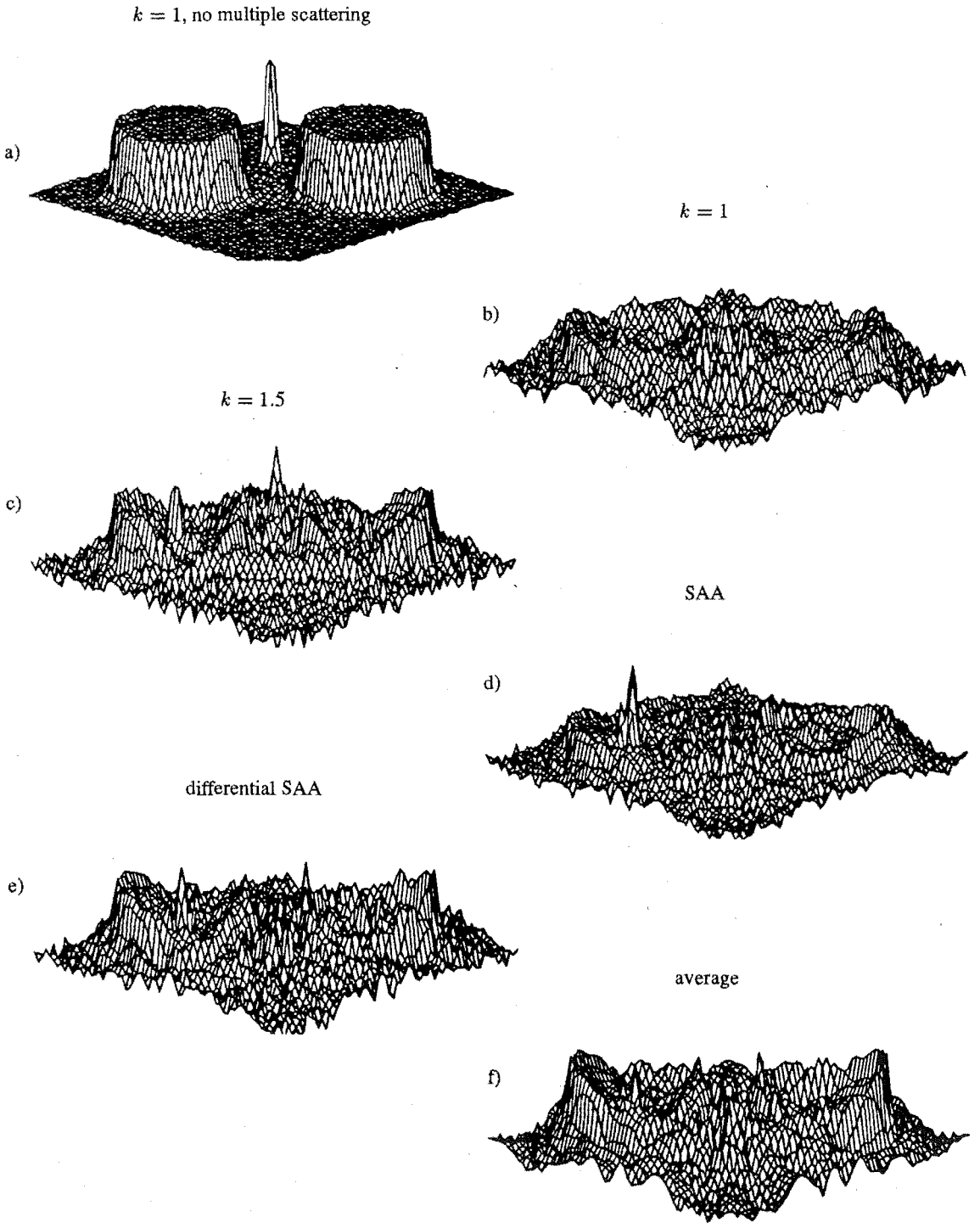

Figure 3.9 The effect of SAA processing on the reconstruction of ν by Born inversion. The object is described by $\mathbf{x}_1 = (-3,-3)$, $\mathbf{x}_2 = (3,3)$, $\mathbf{x}_3 = (-3,3)$, $2r_{1,2} = 6\lambda$, $2r_3 = 0.5\lambda$, $\nu_{1,2} = 1.1$, and $\nu_3 = 1.15$. Descriptions of subfigures are contained in the caption to figure 3.8.

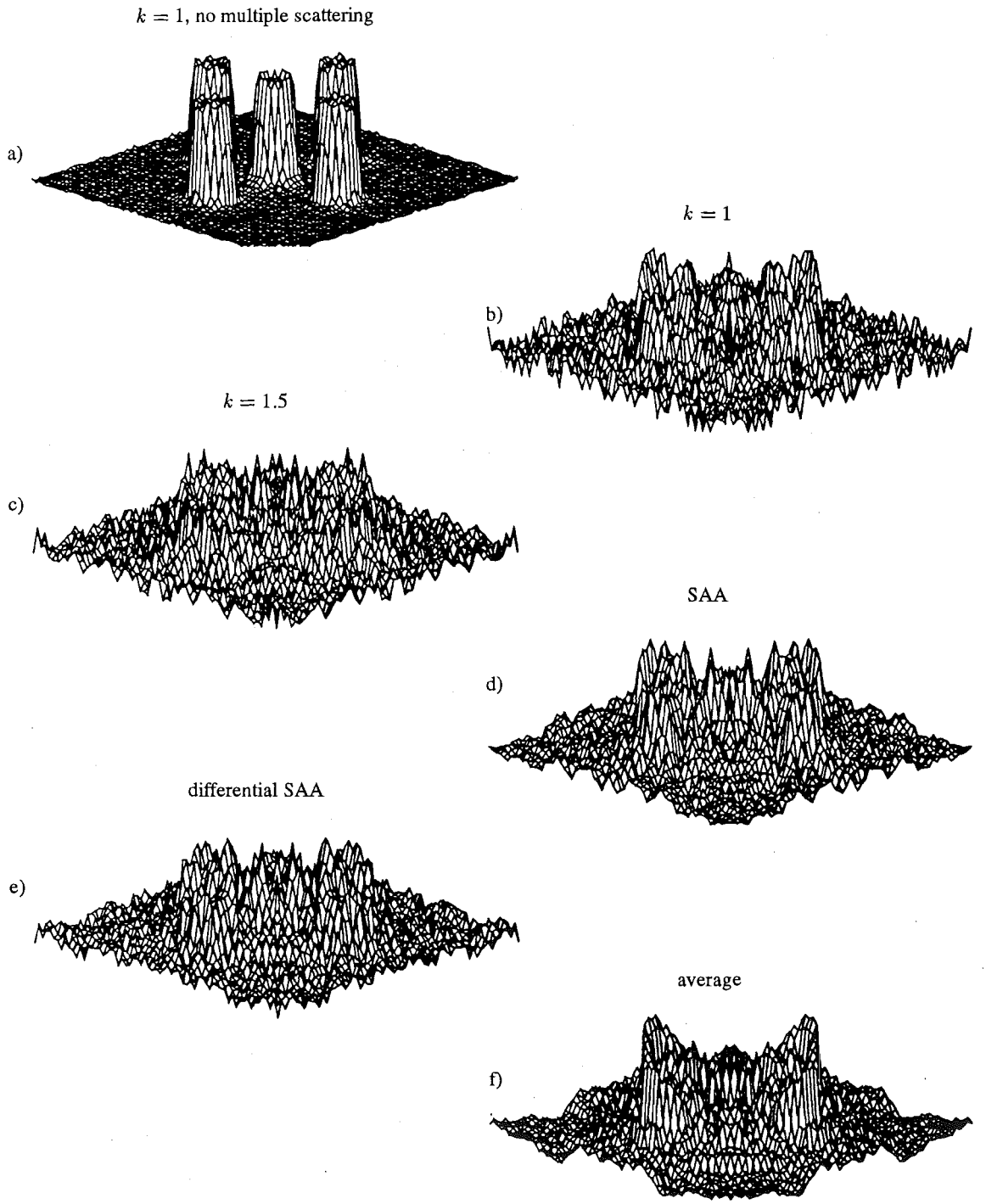

Figure 3.10 The effect of SAA processing on the reconstruction of ν by Born inversion. The object is described by $\mathbf{x}_1 = (-4, 0)$, $\mathbf{x}_2 = (0, -4)$, $\mathbf{x}_3 = (0, 4)$, $\mathbf{x}_4 = (0, 0)$, $\mathbf{x}_5 = (4, 0)$, $2r_{1,2,3,4,5} = 2\lambda$, and $\nu_{1,2} = 1.5$. Descriptions of subfigures are contained in the caption to figure 3.8.

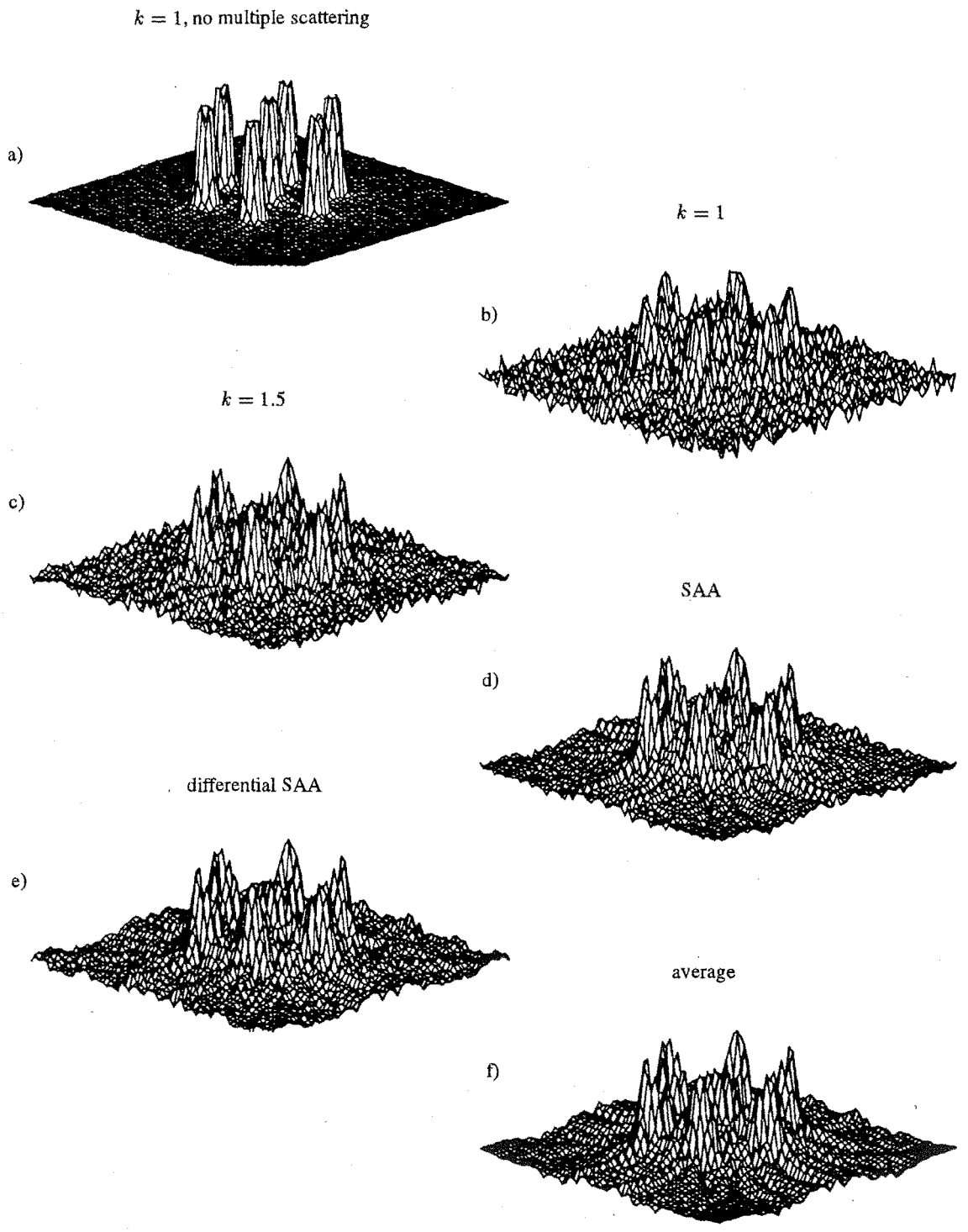

Figure 3.11 The effect of SAA processing on the reconstruction of ν by Born inversion. The object is described by $\mathbf{x}_1 = (-3,0)$, $\mathbf{x}_2 = (-1.5,2.6)$, $\mathbf{x}_3 = (-1.5,-2.6)$, $\mathbf{x}_4 = (0,0)$, $\mathbf{x}_5 = (1.5,2.6)$, $\mathbf{x}_6 = (1.5,-2.6)$, $\mathbf{x}_7 = (3,0)$, $2r_{1,2,3,4,5,6} = \lambda$, and all cylinders are totally reflecting. Descriptions of subfigures are contained in the caption to figure 3.8.

3.1.8 Discussion

Comparison of SAA'd reconstructions with those from standard Born inversion immediately reveals that SAA appears to be unable to compensate for distortion caused by the inaccuracy of the Born approximation. All of the results shown in figures 3.8-3.11 are similar in that the processed reconstructions are arguably better than the reconstruction for $k = 1$. Certainly the background 'noise' level is reduced and the object boundaries appear more defined, although the computational cost of this relatively minor improvement in image quality is considerable. This improvement has also been demonstrated experimentally, although the use of fewer frequencies made the results less obvious [Gehlbach and Sommer, 1987]. However, the failure of the SAA concept is evidenced by the average (no shift) reconstruction being optimum in all cases.

It is possible that SAA processing fails because the distortion is too severe. However, this explanation seems unlikely given that one of the strengths of SAA processing is its ability to handle high noise levels. In fact, in many applications of SAA the object form is completely indecipherable from images at single frequencies. It therefore appears that the supposition that distortion in Born inversion is not representable by a convolution is accurate. Evidence to support this statement can be summarized as:

1. The brightest pixel in the image is not necessarily related to the cylinder with the largest refractive index.

2. The distortion in Born inversion does not involve a shift in position, yet the form of the distortion changes markedly with frequency, even in the absence of multiple scattering.

3. Distortion in ultrasound CT imaging is not well modeled by a convolution unless the distorting medium lies between the object and the receivers, but closer to the receivers [Minard *et al.*, 1985].

The argument for the effectiveness of SAA in reducing multiple scattering relies on the greater path length, and thus susceptability to destructive interference, of the multiple scattering. It should therefore apply in the diffraction tomography context. However, SAA also relies on finding a suitable reference which is less distorted than the rest of the image. Since it appears that the distortion in Born inversion cannot be represented by a convolution, a suitable SAA reference is unavailable. This point is well illustrated by the 'brightest' pixel in figure 3.5(e).

With regard to obtaining a suitable SAA reference, differential SAA is no more successful than conventional SAA. However, diffraction tomography is unlikely to be a suitable context to test conventional means of ensemble image processing, since it appears that the distortion cannot be modeled by a convolution. It therefore provides an unsuitable situation to test differential SAA, which may work successfully in a different context.

Given that the refractive index is real, it could be argued that the most accurately reconstructed part of the image, and so the best part to use as a reference, is where the imaginary part is small and the real part is appreciable. Figure 3.12 shows the real and imaginary parts of the reconstruction in figure 3.8(b). It illustrates that where the imaginary part is smallest is certainly not where the magnitude is largest. Thus,

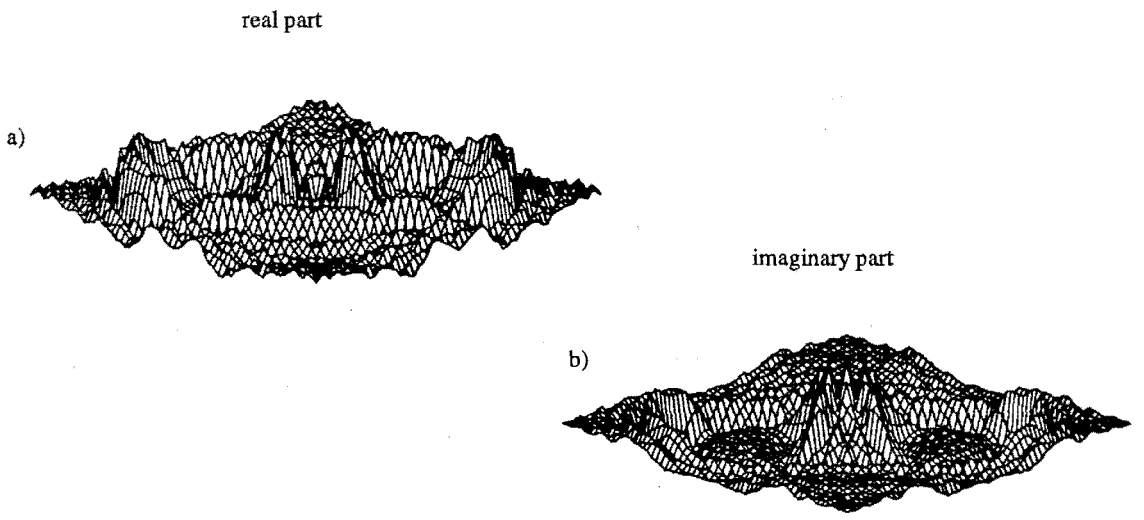

Figure 3.12 An indication of the suitability of the SAA reference. (a) and (b) are, respectively, the real part and the imaginary part of $\nu_b^2(\mathbf{x}) - 1$.

one might immediately consider attempting to use a point where the imaginary part is zero as a reference. However, this is exactly what the simple averaging shown in figures 3.8-3.11 is doing, because where the imaginary part is zero, the phase is zero, and so no phase shift is required. Thus, Born inversion appears unable to provide a suitable reference point for SAA.

The above investigation suggests that distortion in Born inversion is of a different form than can be handled by ensemble image processing techniques. It is therefore difficult to imagine how reconstructions obtained using a non-iterative (i.e. non-exact) formulation of diffraction might be improved by subsequent processing. Note that this comment applies to Rytov inversion, extensions to both Born and Rytov inversion, and all inverse methods based on explicit formulations of diffraction. When using such methods, the relative path length through the object can be well compensated, perhaps by a JWKB method which accounts for phase shift [Bates, 1988]. However, where there are multiple components (as will usually occur in practice) severe distortion can occur even if the deviation in refractive index from an average, or slowly varying background, is only very slight. This shortcoming of explicit diffraction tomography formulations indicates the importance of the bent-ray CT approach now developed.

3.2 Bent-Ray Computed Tomography (CT)

In a recent review of inverse scattering [Bates *et al.*, 1991] we conclude that there is a real need for the development of inverse scattering algorithms intermediate in accuracy between the exact and approximate solutions which currently exist. The former require large amounts of computation, while the latter assume that refraction can be completely, or partly, neglected. Therefore, the desired algorithm will need to be approximate, but take quantitative account of refraction. This section details such an algorithm which was initially proposed in Bates *et al.* [1991] and further developed in Enright *et al.* [1992].

The proposed algorithm is intended for media in which wave motion can be adequately characterized by the eikonal equation (2.22), the derivation, accuracy and applicability of which have been discussed in section 2.4. Reconstructions of the refractive index distribution are derived from travel-time measurements made of radiation passing through Υ_-, but do not assume that refraction is negligible. Solutions to this type of inverse problem, known as bent-ray CT, have previously been proposed, particularly in the context of ultrasonic transmission tomography and seismic tomography. Iterative approaches involving ray tracing immediately suggest themselves and have been developed [Berryman, 1990; Cha and Vest, 1981; Dines and Lytle, 1979a; Lytle and Dines, 1980; McKinnon and Bates, 1980; Schomberg, 1978]. Perturbation solutions that do not require ray tracing have also been proposed [Bates and McKinnon, 1979; Norton and Linzer, 1982], but these are limited by the assumption that the rays do not bend far from straight paths, i.e. the distribution contains only small variations in refractive index. The advantage of the method presented here is that rays are not assumed to be straight (or even almost straight), yet ray tracing is not required.

The bent-ray CT problem is outlined in section 3.2.1, and the proposed reconstruction algorithm described in sections 3.2.2 and 3.2.3. Section 3.2.4 presents the simplified form of this algorithm appropriate when the refractive index is circularly symmetric. Reconstructions of some circularly symmetric distributions are then presented in section 3.2.5 and these results discussed in section 3.2.6.

3.2.1 The bent-ray CT problem

In order to define what is here called the (2D) bent-ray CT problem, consider an emitter at Q and a receiver of the wave motion at the point Q', both on the circle of radius a shown in figure 3.13. Assume that a short enough pulse can be emitted such that the travel-time (or electrical path length)

$$S(Q',Q) = \int_Q^{Q'} \nu ds \tag{3.17}$$

can be measured to whatever accuracy is desired, where ds is the element of arc along the ray path (i.e. the dashed line in figure 3.13, as $P \to Q'$) from Q to Q'. Note that the accuracy with which $S(P,Q)$ can be determined in practice improves as the pulse is narrowed or as the bandwidth of the wave motion is increased. The bent-ray CT problem is then: given the refractive index, ν, at points on the boundary and $S(Q',Q)$ for pairs, (Q',Q), of receiver-emitter points, estimate ν for all points P contained within the circle of radius a.

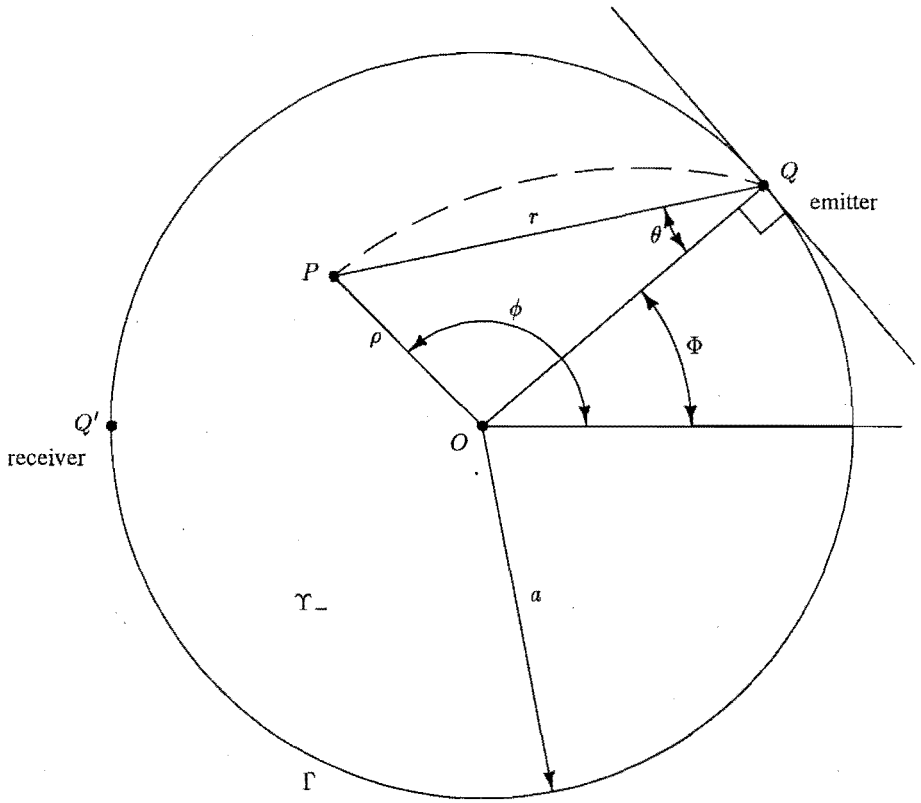

Figure 3.13 Coordinates and geometry for the bent-ray CT problem. Q is an emitter, Q' a receiver, and P an arbitrary point in Υ_-. The dashed line indicates the actual ray path, satisfying the eikonal, from Q to P, or *vice versa*. The circle of radius a, centered on O, is taken to be both Υ_{obs} and Υ_{inc}. Note the use of cylindrical polar coordinate systems.

The refractive index is assumed to vary sufficiently slowly that the electrical path length is related to the refractive index through the eikonal equation (see section 2.4)

$$\nabla_P S(P,Q) \cdot \nabla_P S(P,Q) = \nu^2(P) \tag{3.18}$$

where the subscript P on ∇ implies that the derivatives are to be taken at P. It is apparent that once $S(P,Q)$ is determined, $\nu(P)$ is immediately available as $|\nabla_P S(P,Q)|$. Professor Bates' insight, which led to the approach described below, was that it should be possible to determine $S(P,Q)$ directly, rather than through the computationally expensive process of ray tracing. The problem therefore reduces to one of determining $S(P,Q)$ for all P.

Writing the electrical path length of the ray from Q to P as

$$S = S(P,Q) = S(r;\theta,\rho;\phi) \tag{3.19}$$

emphasizes that the shape of the wavefronts at P depend, in general, on the location of P and Q. Consider the geometry, depicted in figure 3.14, of a particular $S(P,Q)$ with fixed emitter point Q, but P varying. If there are no caustics $S(P,Q)$ will be zero when $P = Q$, and continuous and positive for all other P. The same argument with P fixed

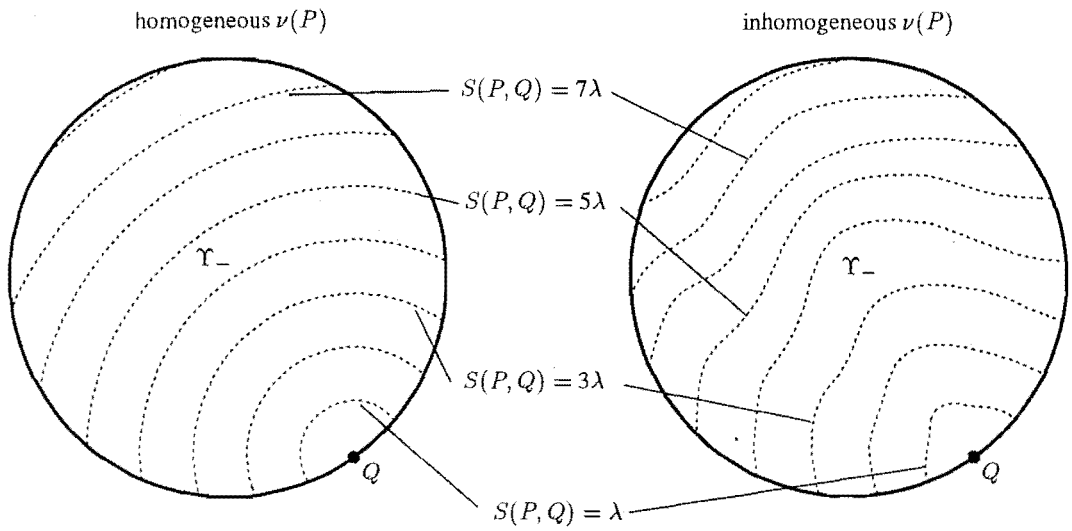

Figure 3.14 Behaviour of $S(P,Q)$, or equivalently, wavefronts of ψ_{inc} in Υ_-. Q is the fixed emitter position.

and Q varying shows that $S(P,Q)$ is continuous for all P and Q. $\nabla S(P,Q)$ is also continuous, provided $\nu(\mathbf{x})$ is continuous. The continuity of $S(P,Q)$ means that it can be accurately described by a series representation. Provided the series representation can accommodate discontinuities, even caustics can be handled, although these must not occur on the boundary. It is worth noting that caustics are unlikely to occur in media where the eikonal is appropriate. Writing the series as

$$S(r;\theta,\rho;\phi) = \sum_{l,m,n} A_{l,m,n} S(r;\theta,\rho;\phi,l,m,n) \tag{3.20}$$

where the $A_{l,m,n}$ are coefficients and $S(r;\theta,\rho;\phi,l,m,n)$ is a series representation, changes the problem to one of choosing $S(r;\theta,\rho;\phi,l,m,n)$ and then determining the $A_{l,m,n}$. Note that the series coefficients are dependent on only three parameters, since the positions of P and Q can be described by three coordinates.

3.2.2 Choosing a series representation

In choosing a series representation, it is important to realize that an expression which satisfies some or all of the constraints on $S(r;\theta,\rho;\phi)$ will gain a computational advantage. For instance, when $\nu(\rho \in \Upsilon_-;\phi)$ is replaced by its average value, $\bar{\nu}$, then $S(r;\theta,\rho;\phi) = \bar{\nu}r$, where r is the physical length of the straight line QP (see figure 3.13). Therefore, it seems appropriate to base a general representation for S, valid for arbitrary variations of $\nu(\rho;\phi)$, on powers of r. A representation which is a combination of a Fourier and power series has been found to be adequate for reconstruction

of nontrivial refractive index distributions, i.e.

$$S(r;\theta,\rho;\phi) = S(P,Q) \approx \left(\sum_{l=-L}^{L} A_l e^{jl\Phi}\right) r + \sum_{l=-L}^{L}\sum_{m=-M}^{M}\sum_{n=2}^{N} B_{l,m,n} r^n e^{j(2m\theta+l\Phi)} \tag{3.21}$$

where the coordinates $(r;\theta;\Phi)$ are shown in figure 3.13 and the approximation arises because of the finite limits. The A_l and $B_{l,m,n}$ are complex-valued expansion coefficients required to satisfy $A_l^* = -A_{-l}$ and $B_{l,m,n}^* = -B_{-l,-m,n}$ (an asterisk denotes complex conjugation) to ensure that $S(P,Q)$ is real. Positive integers L, M and N need to be chosen so that (3.21) can adequately represent the spatial variation of $\nu(P)$. The power series expansion in r^n has terms only for $n > 1$, firstly so that the path length at the emitter points (where $r = 0$) is zero, and secondly so that the refractive index at the emitter points is independent of θ. This second point can be explained more simply following (3.22). Because of its Fourier series character, the representation (3.21) can accommodate discontinuities in $S(P,Q)$, i.e. caustics, along isolated curves in Υ_-. The question of an optimal series representation is not treated here, although alternative representations are discussed in section 4.3. Note that the available resolution of the representation, which depends on L, M and N, is bound by the finite data set.

Substitution of the chosen series representation (3.21) into (3.18) gives an expression relating the series parameters to the refractive index, i.e.

$$\begin{aligned}\nu^2(P) = \nabla_P S(P,Q)\cdot\nabla_P S(P,Q) \approx &\left(\sum_{l=-L}^{L} A_l e^{jl\Phi}\right)^2 \\ &+ 2\left(\sum_{l=-L}^{L} A_l e^{jl\Phi}\right)\sum_{l=-L}^{L}\sum_{m=-M}^{M}\sum_{n=2}^{N} B_{l,m,n} n r^{n-1} e^{j(2m\theta+l\Phi)} \\ &+ \sum_{l,l'=-L}^{L}\sum_{m,m'=-M}^{M}\sum_{n,n'=2}^{N} B_{l,m,n}B_{l',m',n'} r^{n+n'-2}(nn'-4mm')e^{j(2(m+m')\theta+(l+l')\Phi)}\end{aligned} \tag{3.22}$$

As in (3.21), the approximation arises because of the finite limits on the summation. Also, as mentioned above, $n > 1$, so that at the emitter points (where $r = 0$) (3.22) reduces to the first term, which can be directly related to the known refractive indices on the boundary. This term was chosen to be independent of θ since the refractive index at the emitter points is independent of θ. Having decided on a representation, it now remains to determine the A_l and $B_{l,m,n}$ from the data.

3.2.3 Solving for the series coefficients

From both theoretical and practical viewpoints, it is convenient to take the emitter and receiver points to be equally spaced. $(2L+1)$ of each are considered. As implied previously, data for this problem consist of the quantities

$$S_{l,\ell} = S(Q_l', Q_\ell) \tag{3.23}$$

where the Q_l' and Q_ℓ are receivers and transmitters of wave motion, respectively. The angular coordinates of Q_l' and Q_ℓ are $\Phi_l = 2l\pi/(2L+1)$ and $\Phi_\ell = 2\ell\pi/(2L+1)$,

respectively, with the integers l and ℓ spanning the ranges $0 \leq |l| \leq L$ and $0 \leq |\ell| \leq L$. For the boundary conditions, the known refractive index at all receiver points Q'_l, represented as ν_l, is used, i.e.

$$\nu_l^2 = \nabla_P S(Q'_l, Q_\ell) \cdot \nabla_P S(Q'_l, Q_\ell) \tag{3.24}$$

The A_l can then be determined by noting that when emitter and receiver points coincide $r = 0$, and (3.22) reduces to

$$\nu_l^2 = \nabla_P S(Q'_l, Q_l) \cdot \nabla_P S(Q'_l, Q_l) = \left(\sum_{l'=-L}^{L} A_{l'} e^{j2\pi l' \Phi_l} \right)^2 \tag{3.25}$$

Applying the discrete Fourier transform [Bates and McDonnell, 1989] shows that, because of the series representation used, the $A_{l'}$ are directly related to the data, ν_l, i.e.

$$A_{l'} = \frac{1}{2L+1} \sum_{l=-L}^{L} \nu_l e^{-j2\pi l' \Phi_l} \quad \text{for} \quad -L \leq l' \leq L \tag{3.26}$$

and the remaining problem is to solve for the $B_{l,m,n}$ in (3.21). Note that solving for the $B_{l,m,n}$ is effectively determining $S(P, Q)$ for $P \in \Upsilon_-$.

Equation (3.18) is the equation available to describe $S(P, Q)$ for $P \in \Upsilon$. Since $\nu(P)$ is a property of the medium, it is independent of where the wave motion originates. Equation (3.18) is therefore sufficient to enable the problem to be solved because the $\nabla_P S(P, Q) \cdot \nabla_P S(P, Q)$ are equal for all Q and can also be equated for all P. However, a more computationally convenient way to determine the $B_{l,m,n}$ is apparent after differentiating (3.18) with respect to Q to give

$$\nabla_Q [\nabla_P S(P, Q) \cdot \nabla_P S(P, Q)] = 0 \tag{3.27}$$

Equation (3.27) is satisfied by forcing $\nabla_P S(P, Q) \cdot \nabla_P S(P, Q)$ to be independent of Φ, the angle to Q.

To achieve this independence, note that $S(P, Q)$ is finite and well behaved (if not necessarily continuous). It, and therefore $\nabla_P S(P, Q) \cdot \nabla_P S(P, Q)$, can be represented by a Fourier series expansion containing orthogonal functions of the emitter position Φ, i.e.

$$\nabla_P S(P, Q) \cdot \nabla_P S(P, Q) = \sum_{\mu=-L}^{L} C_\mu \, e^{j2\pi\mu\Phi} \tag{3.28}$$

where the orthogonal functions are here chosen to be $e^{j2\pi\mu\Phi}$ and the C_μ are the coefficients of each function. Because of the orthogonality, (3.28) is independent of Φ only if the C_μ are zero for all $|\mu| > 0$, i.e.

$$\sum_{l=-L}^{L} [\nabla_P S(P, Q_l) \cdot \nabla_P S(P, Q_l)] \, e^{j2\pi\mu\Phi_l} = 0 \quad \text{for} \quad 0 < |\mu| \leq L \tag{3.29}$$

Substituting (3.22) into (3.29) produces a set of equations where the only unknowns are the desired $B_{l,m,n}$ coefficients. Remember that the bent-ray CT problem is solved when

a number of the $B_{l,m,n}$, sufficient to characterize $\nu(P)$ (or equivalently $S(P,Q)$) to the desired resolution, have been determined to an adequate accuracy.

The only problem remaining is (3.22) being quadratic in $B_{l,m,n}$. It must, therefore, be linearized with the $B_{l,m,n}$ rewritten as

$$B_{l,m,n} = X_{l,m,n} - y_{l,m,n} \tag{3.30}$$

on the understanding that, at each iteration, the $X_{l,m,n}$ are known and the $y_{l,m,n}$ are unknown. The first iteration does not require an initial estimate for the $X_{l,m,n}$ since these are taken to be zero. By substitution of (3.30) into (3.22) and neglecting terms quadratic in $y_{l,m,n}$, (3.29) is linearized in the unknown $y_{l,m,n}$.

Thus, there are three sets of linear equations which have been developed for $B_{l,m,n}$, or equivalently $y_{l,m,n}$. These are:

1. The equations obtained by substituting (3.30) into (3.22), neglecting terms quadratic in $y_{l,m,n}$ and substituting the result into (3.29).

2. The equations obtained by substituting (3.30) into (3.22), neglecting terms quadratic in $y_{l,m,n}$ and solving for the refractive index on the boundary where $P = Q'_l$, i.e. (3.24).

3. The equations obtained by solving (3.21) for the measurement data where $P = Q'_l$.

A standard least squares package can now be invoked to solve the generally overdetermined set of linear equations in $y_{l,m,n}$. After solving for $y_{l,m,n}$, each $X_{l,m,n}$ is updated by subtracting $y_{l,m,n}$ from the present value of $X_{l,m,n}$ (as per (3.30)). These new $X_{l,m,n}$ are substituted for the $B_{l,m,n}$ in (3.22) yielding a new estimate of $\nu^2(P)$. This completes an iteration, which can be repeated until the change in $\nu^2(P)$ is sufficiently small.

3.2.4 Formulation for circularly symmetric media

When the refractive index distribution is circularly symmetric, i.e. $\nu = \nu(\rho)$, the solution of the bent-ray tomographic problem is known. In seismology it is referred to as the Herglotz-Wiechert formula [Aki and Richards, 1980]. However, the circularly symmetric situation allows the feasibility of the above approach to be determined before going to the trouble of developing algorithms for two and three dimensions. Because of the symmetry, only one emitter point, Q_0 say, needs to be considered and (3.21) can be replaced by

$$S(P,Q_0) = \nu_\Gamma r + \sum_{m=0}^{M} \sum_{n=2}^{N} B_{m,n} r^n \cos(2m\theta) \tag{3.31}$$

where ν_Γ is the known refractive index at the boundary Γ (see figure 3.13). The data are the S_l defined by

$$S_l = S(Q'_l, Q_0) \quad \text{for} \quad 0 \leq l \leq L \tag{3.32}$$

where the angular coordinates of Q'_l, Φ_l, need be defined only within the range $[0,\pi]$ because of the symmetry. Here $\Phi_l = (2l+1)\pi/(2L+1)$. The known refractive index ν_Γ on the boundary is satisfied by (3.31) at the receiver points if

$$\nabla_P S(Q'_l, Q_0) \cdot \nabla_P S(Q'_l, Q_0) = \nu_\Gamma^2 \quad \text{for} \quad 0 \leq l \leq L \tag{3.33}$$

The circularly symmetric version of (3.22) is

$$\nabla_P S(P,Q_0)\cdot\nabla_P S(P,Q_0) = \nu_\Gamma^2 + 2\nu_\Gamma \sum_{m=0}^{M}\sum_{n=2}^{N} B_{m,n} n r^{n-1}\cos(2m\theta)$$

$$+ \sum_{m,m'=0}^{M}\sum_{n,n'=2}^{N} B_{m,n}B_{m',n'} r^{n+n'-2}. \qquad (3.34)$$

$$(nn'\cos(2m\theta)\cos(2m'\theta) + 4mm'\sin(2m\theta)\sin(2m'\theta))$$

and of (3.29) is

$$\sum_{l=0}^{L}[\nabla_P S(P(\rho;\phi_l),Q_0)\cdot\nabla_P S(P(\rho;\phi_l),Q_0)]\cos(2\pi\mu\phi_l) = 0 \quad \text{for} \quad 0 < \mu \leq L \qquad (3.35)$$

Equation (3.35) can be solved at a sufficient number of discrete values for ρ, say ρ_j where $0 \leq j \leq J$, to yield a set of linear equations that is not underdetermined. Since there are $(M+1)(N-1)$ unknown coefficients, $(L+1)$ equations arising out of the measurement data, $(L+1)$ boundary equations and $(J+1)L$ equations arising from (3.35), the system of linear equations for a circularly symmetric distribution will not be underdetermined provided

$$J \geq [(M+1)(N-1) - 3L - 2]/L \qquad (3.36)$$

Before considering any results from the above method, it is important to appreciate a possibly significant limitation on the bent-ray approach to computed tomography. The paths of rays through Υ_- are determined by the refractive index distibution and do not necessarily pass through all parts of Υ_-. If the distribution is such that no rays reach a particular part of the boundary then no measurement data can be taken in that region. This problem is known as existence of a *low velocity zone* (LVZ) in ν and will occur in a circularly symmetric refractive index distribution if [Aki and Richards, 1980]

$$\frac{d(\nu\rho)}{d\rho} < 0 \qquad (3.37)$$

If a LVZ exists, then the solution for ν in the LVZ is normally nonunique. This problem can be neatly circumvented by leaving out (from the set of linear equations to be solved) the corresponding equation for the measurement data where no ray links a particular receiver-transmitter pair. The solution is then unique, although it cannot of course be expected to be accurate in the LVZ where rays do not travel. Because of the use of a series representation, the solution in the LVZ will in fact be a smoothed version of the true refractive index distribution. Note that this problem is considerably reduced when $\nu(\mathbf{x})$ can vary in both ρ and ϕ, because rays reach all receivers most of the time. Another closely related problem is that rays may not enter an internal region of Υ_- [McKinnon and Bates, 1980]. Such regions are therefore impossible to image and will render the solution partially non-unique [Berryman, 1990]. Once again, because of the series representation, the bent-ray CT solution in these regions will be a smoothed version of the true refractive index distribution.

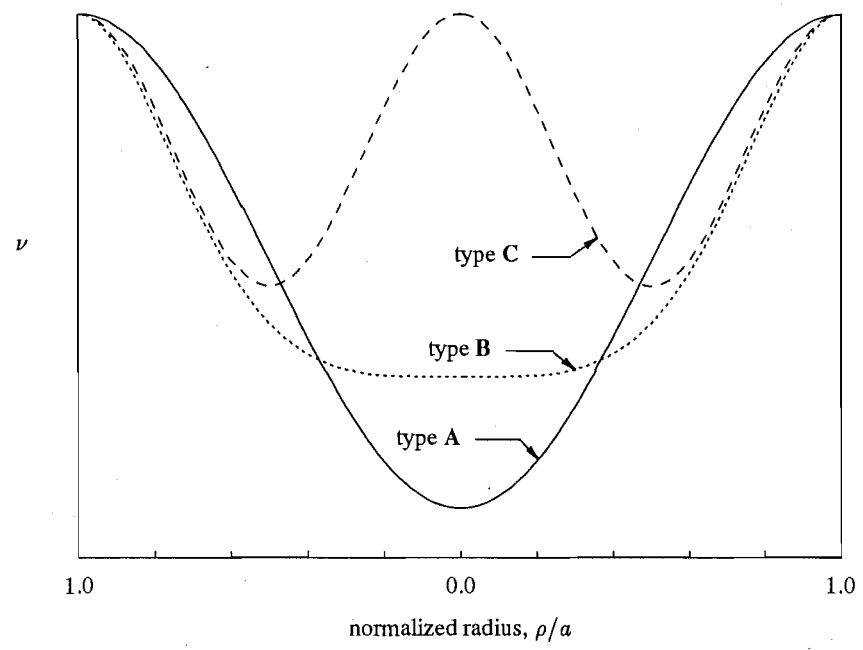

Figure 3.15 Three distributions to be reconstructed, denoted types **A**, **B** and **C**, plotted across their diameter to show circular symmetry.

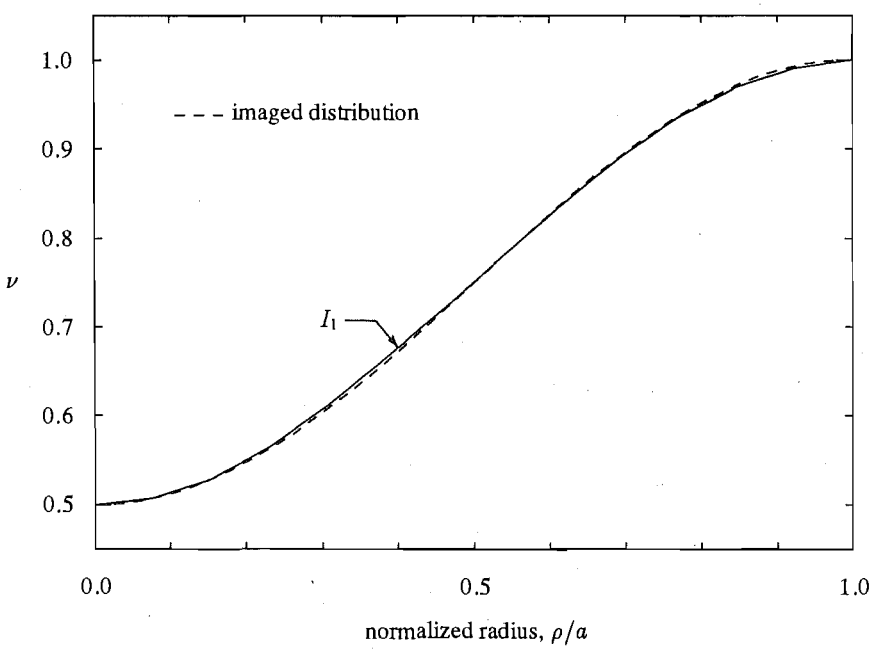

Figure 3.16 Reconstruction of a type **A** distribution with range $0.5 \leq \nu \leq 1.0$ and representation $L = 9$, $M = N = 11$, $J = 12$.

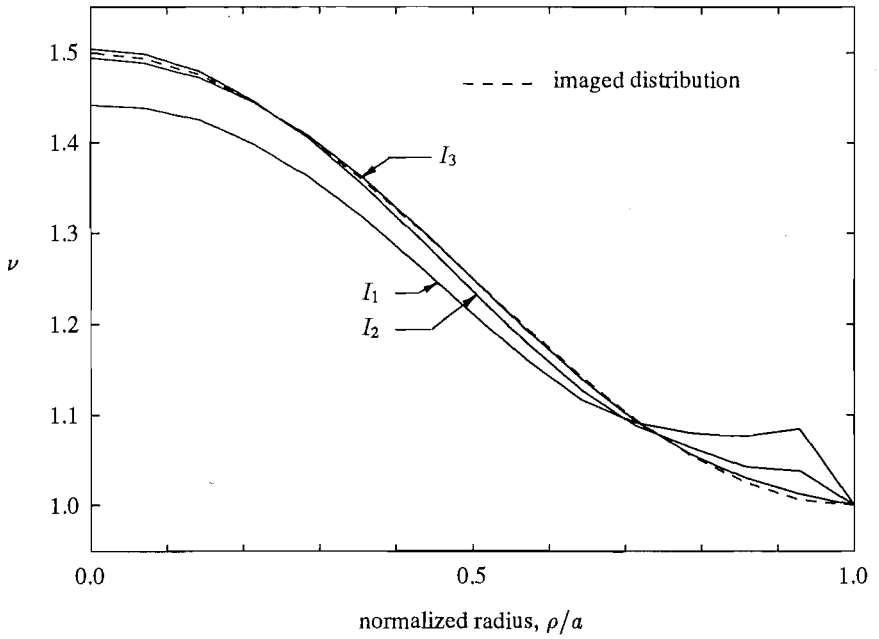

Figure 3.17 Reconstruction of a type **A** distribution with range $1.0 \leq \nu \leq 1.5$ and representation $L = M = N = J = 14$.

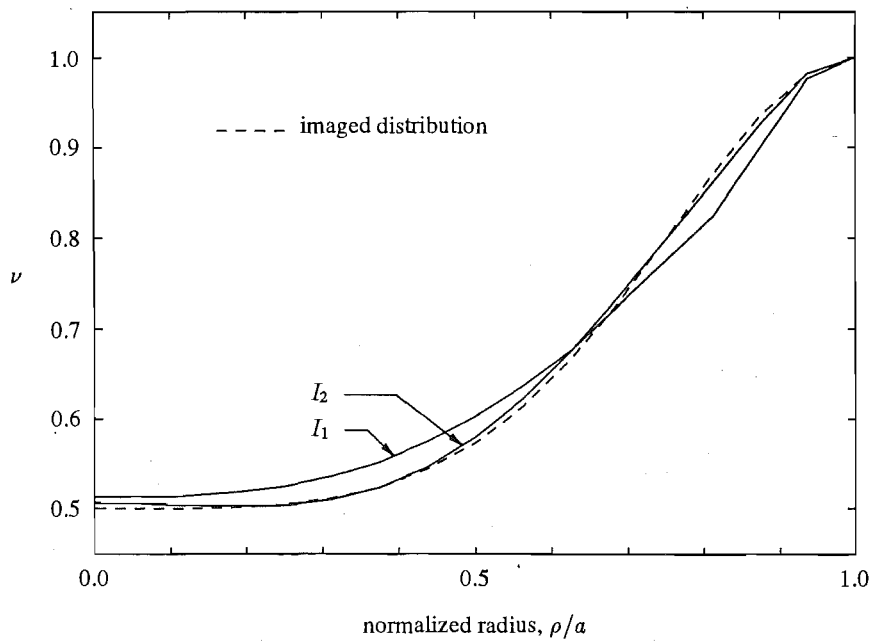

Figure 3.18 Reconstruction of a type **B** distribution with range $0.5 \leq \nu \leq 1.0$ and representation $L = 14$, $M = N = 14$, $J = 16$.

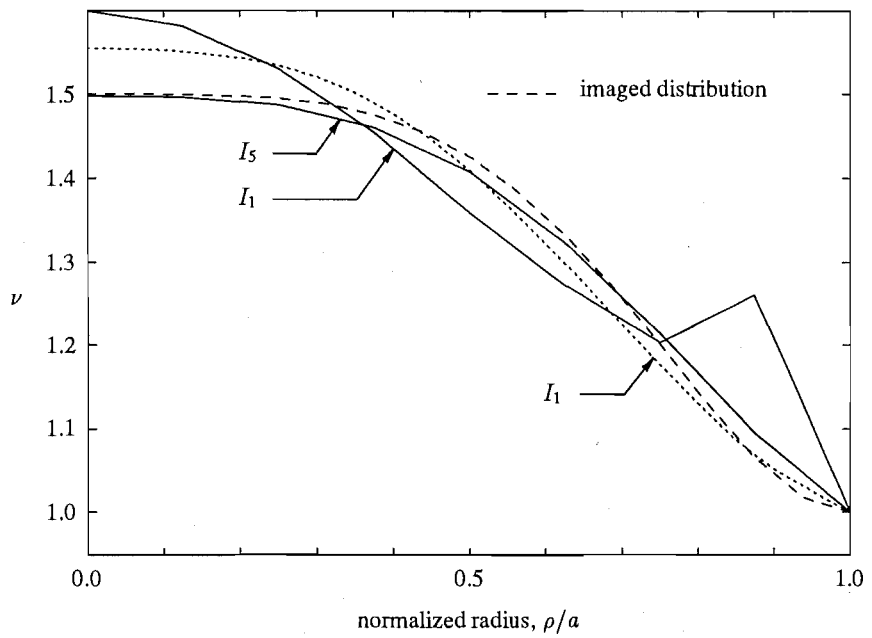

Figure 3.19 Reconstruction of a type **B** distribution with range $1.0 \leq \nu \leq 1.5$ and representations $L = M = N = 9$, $J = 8$ for the solid line reconstructions, $L = M = N = J = 20$ for the dotted line reconstruction.

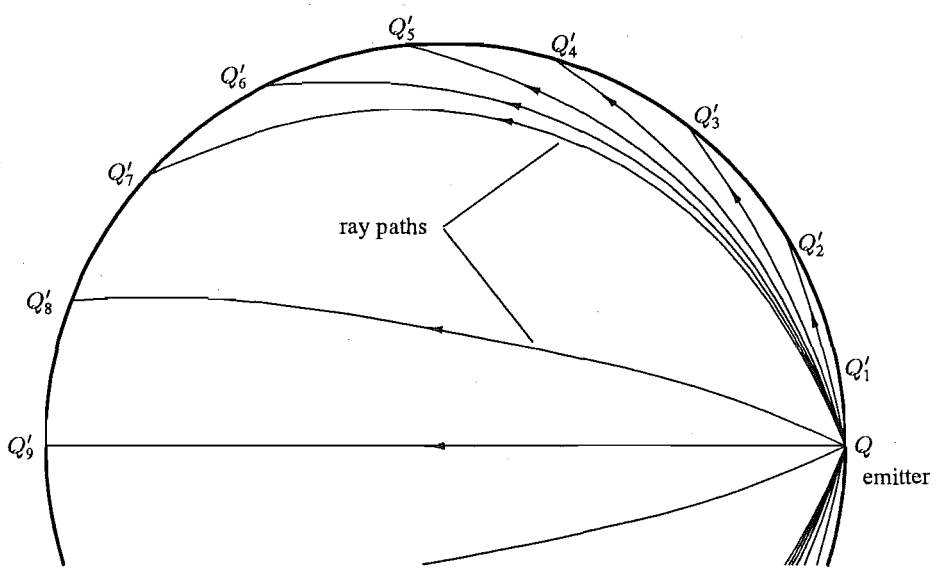

Figure 3.20 Ray paths between emitter and receivers for the reconstruction in figure 3.19. Ray paths are required for only half of the object due to the circular symmetry of the refractive index distribution.

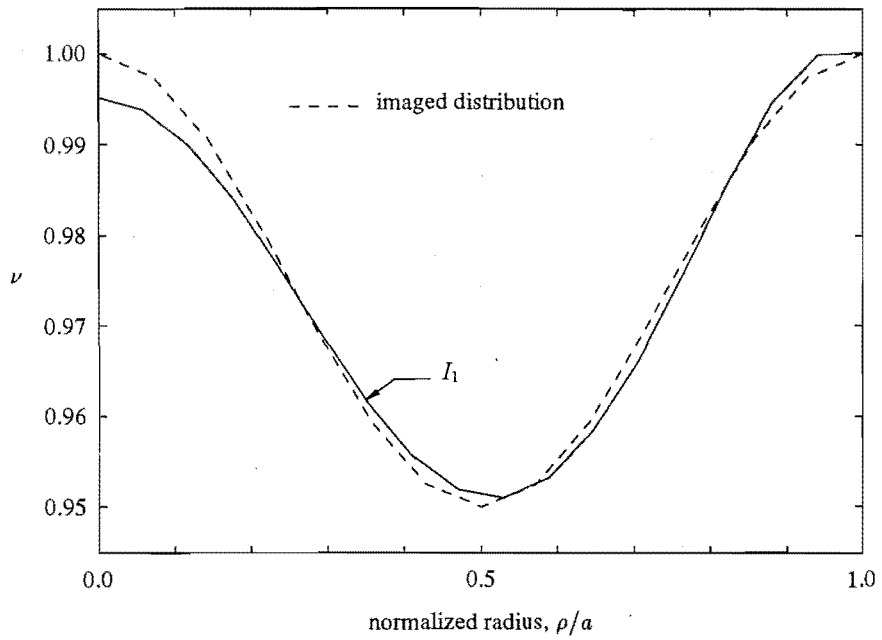

Figure 3.21 Reconstruction of a type C distribution with range $0.95 \leq \nu \leq 1.00$ and representation $L = 20, M = 20, N = 18, J = 17$.

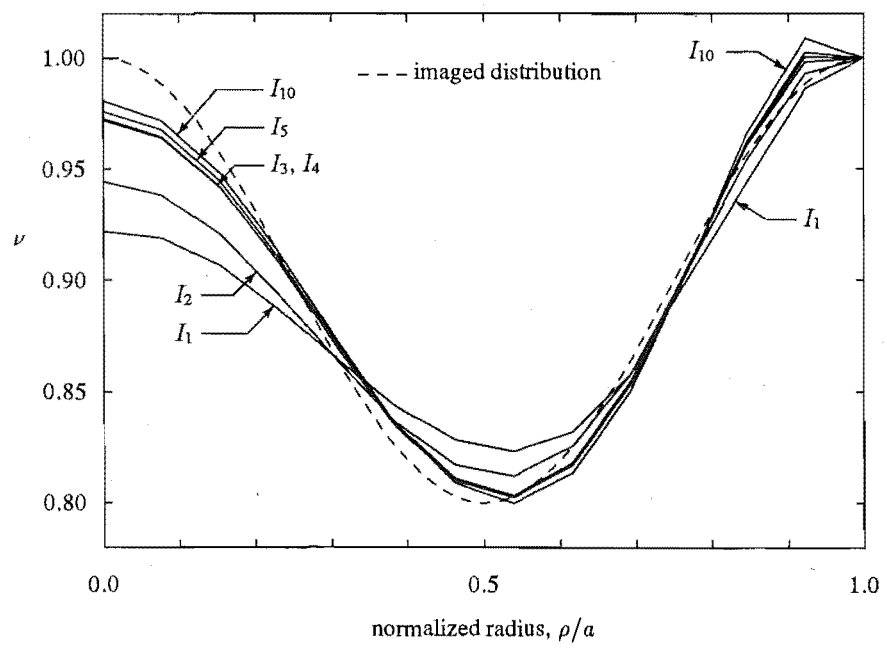

Figure 3.22 Reconstruction of a type C distribution with range $0.8 \leq \nu \leq 1.00$ and representation $L = 14, M = N = 14, J = 12$.

3.2.5 Results for circularly symmetric media

The iterative approach proposed in section 3.2.4 has been used to reconstruct circularly symmetric refractive index distributions from travel-time estimates for three types of distributions. These distributions are shown in figure 3.15 and are referred to as types **A**, **B** and **C**. The distributions have been plotted across their entire diameter to depict the circular symmetry, whereas in figures 3.16-3.22 results are plotted over only the distributions' radii. It should be noted that the distributions are unity on their boundaries and their maximum amplitude variations are as yet unspecified.

The above distributions are sufficiently smooth that they avoid the existence of a low velocity zone, (3.37), provided the amplitude variation in ν lies within the ranges

$$\begin{aligned} \nu_{\max} &\leq 1.45 \quad \text{type } \mathbf{A} \\ \nu_{\max} &\leq 0.64 \quad \text{type } \mathbf{B} \\ -0.59 \leq \nu_{\max} &\leq 0.49 \quad \text{type } \mathbf{C} \end{aligned} \tag{3.38}$$

where $\nu_{\max}$ is the maximum deviation from unity. Note that all the distributions imaged in figures 3.16-3.19 and 3.21-3.22 fall inside the range specified in (3.38).

Travel-time data, $S(Q_l', Q_0)$, for each refractive index distribution were determined as described in section 2.4 and no *a priori* assumptions about the refractive index distribution were required by the reconstruction algorithm. Solution points were taken at discrete radii, ρ_j, equi-spaced in the range $[0, a]$ and the n^{th} iterative reconstruction for $\nu(\rho)$ is denoted by I_n. Note that $I_0 = 1$ for all ρ_j. The power of the proposed approach is its ability to reconstruct refractive index distributions which differ significantly from unity (although they must be sufficiently smooth that the eikonal equation is a reasonable approximation). Results are therefore given for refractive index distributions containing 50% variations in refractive index. Such large variations are unlikely to occur in a typical electromagnetic or ultrasonic imaging problem [Bolomey *et al.*, 1991; Broquetas *et al.*, 1991; Caorsi *et al.*, 1991; Tabbara *et al.*, 1988] and therefore provide a stringent test of the new bent-ray CT algorithm. Smaller refractive index variations than those shown result in better intial estimates, I_1, and more rapid convergence to the true distribution.

Reconstructions are shown for two examples of each of the three types of refractive index distribution shown in figure 3.15. In figure 3.16 the reconstruction is very close to the imaged distribution after the first iteration. Similar accuracy is achieved in figure 3.17 after three iterations with the chosen values for L, M, N and J. A similar difference in rate of convergence to the true distribution is also observed when comparing figures 3.18 and 3.19. The reason for this difference is, as intimated in section 3.2.4, rays tend to avoid regions of high refractive index. These regions are therefore correspondingly more difficult to image by a bent-ray, or any other approach. The extent of the ray bending is illustrated in figure 3.20, which shows the rays corresponding to the solid line reconstructions in figure 3.19. This figure certainly demonstrates the requirement for a bent-ray approach to the problem. In particular, the ray joining Q and Q_7' leaves Q at an angle of 49° to the line joining the two positions. Despite the difficulty of the reconstruction process evidenced by the ray paths in figure 3.20, all reconstructions converge to the true distribution (to within a small percentage of the total spatial variation). Figure 3.19 shows reconstructions for different limits on the path length series. The effect of this is discussed in section 3.2.6. Finally, figures 3.21 and 3.22 demonstrate

that accurate reconstructions are also achieved for more rapidly varying refractive index distributions, with figure 3.22 showing the convergence properties of the new bent-ray CT algorithm.

3.2.6 Discussion

The reconstructions in section 3.2.5 demonstrate that the new bent-ray CT solution is both accurate and able to handle very large variations in refractive index. Remember that the variations are relative to an arbitrary background refractive index which has been chosen as unity for the reconstructions shown. This background refractive could be appropriately higher or lower, but importantly would involve no increase in the complication of the reconstruction process. Thus, this formulation is particularly appropriate for imaging objects where the refractive index is significantly different from unity.

With regard to the choice of objects to reconstruct, it is important to appreciate that the representation for ν is based on ray parameters r and θ (see (3.31)), i.e.

$$\nu(\rho) = f(r;\theta) \tag{3.39}$$

So, although the imaged distributions are simple functions of ρ, they are in fact representative of a more general class of refractive index distribution and are a more severe test of the new bent-ray CT algorithm than may be initially apparent. This point is confirmed by comparing figure 3.16 with figure 3.18. Although the form of ρ dependence differs, the reconstruction is equally successful in both figures. Note also that reconstructions are plotted only across a radius, rather than a diameter, and so the degree of variation being reconstructed is better illustrated in figure 3.15.

Equation (3.39) makes it apparent that the resolution of the solution for ν does not depend on L, M or N in a simple fashion. More receivers would appear to offer more information and therefore permit greater resolution. Experience gained in forming the reconstructions in section 3.2.5 (see figure 3.19 in particular) certainly shows that increasing L, M and N results in more accurate initial estimates of the refractive index distribution. However, the accuracy of the final reconstruction is relatively independent of L, M and N, and reducing these limits reduces the computation involved in each iteration considerably. A lower limit on the number of solution points, J, is provided by (3.36) and is closely related to choice of L, M and N. While increasing J makes the system of equations to solve more overdetermined, it seems to slow convergence near the boundary. Presumably this is because less emphasis is placed on equations involving measurement data. The question of an optimum choice for J, L, M and N can be answered only once alternate series representations have been tested, and more importantly, once a true two dimensional formulation has been implemented. However, in the circularly symmetric situation a wide range of values for these limits produces accurate reconstructions, although iteration is required when smaller limits are used.

The question of an optimum series representation is perhaps more important, since the general approach described here can be expected to give accurate reconstructions with different representations, presumably with different resolution and convergence properties. Options for alternative series representations are discussed in section 4.3. Note that whatever the series representation, since the method is based on the eikonal

equation (as all approximate formulations capable of handling appreciable refraction must be), it cannot be expected to accommodate very rapid changes in refractive index.

The approach proposed here solves the bent-ray CT problem through a set of linear equations, rather than through the conventional process of ray tracing. Ray tracing has also been demonstrated to give accurate reconstructions of similar refractive index distributions to those imaged here [Cha and Vest, 1981]. Indeed, both approaches are based on the eikonal equation and can therefore be expected to have similar validity and accuracy. While the ray tracing approach has not been implemented by the author, a good idea of the computation involved is afforded by the computation required to solve the direct problem associated with the reconstructions in section 3.2.5. As an example, the ray-tracing solutions to the direct problem for the solid reconstructions in figure 3.19 took $37s$ and $124s$ CPU time, respectively, for step sizes of 1% and 0.2% of the radius, a. In contrast, the reconstruction in figure 3.19 took $456s$ CPU time per iteration, although actually solving the linear equations required only $60s$ of the $456s$, with the remaining time spent formulating the equations to solve. Clearly, these times suggest that a ray tracing scheme would be faster than the current implementation of the new bent-ray CT algorithm. However, if a series can be developed which simplifies the equation forming and/or solving process, then the new algorithm may have a speed advantage. This comparison of times taken is of course simplistic in that it ignores the accuracy and resolution of the two reconstruction methods. It is included to show that, for the one dimensional case, the two methods appear to have similar computational cost. A more complete comparison will be required once a two dimensional algorithm is implemented, for the extra dimension may alter the computational requirements significantly. If the new bent-ray CT algorithm does have an advantage, it may be through the stabilizing influence of the series representation. Thus, the new algorithm can be expected to give a smoothed version of a rapidly varying refractive index distribution where the ray tracing approach may not converge to a solution. Considerable further development of this algorithm, followed by comparisons of reconstructions made in two dimensions, will be required before it will be possible to prefer either approach.

CHAPTER 4

Conclusions and Suggestions for Further Scattering Research

The aim of Part I of this thesis has been to investigate the accuracy of two approximate formulations of scattering, geometrical optics (GO) and the Born approximation, and more importantly, two new inverse methods based on these approximations. This chapter summarizes the results contained in Chapters 2 and 3, and draws some conclusions about future progress in diffraction tomography and imaging in general. It finishes with some suggestions for further investigation of the proposed bent-ray CT approach.

4.1 Scattering and Shift-and-add (SAA)

The Born approximation is widely used to simplify both direct and inverse scattering problems, although it is inaccurate unless the maximum relative path length through the object is considerably less than a wavelength. An alternative analytically solvable solution to the Helmholtz equation is provided by GO. Geometrical optics was found to be unsuitable for homogeneous objects with dimensions of less than 20λ, although when $\nu \not\approx 1$ it was found to be more appropriate for such objects than the Born approximation.

Exact, Fourier interpolation and backpropagation methods for performing Born inversion have been considered. Backpropagation was explicitly formulated for the first time for receivers in the far-field. A comparison of backpropagation and Fourier interpolation showed that, in the simulation situation, Fourier interpolation is clearly preferable because of its better resolution and much lower computational cost. Examples of reconstructions using Born inversion were then provided for multi-cylinder objects where the direct problem had been solved exactly. Comparison of these 'exact' reconstructions with reconstructions where no, or only first order, multiple scattering was considered, demonstrated that, for the purposes of evaluating inverse methods, only first order multiple scattering need be considered in solving the direct problem. Multiple scattering was shown to cause significant distortion, even with refractive indices of approximately unity, provided that the individual cylinders in a multi-cylinder object were large and reasonably close together. Equally important, multiple scattering was shown to cause less distortion when cylinder dimensions were small relative to their separation, even though the refractive indices of the cylinders could be large. Furthermore, the distortion in Born inversion was demonstrated to be related only loosely to the maximum distance

between wavefronts of ψ and ψ_{inc}, although this distance is commonly believed to be the only factor determining distortion [Wombell and Fiddy, 1987; Slaney *et al.*, 1984].

Shift-and-add (SAA) is a method for processing an ensemble of images. It has been previously proposed as a suitable way to reduce the distortion in Born inversion. The combination of SAA and Born inversion was comprehensively evaluated, but failed to achieve the anticipated image enhancement. This failure was attributed to the form of the distortion in Born inversion which does not appear to be predominantly described by a convolution. An alternative form of SAA, termed differential SAA, has been previously suggested as a more appropriate ensemble processing scheme when the object is piecewise continuous. Differential SAA was tested in two dimensions for the first time, but was also unsuccessful. However, images obtained from Born inversion do not provide a suitable test of differential SAA because of the form of the distortion. Thus, differential SAA may prove to be a useful alternative to SAA in different imaging contexts. While SAA was said to be unsuccessful, this lack of success refers to the anticipated compensation for all the failings of Born inversion. SAA processing did, in fact, result in improved object localization and reduced background noise, although these were less than those achieved by straightforward averaging of the ensemble of images. Therefore, some form of averaging over reconstructions at different frequencies can be expected to reduce errors due to measurement noise and imperfections in the measurement apparatus.

The distortion arising in Born inversion appears to be of a different form than can be handled by ensemble processing techniques. It is therefore difficult to imagine how reconstructions obtained based on a non-iterative (i.e. non-exact) formulation of diffraction might be significantly improved by subsequent processing. Note that this comment applies to Rytov inversion, extensions to both Born and Rytov inversion, and all inversion methods based on explicit formulations of diffraction. Even if the relative path length through the object is well compensated, perhaps by a JWKB method [Bates, 1988], when there are multiple components (as will usually occur in practice) severe distortion can occur even if the deviation in refractive index from an average, or slowly varying background, is only very slight. Given the continuing rapid increase in available processing power, it seems likely that practical inversion methods will therefore move to iterative imaging solutions, although these may well be based on formulations like the Born approximation. Particularly promising examples have been published recently by Wang and Chew [1989], Chew and Wang [1990] and Joachimowicz *et al.* [1991].

4.2 Bent-Ray CT

A novel algorithm for solving the bent-ray CT problem has been developed for the general two dimensional problem and tested on circularly symmetric refractive index distributions. Accurate reconstructions have been obtained for distributions containing large (50%) deviations in refractive index. The basis for the proposed algorithm is a novel ray description, which allows the refractive index distribution to be found by solution of linear equations, rather than through the conventional process of ray tracing. Some comments comparing the new bent-ray CT algorithm with the ray tracing approach

have been made and suggest that the conventional approach may be faster. However, a major limitation to accurate appraisal of the new algorithm is that it remains untested on general two dimensional distributions or in the presence of noise. Further investigation of alternative series representations, and more particularly, how the series coefficients are computed, may also result in dramatic improvements to the new algorithm. If the new bent-ray CT algorithm, as currently implemented, does have an advantage, it may be through the stabilizing influence of the series representation. Thus, the new algorithm can be expected to give a smoothed version of a rapidly varying refractive index distribution where the ray tracing approach may not converge to a solution. It is clear that an informed decision which prefers either approach must await further development of the new algorithm. Section 4.3 contains some suggestions for this development.

Bent-ray CT solutions, which are able to handle appreciable ray bending, must be based on the eikonal equation. In realistically sized objects they are therefore able to handle much larger variations in refractive index than explicit diffraction tomography solutions, e.g. Born and Rytov inversion [Keller, 1969], while avoiding the computational consequences of an exact solution. However, the problem lies in the assumption that the refractive index varies sufficiently slowly that a high frequency approximation is appropriate. Bent-ray CT solutions are therefore unable to accurately place discontinuities or rapid variations in refractive index, which tend to be the regions of most interest when interpreting reconstructions [Broquetas *et al.*, 1991]. As remarked in section 4.1, in the long term, practical inverse algorithms are likely to move to the use of iterative-exact solutions to the Helmholtz equation. These are likely to be based on Newton-type iterative schemes [Connolly and Wall, 1990; Wang and Chew, 1989; Chew and Wang, 1990], which can be expected to converge rapidly when close to the true reconstruction, but not initially. Thus, an accurate estimate of the background refractive index distribution will allow most of the initial (and more unproductive) iterations to be avoided and can best be provided by a bent-ray CT solution. Because the computation involved in the bent-ray CT solution can be expected to be negligible compared to that associated with even one iteration of an exact method, this approach will result in vast computational savings relative to the exact method where no initial estimate of the refractive index is used [Garnero *et al.*, 1991; Joachimowicz *et al.*, 1991]. It may even allow the solution to be found when the naive exact method will not converge. Also, due to the relative insignificance of the associated computation, the accuracy and stability of the bent-ray CT solution will be the most important considerations. These points may favour the new bent-ray CT algorithm.

4.3 Further Bent-Ray CT Research

The ability of the new bent-ray CT algorithm to reconstruct circularly symmetric refractive index distributions has been demonstrated in section 3.2.5. Although the algorithm has been formulated for the general two dimensional problem, this formulation now needs to be implemented to further confirm the feasibility of the new approach. Equally important in the development of the new approach is further investigation of alternative series representations (3.21) for the path length. The convergence properties of the

algorithm will depend on how well the series representation describes the variation in path length with P. An additional constraint that may be important in this context, but which has not been used to obtain the results in section 3.2.5, is now considered.

The path taken by energy propagating from point Q to point P is the same as that of the energy propagating from P to Q, i.e.

$$S(r;\theta,\rho;\phi) = S(\rho;\phi,r;\theta) \tag{4.1}$$

The series representation could be chosen to comply with this reciprocity condition, thereby implicitly satisfying a known property of the wave motion. As an example, a representation of the form

$$S(r;\theta,\rho;\phi) = \sum_{l,m,n} A_{l,m,n}[\mathcal{R}_m(r;\theta)\,\mathcal{S}_n(\rho;\phi) + \mathcal{R}_m(\rho;\phi)\,\mathcal{S}_n(r;\theta)]r^l \tag{4.2}$$

ensures that $S(r;\theta,\rho;\phi)$ satisfies (4.1), where the $A_{l,m,n}$ are constant expansion coefficients, and the $\mathcal{R}_m(\rho;\phi)$ and $\mathcal{S}_n(\rho;\phi)$ are suitable basis functions.

Another possibly useful simplification of the new bent-ray CT approach would be to replace the first term in the series representation (3.21) by $\bar{\nu}r$. This recognizes that in practical applications the object will generally be surrounded by a material of constant refractive index, e.g. air or water. The range of N in the series could then be extended to include unity, which would enable the second component of the series to have terms in r and may allow variations in path length to be better represented.

Additionally, computational advantage could be gained in evaluating the eikonal's independence with respect to the transmitter coordinate, Φ. Specifically, if $\nabla_P S(P,Q) \cdot \nabla_P S(P,Q)$ was composed of basis functions orthogonal in Φ, the summation over Φ in (3.29) would not be necessary and most of the computational effort associated with the present formulation would be avoided. However, it is far from obvious how this orthogonality might be achieved while retaining a series representation related to the physical path length of the ray from Q to P. Without such a relationship, experience suggests that the new bent-ray CT approach could not be expected to converge to the true solution.

Finally, the new bent-ray CT algorithm does not require any *a priori* information about the form of the refractive index distribution to be reconstructed. On the first iteration the distribution is assumed to be homogeneous, as all series coefficients are set to zero. However, if *a priori* information about the distribution is available, then an initial estimation of the series coefficients could be calculated based on the linearization of (3.21) outlined in section 3.2.3.

Part II

ACTH Regulation

CHAPTER 5

Background to ACTH Regulation

It is well known that *stress* is an unavoidable and potentially harmful fact of life. Indeed excessive mental stress is becoming recognized as a predominant factor behind many illnesses and deaths in industrialized nations [Lockshin and Zakeri, 1990; Riley, 1981]. However, it is also true that stress *hormones*, which (along with other factors) mediate our response to stress, are essential to allow us to meet physical challenges. In times of physical stress they stimulate the heart, increase respiration, shunt blood from the internal organs and skin to the skeletal muscles, decrease pain, and have a host of other actions that contribute to our ability to engage in sustained physical activity. In fact, animals deprived of stress hormones are incapable of sustained effort and readily succumb to conditions easily tolerated by individuals with healthy hormone systems [Martin, 1985]. It is apparent that a better understanding of how the body copes with stress may lead to improved means of controlling its effects, both in the medical context, such as during infections and operations, and in psychological and social situations. It is also worth noting that over 50% of New Zealand's export earnings are derived from farm animals [Statistics, 1991], yet the effect of stress (e.g. tailing, castration, shearing, dehorning, weaning, and confinement) on the productivity of farm animals is only just beginning to be appreciated [Griffin, 1989; Smith, 1990].

Adrenocorticotropic hormone (ACTH), which is also known as *adrenocorticotropin* or *corticotropin*, is the major hormone released from the *pituitary gland* in response to stress. It is now generally accepted that the main factors influencing ACTH secretion are *corticotropin releasing hormone* (CRH), *arginine vasopressin* (AVP) and *cortisol* (F). The research described in Chapter 7 is an analysis and interpretation of how the pituitary concentrations of these hormones regulate ACTH secretion. This chapter and Chapter 6 provide the background information for this research. Section 5.1 sets out the necessary anatomical details, while section 5.2 presents the current understanding of ACTH regulation. The contents of these two sections are then briefly summarized in section 5.3 to focus the thoughts of the non-Endocrinologist. Emphasis is on the horse, or *equine*, and human systems.

5.1 Components of the Stress Axis

The hormone, or *endocrine* system is responsible for maintaining the body's closely regulated internal environment. It can be somewhat artificially divided into three axes which are concerned with regulation of different bodily activities - reproduction, growth and metabolism, and response to stress. Although the three axes are closely interrelated, only the stress, or *adrenal* axis is covered here in any detail. Its major components are the subject of the remainder of section 5.1.

5.1.1 The Pituitary Gland

The pituitary gland is the principal site of ACTH synthesis and release. In mammals it is suspended below the *hypothalamus* by the infundibulum and lies in a hollow at the base of the skull, completely overlaid by the brain [Holmes and Ball, 1974]. It has two major subdivisions. The *adenohypophysis*, or glandular portion, is distinct from the hypothalamus, but is regulated by hypothalamic releasing hormones which travel to it via the hypothalamo-pituitary portal blood vessels. It contains cells that synthesize and secrete hormones. By far the largest component of the adenohypophysis is the *pars distalis*. The other components are the pars intermedia and the pars tuberalis.

The other subdivision, called the *neurohypophysis*, is an extension of the hypothalamus. It does not produce hormones, but stores some of those synthesized in the hypothalamus before releasing them into the blood. The neurohypophysis consists of three main parts, as shown in figure 5.1. The *median eminence* (ME) lies at the base of the hypothalamus where it releases adenohypophysial regulators into the capillaries of the hypothalamo-pituitary portal system. The *infundibular stem* is the stalk of nerve fibres linking the hypothalamus with the *neural lobe* [Porter *et al.*, 1974]. In the neural lobe nerve fibres from the hypothalamus release their hormones - principally AVP and

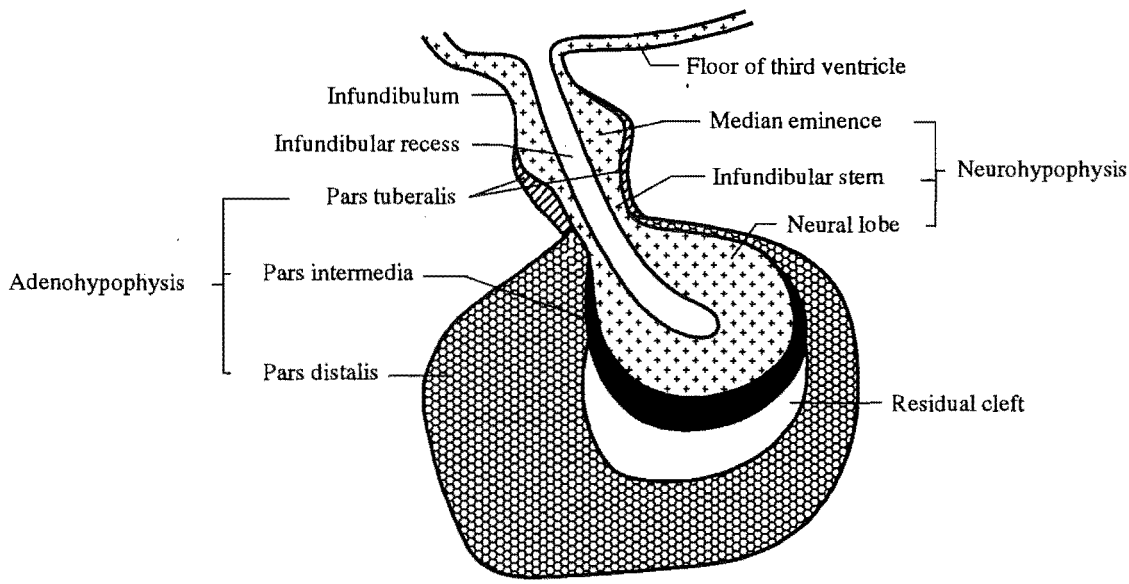

Figure 5.1 Structure of the pituitary gland. (Reproduced from [Martin, 1985].)

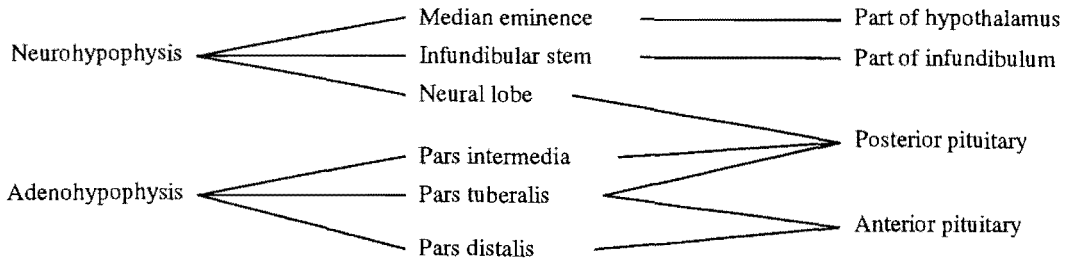

Figure 5.2 Relationships between subdivisions of the pituitary gland. The names anterior and posterior pituitary arise from the experimental situation where an attempt is made to separate the adenohypophysis from the neurohypophysis [Holmes and Ball, 1974].

oxytocin - into blood vessels. The relationships between the various parts of the pituitary gland are shown diagramatically in figure 5.2.

The pituitary cells which produce ACTH are called *corticotropes*, and comprise 3-15% of the cells in the adenohypophysis [Childs *et al.*, 1987; Jia *et al.*, 1991]. This percentage, and the percentage of corticotropes actually secreting ACTH, are dependent on adrenal axis activity [Gertz *et al.*, 1987; Leong, 1988]. Corticotropes synthesize large proteins called pro-opio-melanocortins (POMCs) that are subsequently cleaved to yield ACTH, lipotropin (β-LPH), N-POMC, endorphins, and other biologically active peptides. Upon stimulation, the first three of these peptides are released in equimolar amounts [King and Baertschi, 1990]. Their major physiological effects seem to be restricted to the adrenal gland and mediated by ACTH and N-POMC, with N-POMC potentiating the effects of ACTH, although it is inactive by itself [Al-Dujaili *et al.*, 1981; Lowry *et al.*, 1986].

5.1.2 The Hypothalamus

The hypothalamus forms the floor and lower lateral walls of the third ventricle of the brain. It is the principal source of pituitary concentrations of AVP, CRH and other possible ACTH regulators. It consists of neurons, which group themselves into magnocellular nuclei - clusters of neurons with mainly large cell bodies, and parvocellular nuclei - less uniform clusters of mostly smaller neuron cell bodies. Neurons can also be grouped according to their locations, for example; the paraventricular nuclei (PVN) lie close to the third ventricle, and the supraoptic nuclei (SON) are located above the crossing of the optic nerves. Bundles of long axons, the infundibular stem, connect magnocellular nuclei of the PVN and SON to the neural lobe of the pituitary (see figure 5.3). In mammals the main hormones synthesized within these nuclei are AVP and oxytocin. Parvocellular nuclei of the PVN synthesize CRH, AVP, oxytocin and many other hypothalamic hormones. Regulators made in these nuclei are sent exclusively down relatively short, fine axons that project to the external zone of the median eminence and terminate close to the blood vessels of the hypothalamo-pituitary portal system [Merchenthaler *et al.*, 1984]. These hormones, or releasing factors, then travel through the long portal vessels, which pass down the infundibular stem, to the pars distalis (see figures 5.1 and 5.3).

Interestingly, AVP is present in approximately 2% of CRH-containing parvocellular PVN nuclei [Kiss *et al.*, 1984; Sawchenko *et al.*, 1984], and approximately 44% of secretory granules in the external zone of the rat median eminence contain both CRH and AVP [Whitnall and Gainer, 1988; Wolfson *et al.*, 1985]. In rats which have had their adrenal glands removed there is no *glucocorticoid* feedback to supress hormone synthesis, and colocalization of CRH and AVP may reach 90% [Whitnall *et al.*, 1985]. If this colocalization is physiological it is significant in supporting the synergism between AVP and CRH.

5.1.3 The Adrenal Glands

The mammalian adrenal (or suprarenal) glands are located above the kidneys. Their outer region, or cortex contains the cells that synthesize and release glucocorticoids. Glucocorticoids inhibit ACTH secretion, and thus form a negative feedback loop since glucocorticoid secretion appears to be controlled nearly exclusively by ACTH [Keller-Wood *et al.*, 1984]. The major glucocorticoid for humans, horses, monkeys and some other mammals is cortisol [Ng *et al.*, 1981]. The effects of cortisol are discussed further in section 5.2.4.

5.2 Adrenocorticotropic Hormone (ACTH) and its Regulation

ACTH is principally synthesized in, and released from, corticotropes in the pars distalis (see figure 5.1). Its synthesis was briefly described in section 5.1.1 and its regulation is the topic of the rest of this chapter (see also figure 5.3). The primary purpose of ACTH is to stimulate secretion of glucocorticoids, mainly cortisol, from the adrenal cortex in response to stress.

The regulation of ACTH is a large and continually expanding research area. To draw up a long list of substances influencing ACTH secretion is easy, but to make physiological sense of such a list is much more difficult. A number of excellent recent reviews attempt to do this and the interested reader is referred to these [Antoni, 1986; Axelrod and Reisine, 1984; Emeric-Sauval, 1986; Gibbs, 1986; Jones and Gillham, 1988; King and Baertschi, 1990; Keller-Wood and Dallman, 1984; Lowry *et al.*, 1986; Lundblad and Roberts, 1988; Makara *et al.*, 1984; McEwen *et al.*, 1986; Plotsky *et al.*, 1989; Rivier and Plotsky, 1986; Reisine and Affolter, 1987; Thomson and Smith, 1989]. The rest of section 5.2 will attempt to do the same, with specific emphasis on areas relevant to the research described in subsequent chapters. Figure 5.3 illustrates the current understanding of physiological ACTH regulation. One point that is becoming clear is that the physiological regulation of ACTH depends on a number of factors which are released in proportions that depend on the type of stress involved [Dallman *et al.*, 1987a; Plotsky *et al.*, 1985]. Furthermore, it is clear that control of ACTH secretion is far more complicated than originally thought [Jia *et al.*, 1991; Leong, 1988].

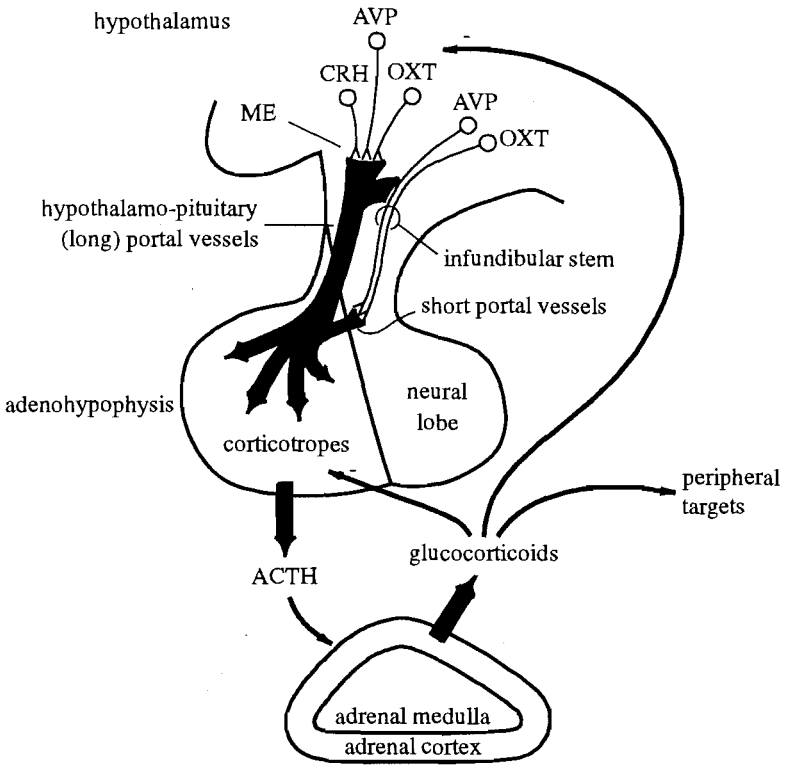

Figure 5.3 Control of ACTH secretion from the adenohypophysis. CRH, AVP and oxytocin (OXT) are synthesized in parvocellular neuclei of the PVN of the hypothalamus and are released from nerve terminals in the median eminence (ME) into the portal blood. AVP and oxytocin are also synthesized in magnocellular neuclei of the PVN and SON, which project to the neural lobe. Most of the portal AVP, and some of the oxytocin, arises from preterminal release by these neurons, with smaller amounts of these hormones reaching the corticotropes through short portal vessels. ACTH is released from corticotropes in the adenohypophysis in response to stimulation by CRH, AVP, and oxytocin, along with other factors. It induces the release of glucocorticoids from the adrenal cortex, which in addition to acting on peripheral targets, feed back to the hypothalamus and corticotropes to inhibit ACTH secretion. (Figure obtained in part from [King and Baertschi, 1990].)

5.2.1 Corticotropin Releasing Hormone (CRH)

Substances stimulating ACTH (corticotropin) secretion have been known to exist since the 1950's [Guillemin and Rosenberg, 1955; Saffran and Schally, 1955]. CRH is still considered by many groups to be the most important of these. Recently, equine CRH has been shown to be identical to human CRH [Livesey *et al.*, 1991], and so it is also identical to rat CRH [Rivier *et al.*, 1983]. Such uniformity across species suggests an important physiological role for CRH. In this context, note that the structure of AVP is identical across all species in which it is present [Martin, 1985].

The pituitary actions of CRH appear to be confined to corticotropes, all of which appear to possess specific, high affinity receptors for CRH [Childs and Unabia, 1990; Childs *et al.*, 1987]. Figure 5.4 illustrates the current knowledge about the intracellular

mechanisms behind ACTH secretion. It should be consulted when reading the rest of this paragraph and for any undefined abbreviations. Binding of CRH to its receptor presumably stimulates the dissociation of the stimulatory nucleotide-binding protein (G_s) into α_s and $\beta \cdot \gamma$ subunits by catalysing the exchange of GTP for GDP on the α_s subunit [Holmes *et al.*, 1984; Perrin *et al.*, 1986]. α_s-GTP stimulates adenylate cyclase (AC), which is the membrane-bound enzyme responsible for catalyzing the production of cyclic adenosine 3,5-monophosphate (cAMP) from Mg^{2+}·ATP [Abou-Samra *et al.*, 1987a]. α_s-GTP also appears to be involved in terminating binding of CRH to its receptor. An increase in intracellular cAMP results in the dissociation of regulatory sub-units from cAMP-dependent protein kinase A, which then regulates the phosphorylation of unidentified protein substrates, leading to increased synthesis and secretion of ACTH [King and Baertschi, 1990]. cAMP may also have a direct effect on Ca^{2+} channels [Thomson and Smith, 1989]. There is compelling evidence to link the ACTH response with a rise in intracellular Ca^{2+}[Guérineau *et al.*, 1991; Leong, 1988], which arrives from the extracellular medium due to the altered electrical status of the corticotrope membrane [Won and Orth, 1990], or through receptor operated channels. The precise mechanism is undetermined. Ca^{2+}-calmodulin kinases, but not internal sequestered Ca^{2+}, also appear to be important [Won and Orth, 1990].

In humans the peripheral effects of CRH are reduced by the presence of a CRH-binding protein, but this does not seem to impair the pituitary actions of hypothalamic CRH [Linton *et al.*, 1990]. Evidence of a CRH-binding protein has recently been found in the horse hypothalamus [Livesey, personal communication], although its purpose there is uncertain. CRH reactivity is found at many sites around the mammalian body, with the highest mean levels occuring in the median eminence [Emeric-Sauval, 1986]. The gut, liver, cerebral cortex, pancreas, lungs, adrenal medulla, and thymus gland are among the peripheral sources of CRH contributing most of the hormone in circulation [Lowry *et al.*, 1986]. Hypothalamic CRH ensures that the corticotropes will always be exposed to higher CRH concentrations than those present in peripheral blood, although under some conditions, e.g. abdominal surgery, peripheral sources of CRH may contribute more to pituitary CRH concentrations than the median eminence [Alexander, unpublished; Donald and Ellis, unpublished; Wittert, unpublished].

Despite its name, CRH is not the only hormone involved in stimulating pituitary ACTH secretion [Gillies *et al.*, 1982; Rivier and Vale, 1983b]. In the past, experimenters have found that pharmacological doses of CRH do indeed stimulate ACTH secretion more than the same quantities of AVP or other regulators [Antoni, 1986; Dallman *et al.*, 1987a; Livesey *et al.*, 1988], however the physiological relevance of these results is questionable. Pregnant women have very high levels of circulating CRH, but only slightly elevated ACTH's [Thomson and Smith, 1989]. Conversely, athletes and Addison's disease patients have lower plasma CRH levels than controls, but higher ACTH concentrations [Wittert *et al.*, 1992; Wittert *et al.*, 1991]. In these situations, either CRH is not the predominant ACTH secretagogue, or its periperal concentrations do not reflect those present in the pituitary. Note that concentrations of ACTH secretagogues at the corticotropes may be enormously greater than those in systemic circulation, due to the tiny amount of blood in the hypothalamo-pituitary portal system. In the horse this ratio of pituitary to jugular concentrations can be as much as 10^4 for AVP, but is less than 50 for CRH [Irvine, unpublished]. So, although AVP is only around 14% as potent a

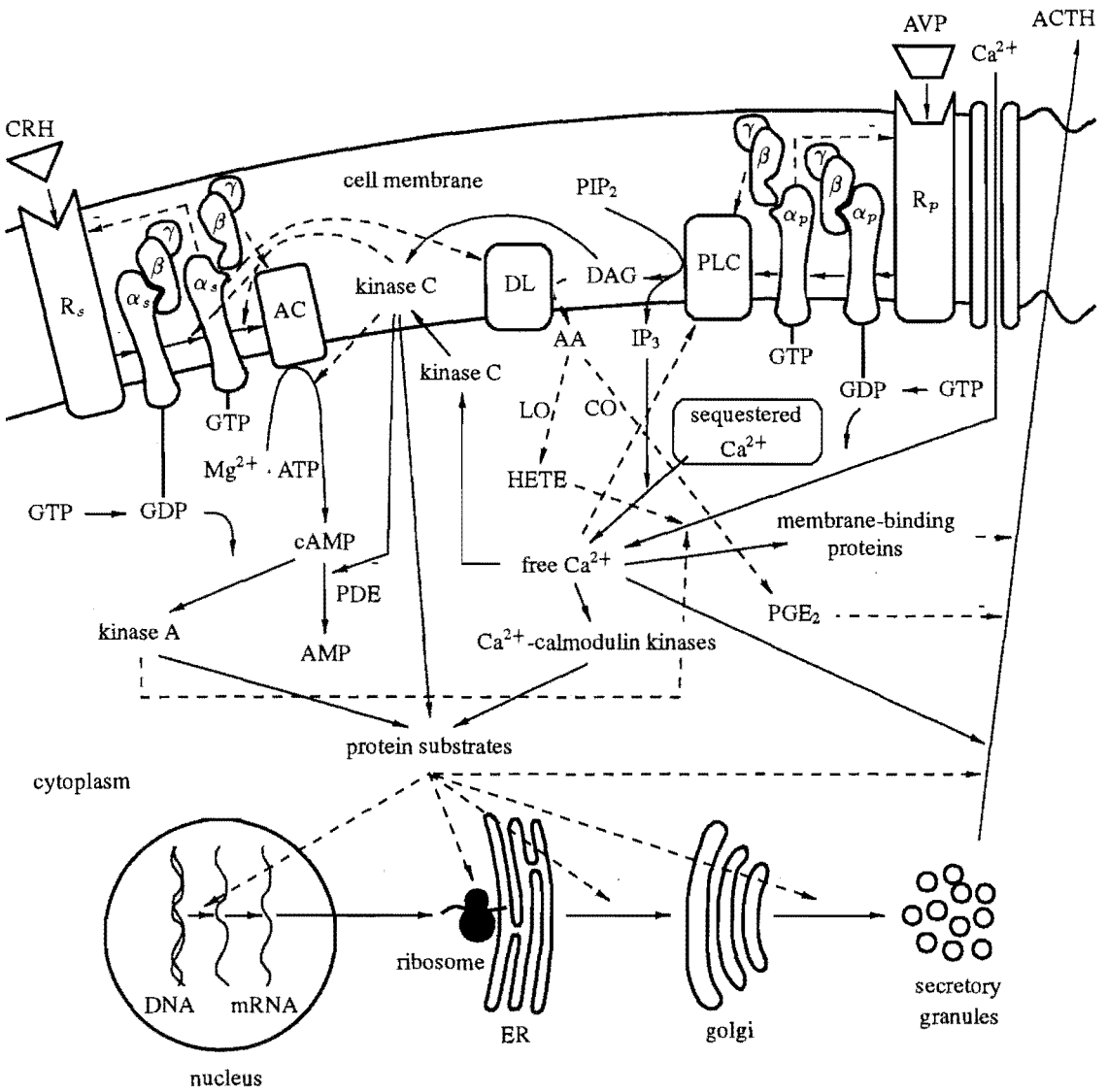

Figure 5.4 Schematic representation of the intracellular mechanisms that lead to ACTH release from corticotropes. Dashed lines represent pathways that are not well understood. All effects are stimulatory, except where '-' signs are present. Abbreviation meanings are: $\alpha_{s/p} \cdot \beta \cdot \gamma$, stimulatory guanine nucleotide-binding protein; AA, arachidonic acid; ATP, adenosine trisphosphate; cAMP, cyclic adenosine 3,5-monophosphate; CO, cycloxygenase; DAG, diacylglycerol; DNA, deoxyribonucleic acad; DL, diacylglyceride lipase; ER, endoplasmic reticulum; GDP, guanosine diphosphate; GTP, guanosine trisphosphate; HETE, 12-OH,5,8,10,14 eicosatetraenoic acid; IP_3, inositol 1,4,5-trisphosphate; mRNA, messenger ribonucleic acid; LO, lipoxygenase; PDE, cAMP phosphodiesterase; PGE_2, prostaglandin E_2; PIP_2, phosphatidylinositol-4,5,bisphosphate; PLC, Phospholipase C; $R_?$, a receptor. The important mechanisms shown above form the basis for a proposed model of ACTH regulation in Chapter 7. Figure obtained in part from [King and Baertschi, 1990].

secretagogue, in the rat, as equimolar CRH [Watanabe and Orth, 1987], it may still be more important than CRH *in vivo*, if circulating concentrations are similar. Obviously, knowledge of hormone concentrations at the pituitary is vital to determine the effects of ACTH secretagogues. Recent *in vivo* experiments in sheep, rats and horses, which sample the blood at the level of the pituitary, have demonstrated much greater rises in AVP than CRH in response to stress [Alexander *et al.*, 1991; Caraty *et al.*, 1990; Engler *et al.*, 1989; Plotsky, 1991; Plotsky *et al.*, 1985]. These observations suggest that AVP may be the more potent secretagogue. Relative receptor concentrations vary between species, and may explain some species differences in responsiveness to AVP and CRH [Liu *et al.*, 1990; Shen *et al.*, 1990]. In addition, the predominance of either AVP, or CRH, in regulating ACTH seems to depend on the type of stress involved [Gibbs, 1986; Plotsky, 1991; Rivier and Plotsky, 1986; Whitnall, 1989], the history of exposure to stress [Silverman *et al.*, 1989], the glucocorticoid concentrations [Childs and Unabia, 1990; Nicholson and Gillham, 1989; Shipston and Antoni, 1991], and possibly the animal's reproductive state [Sawchenko, 1989].

5.2.2 Arginine Vasopressin (AVP)

AVP derives its name from observations that high concentrations stimulate the smooth muscle of the blood vessels to contract, with physiological concentrations being likely to perform some related functions [Share, 1988]. AVP is also known as antidiuretic hormone (ADH), which better describes its major peripheral role in promoting water conservation at the kidney [Martin, 1985].

The importance of AVP in the regulation of the adrenal axis is becoming increasingly evident. *In vitro* it synergizes with CRH to stimulate ACTH secretion [Evans *et al.*, 1988; Marshall *et al.*, 1991] and in some preparations it is the more potent secretagogue [Familari *et al.*, 1989; Liu *et al.*, 1990]. The important role of AVP in physiological ACTH release is well established [Alexander *et al.*, 1988; Brooks, 1989; Bruhn *et al.*, 1984b; DeBold *et al.*, 1984; Ellis *et al.*, 1990; Engler *et al.*, 1989; Gibbs, 1986; Irvine *et al.*, 1989; Linton *et al.*, 1985; Liu *et al.*, 1983; Livesey *et al.*, 1988; Milsom *et al.*, 1985; Plotsky, 1991; Plotsky *et al.*, 1985; Redekopp *et al.*, 1985; Redekopp *et al.*, 1986; Rittmaster *et al.*, 1987; Rivier and Vale, 1983a; Scaccianoce *et al.*, 1991; Whitnall, 1989], with more recent experiments providing good evidence that it is the main ACTH secretagogue, at least in the horse [Alexander *et al.*, 1991].

AVP appears to act through a specific receptor which is expressed by around 80% of corticotropes in the anterior pituitary [Childs and Unabia, 1990; Du Pasquier *et al.*, 1991], and is associated with an intracellular pathway involving phospholipase C (PLC). Consultation of figure 5.4 should help the reader understand the following description of this pathway. Binding of AVP to its receptor presumably stimulates a G-protein (G_p), in much the same way as previously described for CRH. The α_p-GTP subunit activates a membrane-associated enzyme PLC, which is then able to hydrolyze the membrane phospholipid phosphatidylinositol-4,5-bisphosphate (PIP_2). This yields both inositol trisphosphate (IP_3) and diacylglycerol (DAG). IP_3 is water soluble and enters the cytosol to liberate Ca^{2+} from intracellular stores, possibly by binding to portions of the endoplasmic reticulum (ER). DAG remains in the plasma membrane and activates protein kinase C (PKC) which has been translocated to the membrane by Ca^{2+}.

Activated PKC phosphorylates unidentified protein substrates, leading to increased secretion, and possible synthesis of ACTH [King and Baertschi, 1990]. In addition, PKC feeds back to decrease IP_3 production and increase IP_3 metabolism, thus controling the rise in cytosolic Ca^{2+}[Abou-Samra *et al.*, 1987b]. Along with activating protein kinase C, DAG is also hydrolyzed to arachidonic acid (AA) by diacylglyceride lipase. Like CRH, AVP also leads to activation of plasma membrane Ca^{2+}channels, although these may be different to those activated by CRH [Aguilera *et al.*, 1986]. The end result of *in vitro* activation of this pathway by AVP is an initial transient spike of ACTH, followed by a sustained plateau response that persists for as long as AVP is present [Oki *et al.*, 1990]. The initial spike of ACTH seems to be principally mediated through IP_3 and sequestered Ca^{2+}. The sustained plateau depends on calmodulin activation and extracellular Ca^{2+}influx through voltage-sensitive Ca^{2+}channels, as a result of protein kinase C activation [Koch and Lutz-Bucher, 1991; Oki *et al.*, 1990; Won *et al.*, 1990].

Most of the AVP reaching corticotropes appears to be secreted into the hypothalamo-pituitary portal vessels as a consequence of preterminal release from magnocellular neurons which project to the neural lobe [Antoni *et al.*, 1990]. Neurons which project from the PVN to the external zone of the median eminence also release AVP into the hypothalamo-pituitary portal vessels [Zimmerman and Silverman, 1983], and it is conceivable that additional AVP may reach these vessels by retrograde flow from the neural lobe [Oliver *et al.*, 1977], although this is controversial [Bergland and Page, 1978; Recht *et al.*, 1981]. In addition, high concentrations of AVP reach corticotropes through a capilliary plexus shared by the pars distalis and neural lobe, known as short portal vessels [Bergland and Page, 1979; Bergland and Page, 1978]. Thus, two distinct populations of neurons supply AVP to corticotropes: magnocellular neurons from the PVN and SON which terminate in the neural lobe, and parvocellular neurons from the PVN which terminate in the median eminence [Antoni *et al.*, 1990; Defendi and Zimmerman, 1978; Gibbs, 1986]. The percentage of AVP released from the hypothalamus which eventually perfuses the corticotropes is still a matter for debate [Antoni, 1986].

5.2.3 Potentiation

The terms *potentiation* and *synergism* are used synonymously here to mean that when two compounds act together they produce a greater effect than the sum of the effects of each acting alone. Potentiation between CRH and AVP is an important component in the multifactorial regulation of ACTH production [Evans *et al.*, 1988]. AVP administered with maximally stimulating concentrations of CRH greatly increases ACTH release [Gillies *et al.*, 1982], and concentrations of either secretagogue, which are too low to elicit a response singly, are able to potentiate the response to the other [Marshall *et al.*, 1991]. In addition, dose response curves for combined AVP and CRH are much steeper than those for either secretagogue alone [Rivier and Vale, 1983a]. CRH has also been observed to synergise with other compounds (e.g. oxytocin), although the physiological relevance of this is not established.

The physiological understanding of potentiation may be changing. While most researchers have shown that low levels of AVP potentiate the ACTH response to CRH [Antoni, 1986], low concentrations of CRH are also able to potentiate the ACTH response to AVP [Marshall *et al.*, 1991]. In the light of recent findings on the relative physiological

effects of CRH and AVP [Alexander *et al.*, 1991], the second situation may be more realistic, although species variations are also possible.

Most corticotropes are responsive to both CRH and AVP [Jia *et al.*, 1991], and so the interaction of CRH- and AVP-responsive intracellular messenger systems in the corticotrope provides some logical explanation for the synergism between CRH and AVP. Potentiation by AVP of the action of CRH on cAMP is the best established of many possible interactions [Abou-Samra *et al.*, 1987c; Labrie *et al.*, 1987; Thomson and Smith, 1989]. This interaction appears to depend on protein kinase C, which may increase cAMP accumulation by phosphorylating cAMP-dependent phosphodiesterase (PDE), the CRH receptor, its associated nucleotide-binding protein (G_s), or adenylate cyclase (AC) (see figure 5.4) [Bilezikjian and Vale, 1987; King and Baertschi, 1990]. The most substantiated of these mechanisms is the decrease in cAMP degradation with PDE inactivation. Evidence that potentiation does not occur when AVP application precedes that of CRH [Watanabe and Orth, 1987], suggests that the other mechanisms are less physiologically relevant.

There is also evidence that protein kinase A, kinase C and Ca^{2+}-calmodulin kinases could interact by phosphorylating substrates involved in ACTH release, so giving rise to potentiation [Antoni, 1986; King and Baertschi, 1990]. Furthermore, there is evidence that potentiation may occur due to paracrine interactions between corticotropes [Schwartz, 1990], but this will be discussed in Chapter 7. AVP and CRH both increase cytosolic Ca^{2+}, but convergence of these two pathways to potentiate ACTH release is unlikely given evidence that Ca^{2+}removal does not affect synergism [Oki *et al.*, 1991; Oki *et al.*, 1990; Won *et al.*, 1990]. Similarly, arachidonic acid metabolism, which is stimulated by both secretagogues to open Ca^{2+}channels, is unlikely to be involved in synergism.

Pretreatment by AVP increases the number of CRH-receptive pituitary cells and vice versa [Childs and Unabia, 1989; Childs, 1987]. This effect will aid potentiation although it may not be rapid enough to explain any immediate synergistic effects. AVP pretreatment also seems to prepare ACTH secretory granules for more efficient secretion [Childs, 1987], while both AVP and CRH are able to stimulate ACTH synthesis, depending on the species [Autelitano *et al.*, 1990; Liu *et al.*, 1990; Murakami *et al.*, 1984]. Potentiation may be aided by a host of such mechanisms. Another effect which has been demonstrated *in vitro* is *desensitization*, which describes reduced ACTH responsiveness following repeated stimulation of corticotropes [Aguilera *et al.*, 1987; Evans *et al.*, 1988]. This effect is currently considered to be unimportant *in vivo* [Schopohl *et al.*, 1986]. The opposite effect of increased secretory ability following stimulation has also been observed [Antoni and Dayanithi, 1990; Watanabe and Orth, 1987].

5.2.4 Cortisol (F)

ACTH induces the release of glucocorticoids from the adrenal cortex. These, in turn, act at multiple sites around the body to alleviate the conditions which stimulated ACTH release, and also attenuate ACTH secretion in a very tightly regulated fashion [Grossman and Tsagarakis, 1989; Keller-Wood and Dallman, 1984; Livesey *et al.*, 1988]. The major glucocorticoid for humans, horses, monkeys and some other mammals is cortisol [Ng *et al.*, 1981].

At the level of the pituitary, cortisol appears to block ACTH synthesis by suppressing transcription of the POMC gene [Lundblad and Roberts, 1988; Roberts *et al.*, 1987]. It blocks ACTH release by decreasing the rise in intracellular Ca^{2+} which preceeds ACTH release and possibly by also reducing cAMP accumulation [King and Baertschi, 1990; Oki *et al.*, 1991]. In addition, cortisol effects the expression of AVP and CRH receptors by corticotropes [Childs and Unabia, 1990].

While part of the cortisol negative feedback signal is mediated at the level of the corticotrope [Roberts *et al.*, 1987], a proportion also acts at the hypothalamus and *hippocampus* to reduce ACTH secretagogues [Canny, 1990; Dallman *et al.*, 1987b; Levin *et al.*, 1988; Spinedi *et al.*, 1991]. Interestingly, while the hippocampal relationship between cortisol and CRH inhibition appears essentially linear, there may be a nonlinear threshold relationship with AVP and oxytocin [Sapolsky *et al.*, 1990]. This is supported by observations that AVP concentrations increase more than those of CRH following cortisol removal or suppression [Alexander, unpublished; Plotsky and Sawchenko, 1987], suggesting that AVP and oxytocin may be subject to tighter feedback control. Recent *in vitro* research also demonstrates that glucocorticoids are more effective at blocking the ACTH response to CRH than AVP [Nicholson and Gillham, 1989; Oki *et al.*, 1991; Shipston and Antoni, 1991]. One of the major conclusions in Chapter 7 concerns the relative importance of these two effects *in vivo*.

Wherever cortisol acts, and this is not yet well defined, in the pituitary there appears to be a complicated temporal relationship between cortisol concentrations and the resulting inhibition of ACTH, even though such a relationship in a feedback loop is destabilizing. Three distinct phases of inhibition have been observed: fast – within seconds to minutes, intermediate – 2-10 hours, and slow – hours to days [Dayanithi and Antoni, 1989; Keller-Wood and Dallman, 1984]. The slow domain is only observed after chronic elevation of cortisol, and hence, is not of physiological relevance. Intermediate domain feedback requires that the glucocorticoid history be known to predict ACTH response to secretagogues, while inhibition of ACTH by fast feedback may be linearly related to the rate of glucocorticoid increase [Keller-Wood and Dallman, 1984].

5.2.5 Additional ACTH regulators

In the rat elevated oxytocin levels act to release ACTH *in vivo* [Rivier and Vale, 1985], but in other species oxytocin has variable effects on ACTH secretion [Gibbs, 1986]. More recent research demonstrates significant correlation between oxytocin and ACTH in the horse, but only when sex hormones are elevated [Irvine, unpublished]. This suggests that, although its physiological importance is unproven, in some situations oxytocin may well regulate ACTH release, both on its own and in synergy with CRH.

Angiotensin II causes ACTH release from dispersed rat pituitary cells [Ganong and Murakami, 1987], but infusion of acute levels of angiotensin II has not been shown to regulate ACTH secretion *in vivo* [Brooks, 1989]. Therefore angiotensin II's physiological role in ACTH release appears to be in stimulating CRH secretion, and not through a direct action on corticotropes.

In the rat catecholamines appear to influence ACTH release *in vivo* [Bruhn *et al.*, 1984a; Plotsky *et al.*, 1989], but in non-rodents it seems that catecholamines do not exert a significant influence on ACTH secretion at the level of the pituitary, although

they may well facilitate CRH secretion [Milsom *et al.*, 1986; Palkovits, 1987; Plotsky *et al.*, 1989].

Administration of the opioid receptor antagonist, naloxone, increases both basal and stress-induced ACTH secretion [Irvine and Alexander, unpublished; Negro-Vilar *et al.*, 1987]. This effect indicates that an endogenous opioid, of unknown nature, inhibits physiological ACTH release.

Atrial natriuretic factor has been recently proposed as a physiological ACTH inhibitor [Fink *et al.*, 1991].

In addition to the compounds listed above, a number of other substances are able to influence ACTH secretion from pituitary, fetal, or tumor tissue, although their physiological importance is doubtful [Antoni, 1986].

There is also the possibility that additional physiological ACTH regulators are still undiscovered. In support of this idea are observations that: (a) median eminence extract has significantly greater ACTH releasing ability than can be accounted for by its AVP and CRH content [Buckingham, 1985; Ellis, unpublished]; (b) median eminence extract contains ACTH regulators that have different molecular weights to AVP and CRH [Gillies *et al.*, 1984]; (c) removal of hypothalamic input leads to a rise in basal levels of ACTH [Engler *et al.*, 1988]; (d) partial purification of an ACTH-inhibiting factor has been reported [Redei and Evans, 1989]; and (e) in pituitary blood peaks of ACTH cannot always be associated with AVP or CRH peaks [Engler *et al.*, 1989] (see also section 7.2).

5.3 Summary

Sections 5.1 and 5.2 have provided the background to ACTH regulation, while also including information (e.g. intracellular mechanisms) which would be clumsy if included in the context of the research which follows. In brief, AVP and CRH are produced in the hypothalamus in response to stress and travel, via different paths, to the pituitary where they stimulate secretion of ACTH from corticotropes. They act through different intracellular pathways, and hence, result in ACTH responses with different profiles. These intracellular pathways also interact so that when CRH and AVP are both present the ACTH response is greater than the sum of the separate individual responses. ACTH travels from the pituitary to the adrenal glands where it stimulates production of cortisol which helps the animal respond to the initial stress. In addition, cortisol feeds back to the brain to reduce AVP and CRH secretion, and to the pituitary to reduce ACTH release.

If effects at all components of the adrenal axis are considered, cortisol has the greatest influence on ACTH secretion, although at the corticotrope the magnitude of the influences of AVP, CRH and cortisol appear to be more similar and depend on the type of stress, the stress history, the animal, and the species involved. ACTH secretion may also be affected by other hormones such as oxytocin.

CHAPTER 6

Analysis of Experimental Data

All investigations of ACTH regulation are based around experimental data, which is subject to both unavoidable error and problems with experimental procedures. This chapter deals with these difficulties, thus enabling data obtained using different experimental techniques to be combined usefully to investigate physiological ACTH regulation. Sections 6.1 and 6.2 discuss the advantages and disadvantages of some important *in vivo* and *in vitro* experimental methods. Emphasis is on the novel technique of sampling the blood leaving the pituitary, pioneered by Irvine and Alexander [1987], which provides the majority of the data on which the research contained in Part II of this thesis is based. The author is extremely grateful to Professor Cliff Irvine and Dr Sue Alexander for providing this data. Its non-ideal nature is investigated further in section 6.3, in particular the effects of sampling rate and blood flow variations.

6.1 *In Vivo* Experimental Techniques

Corticotropes in the adenohypophysis synthesize and secrete ACTH in response to receptor binding of AVP, CRH, cortisol and possibly some other less important factors. It is also possible that communication between cells occurs, presumably by transfer of analogs of intracellular messengers, and that this may influence ACTH release [Jia *et al.*, 1991; Schwartz, 1990]. The important fact is that ACTH release depends exclusively on the concentrations of relevant substances which are perifusing, or have perifused, the corticotropes. *In vivo* experiments which try to estimate these concentrations are fraught with difficulties of access to the hypothalamo-pituitary region, while interpretation of the measurements made is impeded by the *in vivo* environment. One is unable to identify the direct effects of ACTH secretagogues unambiguously, as they will have non-specific pituitary and extra-pituitary actions, and these effects may be modulated by factors which are not measured or even identified. In addition, attempts to identify the response to a particular hormone, through a systemic administration scheme designed to duplicate pituitary concentrations, may require up to a 10^4 fold increase in peripheral concentrations. Such high peripheral concentrations may cause important non-specific effects. Nevertheless, such *in vivo* experiments are essential to understanding the physiological regulation of ACTH secretion.

6.1.1 Non-invasive pituitary effluent sampling (PES)

A "non-invasive" method to directly measure pituitary effluent in the horse has been recently developed and verified by Irvine and Alexander [1987]. The method begins with placement of a cannula into an incision in the facial vein. The cannula is then manipulated into the venous drainage system of the head, so that the tip lies in the intercavernous sinus (ICS) close to the outlet of the pituitary veins, as shown in figure 6.1. This method of sampling pituitary effluent, henceforth termed PES, is feasible only in the horse due to the unique venous drainage of its pituitary [Sisson, 1914]. In contrast, blood in the cavernous sinus of the sheep [McFarland *et al.*, 1960] and the monkey [Neill *et al.*, 1977], does not contain high concentrations of hypothalamic and pituitary hormones. Cannula placement and blood collection are carried out painlessly in fully conscious, ambulatory, unstressed animals. The remarkable affinity between horse and human, along with the non-invasive nature of this cannulation technique, then enables the adrenal axis to be studied under stress-free and totally physiological conditions.

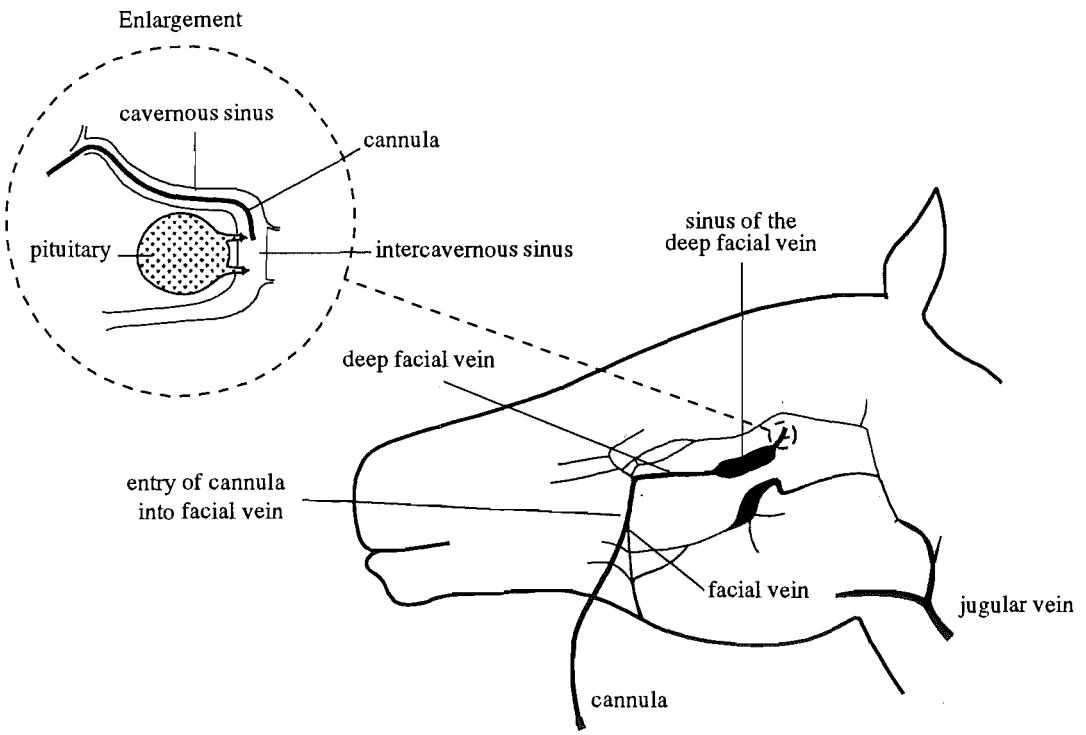

Figure 6.1 Pathway of the cannula through the veins of the horse head to the outlet of the pituitary. (Reproduced from [Irvine and Alexander, 1987])

Throughout this thesis emphasis is placed on the physiological relevance of any experimental findings. This is because the majority of *in vivo* experiments investigating the adrenal axis involve either pharmacological hormone administration, or subjects which are already under considerable stress, and hence, the results are difficult to relate to the normal operation of the adrenal axis. A major advantage of PES is that the animal is in a completely normal state, and sampling can continue even during vigorous exercise. Furthermore, the large blood volume of the horse permits collection of 3ml of pituitary effluent every 30*s*, while removing only around 30% of pituitary hormone

secretion. The importance of sampling at this rate will be discussed in section 6.3.4, while 3ml samples permit ACTH, CRH, AVP, oxytocin and cortisol to be assayed in the same sample. Removal of approximately 30% of the ACTH produced will cause some peripheral reduction in the cortisol response to stress, compared to controls, but this is unlikely to have a major effect on ACTH regulation at the level of the corticotrope. The total amount of blood removed is less than 4% of the total blood volume, even when experiments take 500 samples. PES also allows animals to be used for long term studies because correct cannulation has no adverse effects on a horse's well-being.

One disadvantage of PES by ICS cannulation is that it is possible only in the horse. The horse is not widely used as either an endocrinological model or an experimental subject, and so basic knowledge of equine hypothalamic and pituitary function is limited. However, hormones at each tier of the adrenal axis are structurally identical to those in the human [Livesey *et al.*, 1991; Martin, 1985; Ng *et al.*, 1981], and cortisol is the principal glucocorticoid [James *et al.*, 1970], so biochemically the horse is closely related to the human.

6.1.2 Sampling pituitary portal blood

Hypothalamic hormone concentrations may be obtained by sampling blood from the portal vessels connecting the median eminence to the adenohypophysis. This experimental method has been used on rats, sheep and monkeys [Plotsky, 1991; Engler *et al.*, 1989]. In preparation for portal blood collection, animals are subjected to urethane anethesia and considerable acute surgical intervention. Therefore measurements of hormone concentrations in the portal blood represent changes after an initial marked perturbation of the adrenal axis, and their physiological relevance is doubtful [Plotsky, 1991; Plotsky and Vale, 1984]. An indication of the size of the perturbation in transnasal collection of pituitary portal blood in the sheep is given by the relative basal portal concentrations of adrenal axis hormones: CRH 18–127pmol/l basal, AVP 20–2034pmol/l basal, systemic ACTH 15–30pmol/l [Engler *et al.*, 1989]. These concentrations are much higher than those measured by PES in unstressed horses, e.g. CRH 0–2pmol/l basal, AVP 0-5pmol/l basal and systemic ACTH 10pmol/l.

Comparison of these figures shows that portal sampling experiments have less physiological relevance than PES experiments in the horse, which is presumably a very important consideration in the study of the adrenal axis. Since portal blood measurements in the rat and monkey involve substantial tissue damage, there are also likely to be disproportionately high levels of CRH arriving from "tissue" sources. In addition, the small volume of blood in the long portal vessels restricts sampling to once every 5 minutes in the sheep [Engler *et al.*, 1989], and once every 20 minutes in the rat [Plotsky, 1991]. PES has shown that intervals of hormone secretion occasionally last less than $20s$ and often less than $60s$. Portal sampling therefore misses much of the hormone signal, where the missing "information" may be particularly important in understanding the adrenal axis (see section 6.3.4).

6.1.3 Sampling circulating blood

Because of the enormous dilution of pituitary blood that occurs after it leaves the pituitary, circulating hormone concentrations do not reflect those at the pituitary. Instead, they result from the combined influences of prior and ongoing hormone secretion, along with relevant hormone distribution and elimination kinetics, associated with metabolism and/or removal of intact hormone from the circulation. One simple method to obtain pituitary hormone concentrations, at least from the experimentalist's viewpoint, is to reconstruct them from their concentrations in circulating blood using deconvolution. If a rise in peripheral hormone concentration is attributed to an episode of secretion by the hypothalamus or pituitary, and some assumptions are made about the disappearance kinetics, then deconvolution of peripheral blood concentrations can be used to estimate pituitary concentrations of the hormone in question [Veldhuis and Johnson, 1990a; Veldhuis, 1991]. Providing pituitary hormone concentrations consist of large well spaced (compared to plasma half life) pulses of secretion, separated by regions of low secretion, and there are no significant peripheral sources of hormone, then this technique has the potential to work well, particularly when one has good models of hormone secretion and disappearance. It seems to be a useful method for studying the reproductive axis [O'Sullivan and O'Sullivan, 1988; Hindmarsh *et al.*, 1990; Veldhuis *et al.*, 1990b; Veldhuis, 1991], although the deconvolution model has not been validated *in vivo*. There may, however, be some major problems associated with its application to the adrenal axis.

PES has demonstrated that large pulses of ACTH and AVP may last less than $30s$, and more importantly, that they may be separated by less than $30s$. Since the half lives of these hormones are around 5-8 [López and Negro-Vilar, 1988], and 4-6 minutes [Lauson, 1974] respectively, the plasma hormone concentrations may fall by less than the assay error between such pulses, making recovery of meaningful information about these pulses difficult, even when the pulses are large. In addition, pituitary AVP and ACTH concentrations may be up to 500 and 50 fold greater, respectively, than peripheral concentrations, even under physiological conditions [Redekopp *et al.*, 1986]. This dramatically increases the noise sensitivity of any quantitative estimate of their pituitary concentrations from those in peripheral blood. Furthermore, the importance of rapid variations in adrenal axis hormones has been uncovered by PES [Alexander *et al.*, 1991], and is supported by the work in this thesis. 10 minute sampling seems to be most commonly used for deconvolution [Veldhuis *et al.*, 1990a], but this sampling rate has the potential to recover only between 5 and 25% of the variation in pituitary concentrations of ACTH or AVP (see section 6.3.4). Deconvolution will obviously recover less than this. Attempts to recover more information by deconvolving more rapid samples [Iranmanesh *et al.*, 1990] are compromised by the ill-posed nature of the process (i.e. it is inherently noise sensitive), and when the sampling interval is much less than the half life of a hormone, typical assay noise may prevent one from obtaining virtually any useful information, except about large peaks [Veldhuis and Johnson, 1990b]. Deconvolution therefore appears unable to reveal the rich nature of variations in many pituitary hormones which has been uncovered by PES, and which is hinted at by spectral analysis of rapidly sampled plasma hormone concentrations [Carnes *et al.*, 1991].

Another problem with using deconvolution to estimate pituitary concentrations of adrenal axis hormones is that in mammals CRH is mainly produced by peripheral sources, rather than in the hypothalamus [Alexander, unpublished]. Under these circumstances, one can attempt to reconstruct CRH secretion, but the reconstruction will not reflect CRH concentrations at the corticotropes.

6.1.4 Adrenal axis manipulation

A number of experimental techniques are available to isolate various aspects of the adrenal axis, including surgical lesioning/removal of adrenal axis pathways or components, immunoneutralization of ACTH regulators and administration of ACTH regulator receptor antagonists. In interpreting results obtained using such techniques, one should not neglect their substantial side-effects [Antoni, 1986].

6.2 *In Vitro* Experimental Techniques

Although *in vitro* studies have provided a wealth of information on corticotrope function, isolated endocrine cells do not always behave in the same way as they do in the whole animal. Enzymatic dispersion may disrupt paracrine interactions between cells, and can compromise cell-surface proteins [Antoni, 1986]. Furthermore, suspension in aqueous medium will cause profound alterations in the shape of cells. Normally, corticotropes have a stellate appearance, with numerous processes 50-100μm long, however in suspension they are round (minimal surface) [Childs, 1987]. This, in all likelihood, is associated with changes in cytoskeletal organization, which could have marked effects on cell surface receptors and secretory processes [Antoni, 1986]. It would appear that dispersion reduces the response of corticotropes to AVP more than the response to CRH [Evans, personal communication; Rivier and Vale, 1983a]. This effect may explain some of the discrepancies between *in vitro* and *in vivo* studies. Other examples of changes in secretory processes are the increase in secretagogue concentration required to stimulate secretion *in vitro*, and the change in ratio of maximum to basal ACTH secretion from greater than 500 *in vivo* to approximately 10 in some *in vitro* preparations [Schwartz, 1990].

Cultured pituitary cells can also develop novel properties, which may not be relevant to conditions *in vivo* [Antoni, 1986]. Furthermore, the type of *in vitro* system used can influence results, with the response of corticotropes to CRF and AVP depending on the amount of time the cells have spent in culture, and on whether a static medium or perifusion system is employed [Evans *et al.*, 1992; Watanabe and Orth, 1988].

Another major obstacle to *in vitro* investigation of corticotrope activity is that corticotropes only comprise a small percentage of the cells in the adenohypophysis [Jia *et al.*, 1991]. Efficient and economical methods for obtaining high concentrations of corticotropes have yet to be developed, and this makes experiments to determine the cellular effects of ACTH regulators more difficult. A line of cells which secrete ACTH has been developed, but these AtT-20 cells express functional receptors for hormones that do not influence ACTH release by normal corticotropes, whereas they fail to respond to AVP [Axelrod and Reisine, 1984]. Results obtained from these cells have provided valuable

information on intracellular mechanisms, but the relevance of these results to normal corticotropes is clearly questionable.

6.2.1 Perifusion systems

Perifusion systems consist of a column containing dispersed cells, through which a medium containing test substances is pumped. They provide the best *in vitro* approximation to the operation of the pituitary, and if the column volumes are small enough, can duplicate normal hormone dynamics [Watanabe and Orth, 1987]. Other advantages over alternative *in vitro* techniques include minimizing hormone degradation, avoiding effects of nutrient depletion and metabolite accumulation, and cells can be repetitively stimulated to test reproducibility.

6.2.2 Static cell culture and single cell experiments

Static cell culture experiments involve incubating cells with test solutions in containers for a substantial amount of time. The concentration of products, or effect on cells, is then measured. Such experiments are simpler and cheaper to perform than perifusion experiments, but they give limited information about the time course of effects. In particular, the effects of CRH, AVP and cortisol on ACTH release are all time dependent [Oki *et al.*, 1991; Shipston and Antoni, 1991], limiting the interpretation of results from cell culture experiments.

Single cell studies involve observing the behaviour of single cells in response to test solutions. These experiments are most useful for determining the intracellular steps between corticotrope stimulation and ACTH secretion, along with information on the corticotropes involved.

6.3 Comments on PES Data

PES allows blood leaving the pituitary to be rapidly sampled under totally physiological experimental conditions. The data obtained opens an invaluable window on the operation of the endocrine system, but there are some problems in using it to study ACTH regulation at the corticotropes. Hormone concentrations in the adenohypophysis are continuously varying quantities which cannot be measured exactly, since: (a) the sampling process introduces distortion; (b) blood flow variations in the ICS may stop measured hormone concentrations from representing secretion rates; and (c) hormone concentrations in the ICS are not the same as those present at the corticotropes. This section sets out the effects of these three factors on the data produced by PES. Since the term *pulse* is used repeatedly herein, it is appropriate to define it as a significant rise followed by a significant fall in hormone concentration. Note that it is a single event having no association with a rhythm.

6.3.1 What is measured by PES?

A substantial proportion of the blood measured by PES has come from the neural lobe of the pituitary, and consequently, has not perifused the corticotropes in the adenohypophysis. The presence of this blood dilutes concentrations of adenohypophysial hormones and hormones produced by the hypothalamus which are released only into the adenohypophysis. One can calculate the dilution involved by comparing Luteinizing Hormone (LH) responses to endogenously generated and exogenously administered Gonadotropin Releasing Hormone (GnRH) pulses using

$$\text{dilution} = \frac{\text{LH}^{\text{endog}}}{\text{LH}^{\text{exog}}} \cdot \frac{\text{GnRH}^{\text{exog}}}{\text{GnRH}^{\text{endog}}} \tag{6.1}$$

where quantities in (6.1) represent the total amount of hormone in the pulse under consideration. Reproductive axis hormones are used because: (a) the dynamics of endogenous and exogenous GnRH are very similar (many hypothalamic hormones are produced in much shorter pulses); (b) GnRH pulses almost always cause LH pulses; and (c) LH is released solely from cells in the adenohypophysis. Equation (6.1) is derived with the knowledge that exogenous GnRH will be present in all blood entering the ICS in equal concentrations (neglecting any delays), while endogenous GnRH will be diluted by the unknown amount of blood. Thus, if the two LH pulses resulting from endogenous and exogenous GnRH pulses are the same size then the dilution of blood from the adenohypophysis is the ratio of the sizes of the GnRH pulses. If the LH pulses are not the same size then the dilution also depends directly on the LH size ratio. Performing the calculation in (6.1) using PES data shows that the dilution factor is usually around 10, although it may be dependent on reproductive state since dilutions of 2 and 10 have been observed in the same individual [Irvine, unpublished].

Equating a change in peripheral hormone concentration to the difference between hormone input from the pituitary and hormone loss due to metabolism allows the average blood flow past the tip of the ICS cannula to be determined by

$$F_{\text{ICS}} = \frac{[C^X_{\text{jug}}(T) - C^X_{\text{jug}}(0)]F_{\text{jug}} + L^X}{\int_0^T C^X_{\text{ICS}}(t) - C^X_{\text{jug}}(t)dt} \tag{6.2}$$

where $C^X_{\text{jug}}(t)$ and $C^X_{\text{ICS}}(t)$ are the concentrations of X in the general circulation and in the ICS respectively, L^X is the total amount of hormone eliminated from the blood between time 0 and T, and F_{jug} is the circulating blood volume (assumed constant). Information about blood flow through the pituitary [Porter *et al.*, 1970] then suggests that in good canulations approximately 75% of the blood sampled has entered the ICS directly from the pituitary [Irvine and Alexander, 1987].

The effect of neural lobe blood on concentrations of hormones like AVP and oxytocin is undetermined, since these hormones are released in both the neural lobe and the adenohypophysis. This means that PES may be unable to establish AVP and oxytocin concentrations at the corticotropes, and, in a worst case scenario, could not even establish their dynamics. Fortunately, recent research suggests that most of the AVP perifusing the corticotropes is derived from the same hypothalamic neurons that release AVP into the neural lobe [Antoni *et al.*, 1990], and that AVP concentrations measured by PES

have very similar dynamics to those in the adenohypophysis [Alexander *et al.*, 1988; Irvine *et al.*, 1989].

CRH is not released in the neural lobe, but under physiological conditions CRH concentrations measured by PES closely approximate those in systemic circulation, with a large gradient between pituitary and circulating concentrations occurring only as a result of chronic stress [Alexander, unpublished]. These results indicate that, under physiological conditions, PES provides more information about AVP concentrations than CRH concentrations at the corticotropes, even though initially one might assume the opposite. PES does, of course, provide excellent information about ACTH concentrations at the corticotropes.

6.3.2 Details of the most used experiments

In the course of subsequent analyses and discussions a limited set of "more informative" experiments will be referred to repeatedly. The complete set of adrenal axis experiments will be used only occasionally. To facilitate referencing this data, and to avoid repetition, this section sets out details on the most referred to experiments. All, or part of the data for experiments Horse79, Horse89 and Horse95 are also plotted so they can be used to support statements in the text.

Horse60: 300 samples were taken at 20s intervals. The horse was a mare called Annin. 0.15 units/kg of insulin were injected into the jugular at sample 125. ACTH, AVP and prolactin were measured in all samples.

Horse79: 226 samples were taken at 30s intervals, apart from between 53 and 81 minutes, when samples were taken at 1 and 5 minute intervals. The horse was a mare called Ellen. Boluses of 3μg AVP (42.5), 1μg CRH (91), 0.5μg CRH (106) and 3μg AVP (121) + 0.5μg CRH (120.5) were administered at the times shown in brackets. ACTH, AVP and CRH were measured in all samples.

Horse89: 500 samples were taken at 30s intervals. The horse was a mare called Matai Mist. At the beginning of the experiment 1.25g of metapyrone was injected in a 12.5ml bolus, followed by metapyrone infusion at a rate of 0.05g/min until 20 minutes before the end of the experiment. Metapyrone blocks the final stage in cortisol synthesis [Little *et al.*, 1958] and so reduces cortisol concentrations to very low levels. ACTH (1-500), AVP (1-460) and CRH (98-383) were measured in the samples indicated in brackets.

Horse95: The experimental scheme was identical to that for Horse89, but the horse was a mare called Premi. ACTH (1-472), AVP (1-472) and CRH (165-472) were measured in the samples indicated in brackets, although CRH was only assayed for alternate samples.

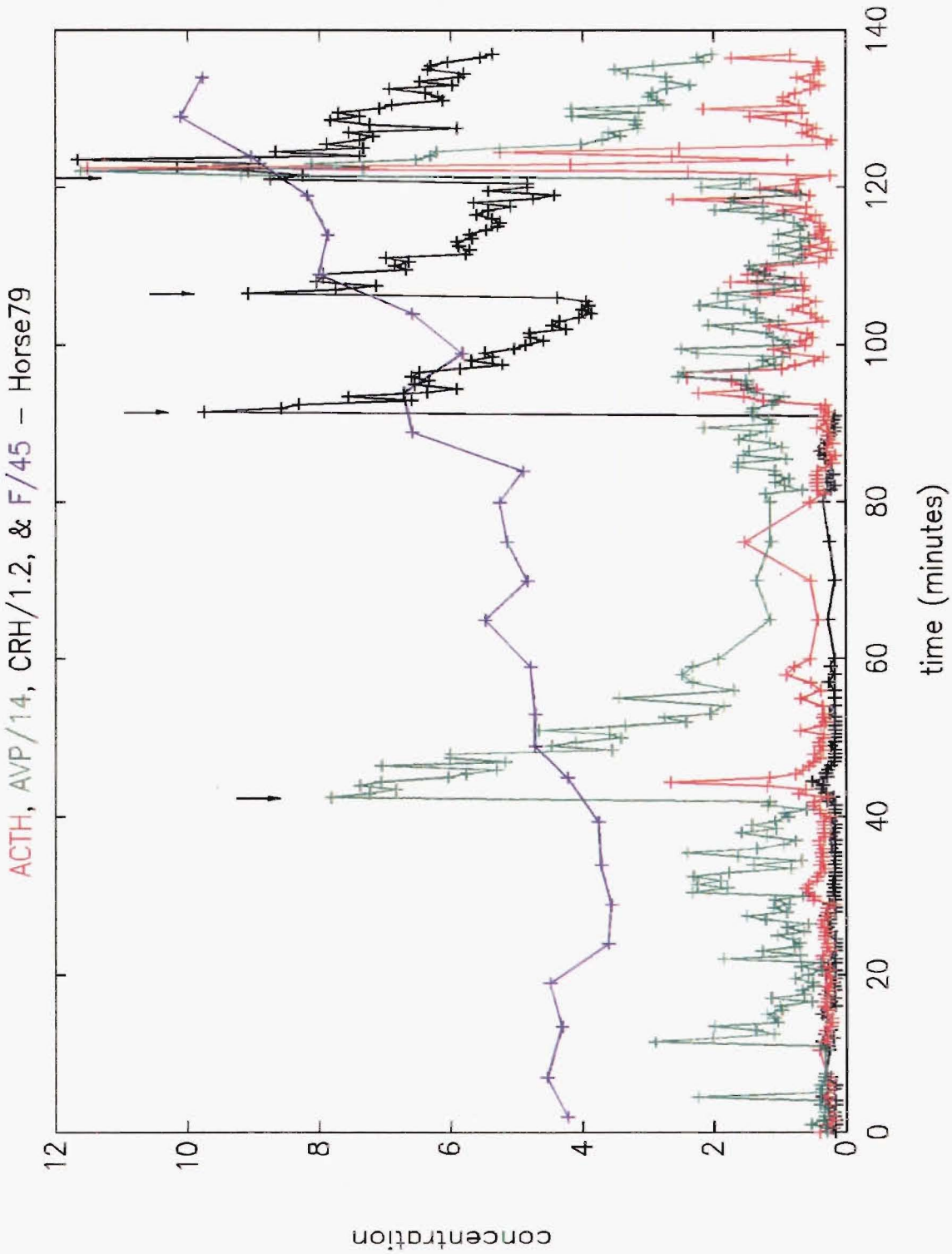

Figure 6.2 Concentrations of hormones measured in experiment Horse79. ACTH, in μg/l, is in red. AVP and CRH, in pmol/l, are in green and black respectively. Cortisol, in nmol/l, is in blue. Timing of AVP and CRH administration, which is described in the text, is indicated by 4 arrows.

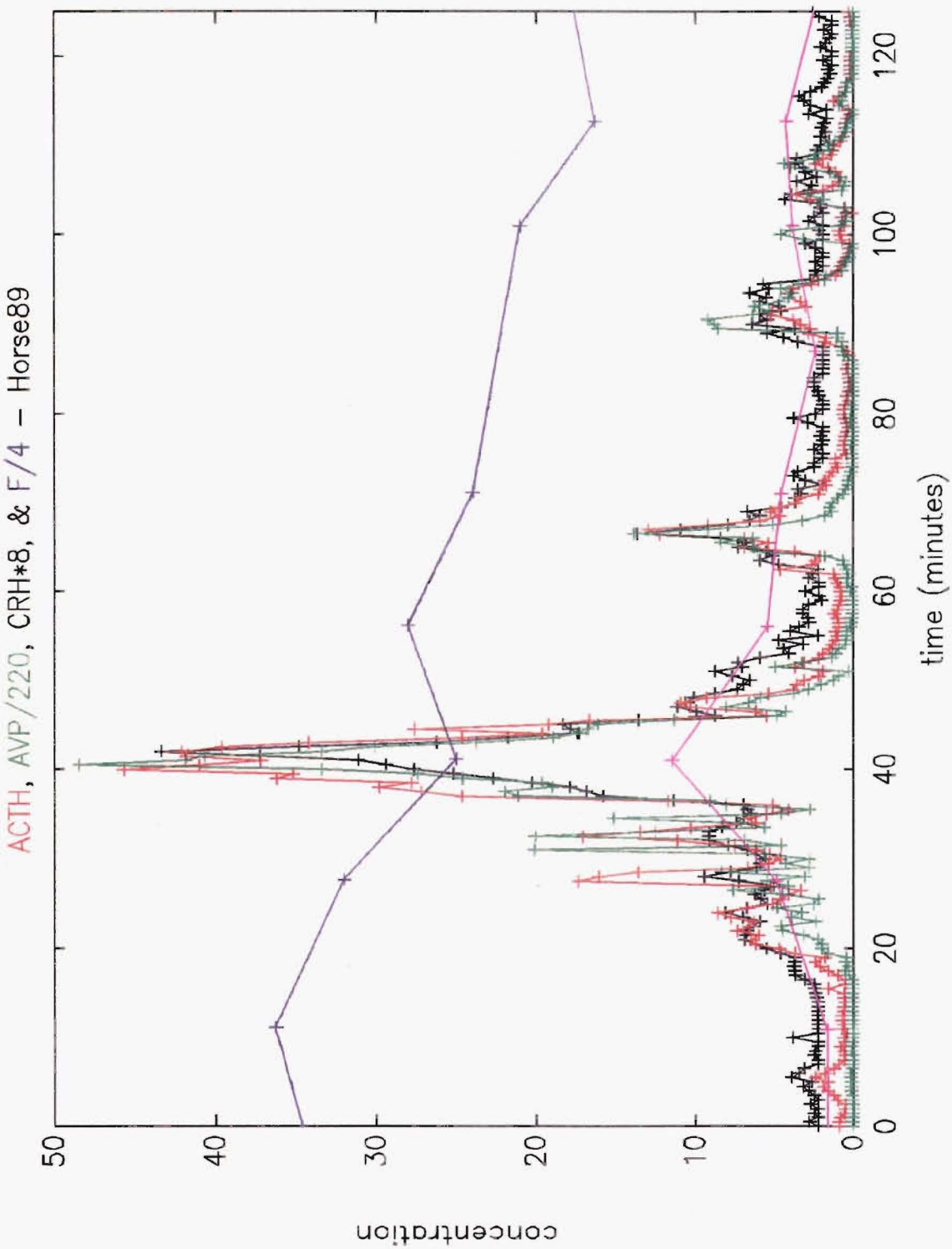

Figure 6.3 Concentrations of hormones measured in the part of experiment Horse89 where samples were assayed for CRH. Note that time zero therefore equates to sample 98 in the experiment. ACTH, in μg/l, is in red. AVP, CRH, and peripheral CRH, in pmol/l, are in green, black, and pink respectively. Cortisol, in nmol/l, is in blue. Cortisol concentrations plotted are as determined by the assay, but will exceed actual cortisol concentrations due to substantial crossreaction with 11-deoxycortisol.

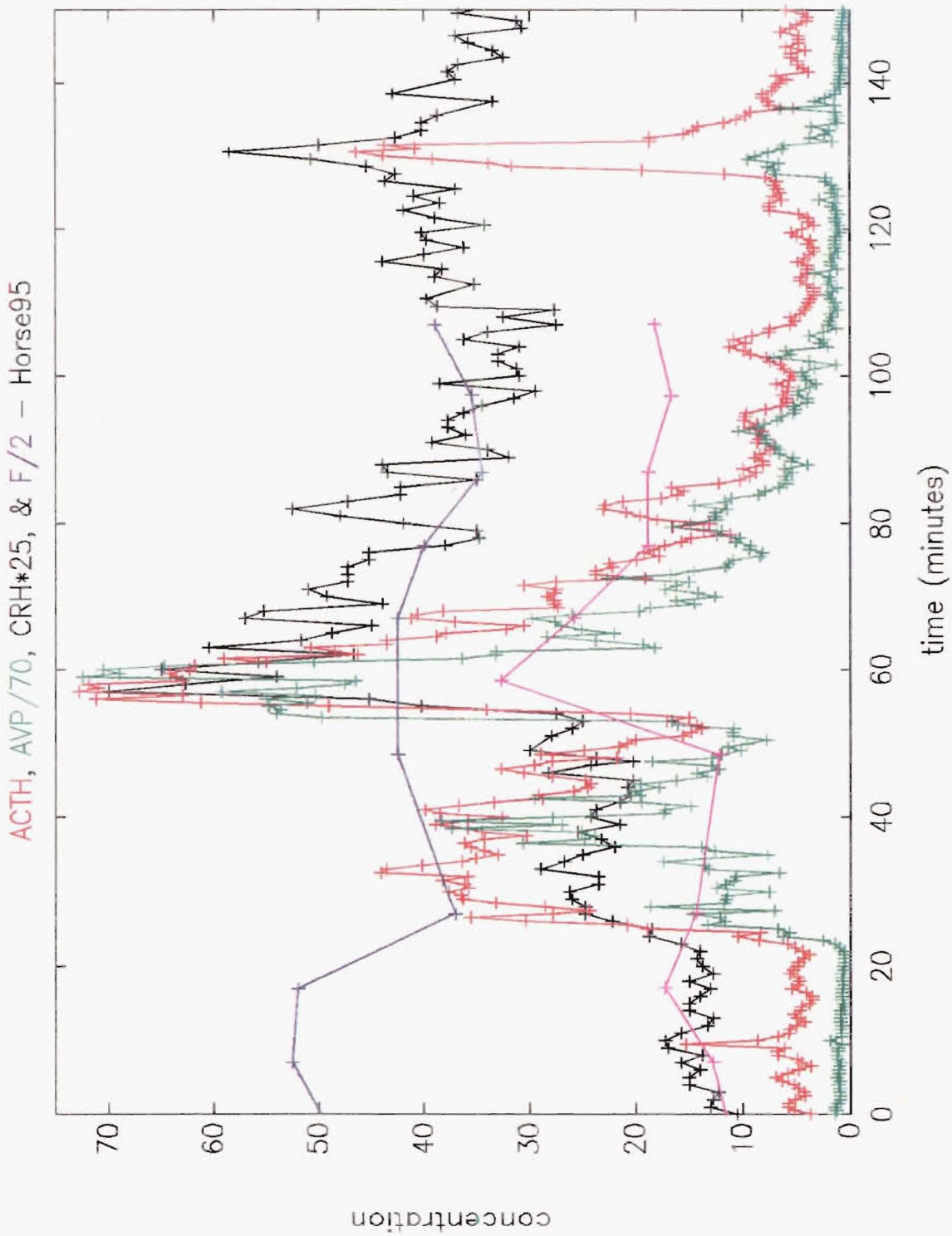

Figure 6.4 Concentrations of hormones measured in the part of experiment Horse95 where samples were assayed for CRH. Note that time zero therefore equates to sample 165 in the experiment. ACTH, in μg/l, is in red. AVP, CRH, and peripheral CRH, in pmol/l, are in green, black, and pink respectively. Cortisol, in nmol/l, is in blue. Cortisol concentrations plotted are as determined by the assay, but will exceed actual cortisol concentrations due to substantial crossreaction with 11-deoxycortisol.

6.3.3 Assays and data accuracy

The concentration of the main adrenal axis hormones in a blood sample is most accurately determined by radioimmunoassay (RIA) [Chard, 1982]. The basic principle behind RIA is illustrated for ACTH in figure 6.5. As the concentration of ACTH in the blood sample increases, so the ratio of labelled to unlabelled ACTH decreases. Therefore, less labelled ACTH becomes bound to the antibody and the radioactivity of the precipitate decreases. Thus, the radioactivity of the precipitate is a measure of the ACTH concentration in the original sample. Once radioactivity "counts" have been obtained for samples containing known amounts of ACTH, a standard curve can be drawn. The amount of ACTH in an unknown sample can then be determined from the curve. A typical standard curve is shown in figure 6.6.

At the left and right ends of the standard curve the labelled ACTH (or any other hormone to be assayed) is, respectively, almost completely bound to the antibody and completely free. In these regions, changes in the concentration of unlabelled ACTH produce only minor variations in the amount of bound labelled ACTH, and so the assay is inaccurate. Between these extremes, small changes in unlabelled ACTH produce a significant alteration in the amount of bound labelled ACTH. This region, the middle section of the standard curve, represents the effective range of the assay. A typical

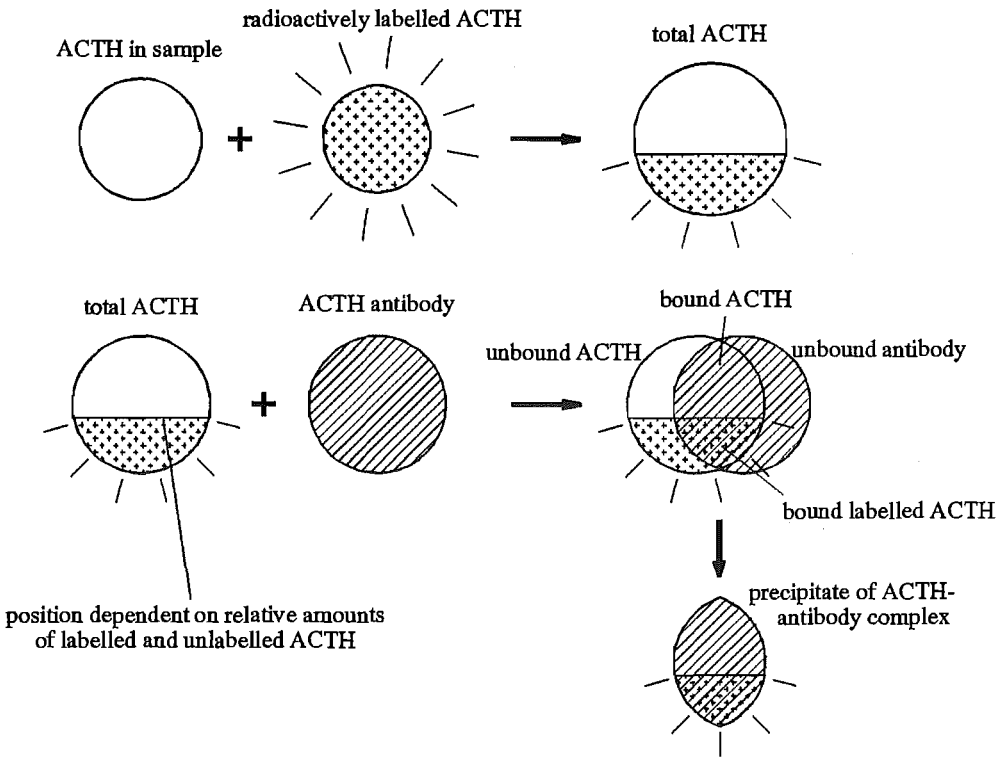

Figure 6.5 The basic principle of a RIA, illustrated for ACTH. A specified quantity of radioactively labelled ACTH is added to the sample in which ACTH is to be measured. An ACTH antibody is then added to the mixture where it binds with some of the ACTH. Finally, the antibody-ACTH complex is precipitated out, and its radioactivity determined.

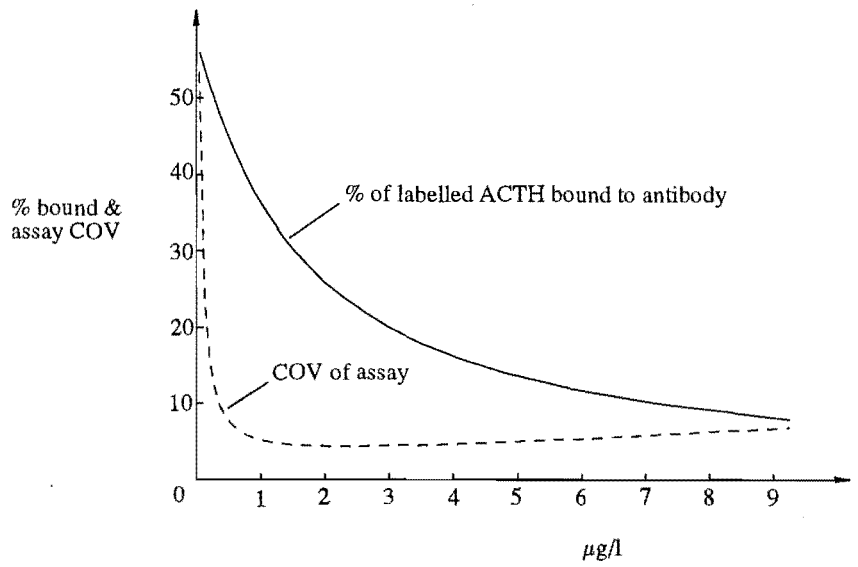

Figure 6.6 A typical standard curve for the ACTH assay, along with the coefficient of variation of the measurement.

variation in assay accuracy is also shown in figure 6.6. Table 6.1 gives some examples of signal to assay noise ratio (SNR), and average assay coefficient of variation ($\overline{\text{COV}}_{\text{assay}}$), which have been determined by

$$n_X = X.\text{COV}_{\text{assay}}(X).\kappa \tag{6.3}$$

$$\text{N(f)} = \sum_{i=1}^{10^5} |\mathcal{F}[\text{wind}(n_X)]|/10^5 \tag{6.4}$$

$$\text{S(f)} = |\mathcal{F}[\text{wind}(X(t) - \bar{X})]| \tag{6.5}$$

$$\text{SNR} = \int_0^{\text{f}_s/2} \text{S}^2(\text{f})\, d\text{f} \Big/ \int_0^{\text{f}_s/2} \text{N}^2(\text{f})\, d\text{f} \quad \text{and} \tag{6.6}$$

$$\overline{\text{COV}}_{\text{assay}} = \frac{1}{\sqrt{\text{SNR} + 1}} \tag{6.7}$$

where X is the concentration of the hormone in question, n_X is a typical assay noise sequence associated with X, κ is a zero mean random sequence with unit standard deviation, N(f) is the magnitude of the spectrum of n_X, $\mathcal{F}$ is the temporal Fourier transform operator [Bracewell, 1978], 'wind' is a Hamming window which is used to reduce the noise caused by mismatch between the beginning and end of the data [Harris, 1978], and S(f) is the magnitude of the spectrum of X. Equations (6.3)-(6.7) use the standard curve to determine the error in each sample and assume that this error is normally distributed.

Additional error will arise from mixing in the catheter and division of blood into samples, but these effects are small [Irvine, personal communication]. So, although assays are performed in duplicate, apart from for CRH, and repeated if the replication

Experiment	Hormone	SNR (assay noise)	$\overline{COV}_{assay}$
Horse60	ACTH	23 dB	7%
	AVP	18 dB	13%
	PROL	16 dB	15%
Horse79	ACTH	24 db	7%
	AVP	18 dB	12%
	CRH	20 dB	10%
Horse89	ACTH	24 db	6%
	AVP	28 dB	4%
	CRH	19 dB	12%

Table 6.1 Some signal-to-noise ratios and average assay COVs for ICS hormone concentrations and corresponding assay noise. The average interassay relative error can be obtained by multiplying the figures in the last column by $\sqrt{8}$.

is unsatisfactory, or the concentration does not fall on a satisfactory part of the standard curve, the assay is usually the major source of data error. This error (see table 6.1) is much higher than those found in a typical engineering context and has profound effects on the accuracy which can be obtained in any of the following analyses.

6.3.4 Sampling and sampling rate

This subsection considers the spectral content of AVP, CRH and ACTH, and makes some comments on the effects of using different sampling rates. Spectral analysis has been used elsewhere to reveal the multifactorial frequency structure of plasma ACTH concentrations [Carnes *et al.*, 1991], but the existence of high frequencies in PES data is demonstrated more simply by the occurrence of significant AVP and ACTH peaks which last less than $30s$. In addition, there appears to be no consistent frequency structure to pituitary adrenal-axis hormone concentrations. This is supported by observations that the variation in plasma ACTH spectra is greater within control groups, than between them [Carnes *et al.*, 1991].

PES involves collecting ICS blood over an interval of time, usually $30s$. When this sample is assayed, what is measured is the average hormone concentration over the sampling interval. This smoothing effect is unavoidable, since instantaneous sampling (collecting all the blood at one time) would cause unphysiological blood flow around the cannula, deprive target organs of hormones, and the source of the sample would be uncertain. A mathematically equivalent model of the actual sampling process is shown in figure 6.7. In the model, the actual hormone concentration in the ICS is averaged over the sampling interval, before being sampled by an instantaneous sampler and having assay noise added.

In the absence of noise, the input signal in figure 6.7 could be recovered exactly, provided that the sampling rate was high enough [Haykin, 1983]. In the presence of noise, the effects of averaging can not be removed, but this distortion does provide a rough anti-aliassing filter. The SNR can be improved by sampling more rapidly, but this must be offset against the increased cost and effort involved in more rapid sampling, provided that more rapid sampling is possible of course.

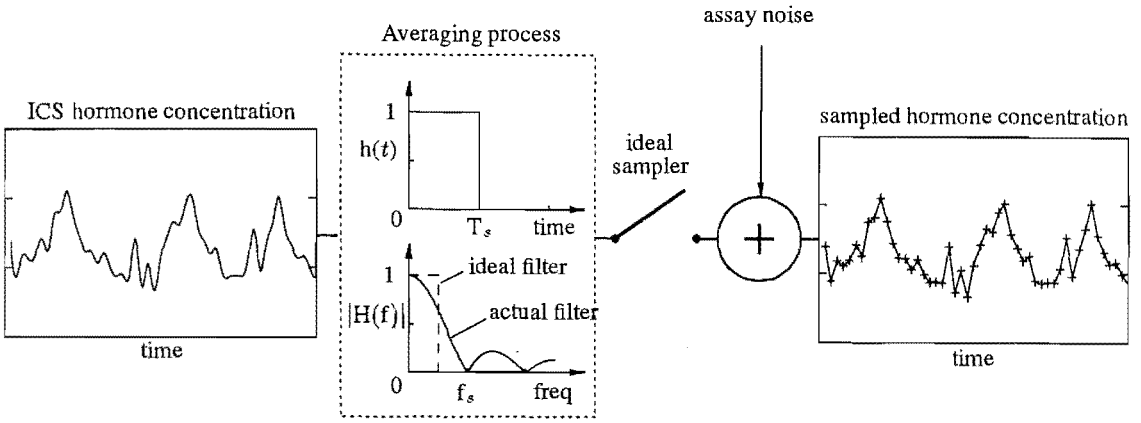

Figure 6.7 Model of the sampling process. The hormone concentration in the ICS is averaged over the sampling interval. The average is then sampled and assay noise is added.

The effect of sampling rate was quantitatively investigated using data from experiments Horse60, Horse73 and Horse89. These experiments were chosen because: (a) they contain concurrent samples with few missing samples - this is essential for spectral analysis; (b) the sampling rate appears to be high enough to avoid serious aliassing; (c) sufficient samples were taken to give one confidence in the spectra, and to allow good statistical significance; and (d) the animals did not receive bolus injections of ACTH secretagogues (i.e. ACTH secretion is endogenously driven, at least at the level of the corticotrope). Figure 6.8 illustrates the ACTH concentrations measured in experiment Horse60.

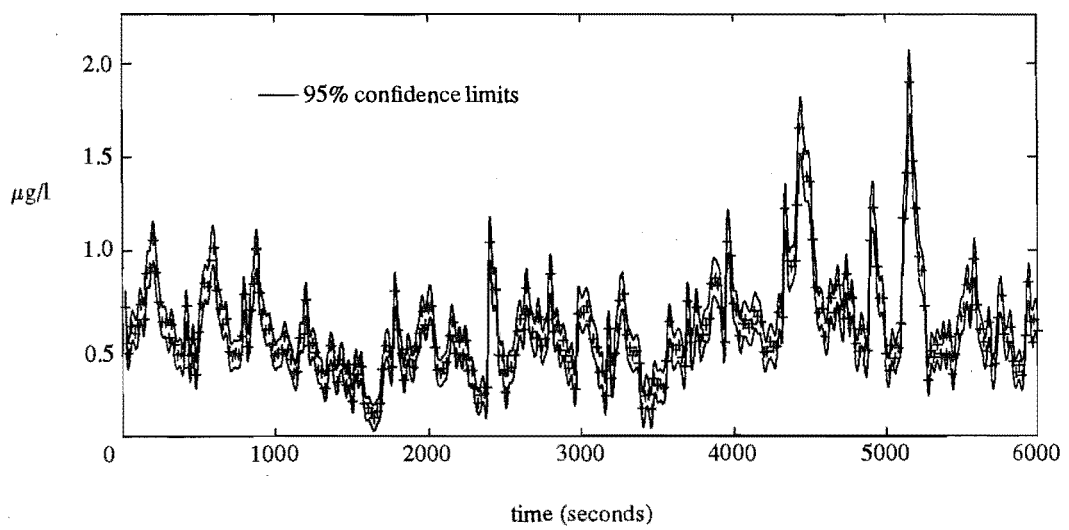

Figure 6.8 95% confidence limits on the ACTH concentrations in experiment Horse60. Data points are marked by a +.

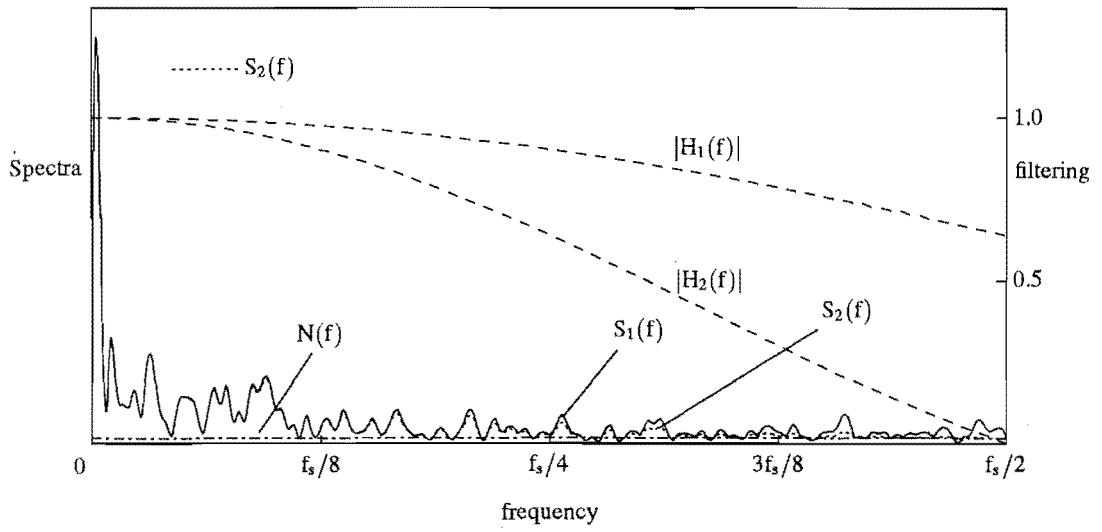

Figure 6.9 Spectra magnitudes of ACTH concentrations ($S_1(f)$) and assay noise ($N(f)$) from experiment Horse60, with sampling frequency $f_s = 1/20$ samples/s. In the figure a frequency of $f_s/2$ corresponds to hormone concentration peaks defined by one point, while $f_s/4$ corresponds to peaks defined by two points, and so on. The curve labelled $|H_1(f)|$ is the effect on the spectrum of averaging the ACTH over the entire $20s$ sampling interval, and is calculated using (6.9). Similarly the curve labelled $|H_2(f)|$ shows the effect on the spectrum of sampling at $40s$ intervals, while the curve labelled $S_2(f)$ demonstrates this effect for the ACTH spectrum shown.

The information needed to determine the effects of different sampling rates is shown in figure 6.9, and has been determined using (6.3)-(6.5), (6.8) and (6.9). $S_1(f)$, which is the magnitude of the spectrum of the ACTH concentrations in figure 6.8, indicates that much of the variation in ACTH concentration occurs relatively slowly, with the spectral content of the time series (difference between signal and noise) falling off to almost zero at half of the sampling frequency. This is gratifying and suggests that a $20s$ sampling rate has avoided much aliassing in this particular experiment. If one assumes that there is insignificant aliassing in this data then the effects of sampling at slower rates can be estimated. Slower sampling causes the original spectrum $S_1(f)$ (determined by sampling every $20s$ in the example shown in figure 6.9) to be 'filtered' to produce a new spectrum $S_2(f)$ such that

$$S_2(f) = [S_1(f) - N(f)]\frac{|H_2(f)|}{|H_1(f)|} + N(f) \tag{6.8}$$

$$\text{where} \quad |H(f)| = \sin(\pi f/f_s)/(\pi f/f_s) \tag{6.9}$$

and f_s is the sampling rate. Unfortunately it is not just the attenuation of the signal due to 'filtering' that is important. Those spectral components above half the new sampling frequency will be aliassed down into the new spectrum and appear as noise. Figure 6.10 illustrates these effects in the time domain. So, not only will some of the signal be lost, but aliassing will increase the noise.

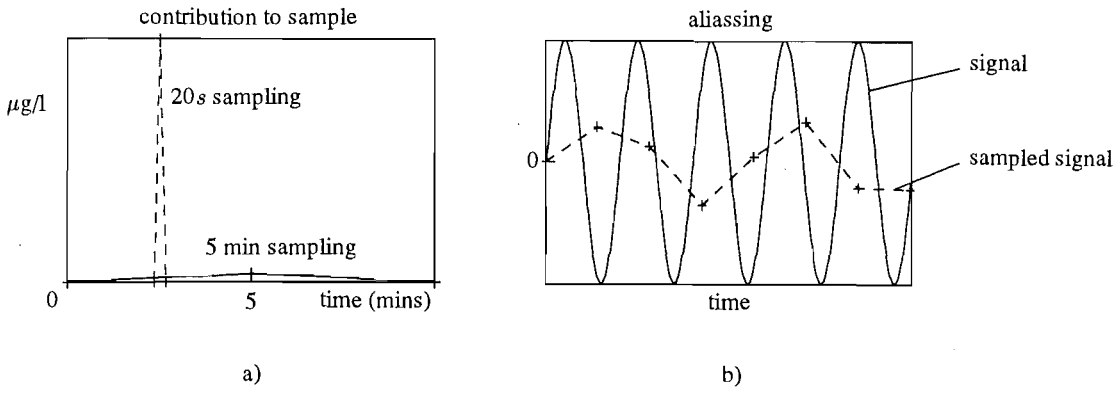

Figure 6.10 The time domain effects of a low sampling rate. Points represent the integral of the signal between samples. In (a) a secretory episode which lasts less than $20s$ contributes a large amount of 'signal' if the sampling interval is $20s$, but only a small amount if the sampling interval is 5 minutes. In (b) the true signal is misrepresented by inadequate sampling, an effect which is known as aliassing.

Ideally, one would like to sample very rapidly, and then low pass filter the signal at just above its highest frequency component to reduce the noise. In reality, the choice of a sampling strategy will always be a trade off between the extra information obtained and the cost to obtain it. The cost in materials will be proportional to the sampling rate, i.e. doubling the sampling rate doubles the cost. A measure of the information obtained as a function of sampling rate is vital to making the 'best' choice for a particular application.

A good measure of the amount of signal is the area between the magnitude of the hormone spectrum and the magnitude of the noise spectrum (assay + aliassing), because this quantity is directly proportional to the size of the signal in the time domain. Using the notation in figure 6.9 this quantity is given by

$$\mathcal{S}(f_{s2}) = \int_0^{f_{s2}/2} [S_2(f) - N(f)]df - \int_{f_{s2}/2}^{f_{s1}/2} pos[S_2(f) - N(f)]df \qquad (6.10)$$

where f_{s1} and f_{s2} are the original and new sampling frequencies respectively, and 'pos' indicates that only positive values are used. It is important to realize that while $\mathcal{S}(f_{s2})$ is the amount of 'signal' recovered by sampling at f_{s2}, it does not indicate how the pituitary responds to this signal. For instance, the pituitary may only respond to rapid changes in the signal. Alternatively, it may just respond to the average concentration of releasing factors. If this were the case, high frequency information would not be necessary to understand the operation of the pituitary, and it would be sensible to use either a slower sampling rate to reduce expense, or filtering to reduce noise. While the dynamic nature of hormone release is believed to convey important biochemical information, current understanding of what constitutes the most important part of the signal seems to be very limited.

The amount of *information* contained in any region of an ACTH, AVP, CRH, or cortisol spectrum will be determined only with a much better understanding of the pituitary than is presently available. However, the small value of the delay between ACTH secretagogue and ACTH release (see section 7.2) suggests that high frequency variations in ACTH secretagogue concentrations are very important signals to the pituitary. In addition, hormone concentrations obtained by portal sampling, which measures only

low frequency information, seem much more difficult to relate to one another than those obtained using PES [Alexander *et al.*, 1991; Engler *et al.*, 1989]. Another argument is that until the signal that the pituitary is responding to is known, then every effort should be made to obtain as much information about hormone dynamics as possible. Perhaps the strongest support for the information contained in high frequency hormone variations comes from the research described in section 7.5.3. This work would not be possible with sampling intervals of 2 minutes or longer. Thus it appears that measuring rapid variations in AVP, CRH and ACTH is necessary to understand ACTH regulation, and that $\mathcal{S}(f_{s2})$ is a good measure of the information recovered by sampling.

The amount of signal recovered by sampling is plotted in figures 6.11-6.13 as a function of sampling rate, and as a ratio of the value when $f_{s2} = f_{s1}$. Curve A is of most interest and so the assay cost shown corresponds to this sampling strategy. Of particular note is the steepness of almost all curves at low sampling intervals showing: (a) the value of rapid sampling; and (b) that considerably more information can be obtained by sampling even more rapidly. Results from experiments Horse60 and Horse73 are presumably more applicable to the physiological situation, given that no major manipulations of the adrenal axis took place in these experiments. The rapid decline in the curves for experiment Horse73 shows the importance of rapid sampling in this experiment, due to the more rapid fluctuations in ACTH and AVP concentrations. Horse73 is an exercise experiment and inspection of the data from other exercise experiments

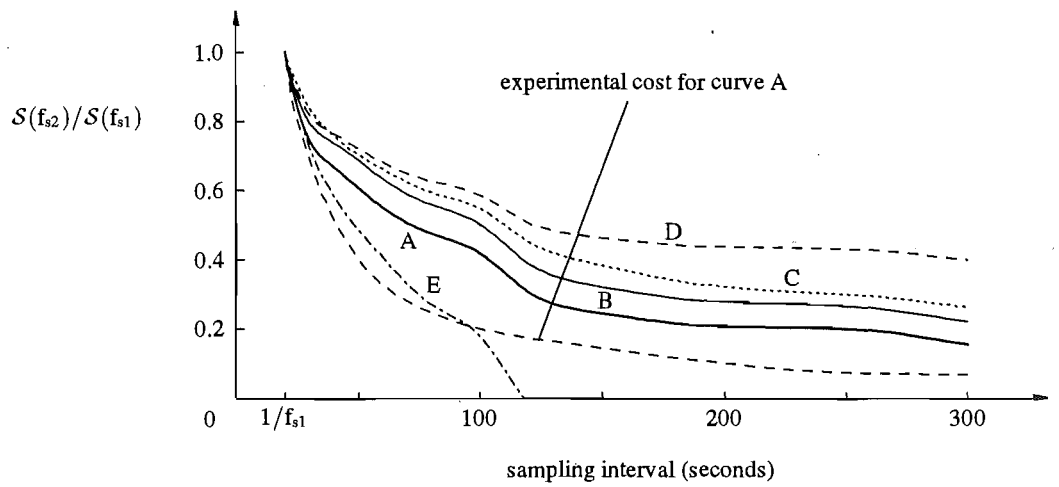

Figure 6.11 Relative ACTH signal as a function of the interval between samples ($= 1/f_{s2}$) for experiment Horse60, determined using (6.10). The original sampling strategy is taken to provide unit signal. Curve A is the signal variation recovered, as a function of the sampling interval, when blood is collected over the whole sampling interval. Curve B is the same, but the experiment length is increased to provide the same total number of samples as the original experiment. Curve C shows the best result that can be acheived by ideal filtering [Haykin, 1983] and then sampling. Curve D is the same as A, but for the entire signal, not just the signal variation, i.e. it includes the d.c. term in the spectrum. Curve E is also the same as A, but the time over which blood is collected remains fixed, i.e. $20s$, in this case, while the sampling interval varies. Negative values correspond to a sampling strategy which provides no useful information. The relative material cost of performing experiments corresponding to curve A is also given. Note that the experiment cost corresponding to curve B is independent of sampling rate.

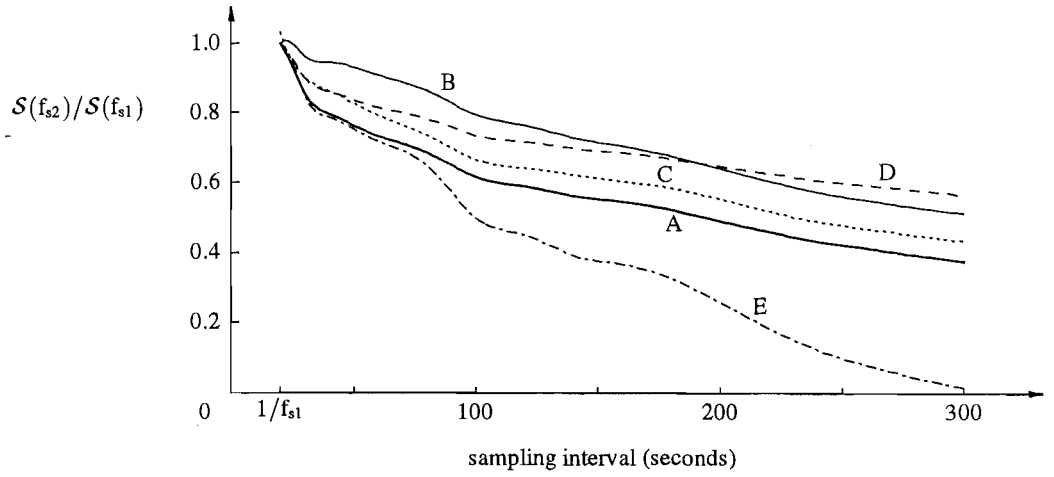

Figure 6.12 Relative AVP signal as a function of the interval between samples for experiment Horse60. The curve labels are explained in figure 6.11.

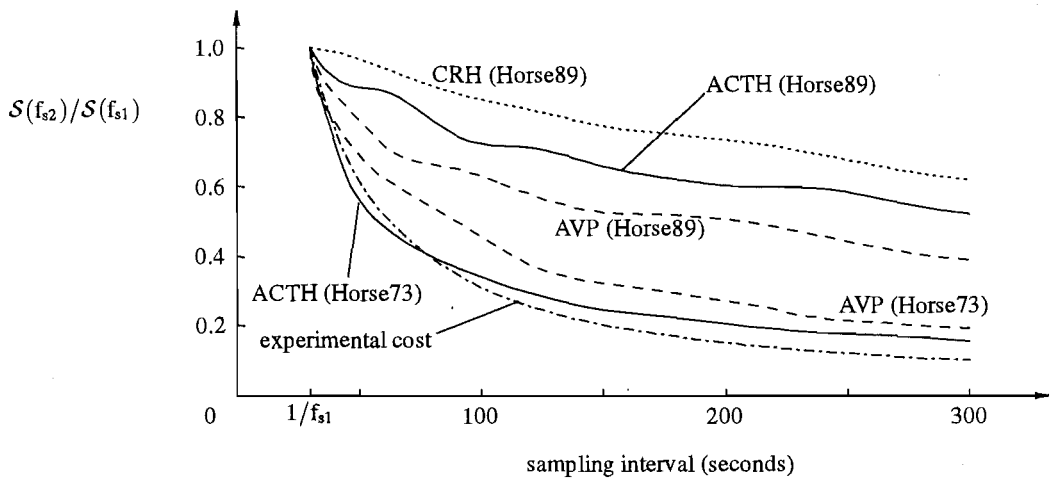

Figure 6.13 Relative ACTH, AVP and CRH signals as a function of the interval between samples for experiments Horse73 and Horse89. These curves, apart from the cost function, correspond to curve A in figures 6.11 and 6.12, and are shown here for comparison with these figures.

also suggests that hormone concentrations vary more rapidly during exercise, although lack of contiguous samples prevents a formal analysis. This is equivalent to saying that hormone pulses occur more frequently, but be careful to avoid the idea that pulse frequency has increased. The slower decline of signal, with increased sampling interval, for experiment Horse89 is due to the large, but broad, hormone peaks that occur as a result of metapyrone administration.

In the light of the results in figures 6.11-6.13 it is appropriate to make some recommendations for a sampling strategy. ACTH and AVP need to be sampled as rapidly as economically possible, since the amount of signal recovered decreases rapidly as the sampling interval is increased. It is apparent, from the slope of the AVP and ACTH curves when $f_{s2} = f_{s1}$, that significantly more signal could be recorded by a relatively small decrease in sampling interval, and one might consider this justification for decreasing the sampling interval. However, the cost function is also very steep in this

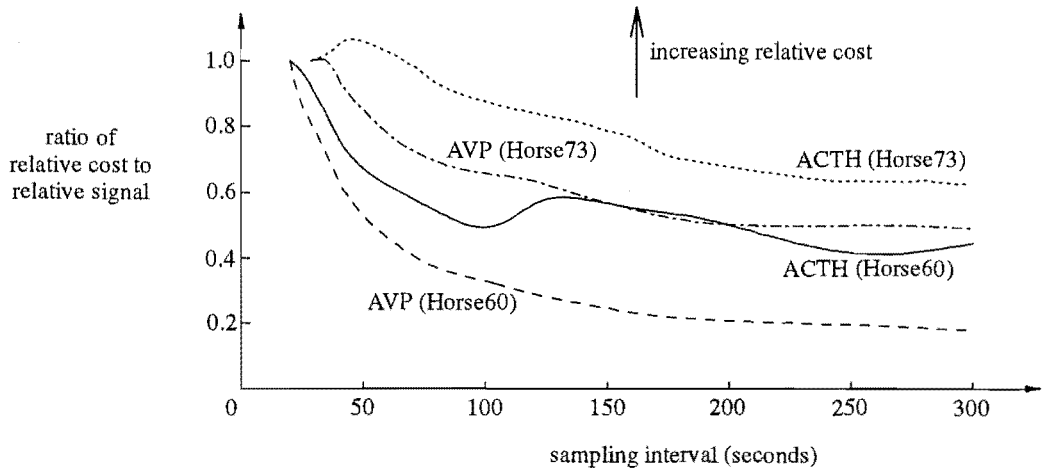

Figure 6.14 Relative assay cost to recover a given amount of signal, i.e. the higher the curve the greater the cost of recovering the signal. Curves shown are derived from those labelled A in figures 6.11 and 6.12, those for experiment Horse73 in figure 6.13, and the relative experimental cost shown in figures 6.11 and 6.13.

region, and hence, the relative cost is generally rising as the sampling interval decreases. Figure 6.14 illustrates the diminishing return when an attempt to recover more signal by sampling more quickly is made. It is important to note the small overall variation in relative cost for hormones from experiment Horse73, and in particular, the decrease around the 30s sampling interval, which suggests that rapid sampling is actually "value for money" in exercise experiments. This result argues for a decrease in sampling interval for exercise experiments. Apart from the burden of increased actual cost it is also vital to assess whether the increased signal recovered (and this analysis certainly indicates that there is more to be recovered) by more rapid sampling is the best way to investigate ACTH regulation. Given the lack of sophistication of current data analysis, it seems that experimental money is best spread around a greater number of experiments, and that what is now most urgently required is a concerted effort to develop more sophisticated techniques for interpreting data sampled at 30s intervals (see also section 7.1). So, in conclusion, the increased expense of faster sampling does not appear to be justified, yet!

Special circumstances apply for sampling CRH since the signal does not decrease rapidly with increasing sampling interval (see figure 6.13), and a large volume of plasma is required for the extracted assay. Figure 6.15 attempts to illustrate the signal recovered by some sampling strategies for the CRH concentrations measured in experiment Horse89. It suggests that considerable advantage can be gained from filtering the rapidly sampled CRH data and that this is the best way to maximize CRH signal in experiment Horse89 (i.e. curve B is above A, C and D). Furthermore, the unfiltered data is also available to determine the timing of associated CRH and ACTH concentration changes.

It is also important to determine how CRH signal varies when CRH concentrations are physiological, i.e. <1pmol/l. Since sufficient contiguous samples of physiological CRH levels were unavailable, the CRH data from experiment Horse89 was used, but the assay error was assumed to vary in the same way as it would if the CRH concentration was <1pmol/l. Due to the shape of the standard curve in this region, extracting twice the plasma approximately halves the assay noise. Curve E in figure 6.15 shows the signal

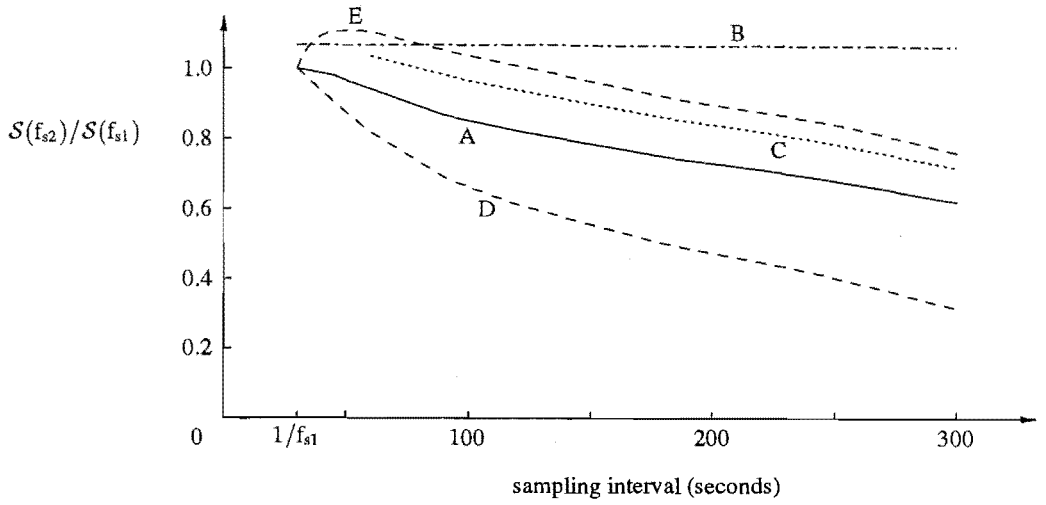

Figure 6.15 Relative CRH signal as a function of the interval between samples for experiment Horse89. Curve A corresponds to curve A in figure 6.11. Curve B shows the maximum signal content obtainable with ideal filtering of the original signal. Curve C indicates the effect of performing assays in duplicate once there is enough plasma. Curve D is an attempt to estimate the effect of combining the original samples, extracting, then assaying in singlicate. The reason that it is lower than curve A is that $\overline{\text{COV}}_{\text{assay}}$ for this data (see table 6.1) is above the optimum point on the standard curve, hence the error rises with increasing concentration. Curve E, for comparison, corresponds to curve D, but used a simulation to determine $S(f_{s2})$ for the situation where CRH concentrations are near the detection limit of the assay.

recovered. It indicates that when CRH concentrations are physiological it is better to sample at 60s intervals rather than 30s intervals. The reason is that the signal-to-noise advantage gained by extracting twice the plasma outweighs the loss of signal due to slower sampling. Note that at sampling intervals above 60s the loss of signal with slower sampling becomes more important.

In summary, when physiological CRH concentrations are expected, some initial samples should be taken to determine an approximate CRH level, and if this level is low, adjacent samples should be pooled for assay in singlicate. However, the decision to use sample pooling for the CRH assay, when physiological CRH concentrations are expected, should not be taken lightly. While rapid sampling, followed by filtering will always give near-optimum signal improvement, sample pooling will dramatically reduce the signal recovered if CRH levels are high (see curve D in figure 6.15). Thus if any adrenal axis manipulations are planned, CRH should be sampled as rapidly as AVP and ACTH.

In the above analysis no attempt has been made to account for biological noise, which is noise that occurs in addition to assay noise. This is because there is not enough information on this type of noise to allow its effects to be usefully incorporated into a quantitative analysis. Certainly, the effects of biological noise will be reduced by any filtering, i.e. curve B in figure 6.15 will move up. It is difficult to say much more than that. Rapid sampling may tend to increase biological noise because of the increased strain on experimenters and experimental equipment. Slow sampling will increase its contribution to aliassing. These effects can be expected to cancel to some

extent. Since biological noise appears to be much less of a problem with PES than assay noise, combined with an expected cancellation effect, it seems unlikely to have much influence on the results in figures 6.11-6.15.

Finally, it is important to appreciate that the results in figures 6.11-6.15 apply equally well for all *in vivo* ACTH, AVP and CRH measurement. They therefore provide an upper limit on the signal that can be recovered by portal sampling or peripheral sampling with deconvolution, relative to that recovered by PES.

6.3.5 Blood flow effects

The cavernous sinuses and the ICS link dorsal and ventral, right and left, large low-pressure venous circuits (see figure 6.1). It is therefore possible that the volume and direction of blood flow past the ICS cannula might be affected by sporadic events such as changes in head position and chewing, which intermittently compresses the deep facial vein. Such alterations in blood flow would cause changes in hormone concentrations at the cannula tip. Simultaneous changes in supposedly unrelated hormones have been observed in PES data, so it is important to know the effect, if any, that blood flow variations might have on the data. Visual inspection of hormone patterns indicates that there is no consistent relationship with either eating or head position [Irvine and Alexander, 1987]. Chewing is unlikely to have an effect since a 30s sample averages over many chewing motions and, although a low head position causes swelling of the facial veins, the head is generally raised during sampling. Furthermore, concentration changes in hormones are sometimes very large and generally asynchronous, showing that blood flow variations are not solely responsible for the pulses observed.

Measured hormone concentrations can be described by

$$C^X_{\text{ICS}} = (R^X_{\text{pit}} + C^X_{\text{jug}}[F_{\text{ICS}} - F_{\text{pit}}])/F_{\text{ICS}} \tag{6.11}$$

$$\approx R^X_{\text{pit}}/F_{\text{ICS}} \quad \text{given} \quad C^X_{\text{jug}} \ll C^X_{\text{pit}} \tag{6.12}$$

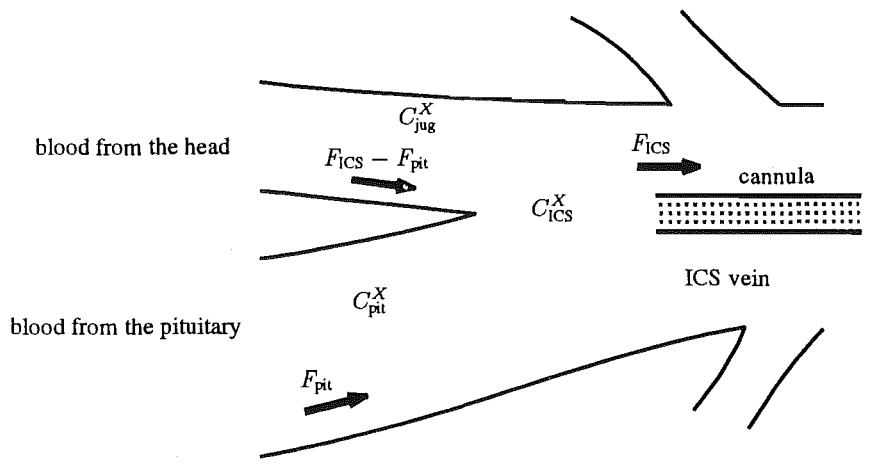

Figure 6.16 Blood flow in the ICS in the area around the cannula tip. C is a concentration, F is a blood flow and X is the hormone in question.

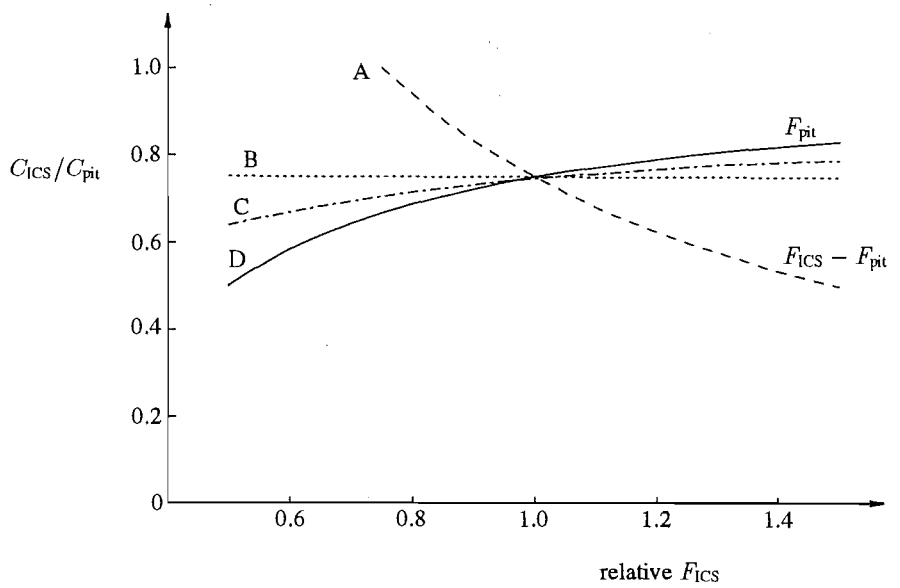

Figure 6.17 The possible variation in the ratio C_{ICS}/C_{pit} as a result of changes in blood flow in the ICS. Curve A shows the maximum variation possible, given that all of the variation in ICS blood flow occurs in the blood from the head ($F_{ICS} - F_{pit}$). Curve B shows that if blood flow changes occur equally in both flows entering the ICS, then ICS hormone concentration variations are identical (relatively) to those in the pituitary. Curve C is the likely effect of blood flow variations, given that variations are likely to affect the lower pressure F_{pit} more than the flow from the head. Curve D show the maximum variation possible, given that all the variation occurs in F_{pit}.

so blood flow variations may be erronously interpreted as changes in secretion. The notation used in (6.11) is explained in figure 6.16, with R^X_{pit} being the rate of secretion of hormone X by the pituitary or hypothalamus.

Equation (6.12) can also be written as

$$C^X_{ICS} \approx C^X_{pit} F_{pit}/F_{ICS} \tag{6.13}$$

Note that C^X_{pit} and R^X_{pit} are the quantities of most interest for hypothalamic and pituitary derived hormones respectively. For a good cannulation, measurements indicate that [Irvine and Alexander, 1987]

$$F_{pit} \approx 0.75 F_{ICS} \tag{6.14}$$

If (6.14) holds during changes in blood flow, then (6.13) means that the variations measured by PES are also occurring at the corticotropes. Otherwise, figure 6.17 indicates the range of possible variation in the ratio C_{ICS}/C_{pit}. The most likely dependence of C_{ICS}/C_{pit} on F_{ICS} is, from curve C in figure 6.17,

$$\text{percentage} \left[\frac{\mathrm{d}C_{ICS}/C_{pit}}{\mathrm{d}F_{ICS}}\right] \approx 0.15 \quad \text{at relative } F_{ICS} = 1.0 \tag{6.15}$$

which shows that reasonable changes in blood flow do not actually affect interpretation of adenohypophysial hormone concentrations very much. Interpretation of secretion rates is not so accurate with

$$\text{percentage} \left[\frac{\mathrm{d}R^X_{pit}}{\mathrm{d}F_{ICS}}\right] = 1.0 \quad \text{at relative } F_{ICS} = 1.0 \tag{6.16}$$

The above analysis is simplistic in that it neglects the blood flow dependent relationship between C_{pit}^{X} and the concentration of X in the adenohypophysis. Too little is known about hypothalamic/pituitary vasculature to sensibly include such a relationship into (6.11). What the above analysis does show is that interpretation of adenohypophysial hormone concentrations is likely to be substantially less affected by blood flow variations than interpretation of hypothalamic or pituitary secretion rates.

Determining the size of blood flow variations is difficult because many of the hormones measured are inter-dependent, and so relationships between hormones may be the result of blood flow variations, or the physiological influence of one hormone on another. One way to distinguish these two sources of synchronicity in the data is the delay between concentrations changes. There will be no delay between changes caused by blood flow variation, while there may be a delay, depending on sampling rate, if one hormone is influencing the other (see section 7.2).

Two measures of blood flow have been used to investigate the size of possible blood flow variations. The first of these, referred to as method A, recognises that blood flow variations will cause the same relative changes in all hormone concentrations, and so examines the correlation of relative hormone concentration changes. Relative concentration changes are given by

$$A_X = (C_X - C_X^{-1})/(C_X^{-1} + \alpha), \tag{6.17}$$

$$\text{where} \quad \alpha = \begin{cases} 0 & \text{for } \min(C_X) \geq 0.5 \\ 0.5 - \min(C_X) & \text{for } \min(C_X) < 0.5 \end{cases}$$

In (6.17) C_X is the concentration of hormone X, the superscript $^{-1}$ means a delay of one sample, α is a constant (for any particular hormone) which prevents excessive values of A_X for small values of C_X and $\min(x)$ is the minimum value of x.

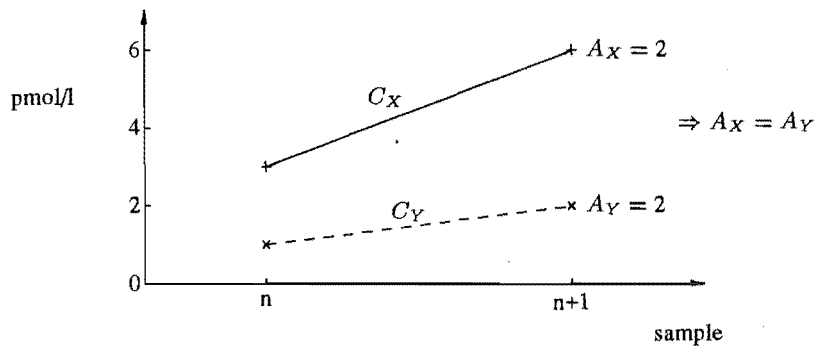

Figure 6.18 Illustration of the transformation described by (6.17).

The effectiveness of (6.17) is illustrated in figure 6.18, where the blood flow is assumed to halve from sample n to sample n+1. From (6.11), if F_{ICS} halves, then the concentrations of hormones X and Y will double, all other variables remaining equal. In this situation, although C_X increases by 3pmol/l and C_Y only increases by 1pmol/l, the measure of relative concentration change is 2 in both cases, i.e. $A_X = A_Y$. The correlation (r_A) between relative concentration changes (A_X and A_Y) is therefore able to emphasise the effects of any blood flow variation in the two series. Results obtained using this method are given a subscript A.

Other comparisons of relative concentration changes, such as

$$\sum(A_X - A_Y)/\mathrm{N} \tag{6.18}$$

where N is the number of samples, were also investigated. However, (6.18) was found to be too non-linear a measure of the relationship between X and Y to be statistically useful. In contrast, correlation is a fairly linear measure of relationship when deviations are small.

A second method, called method B, uses the fact that 30s sampling of hormones produces spectra with only small amounts of energy at high frequencies (i.e. almost all hormone peaks are defined by more than one point), so crosscorrelations between such hormones will vary slowly. Noise on the data will always be present, but its effect is reduced by the crosscorrelation and is well defined statistically. Blood flow variations will appear as a peak in crosscorrelation at zero lag, but have only random effects at other lags. Consequently, a measure of such variations is the deviation of the zero lag crosscorrelation from the smooth curve which is constructed by fitting a spline to all points except the one at zero lag. Although this method is somewhat *ad hoc*, it provides additional support for the more rigorous results obtained using method A.

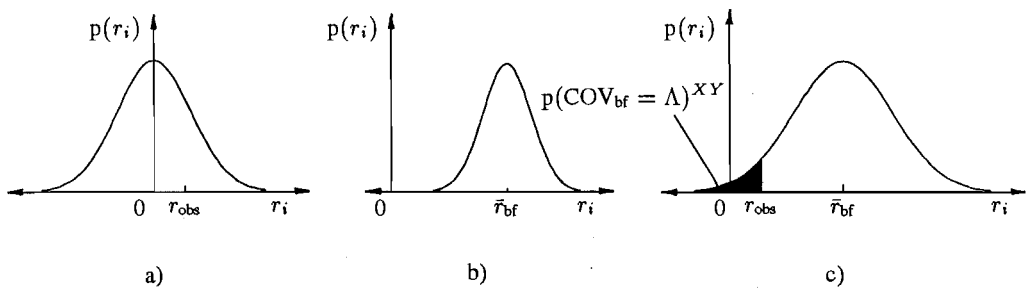

Figure 6.19 Determination of blood flow significance. (a) is the correlation distribution, assuming assay noise and that the two hormones are unrelated, or that they don't change synchronously i.e. $\bar{r} = 0$. It is calculated by setting $\mathrm{COV_{bf}} = 0$ in (6.19). r_{obs} is the correlation between relative variations in hormone concentration, for method A, and the difference between a smooth curve and zero lag crosscorrelation, for method B. (b) illustrates the distribution in correlation which results from an artificial blood flow variation with $\mathrm{COV_{bf}} = \Lambda$. It is calculated by setting the assay noise n_X and n_Y to zero in (6.19). (c) is the sum of (a) and (b), and is calculated using (6.19). The shaded region indicates the probability that r_{obs} could occur, given $\mathrm{COV_{bf}} = \Lambda$, and the assumptions stated in the text.

The assumptions in method A are that the two hormones are either independent or that, on average, changes in the two hormones do not occur synchronously. While these assumptions are violated by many of the hormone pairs (ACTH and AVP in particular), which will result in unrealistically high estimates for average blood flow COV ($\mathrm{COV_{bf}}$), they may be approximately true for others, e.g. AVP and CRH or PROL. It is these hormone pairs which provide the limits on $\mathrm{COV_{bf}}$. The assumption in method B is that the crosscorrelation function is smooth in the region around zero lag. Such gross assumptions are unavoidable because too little is known about the relationships between the measured hormones to do anything more rigorous. Both methods also assume that variations in blood flow are normally distributed.

Figure 6.19 illustrates the determination of upper limits on COV_{bf}. The distributions shown apply to methods A and B, and are determined from simulation of

$$r_i = f\left(\frac{C_X}{1+\frac{COV_{bf}}{100}\kappa_i} + n_X^i\right) \otimes f\left(\frac{C_Y}{1+\frac{COV_{bf}}{100}\kappa_i} + n_Y^i\right) \quad \text{for} \quad i = 1, \ldots, 10^5 \qquad (6.19)$$

where $\otimes$ means crosscorrelation, κ_i are normally distributed, zero mean, random sequences with unit standard deviation, n_X^i and n_Y^i are assay noise sequences, calculated using (6.3), and associated with hormones X and Y, while

$$f(x) = \begin{cases} (x - x^{-1})/(x^{-1} + \alpha) & \text{for method A} \\ x & \text{for method B} \end{cases}$$

as in (6.17). This simulation is designed to reflect the *in vivo* situation as well as possible. Since the correlation between hormones X and Y (say) is independent of that

	Λ where $p(COV_{bf} \geq \Lambda) < 0.05$		
Experiment	$\Lambda = \Lambda_A$	$\Lambda = \Lambda_B$	$\Lambda = \Lambda_A$ or Λ_B
Horse60	10%	5%	5%
Horse79	1%	2%	1%
Horse89	5%	8%	5%

Table 6.2 Upper limits on COV_{bf}, determined using methods A and B. The Λ values for experiment Horse79 are artificially low because some of the concentration changes in this experiment resulted from hormone administration.

Experiment	Hormones	$\bar{r}_A = 0$	COV_{bf}^A where $\bar{r}_{bf} = r_{obs}$
Horse60	ACTH & AVP	0	8%
	ACTH & PROL	0	11%
	AVP & PROL	0	7%
Horse79	ACTH & AVP	0	12%
	ACTH & CRH	0	< 0%
	CRH & AVP	0	< 0%
Horse89	ACTH & AVP	+	< 28%
	ACTH & CRH	+	< 21%
	CRH & AVP	0	< 0%

Table 6.3 Further information on COV_{bf}, determined using method A. The column labelled $\bar{r}_A = 0$ indicates whether the observed correlation between relative variations in the two hormones could occur by chance, if they were unrelated. + therefore denotes that variations in the two hormones are related, at the 95% level. The last column is the COV_{bf} which best predicts r_{obs}, using method A, but assuming that the hormones are unrelated. Where a relationship exists in the previous column, < signs have been inserted because blood flow variations are only required to explain part of r_{obs}. A negative value in three of the seven instances where $\bar{r}_A = 0$, is additional support for the average blood flow effect being small.

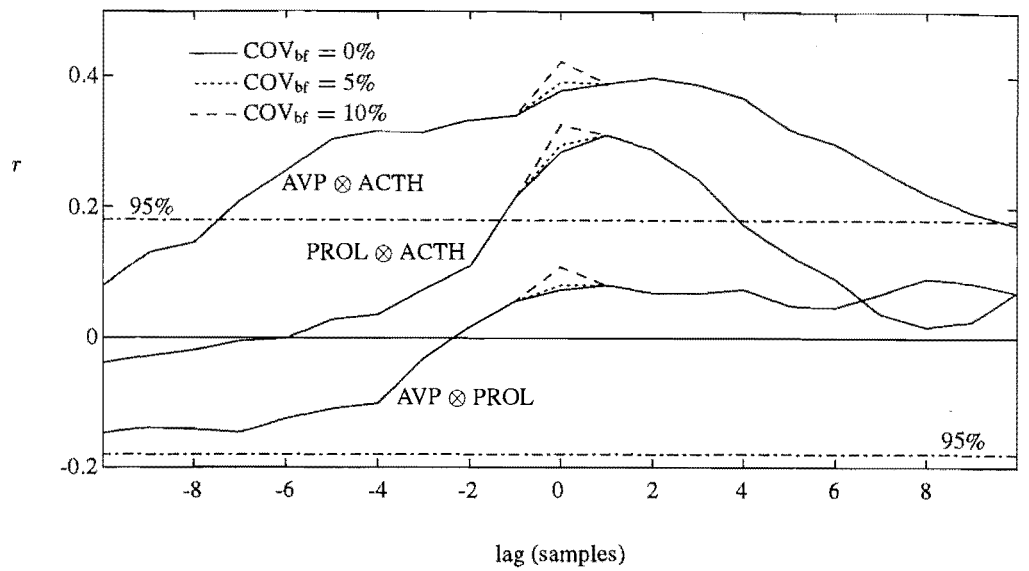

Figure 6.20 Effect of artificial blood flow variation on the crosscorrelation between the hormones measured in experiment Horse60. Curves are a result of simulation using (6.19) with $f(x) = x$. 95% significance limits are shown, and exceeded for two of the hormone pairs, indicating a relationship exists between these pairs. The customary occurrence of the maximum crosscorrelation at a non zero lag aids in the identification of possible blood flow effects, since it is visually easier to identify an assymetry than an increase in the maximum.

between hormones Y and Z (say) [Blank, 1982], the probabilities from two different combinations of hormone pairs can be multiplied to get a tighter limit on $\mathrm{COV_{bf}}$ for any particular experiment. That is, $\mathrm{p(COV_{bf} = \Lambda)}$ is the product of whichever pair of $\mathrm{p(COV_{bf} = \Lambda)^{XY}}$, $\mathrm{p(COV_{bf} = \Lambda)^{YZ}}$ and $\mathrm{p(COV_{bf} = \Lambda)^{XZ}}$ produces the smallest probability. The more expansive form of this probability is $\mathrm{p}(r_{\mathrm{obs}} < r_i$, given $\mathrm{COV_{bf}} = \Lambda)$. This expression better illustrates that if $\mathrm{COV_{bf}}$ equals the Λ values in table 6.2, then the correlation is greater than r_{obs} at least 95% of the time. Λ values in table 6.2 were calculated by incrementing the value of $\mathrm{COV_{bf}}$ in (6.19) until this was achieved. Further information on $\mathrm{COV_{bf}}$, determined using method A, is provided in table 6.3 and summarized in the accompanying caption.

An additional check on the results afforded by methods A and B, referred to as method C, is provided by inspection of the effect of an artificial blood flow on the shape of the crosscorrelation between two hormones, as illustrated in figure 6.20. Method C is really a more interactive form of method B, and indicates that blood flow variations with average COVs of greater than 5% should have an obvious visual effect on the crosscorrelation between hormones.

So, while there is not enough information about the relationships between different hormones to assess the actual value of any blood flow effect present in data, it is possible to put an upper limit on the average effect, for any given data set. In general this limit is less than 5%, based on results from methods A, B and C, which suggests that blood flow variations have a much smaller effect on the data than interrelationships between different hormones, where they exist. In addition, while such variations influence apparent hormone secretion rates, they have less effect on the interpretation of adenohypophysial

hormone concentrations. The size of this effect can be estimated by combining the 5% limit on COV_{bf} with (6.15) to show that, on average, blood flow variations may cause less than a 1% COV in interpretation of adenohypophysial hormone concentrations. Thus PES appears to accurately measure AVP, CRH and ACTH concentrations at corticotropes.

CHAPTER 7

Analysis of ACTH Regulation

The research described in this chapter is an analysis and interpretation of how pituitary concentrations of AVP, CRH and cortisol affect ACTH secretion. Section 7.1 examines the methods which are used in this thesis to investigate the relationships between hormones in PES data and presents some preliminary results. Section 7.2 examines evidence for a delay between presentation of AVP or CRH and ACTH release, and what this may indicate about ACTH secretion. In section 7.3 an existing model of ACTH secretion is introduced and tested using PES data. To complete the background for a more appropriate model, section 7.4 outlines the major experimental results that a successful model should be able to duplicate. Section 7.5 then proposes a model, based on the results of sections 7.1-7.4, and examines what this model can reveal about ACTH regulation.

7.1 Investigating ACTH Regulation

It is apparent that different stressful stimuli evoke specific changes in the release of AVP, CRH, cortisol and other, presumably more minor ACTH regulators [Antoni, 1986; Canny *et al.*, 1989; Engler *et al.*, 1989; Gibbs, 1986; Whitnall, 1989]. These changes constitute a complicated hypothalamic signal, possibly containing both amplitude and frequency coded information, which appears to be decoded by corticotropes, before initiating whatever response is appropriate for the initial stimuli. Consequently, a simple eyeballing approach to analysing relationships between hormones is not entirely satisfactory, and considerable additional information can be gained by using the techniques in this section. Crosscorrelation is the first of these techniques, followed by pulse analysis in section 7.1.2. Results from section 7.1.2 are extended in section 7.2, while introductory comments on modeling in section 7.1.3 foreshadow the modeling based analysis of ACTH regulation contained in sections 7.3-7.5.

7.1.1 Crosscorrelation

Objectivity is essential for any accurate statistical analysis and correlation is the simplest objective method for investigating the relationship between two time series. On a cautionary note, crosscorrelation is best used only in conjuction with other analyses because, although it indicates the presence of a relationship, in its basic form it is unable

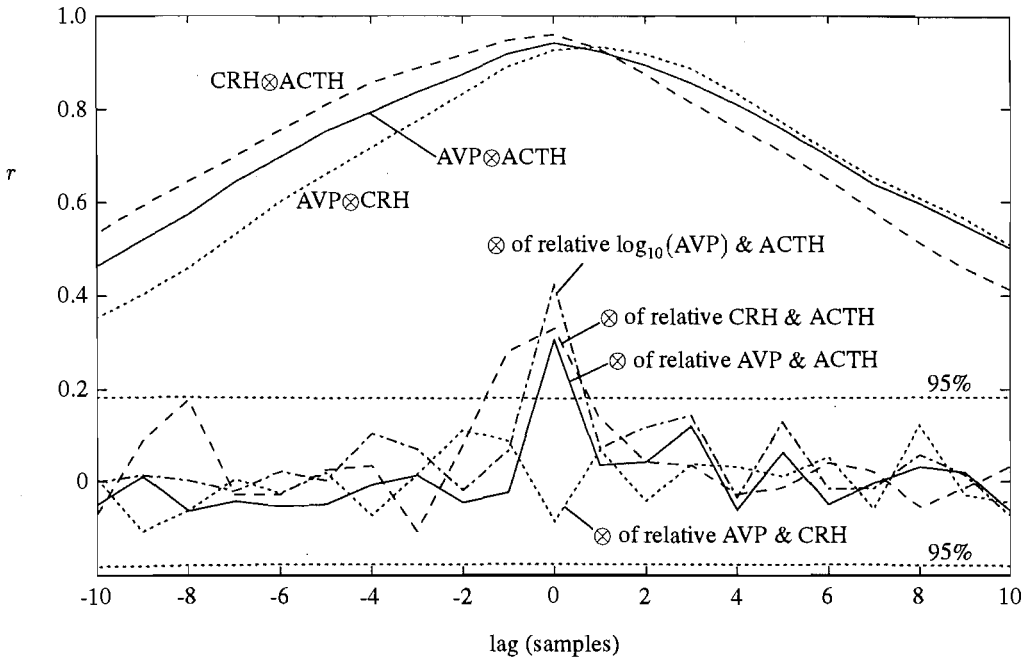

Figure 7.1 Crosscorrelations (⊗) of AVP, CRH and ACTH, along with relative variations determined using (6.17), all from experiment Horse89. 95% confidence limits shown apply to crosscorrelations involving CRH. For AVP⊗ACTH 95% significance at zero lag is when $|r| > 0.14$. A positive lag for $X \otimes Y$ means that Y follows X.

to reveal much about the form of this relationship. Consequently, using crosscorrelation to provide additional support for established relationships between ACTH and its regulators, is likely to be less informative than results from other techniques (e.g. modeling) which seek to determine what the relationships are. Crosscorrelation may also be heavily influenced by trends, like circadian rhythms, or outside factors, which are not of interest or not appreciated. An example is shown in figure 7.1 where AVP and CRH are extremely well correlated (r=0.93 at zero lag). This observation, on its own, supports the suggested physiological role for colocalization of CRH and AVP in granules in the median eminence, particularly since colocalization should be enhanced by the low cortisol levels in this experiment [Whitnall, 1989]. However, further investigation using correlation of relative variations in AVP and CRH shows that the two hormones are not varying synchronously ($r = -0.08$ at zero lag), as they would if released from the same granules. This second observation virtually disproves a physiological role for colocalization in experiment Horse89.

Once correlation has been used to establish whether there is a relationship, it may not be obvious how to proceed with this approach. Additional information can be gained by using crosscorrelation to determine the effects of different transforms on the data, e.g. relative variation or filtering, and this is demonstrated in figures 7.1 and 7.2. In figure 7.1 the magnitude of the crosscorrelation indicates the tight coupling between all three hormones in this experiment, while significant correlation between relative concentration changes supports the idea that individual pulses of AVP and CRH cause pulses of ACTH without delay. The increased correlation between relative

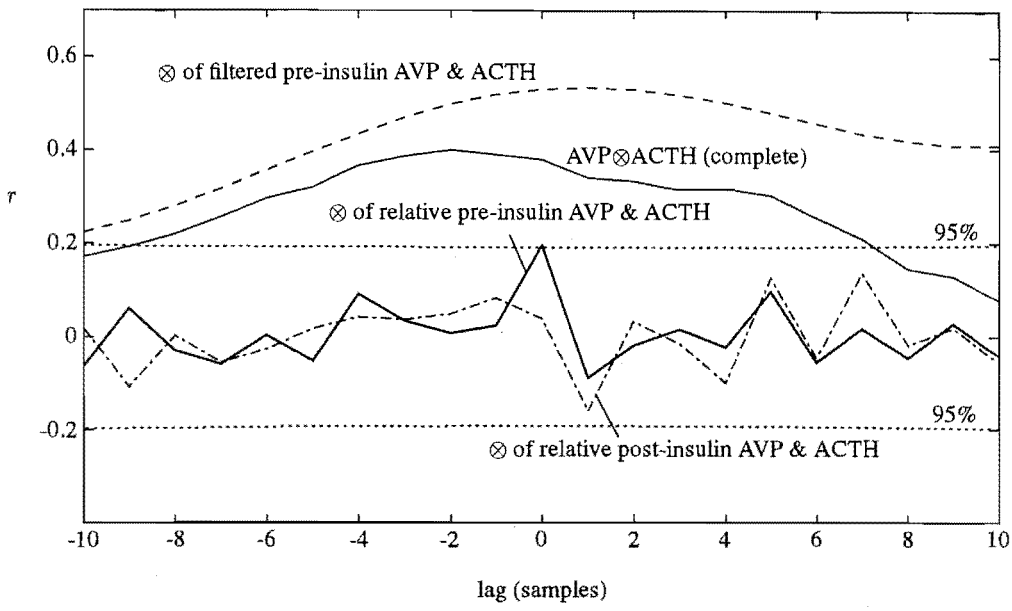

Figure 7.2 Crosscorrelation (⊗) of AVP and ACTH, along with ideal low pass filtered versions ($f_c = 0.15f_s$, where f_c is the cutoff frequency and f_s is the sampling frequency), and relative variations determined using (6.17), all from experiment Horse60. 95% confidence limits shown apply to the crosscorrelation of relative pre-insulin AVP and ACTH. For AVP⊗ACTH 95% significance at zero lag is when $|r| > 0.16$, and for crosscorrelation of relative post-insulin AVP and ACTH, when $|r| > 0.23$.

$\log_{10}$(AVP) and ACTH suggests a non-linear relationship between ACTH and the very high concentrations of AVP which result from metapyrone administration. In figure 7.2 the increased correlation, when the two hormones are low pass filtered, indicates that the relationship between them is closer over a period of minutes than over the sampling interval of $20s$. However, a significant correlation between the relative concentration changes in the two hormones, over the period before insulin administration, supports the hypothesis that individual pulses of AVP normally drive pulses of ACTH. The disappearance of this relationship after insulin administration bears on the discussion in section 6.3.1. It suggests that when AVP is released in an antidiuretic role, PES may be less accurate at measuring the variations in AVP that the corticotropes are exposed to. Note that a significant correlation between AVP and ACTH still exists ($r = 0.22$ [$r = 0.42$ before insulin] at zero lag, not shown), even after insulin administration.

Correlation results for the entire set of rapidly sampled adrenal axis PES experiments with satisfactory assay replication are summarized in table 7.1. The error in CRH columns is typically larger than for AVP columns since not all samples are usually assayed for CRH. AVP is significantly correlated with ACTH in all but one CRH administration experiment, and relative changes in the two hormones are also significantly correlated in 75% of experiments, showing the close relationship between AVP and ACTH. Conversely, the relationship between CRH and ACTH is not nearly as pronounced, or evident in such a variety of experimental situations, although it is highly significant in all of the recent metapyrone experiments. These results support other recent observations [Alexander *et al.*, 1991; Alexander *et al.*, 1988].

Horse	experiment type	AVP⊗ACTH	CRH⊗ACTH	$AVP_A \otimes ACTH_A$	$CRH_A \otimes ACTH_A$
60	insulin	$.38^+$	no CRH	.11	no CRH
62	basal	$.41^+$	$-.57^-$	.00	-.03
63	CRH administration	.00	$.76^+$	.00	$.32^+@40s$
69	exercise	$.46^+$	$.38^+$	$.24^+$	.01
71	metapyrone	$.72^+$	$-.35^-$	$.41^+$	.05
72	exercise	$.55^+$	.17	$.28^+$	-.11
73	basal	$.66^+$	0	$.83^+$	.10
74	basal	$.73^+$	$.42^+$	.07	.06
75	exercise	$.40^+$	-.14	$.33^+$	.22
77	exercise	$.68^+$	-.21	$.62^+$	-.09
79	AVP/CRH admin.	$.43^+$	$.43^+$	$.18^+@30s$	$.19^+@90s$
80	AVP/CRH admin.	$.29^+$	-.26	.12	.01
83	AVP/CRH admin.	$.28^+$	$.40^+$	$.48^+$	.07
84	metapyrone	$.74^+$	$.38^+$	$.47^+$	0.0
85	AVP/CRH admin.	$.57^+$	.22	$.38^+$	-.17
89	metapyrone	$.94^+$	$.95^+$	$.29^+$	$.31^+$
90	AVP/CRH admin.	$.28^+$	.23	$.22^+$	0.0
92	AVP/CRH admin.	$.48^+$	$.48^+$	$.13^+$	.03
93	metapyrone	$.86^+$	$.40^+$	$.48^+$	.07
95	metapyrone	$.86^+$	$.55^+$	$.14^+@30s$	.16
		$95\%^+$	$40\%^+$	$75\%^+$	15% (NS)

Table 7.1 Correlation between ACTH and AVP or CRH. A subscript 'A' means that the hormone concentration has been transformed by (6.17), to emphasize relative variation. Lags of up to 150*s* were considered with the relative correlation, since in some situations delays were apparent. These are denoted by an @, followed by the delay at which the correlation occurred. Positive (negative) significance at the 95% level is denoted by a $^+$ ($^-$) superscript, while NS means not significant. Where a substance is listed under experimental type it was administered to the horse during the experiment. Insulin stimulates AVP release (see section 5.2.2), while metapyrone blocks the final stage in cortisol synthesis [Little *et al.*, 1958]. More details on some of these experiments have been given in section 6.3.2.

7.1.2 Pulse analysis

Traditional methods of crosscorrelation analysis are not adequate for quantifying the linkage between concentration changes in different hormones or for determining details about hormone secretion. In an attempt to provide this information it is desirable to identify, relate and characterize hormone pulses. A large number of pulse identification algorithms are available to assist with these three tasks, and are widely used to interpret serial hormone measurements in terms of pulse frequency and amplitude, and mean peak and trough levels [Kushler and Brown, 1991; Royston, 1989; Urban *et al.*, 1988a; Urban *et al.*, 1988b].

Since hormone pulses are considered by most Endocrinologists to be fundamental in characterizing hormone signals, the endocrinology community has put an enormous amount of effort into developing objective pulse identification algorithms. The difficulty

of this task is indicated by the fact that there is no one 'standard' pulse identification algorithm. While all pulse identification methods can produce sensible results, they may break down in special cases, and all have one or more parameters which are more or less arbitrarily determined. This means that, while they attempt to be objective, pulse identification programs can be configured to 'find' whatever pulses are desired (although this may be a useful attribute). Furthermore, it is assumed that pulses found by pulse identification algorithms reflect, to a useful degree, actual pituitary secretion.

This assumption has been tested *in vivo* by Urban *et al.* [1989] & [1991] who concluded that positive accuracies (likelihood of detecting a real pulse) of >85% can be achieved by the Cluster algorithm [Veldhuis and Johnson, 1986] with reasonable false negative errors (<15%). In assessing the validity of this conclusion it is worth considering that Urban *et al.* [1991] used only instances where hypothalamic electrical activity was obviously followed by FSH release. This forced them to discard much of their data. In addition, Urban *et al.* [1989] commented that peripheral LH pulses follow medial basal hypothalamic electrical activity with a delay of 2-3 minutes. Since they then considered a 60 minute wide window of allowable delay in matching real and detected pulses, good positive accuracy could be expected even if there was no relationship. When only a 15 minute window is considered the average positive accuracy falls to 59%, with range 17-83% (calculated using their data). Finally, when pulse detection methods are used, increased false negative errors mean that 5 and 10 minute sampling is not necessarily more informative than 20 minute sampling [Genazzani and Rodbard, 1991; Urban *et al.*, 1991]. Significant concentration variations in PES reproductive axis data occurring over 30*s* intervals [Irvine, personal communication] (see also section 6.3.4) therefore suggest that: (a) peripherally detected pulses may not accurately represent pituitary secretion; and (b) that some form of data smoothing before pulse detection would be helpful.

Thus, it should be recognised that pulse identification algorithms currently lend a somewhat false air of objectivity to an analysis, although there is no disputing that pulses must be found objectively or the whole analysis is flawed. Another problem, for the purposes of this thesis, is that many of the 'better' pulse identification algorithms achieve advantage by assuming that the pulse rises rapidly and decays exponentially. This model is appropriate for peripheral hormone measurements, but does not apply *in vitro* or for PES, the two experimental methods which provide the data analysed in this chapter.

PES has revealed the complexity of hypothalamic and pituitary adrenal axis hormone secretion. Patterns are neither rhythmic nor regular, showing that the adrenal axis lacks a strict 'timekeeper' as some groups believe exists for the reproductive axis [Knobil, 1981]. In this context, it is interesting (but certainly not surprising!) that Carnes *et al.* [1991] found that visual inspection of rapidly sampled peripheral rat ACTH suggested it has a more complicated repetitive nature than is revealed by pulse identification algorithms. The irregularity of secretion means that conventional methods for analysing hormone secretion (i.e. pulse identification, followed by calculation of pulse frequency) represent an oversimplification of secretory behaviour, and that an approach which uses the entire secretory pattern (e.g. modeling) is likely to be more useful. In addition, relating pulses in different hormones uses no information about the size or shape of these pulses, both of which are likely to be important signals [Guardabasso *et al.*, 1991].

Despite the above mentioned shortcomings of pulse analysis, relating pulses is certainly more quantitative than correlation type analyses, and can provide some useful information about relationships between hormones. Therefore, all ACTH, AVP and CRH pulses in PES experiments with sampling intervals of one minute or less were identified and related to one another. The results are displayed in table 7.2.

Given previous comments, pulses were identified by inspection, with regard to the standard statistical principles on which the more reputable pulse identification algorithms are based, this being considered adequate for the subsequent analysis. The significance of a change in hormone concentration was dependent on:

i. the size of the change in concentration,

ii. the assay error at the concentrations involved and

iii. the square root of the number of samples involved.

Horse	N_{samp}	N_{ACTH}	ACTH←AVP	ACTH←AVP/CRH	AVP↛ACTH	AVP/CRH↛ACTH
60	300	31	87%	≥87%	7%	≈7%
62	124	5	100%	100%	0%	17%
63	64	6	67%	100%	0%	0%
69	84	5	80%	100%	20%	20%
71	418	28	96%	≥96%	27%	≈27%
72	61	6	83%	100%	0%	12%
73	109	26	100%	100%	13%	≈13%
74	238	20	95%	95%	14%	17%
75	42	8	75%	88%	14%	12%
77	38	4	100%	100%	20%	20%
79	226	13	92%	100%	43%	41%
80	230	11	100%	100%	56%	56%
83	278	11	63%	≥73%	47%	≈53%
84	96	13	69%	≥77%	31%	≈29%
85	226	16	81%	≥81%	7%	≈28%
89	460	52	81%	90%	7%	10%
90	222	27	96%	≥96%	24%	≈24%
92	246	27	74%	≥85%	5%	≈4%
93	477	34	65%	≥71%	12%	≈11%
95	472	49	80%	94%	22%	19%
20	4411	392	84.2%	≥91.7%	18.4%	≈21%

Table 7.2 Approximate quantitative relationships between hormones in rapid sampling adrenal axis experiments. N_{samp} is the number of samples in each experiment, N_{ACTH} is the number of ACTH pulses found in each experiment, AVP/CRH means AVP and/or CRH, and → indicates relationship, i.e. ACTH←AVP is the percentage of ACTH pulses related to an AVP pulse, while AVP↛ACTH is the percentage of AVP pulses not related to an ACTH pulse. The last row contains column averages or totals as appropriate. The percentages listed indicate that AVP and CRH may be able to explain the great majority of ACTH events.

Objectivity was carefully considered at all times, and the entire pulse identification procedure was repeated to ensure consistency (or at least consistent subjectivity).

Having identified pulses in the data it is then important to use a consistent and physically meaningful method for relating pulses of AVP or CRH to pulses of ACTH. The delay between pulses was initially required to be in the range -1 sample to +150s. This range was used because assay noise might have caused the onset, or peak, of an ACTH pulse to preceed that of the secretagogue causing it by 1 sample, while the maximum delay apparent in any AVP/CRH bolus administration experiment is 150s. It is perhaps more important to be clear about how the value of the delay was determined since, with 30s sampling, pulses are defined by multiple samples. One must therefore make assumptions about which feature of the AVP or CRH pulse is the signal, and which feature of the ACTH pulse is the response. The features used were the steepest or most rapidly varying of

1. the transition from basal secretion to the leading edge of the two pulses,
2. the peaks of the two pulses, or
3. the steepest sections of the leading edges of the two pulses.

Pulse parameters are listed above in order of preference, since presumably the leading edge is a more important signal than the peak, particularly for AVP [Watanabe and Orth, 1987]. The delay between pulses is then the delay between their most temporally defined aspects as illustrated in figure 7.3, where labels correspond to those used in the above list. Obviously, each pulse in hormone X, say, can be related to only one pulse in hormone Y.

The number of pulses found depends on the pulse parameters emphasized and the level of significance required. For this reason, pulse identification using different methods will always 'find' different numbers of pulses. In contrast, the percentages of related pulses listed in table 7.2 will not vary to the same extent, since adjusting pulse identification parameters to find more ACTH pulses, say, should also find more AVP

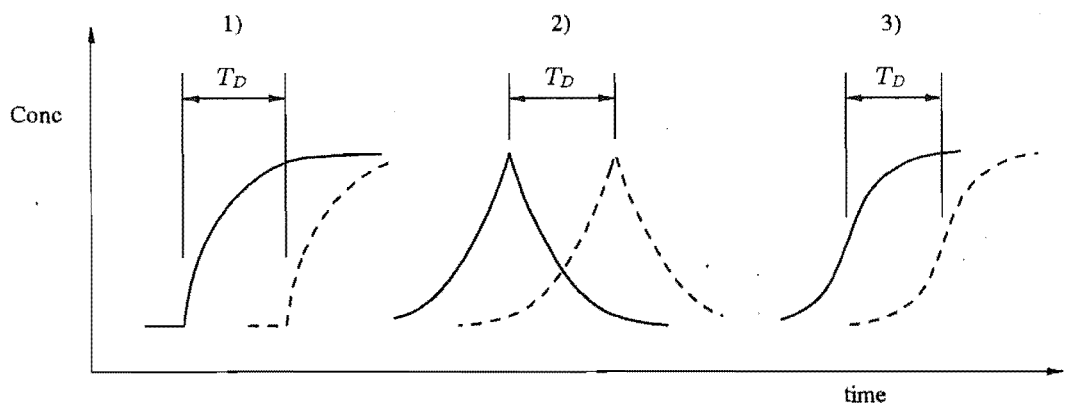

Figure 7.3 Illustration of the delay between pulses in hormone X, say (solid line), and hormone Y (dashed line).

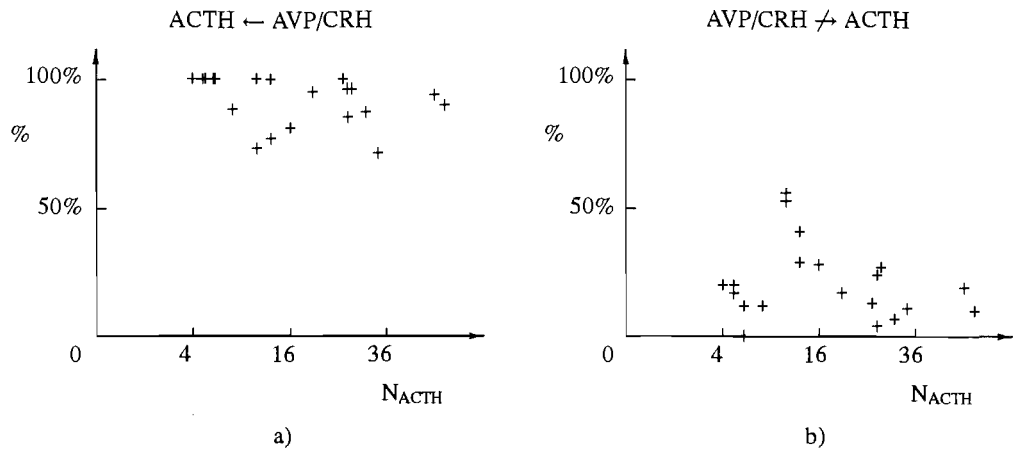

Figure 7.4 Relationships between ACTH, and AVP and CRH pulses. (a) shows the percentage of ACTH pulses which were related to an AVP or CRH pulse. (b) shows the percentage of AVP and CRH pulses which were not related to an ACTH pulse. See table 7.2 for label definitions.

and CRH pulses, although just how many would be difficult to predict. The values in table 7.2 can therefore be regarded as an accurate measure of the relationships between pulses, given the band of allowable delays. Some of these values are also plotted in figure 7.4, which perhaps more clearly illustrates that AVP and CRH may be closely coupled with ACTH. The closeness of this coupling is an important issue and it is therefore essential to consider the effect of incomplete CRH measurement. 8% of all ACTH pulses were associated with CRH pulses in the absence of AVP pulses, but CRH was assayed for only 57% of total experimental time (less if actual sample numbers are used). It is therefore reasonable to predict that an extra 6% of ACTH pulses could have been related to CRH, if CRH had been assayed in all samples. This suggests that in 20 experiments with 4411 total samples, 98% of ACTH pulses may be related to AVP and/or CRH pulses. Additional comments on this percentage follow the analysis of delay between AVP or CRH and ACTH in section 7.2.

Comparison of the columns in table 7.2 also supports another of the findings of the previous subsection, that AVP and ACTH appear to be more closely related than CRH and ACTH, at least in the horse. 70% of ACTH pulses were associated with AVP pulses occurring without CRH pulses. However, only greater than 8% (probably $\approx$14%) were associated with CRH pulses occurring in the absence of AVP pulses. The uncertainty in the percentage arises because of the incomplete CRH data. A more complete comparison of AVP→ACTH vs CRH→ACTH based on relationships between pulses was not attempted because: (a) CRH is typically assayed for only part of an experiment (often less than 50%); (b) under physiological conditions CRH does not appear to be very pulsatile; and (c) the assay error at physiological CRH concentrations is quite large (see section 6.3.3). These factors would strongly bias such a comparison in favour of AVP as the more potent secretagogue.

7.1.3 Modeling

There are complicated mechanisms behind the secretion of ACTH from corticotropes. The previous two subsections have indicated how crosscorrelation and pulse analysis might fail to uncover these. In addition, the basic mechanisms behind ACTH secretion are known, although their dynamics are in dispute, so what appears to be most urgently required is an analysis of the dynamics and interactions of different adrenal axis hormones. Such investigations require thoughtful experimental design, increasingly precise experiments and probably more sophisticated data analysis than has been conducted to date. In this last context, modeling is likely to be more informative than more simplistic data analysis techniques like crosscorrelation and pulse identification.

The foundation of a modeling approach is an accurate model of the mechanisms which are understood to be behind ACTH secretion. This model can then be used, in conjunction with experimental data, to: (a) investigate how well ACTH secretion is actually understood, which is assessed by how well the model 'explains' the data; (b) investigate additional mechanisms or relationships, which, when included in the model, result in a better fit to the data; and (c) plan new experiments to test hypotheses suggested by (b). In this way the entire data set is used, rather than just one aspect of it, and there is greater sensitivity to the more subtle mechanisms behind ACTH secretion, which is perhaps the area where the greatest advances are still to be made.

Section 7.3 initiates such an investigation by applying a model, which has already been proposed, to PES data.

7.2 Delay

In addition to determining the magnitude of the ACTH response to a particular sequence of secretagogue concentrations, a model must also predict the delay by which the response follows the secretagogues, henceforth referred to as T_D. It appears that no attempt has been made to analyse the length of this delay, the cause of it, or even if it exists. This may be because *in vitro* the length of this delay is less than the temporal resolution of most perifusion systems and, hence, it could be regarded as insignificant. However, an investigation seems important because some *in vivo* AVP and CRH bolus administration experiments suggest that the delay may be much larger *in vivo*. Such an investigation may also shed light on mechanisms behind ACTH secretion.

7.2.1 Delay in *in vitro* data

To avoid the effects of a whole host of non-specific influences and unmeasured factors, the simplest place to look for delay is in *in vitro* data, although there is only one source of *in vitro* data with sufficient temporal resolution to show a delay [Watanabe and Orth, 1987; Watanabe *et al.*, 1989]. The method used to determine delays is described in section 7.1.2, since in hormone data it is only feasible to determine delays between pulses. Timing information obtained by comparing, in whatever way, two low hormone concentrations is too sensitive to noise.

Figure 7.5 shows the results from relating pulses of AVP and CRH in the *in vitro* data of Watanabe and Orth [1987] to ACTH pulses in the same data. Observe that there

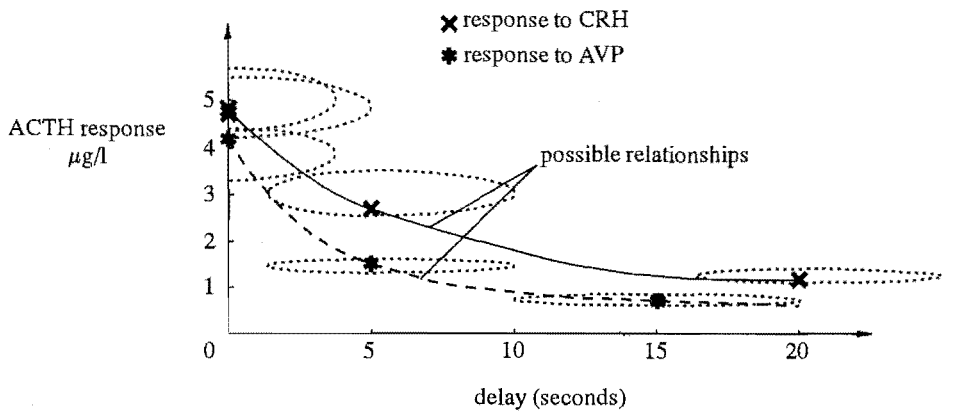

Figure 7.5 The delay between AVP or CRH administration and ACTH release in the perifusion system of Watanabe and Orth [1987]. Maximum uncertainty in the position of a plotted point is indicated by the surrounding ellipse which was determined by inspection.

were four CRH pulses and three AVP pulses. Since the data has virtual step changes in AVP and CRH concentrations occurring in the absence of other changes, this is clearly a stimulus-response relationship. Figure 7.5 therefore indicates that a delay exists, and also suggests that its value varies inversely with the ACTH response.

7.2.2 Mechanisms behind delay

The apparent *in vitro* relationship between ACTH response and delay (see figure 7.5) may arise because the rate limiting step for ACTH release involves the conversion of intracellular substance B to intracellular substance G. This can be represented as

$$\text{AVP or CRH} \quad \cdots \longrightarrow \text{B} \longrightarrow \text{G} \longrightarrow \cdots \quad \text{ACTH} \tag{7.1}$$

from which it can be immediately appreciated that the rate of ACTH release (R_{ACTH}) is proportional to the concentration of B (C_B). This gives the desired relationship for delay, namely

$$T_D \propto \frac{1}{C_B}$$

Alternatively, the rate limiting step might be catalysed by substance E, i.e.

$$\text{AVP or CRH} \quad \cdots \longrightarrow \text{B} \xrightarrow{\text{E}} \text{G} \longrightarrow \cdots \quad \text{ACTH} \tag{7.2}$$

$$\Rightarrow R_{ACTH} \propto f(C_E)$$

$$\Rightarrow T_D \propto \frac{1}{f(C_E)}$$

where $f(\cdot)$ represents the (usually non-linear) relationship between the concentration of E and the rate of ACTH release. The actual rate limiting step in the release of ACTH may, of course, be more complicated. Diffusion may also play a part in the delay, although diffusion times over cellular distances are usually negligible [Florey, 1966].

Therefore, if further evidence supports the type of response/delay relationship suggested by figure 7.5, such a relationship is most likely to be due to a process similar to (7.1) or (7.2).

7.2.3 Can PES measure a delay *in vivo*?

The delay between ACTH and AVP or CRH *in vitro* (see figure 7.5) suggests that PES, with a sampling interval of 30*s*, may have insufficient temporal resolution to estimate delay accurately. However, in some AVP and CRH administration experiments (see figure 6.2) the delay appears to be of the order of 1-2 minutes. This discrepancy is cause for concern when one aims to construct a model of ACTH regulation, based on both *in vitro* and *in vivo* data.

The first step in an investigation of delay *in vivo* is to determine that it actually exists. To this end, the delays associated with all of the relationships in table 7.2 were determined. Figure 7.6 shows the ACTH response as a function of this delay. To be significant the number of relationships with a particular delay must exceed the number that could reasonably occur if the two hormones were unrelated. This is because, even if two hormones are unrelated, identification of some related changes is expected, due to the number of pulses in PES data, and the -30 to 150*s* window of allowable delay. The number of spurious relationships found will depend on the number of pulses, their distribution and the length of the experiment. The number of pulses and the experiment length are measured (see table 7.3), and the most appropriate distribution of events to assume is a uniform distribution, given that pulses of hormone appear to occur at

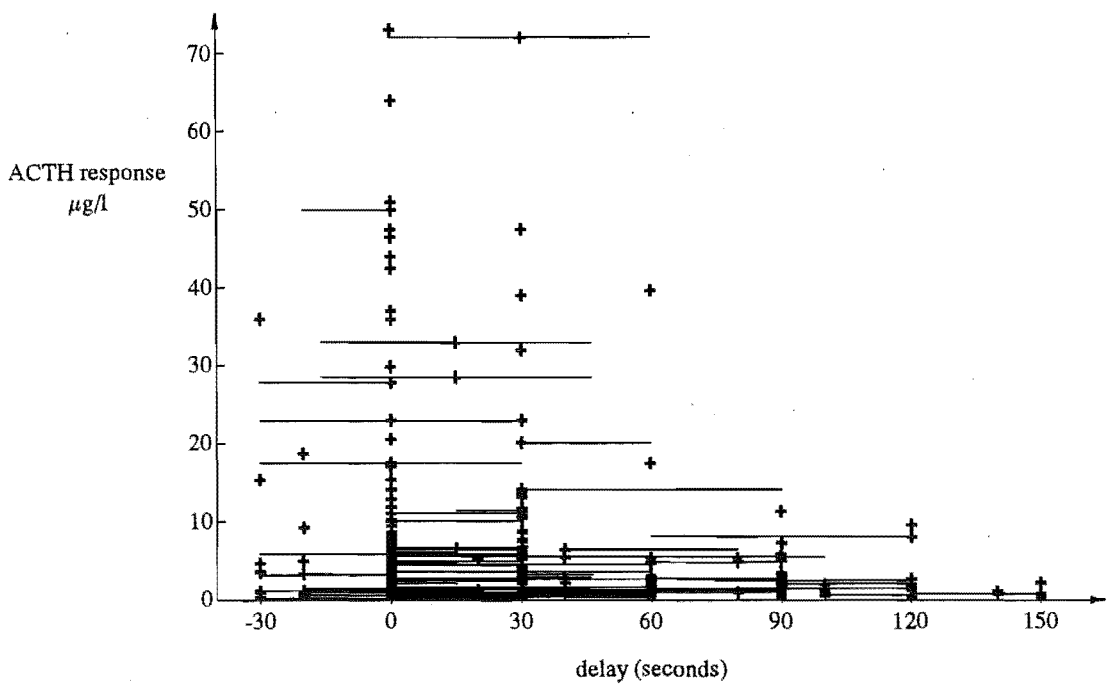

Figure 7.6 The complete set of delays between AVP or CRH and ACTH. Where the temporal error in any point is greater than customary (see figure 7.5 for an indication of customary errors) it is plotted with an error bar. Note that the shape of the pulses often resulted in temporally asymmetric errors.

Horse	effective N_{samp}	sampling interval	N_{ACTH}	$N_{AVP/CRH}$	N_{rel}	$\bar{N}_{sim}$	$N_{rel} \leq \bar{N}_{sim}$
60	300	20s	31	$\geq$29	27	14.0	+
62	122	30s	5	6	5	1.4	+
63	62	20s	6	6	6	2.8	+
69	84	20s	5	6	5	2.1	+
71	358	30s	28	$\geq$37	27	12.3	+
72	59	30s	6	7	6	2.9	+
73	107	30s	26	30	26	17.4	+
74	223	20s	20	23	19	9.8	+
75	42	30s	8	8	7	4.6	
77	38	30s	4	5	4	2.1	
79	219	30s	13	22	13	5.8	+
80	225	30s	11	25	11	5.5	+
83	271	30s	11	$\geq$17	8	3.6	+
84	94	60s	13	$\geq$14	10	5.0	+
85	225	30s	16	$\geq$18	13	5.9	+
89	460	30s	52	52	47	22.6	+
90	210	30s	27	$\geq$34	26	14.6	+
92	235	30s	27	$\geq$24	23	10.9	+
93	470	30s	34	$\geq$27	24	9.4	+
95	472	30s	49	57	46	22.9	+
20	4272		392	$\geq$447	353	175.5	+

Table 7.3 Information for, and results from delay simulation. The effective number of samples used for simulation is less than, or equal to, the number of samples in an experiment. This is because delays are not established where the sampling interval is greater than 1 minute, and some experiments had periods of slower sampling. $N_{AVP/CRH}$ is the number of AVP and CRH pulses found, N_{rel} is the number of relationships between AVP and CRH, and ACTH found, $\bar{N}_{sim}$ is the average number of relationships found by the simulation, and the last column is the result of the single sided test that the number of relationships found is not greater than the number that could occur by chance - N_{sim} (which is a random variable). + denotes significance at the 95% level.

randomly spaced intervals. The expected delay distributions were therefore calculated by simulation, with the appropriate number of ACTH and AVP+CRH pulses for each experiment being randomly assigned to positions amongst the appropriate number of samples. Delays between AVP+CRH and ACTH were then measured, and the whole process repeated 2×10^4 times for each of the 20 experiments. Pulses in the same time series could not occur at adjacent samples, or the first or last sample, and each pulse of ACTH or secretagogue could be used only once. 95% confidence limits on the number of relationships found with a particular delay, in a particular experiment, do not assume that the number is normally distributed. 95% confidence limits on the total number of relationships, with a particular delay, were calculated by summing the squares of the 95% deviations from the mean in individual experiments, and taking the square root (in the same way that when independent normally distributed variables are added together, the variance of the sum is the sum of the individual variances). Delays measured in experiments with 20s sampling were adjusted to be multiples of 30s

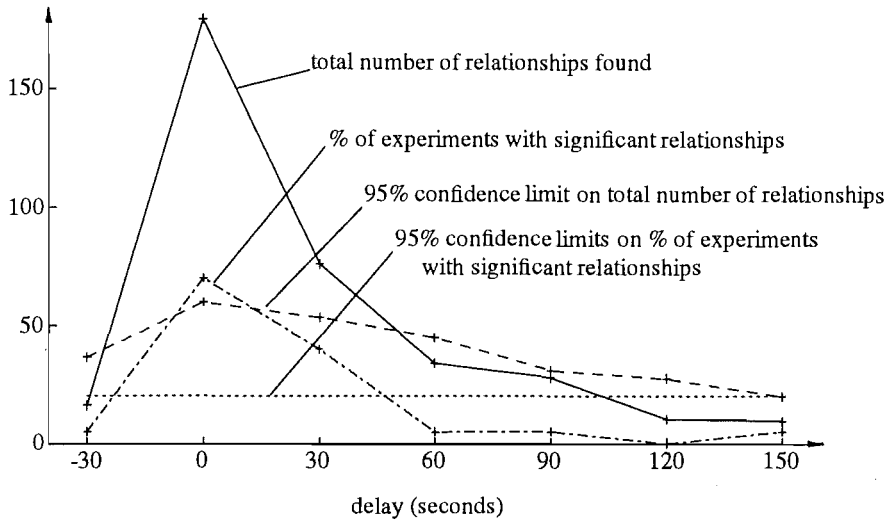

Figure 7.7 Evidence for delay. The solid line is the total number of relationships found in all 20 experiments analysed. 95% confidence limits for this total, were determined by simulation. A significant relationship is only present for delays of 0 and 30s. Also shown is the percentage of individual experiments in which there was a significant relationship, at the 95% level, for a particular delay.

by linear interpolation (i.e. 67% of the number of relationships with 20s delays were assigned to the 30s group, and 33% were assigned to the 0s group), which enabled all experiments to be compared and combined. Statistical limits were unaffected by this transformation, since the simulation used the actual experimental sampling rate and then transformed delays to be multiples of 30s.

The results of this simulation are displayed in table 7.3 and figure 7.7, where they provide the statistical limits for the delay measured in PES data. The last column in table 7.3 shows that, for all but two experiments, the number of relationships found at a significance level of 95% was greater than could be expected on the basis of chance. In the non-significant experiments, four of four, and seven of eight ACTH pulse were related to an AVP or CRH pulse, but the short experiment duration resulted in high uncertainty in the number of relationships which would usually be found. These results provide further evidence for close coupling between AVP and/or CRH and ACTH in all of the experimental situations tested.

There is some uncertainty in the justification for combining all of the PES experiments and examining the total delay (as in figure 7.7). However, the percentage of individual experiments in which any particular delay was found to be significant is also shown in figure 7.7, and would suggest that delays are similarly distributed in all experiments. In fact, this percentage, for delays other than 0 and 30s, is never greater than the average value expected, i.e. 5%.

In conclusion, there are a significant total number of delays with values of 0 and 30s, and a significant number of experiments where there are a significant number of delays with values of 0 and 30s. However, due to sampling in the presence of assay noise, a

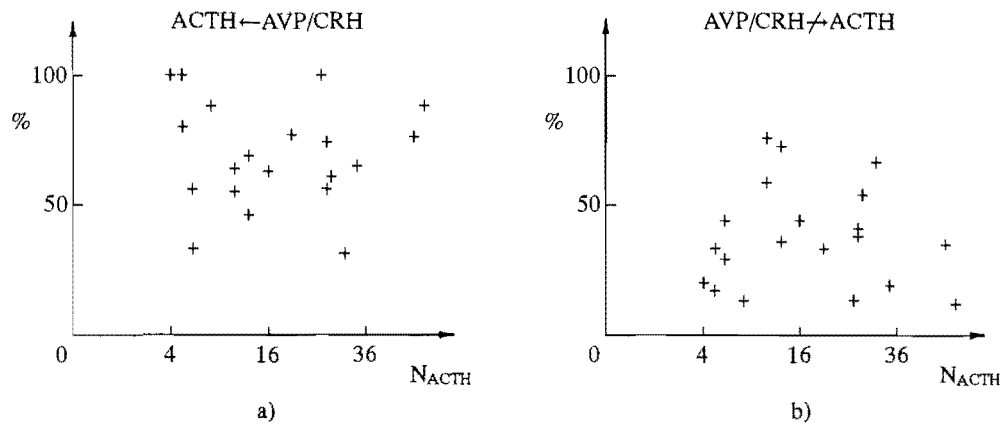

Figure 7.8 Relationships between AVP and/or CRH pulses and ACTH pulses, given that PES is unable to demonstrate a significant delay. (a) shows the percentage of ACTH pulses which can be related to an AVP or CRH pulse. b) shows the percentage of AVP and CRH pulses which are not related to an ACTH pulse. These results are a more accurate measure of the relationships between AVP and/or CRH and ACTH, than those in figure 7.4.

30s delay is not significantly different from no delay. This analysis therefore shows that **a non-zero delay is not apparent in PES data.** A better interpretation of the results in figure 7.7 is that the delay probably has a range of 0-30s, and a distribution weighted towards 0s. This agrees with delays found *in vitro* (see figure 7.5).

This finding has some important implications for the relationships between pulses of AVP and/or CRH and ACTH found in section 7.1.2, since some of these relationships do not satisfy $|\text{delay}| \leq 30s$. Figure 7.8 illustrates the new relationships. The average percentage of ACTH pulses explained by an AVP or CRH pulse drops from $\approx$98% ($\geq$92%) to $\approx$76% ($\geq$71%), while the average percentage of AVP and CRH pulses not associated with an ACTH pulse rises from 21% to 40%. Note that the figure of 76% accounts for unassayed CRH, and assumes that this CRH will have similar delay distribution to that in assayed CRH. These results provide evidence for the existence of additional ACTH secretagogues, as changes in cortisol concentration are unlikely to occur rapidly enough to cause ACTH pulses. They can also be compared with the results of Engler *et al.* [1989] using 5 and 10 minute sampling in 5 sheep, who found that 64% of ACTH pulses occurred with AVP or CRH pulses (calculated from their results). However in assessing the usefulness of Engler *et al.*'s results it must be considered that they found a massive 71% of AVP and/or CRH pulses occurred without ACTH pulses (again calculated from their results), and also that PES using 5 minute sampling shows considerably more concordance between AVP+CRH and ACTH than PES using 30s sampling [Alexander *et al.*, 1991].

7.2.4 Delay with AVP or CRH administration

As mentioned previously, in some situations where AVP or CRH were administered the delay appeared to be of the order of 30s to 2 minutes. The complete set of delays

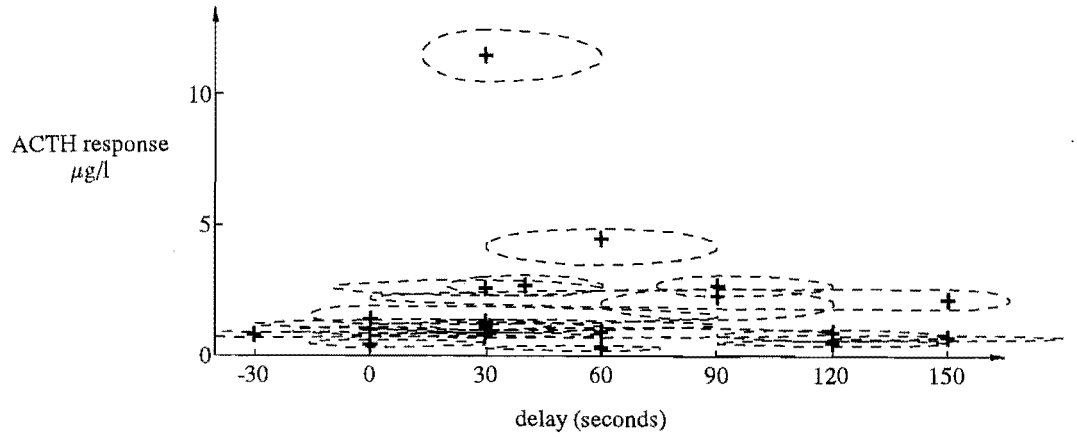

Figure 7.9 Delay between AVP or CRH and ACTH, where the AVP or CRH were administered. Maximum uncertainty in the position of a plotted point is indicated by the surrounding ellipse.

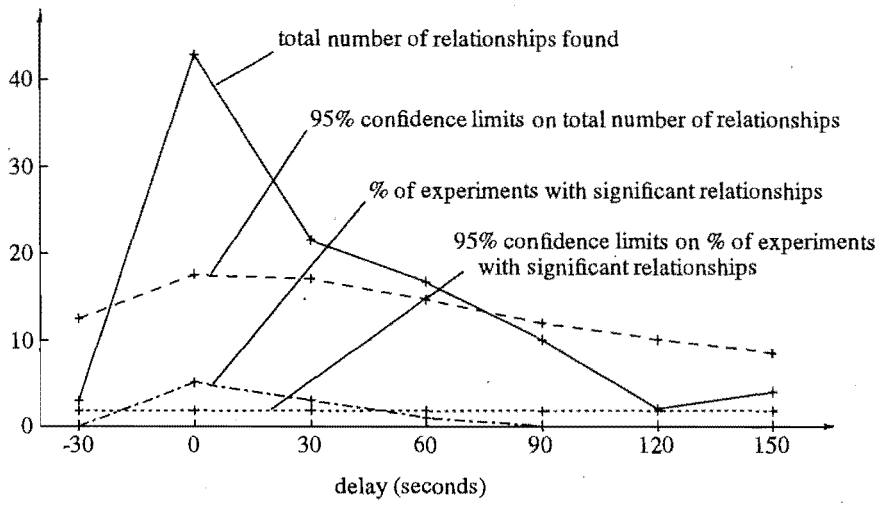

Figure 7.10 Evidence for delay in AVP and CRH administration experiments. The solid line is the sum of the relationships found in the seven AVP and CRH administration experiments, while 95% confidence limits for this sum were determined by simulation. A significant relationship is present at delays of $0s$, $30s$ and $60s$. Also shown is the percentage of individual experiments in which there was a significant relationship, at the 95% level, for a particular delay.

in response to AVP and CRH administration is plotted in figure 7.9, which shows that a good proportion of these delays do not have value zero. A simple explanation for this delay may be difficult to obtain, given that the points in figure 7.9 seem to be randomly distributed, and similarly, there is no consistent bolus delay in individual experiments. Statistical limits on just those delays in response to AVP and CRH boluses cannot be determined, so statistical limits for all delays in bolus administration experiments must be used. The results for this group of experiments are shown in figure 7.10, where the total number of delays is significant at delays of $0s$, $30s$ and $60s$. It therefore appears that the delay may be longer when AVP and/or CRH are administered, although note

that there is not a significant number of individual experiments with significant numbers of delays at $60s$. So, what are the possible explanations for the existence of a longer delay between ACTH and administered AVP or CRH? Several explanations are now postulated.

1. Although both AVP and CRH appear to cause ACTH release *in vitro*, at similar concentrations to those measured in bolus administration experiments [Familari *et al.*, 1989; Watanabe and Orth, 1987], recall the discussion in section 6.3.1. Endogenous hormones are substantially diluted while travelling from the adenohypophysis to the ICS, but exogenously administered hormones are not. PES will therefore underestimate pituitary concentrations of endogenous hormones, and so the ACTH response may not be associated with the secretagogue to which it was related. This, of course, requires that the ACTH response be related to something else, and there are often no other candidates.

2. Administration of a bolus of CRH, or more particularly AVP, may have dramatic non-specific effects which result in reduced blood flow through the pituitary. Part of the bolus would therefore reach the ICS cannula without delay, while part would experience substantial delay in passing through the pituitary. The ACTH response is to the AVP or CRH concentration in the pituitary, and so would be delayed by a similar amount of time. This scenario offers another simple explanation for the apparent situation in some experiments (e.g. Horse79), where small endogenous AVP and ACTH pulses are related with no delay, but there is a substantial delay between administered AVP or CRH and the apparent ACTH response. Problems with such a scenario are described below.

   (a) A delay through the hypothalamus, long portal vessels and pituitary of up to $120s$ (maximum delay minus uncertainty) is implied. While the delay involved has not been accurately measured, $120s$, or approximately 4 times the circulation time of peripheral plasma, seems like a very long time. Experiments to determine the delay through the hypothalamo-pituitary system have been conducted using the ICS catheter system and a labelled tracer, but have not produced clear results [Irvine, personal communication]. Note that such an experiment has the potential to provide extremely important new information on pituitary blood flow, and through deconvolution, the time course of hormone secretion.

   (b) AVP is a potent vasoconstrictor, but long and variable delays also occur with CRH and GnRH administration [Irvine, personal communication], and these hormones are not known to affect blood flow.

   (c) All hormone concentrations should be affected in the same manner, yet no increased correlation is apparent immediately following bolus administration.

   (d) Longer delays, in any particular experiment, seem to occur with lower concentrations of AVP or CRH. However, higher concentrations should have more effect on delay, if the delay is a result of non-specific effects.

(e) Although the ACTH response would occur as a single pulse, the AVP or CRH should increase in two (or more) steps separated in time by the value of the delay. Instead the highest AVP or CRH concentration usually occurs immediately after the bolus. Unfortunately, assay error, combined with a lack of information about pituitary blood flow, makes proving this unlikely.

3. The delay may occur in the pituitary, but to get a whole pituitary full of cells to produce ACTH pulses of short duration, large magnitude and after substantial delay, must require very active control. Such active control should be readily apparent, yet there appears to be no consistent relationship between the delay, in response to a bolus, and ACTH, AVP, CRH, or cortisol. It is difficult to postulate any mechanism operating in millions of corticotropes and capable of producing very short pulses with a randomly variable delay. In addition, if such long delays occur in the pituitary they should be observable *in vitro*.

4. The secretagogue pulse shape may be different when the hormone is administered. Specifically, it is possible that pulses originating in the hypothalamus might have steeper leading edges, and so the pituitary might respond more slowly to exogenously administered secretagogues. The problem with using the rate of change of AVP or CRH concentration as a signal for ACTH release, is that the size of the response should still be related to the delay, but it does not appear to be. There is also no sound *in vitro* evidence for the importance of rate of change, since the often quoted results of McIntosh and McIntosh [1985] rely on some very questionable interpolation to determine slope.

5. Cortisol has a pronounced negative feedback effect on ACTH release and might have some effect on delay. This explanation is not refuted by metapyrone administration experiments, which provide the highest percentage of zero delays, but where the delays are perhaps clearest (e.g. experiment Horse79) delay decreases while cortisol increases. Also, there is no *in vitro* evidence of a relationship between cortisol and delay [Oki *et al.*, 1991].

6. The delay determination scheme may be inappropriate. However, when hormones are administered their dynamics are usually well defined, and hence, the error in the delay is typically smaller than for endogenous pulses.

Since each of the above explanations has a rebuttal, none are individually satisfactory. It is possible that the increased delay with secretagogue administration is due to a combination of the above effects. The increased delay may also be caused by an entirely different mechanism. It seems that the result best illustrated by this analysis is how poorly understood some aspects of pituitary behaviour still are.

7.2.5 Summary

The analysis in this section indicates that the delay between AVP or CRH and ACTH appears to be similar *in vitro* and *in vivo*. Hence, based on *in vitro* studies with greater temporal resolution than PES, there is evidence that this delay is 0-30s, and that it is dose dependent. When AVP and/or CRH are administered in boluses *in vivo*, the delay

appears to be longer, although there is no satisfactory explanation for why this should be so. Under the assumption that PES has insufficient temporal resolution to distinguish a delay, only ≈76% of ACTH pulses can be associated with an AVP or CRH pulse, while 40% of AVP and CRH pulses do not appear to cause ACTH pulses. This is evidence that there are additional ACTH regulators other than AVP, CRH and cortisol.

7.3 The Schwartz Model of ACTH Regulation

The complexity of ACTH regulation is becoming increasingly apparent. One possible way the pituitary could decode the signal received from the hypothalamus is through the involvement of different populations of corticotropes, which would be differentially stimulated by increasing AVP or CRH concentrations. This idea is formalized in a model of ACTH regulation proposed by Schwartz *et al.* [1989a].

7.3.1 Background

It appears that corticotropes in the pars distalis can be subdivided into four groups, on the basis of the secretagogue they respond to [Jia *et al.*, 1991]. These groups are set out in table 7.4. There is also evidence that all corticotropes express receptors for both AVP and CRH [Childs *et al.*, 1987]. This result does not conflict with table 7.4 since AtT-20 cells do not respond to AVP, even though they have AVP receptors [Lutz-Bucher *et al.*, 1987]. In addition, the relative numbers of CRH/AVP receptors on corticotropes seems to be species dependent [Du Pasquier *et al.*, 1991; Shen *et al.*, 1990].

secretagogue responded to	% of corticotropes
medium	6%
CRH only	24%
AVP or CRH	56%
AVP and CRH only	14%

Table 7.4 Approximate percentages of sub-populations of corticotropes in the rat.

Schwartz proposed that the operation of corticotropes in the pars distalis could be modeled by two types of corticotrope, one which responded to AVP, and one which responded to CRH. As a result of a series of cell culture experiments using rat and sheep pituitary tissue [Schwartz *et al.*, 1991; Schwartz, 1990; Schwartz *et al.*, 1989a; Schwartz *et al.*, 1989b; Schwartz and Vale, 1988; Schwartz *et al.*, 1986], Schwartz also proposed the intercellular interactions and intracellular secretory mechanisms illustrated in figure 7.11. The main findings which relate to his model were:

- As AVP or CRH concentration increased, both the number of cells secreting ACTH and the amount of ACTH secreted/cell increased.
- Administration of a cytotoxic analog of CRH, which presumably killed cells expressing CRH receptors, resulted in undiminished response to AVP and increased

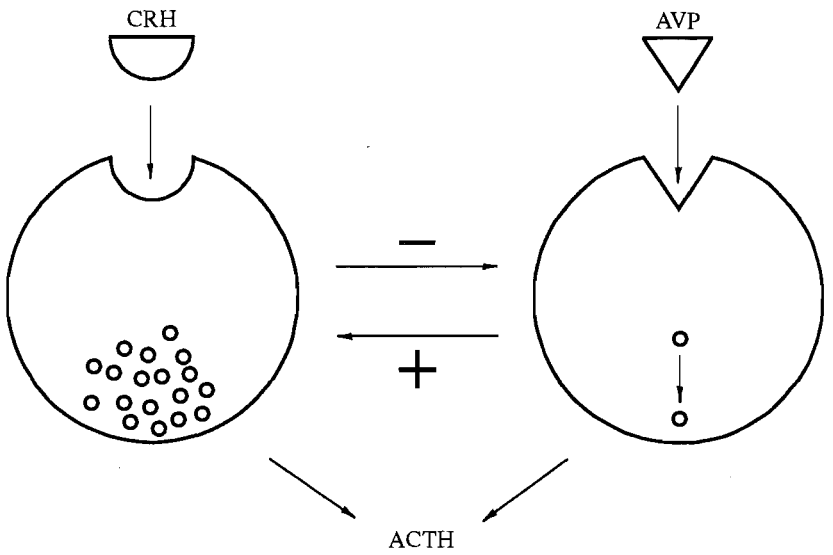

Figure 7.11 The Schwartz model of corticotrope action in the adenohypophysis. One type of corticotrope responds to AVP, stores little ACTH, secretes a stimulatory paracrine factor and is responsible for most basal ACTH secretion. The other type of corticotrope responds to CRH, is responsible for the bulk of stored ACTH, secretes an inhibitory paracrine factor and contributes less to basal secretion. ACTH secretion from AVP-responding corticotropes is constitutive, whereas that from the CRH-responding corticotropes is regulated. (Reproduced from [Schwartz, 1990].)

basal secretion. This result was used to link AVP-stimulated and basal secretion to a constitutive process, and to support the inhibitory effect of CRH on AVP.

- In support of an inhibitory paracrine effect are observations that increasing the separation of cells, and hypothalamus-pituitary disconnection, both caused an increase in basal secretion [Engler *et al.*, 1988; Schwartz, 1990].

Obviously there must also be a positive paracrine interaction to explain potentiation of CRH and AVP on ACTH release. Unfortunately, in the bioassay employed by Schwartz and Vale [1988] the effects of CRH and AVP are only additive and not synergistic as in other *in vitro* systems [Watanabe and Orth, 1988]. It is thus not possible to investigate whether the synergism between CRH and AVP is due to interactions between their two pathways occurring in the same cell, or if the potentiating effect is due to paracrine communication between separate populations of AVP- and CRH-responding cells.

7.3.2 An interpretation of the Schwartz model

A quantitative interpretation of the model in figure 7.11 was required to determine how well it explains PES data, and thus, ACTH secretion *in vivo*. The interpretation made is formally described by (7.3)-(7.7), and is now introduced.

The relationship between the response of a cell and the stimulus is generally a sigmoid function of the form

$$M(x) = x^3/(a^3 + x^3) \tag{7.3}$$

where a determines the 'spread' of the curve along the x-axis. The particular sigmoids used here are specified by choosing $a = 165$ for AVP and $a = 18$ for CRH. The constitutive response of the AVP-responding cell is the sum of basal secretion and the response to a suitably averaged and delayed AVP signal. A delay of 15 minutes was used, which is, if anything, too short. A Hamming window (*wind(x)*) [Harris, 1978] was chosen to emphasize the values near the center of the integration limits, i.e.

$$A(t) = \text{Basal} + 1.5 \int_{t-50}^{t-15} wind(M(\text{AVP}(\tau)))d\tau \tag{7.4}$$

$$\text{where} \quad \text{AVP}(t) = \begin{cases} \text{AVP}(t) & \text{for} \quad t \geq 0 \\ \frac{1}{25}\int_0^{25} \text{AVP}(\tau)d\tau & \text{for} \quad t < 0 \end{cases} \tag{7.5}$$

The ACTH response to CRH is regulated and can written as

$$C(t) = 6M(\text{CRH}(t)) \tag{7.6}$$

Now combining the response of each cell type and including the effects of the intercellular interactions results in the total ACTH response, i.e.

$$\text{ACTH}(t) = A(t)[1 - C(t - 0.5)/2] + C(t)[1 + A(t - 0.5)/2] \tag{7.7}$$

where times are in minute units. Figure 7.12 shows the ACTH predicted by (7.7) on the basis of the AVP and CRH concentrations from experiment Horse79, along with

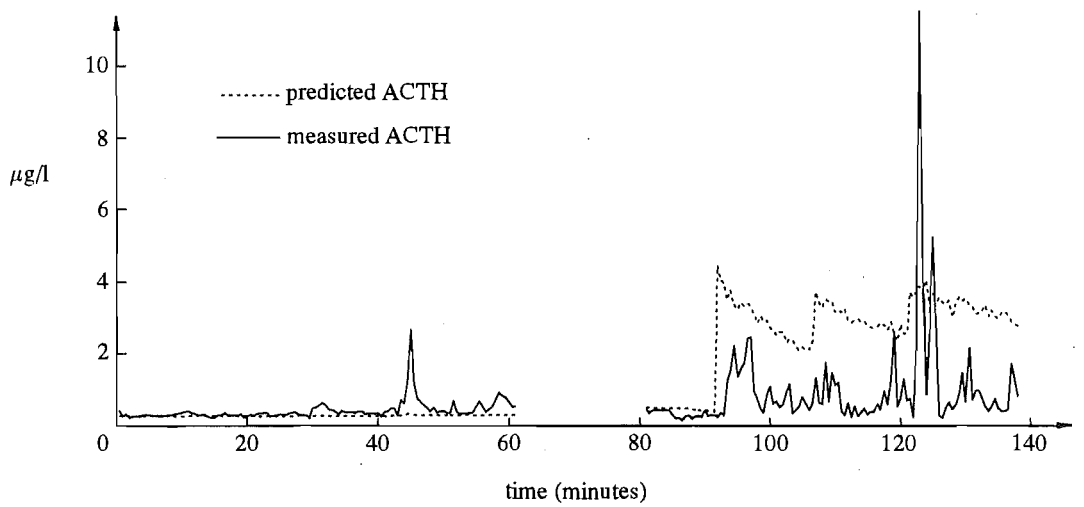

Figure 7.12 Fit of the Schwartz model to the data in experiment Horse79, an AVP and CRH administration experiment. ACTH between 60 and 80 minutes is not shown because the sampling rate was inadequate.

actual ACTH concentrations from this experiment. The complete disparity between the dynamics of the two series makes it obvious that (7.3)-(7.7) are unable to explain ACTH secretion *in vivo*. Some of the problems with the model are outlined below.

One of the cornerstones of Schwartz' work is the removal of corticotropes which are responsive to CRH with a cytotoxic analogue of CRH. However, all corticotropes express CRH receptors [Childs *et al.*, 1987], and can respond to CRH [Jia *et al.*, 1991], so it is uncertain which cells remain viable following this treatment. Presumably cells with smaller numbers of CRH receptors have a greater chance of surviving, but these cells can not be assumed to correspond to corticotropes which respond to AVP. Potentiation between AVP and CRH occurs if CRH is presented first, but not if AVP is presented first [Watanabe and Orth, 1987]. The model in figure 7.11 suggests the opposite. Finally, the constitutive secretory process included in the model can not explain the observed time delay between AVP administration and ACTH response (e.g. $0 - 15s$ [Watanabe and Orth, 1987], <5 min [Evans *et al.*, 1988], <5 min [Mason, 1988], PES $0 - 30s$ (see section 7.2)).

The question of how to make a model which is more sucessful at predicting ACTH secretion then arises.

7.4 Ideas Behind Modeling ACTH Regulation

Schwartz' model in figure 7.11 is principally based on data from static cell culture experiments. In attempting to model the *in vivo* situation in the horse, it is more accurate to base the model on *in vivo* data, or where this is unclear, suitable *in vitro* data.

7.4.1 Summary of results from *in vitro* studies

There have been a large number of relevant *in vitro* studies on the operation of corticotropes, results of which have already been reviewed in section 5.2. Here the intention is to elaborate on those results which have contributed directly to aspects of the model described in section 7.5.

The effects of the more important ACTH secretagogues have been best illustrated by a perifusion system which is capable of $5s$ sampling and which indicates that:

- The ACTH response to a step input of AVP is a brief pulse followed by a plateau phase which continues for as long as AVP remains elevated [Oki *et al.*, 1990; Watanabe and Orth, 1987; Watanabe *et al.*, 1989; Won *et al.*, 1990].
- In contrast, the ACTH response to a step input of CRH is a plateau which continues for as long as CRH remains elevated [Oki *et al.*, 1990; Watanabe and Orth, 1987; Won and Orth, 1990].
- Dexamethasone, which will presumably have a similar effect to cortisol, eliminates the plateau phase of the response to AVP, but leaves the initial peak undiminished [Oki *et al.*, 1991].
- In contrast, dexamethasone reduces the magnitude of the response to CRH [Oki *et al.*, 1991; Won and Orth, 1990].

- Synergism of AVP with CRH occurs only if the AVP pulse occurs with, or after, the CRH pulse [Watanabe and Orth, 1987]. Note that this behaviour can not be explained by the model in figure 7.11. When AVP and CRH are administered together, the shape of the response may resemble the sum of the two responses [Oki *et al.*, 1990].

- The delay between AVP or CRH presentation and ACTH release is 0-20s, which requires a regulated secretory process.

Mechanisms which are likely to be responsible for these results have been discussed in section 5.2. The extent to which these *in vitro* observations coincide with *in vivo* corticotrope behaviour is possibly best decided through their incorporation in a model.

7.4.2 Observations of interest from the horse

Although *in vivo* data are much more difficult to interpret than corresponding *in vitro* data, such interpretation is essential to understanding physiological ACTH regulation. Some *in vivo* observations from the horse, which are important guidelines in formulating a model are:

- Under physiological circumstances ACTH and AVP are secreted in very brief pulses, which occasionally last less than 30s.

- The dynamic ranges of AVP and ACTH concentrations are very large.

- AVP and ACTH are correlated in unstressed horses and all stresses seem to cause increases in AVP, which are associated with increases in ACTH [Alexander *et al.*, 1991].

- Under basal conditions, ICS CRH concentrations are low (typically 0.4-1 pmol/l) and relatively stable. Both at rest, and during stress induced by exercise or hyperosmolality, acute increases in ACTH are not accompanied by CRH rises, although in several horses CRH was observed to increase after exercise [Alexander *et al.*, 1991]. The gradient between ICS and jugular CRH concentrations is usually small, even when the levels are not stable [Alexander, unpublished], and only minor amounts of CRH are removed during passage through the pituitary [Alexander *et al.*, 1991]. In addition, administration of as little as 1μg of CRH is sufficient to stimulate an ACTH response. It therefore appears that in resting horses there is little CRH secretion, and furthermore, that CRH does not drive the acute rises in ACTH observed under some conditions.

- Reductions in blood cortisol levels, induced by metapyrone administration, stimulate a dramatic increase in ACTH secretion which is accompanied by major increases in both CRH and AVP secretion. Although the relative increase in AVP is much greater than that for CRH, in agreement with other studies [Plotsky and Sawchenko, 1987; Sapolsky *et al.*, 1990], the correlation between CRH and ACTH increases dramatically.

7.5 A Proposed Model of ACTH Regulation

The aim of this section is to describe the model illustrated in figure 7.13, which is based on realistic mechanisms operating within or between corticotropes, and has inputs of AVP, CRH and cortisol. This model provides a useful prediction of the ACTH variations measured by PES, and hence, can be used to assess the way in which ACTH release is regulated in the horse.

7.5.1 Background to the model

AVP and CRH stimulate ACTH secretion through different pathways and they may also operate on different corticotrope sub-populations. A model which separates these

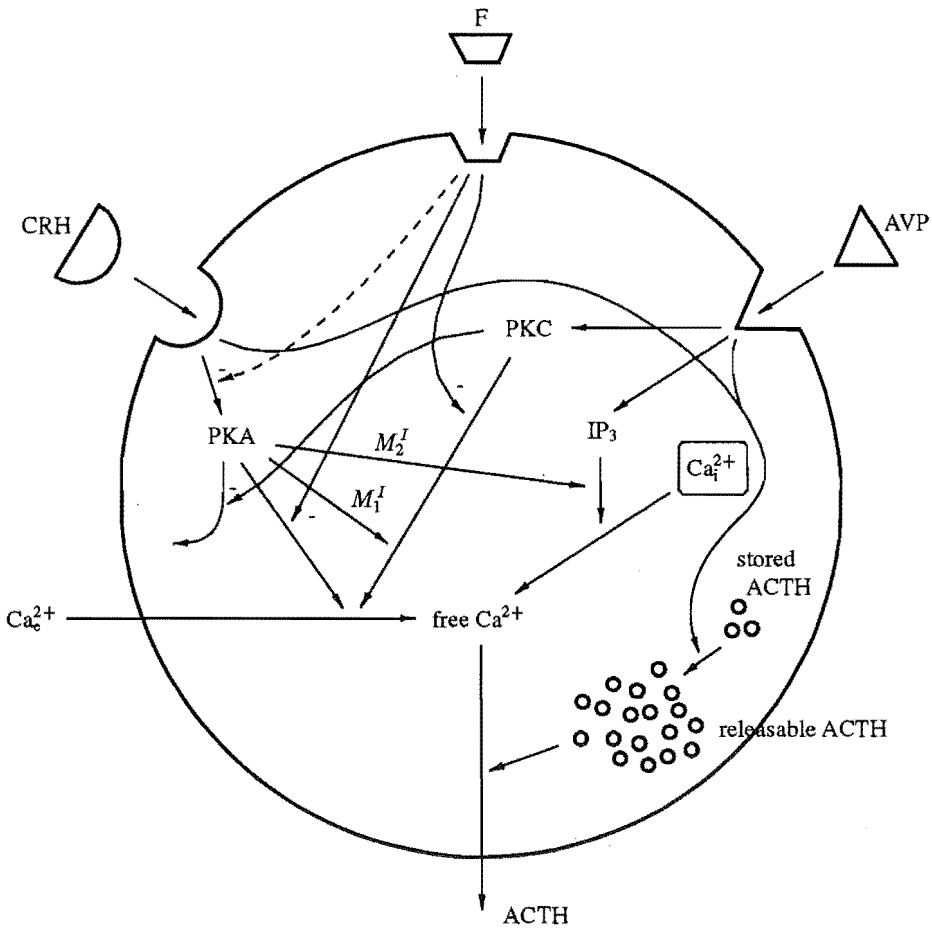

Figure 7.13 A possible model of ACTH regulation. Symbol meanings are: Ca_e^{2+}, extracellular calcium; Ca_i^{2+}, intracellular or sequestered calcium; IP_3, inositol 1,4,5-trisphosphate; PKA, protein kinase A; and PKC, protein kinase C. $M^I_{1\&2}$ are undetermined intracellular messengers. The dashed line represents a possible effect of cortisol on cAMP [Nicholson and Gillham, 1989; Oki *et al.*, 1991], which is not included in the model but which will be discussed with the modeling results. All interactions are stimulatory, except where there is a negative sign. The curved arrow under PKA represents loss of PKA activation (due to cAMP degradation).

pathways is essential since they have different dynamics. However the precise physiology behind the separation is not essential since the one model can represent both situations. The pathways may well both occur in the same cell. Certainly, the greatly increased ratio of AVP to CRH receptors on corticotropes likely in the horse over the rat [Alexander *et al.*, 1991; Du Pasquier *et al.*, 1991; Shen *et al.*, 1990], combined with the corticotrope sub-populations in the rat (see table 7.4), could be interpreted to mean that corticotropes which respond to AVP predominate in the horse.

The close association between Ca^{2+}concentration in the corticotrope and ACTH release has already been reviewed in some detail in section 5.2. It therefore seems sufficient to relate ACTH release directly to Ca^{2+}concentration, which has the advantage that the mechanisms leading to Ca^{2+}concentration changes are better understood than those connecting these changes to ACTH release. Current understanding of the mechanisms behind ACTH release is also reviewed in section 5.2 and illustrated in figure 5.4. The model in figure 7.13 is a simplified version of the mechanisms detailed in figure 5.4, but it retains the important dynamic aspects of each pathway, and incorporates cortisol. No attempt has been made to incorporate the longer term effects of cortisol on protein synthesis [Keller-Wood and Dallman, 1984]. This is because quantitative information on this process is unavailable, and PES experiments are too short to allow the effect to be estimated, except perhaps for the last part of the experiment. The difference equations governing the behaviour of this model are formally written in (7.8)-(7.15) and are now introduced.

Binding of CRH to its receptor causes a rise in cAMP with the relationship being described by f_2. This rise in cAMP is potentiated by PKC (which reduces cAMP degradation through reduction of cAMP phosphodiesterase (PDE) activity (see figure 5.4)) with the relationship being described by one function, f_1, since cAMP equilibrium is assumed to be reached quickly. Two equations are required to describe cAMP accumulation since the rise in ACTH output, in reponse to CRH, occurs more rapidly than the exponential decline following CRH removal. cAMP accumulation is intermediate between CRH binding to its receptor and protein kinase A (PKA) activation. To avoid an additional equation, it is equivalently modeled as PKA activation with the relationship between cAMP and PKA being incorporated into f_2. All of this can be abbreviated to

$$\mathrm{PKA}(t) = \begin{cases} [k_1 + f_1(\mathrm{PKC}(t))]f_2(\mathrm{CRH}(t)) & \mathrm{CRH}(t) \geq \mathrm{CRH}(t-0.5) \\ [k_1 + f_1(\mathrm{PKC}(t))]f_2(\mathrm{CRH}(t))[0.7 - f_1(\mathrm{PKC}(t))] & \\ \quad + \mathrm{PKA}(t-0.5)[0.3 + f_1(\mathrm{PKC}(t))] & \mathrm{CRH}(t) < \mathrm{CRH}(t-0.5) \end{cases} \tag{7.8}$$

where $f_1(\mathrm{PKC}(t)) < 0.7$.

PKC activation occurs in response to AVP binding with its receptor, the activation being described by f_3. Two equations are again required since a rise in PKC activation reaches equilibrium in less than $30s$, while the exponential decline following AVP reduction occurs more slowly. Thus

$$\mathrm{PKC}(t) = \begin{cases} 1.3f_3(\mathrm{AVP}(t)) & \mathrm{AVP}(t) \geq \mathrm{AVP}(t-0.5) \\ f_3(\mathrm{AVP}(t)) + 0.3\mathrm{PKC}(t-0.5) & \mathrm{AVP}(t) < \mathrm{AVP}(t-0.5) \end{cases} \tag{7.9}$$

Binding of AVP to its receptor results in a transient increase in IP_3 production, followed by an increase in IP_3 metabolism. This transient response is equivalently

modeled as a response to an increase in AVP binding, as described by f_4, and an exponential decay, i.e.

$$\mathrm{IP_3}(t) = \begin{cases} f_4(\mathrm{AVP}(t)) - f_4(\mathrm{AVP}(t-0.5)) + 0.4\mathrm{IP_3}(t-0.5) & \mathrm{AVP}(t) \geq \mathrm{AVP}(t-0.5) \\ 0.4\mathrm{IP_3}(t-0.5) & \mathrm{AVP}(t) < \mathrm{AVP}(t-0.5) \end{cases} \tag{7.10}$$

CRH has a synergistic effect on AVP-stimulated free Ca^{2+}concentrations which is here postulated to be mediated by two intra(possibly inter)-cellular messengers, M_1^I and M_2^I. These are generated in response to PKA activation, as described by f_5 and f_6, and metabolized at a constant fractional rate, i.e.

$$M_1^I(t) = f_5(\mathrm{PKA}(t)) + 0.3M_1^I(t-0.5) \tag{7.11}$$

$$M_2^I(t) = f_6(\mathrm{PKA}(t)) + 0.3M_2^I(t-0.5) \tag{7.12}$$

The $Ca_e{}^{2+}$ influx resulting from PKA and PKC activation is reduced by cortisol, as described by f_7, where $f_7(\mathrm{F}(t)) < 1$. The action of the two AVP-stimulated pathways in increasing free $Ca^{2+}$is potentiated by M_1^I and M_2^I. Thus

$$\text{free } \mathrm{Ca^{2+}}(t) = \mathrm{PKA}(t)[1-\mathrm{f_7(F}(t))]+\mathrm{k_2PKC}(t)[1+\mathrm{M_1^I}(t)][1-\mathrm{f_7(F}(t))]+\mathrm{IP_3}(t)[1+\mathrm{M_2^I}(t)] \tag{7.13}$$

The amount of ACTH available for release from corticotropes is depleted by ACTH release, but replenished at a non-zero rate, which depends on AVP [Liu *et al.*, 1990] and CRH [Autelitano *et al.*, 1990], i.e.

$$\mathrm{ACTH_{avail}}(t) = k_3 + f_8(\mathrm{AVP}(t)) + f_9(\mathrm{CRH}(t)) - \mathrm{ACTH}(t-0.5) \tag{7.14}$$

where $\mathrm{ACTH_{avail}}(t)$ is always less than some maximum value.

Finally, the amount of ACTH released depends directly on the free Ca^{2+}concentration in the corticotropes and the amount of ACTH available for secretion, and is described by the (smooth) relationship f_{10}. There is also a small basal component k_4, i.e.

$$\mathrm{ACTH}(t) = \mathrm{Ca^{2+}}(t) f_{10}(\mathrm{ACTH_{avail}}(t)) + k_4 \tag{7.15}$$

k_{1-4} are constants which differ between horse experiments and are fitted by trial and error. $f_{1-10}(x)$ are different monotonically increasing functions of x, typically similar to the sigmoid relationship described by (7.3), although they sometimes have value zero. These functions vary between experiments and have no set form, as is indicated by the example functions in figure 7.14. Some functions are described by a mapping rather than by an equation, since this allowed simpler fitting to the data by the trial and error approach used. Initially this mapping was just by a constant, i.e. $f(x) = kx$. If required by the fitting process, this linear function was changed to a monotonically increasing piecewise linear function, which is presumably more like the highly nonlinear relationships which $f_{1-10}(x)$ represent.

If the reader regards (7.8)-(7.15) as complicated, consider that they are certainly a lot simpler than the real intracellular processes occurring in corticotropes. (7.8)-(7.10), (7.13) and (7.15) are all accurate descriptions of the current understanding of the processes occurring at the intracellular level. Mechanisms behind potentiation are still an area of speculation (see section 5.2.3). (7.11) and (7.12) are a best guess at a

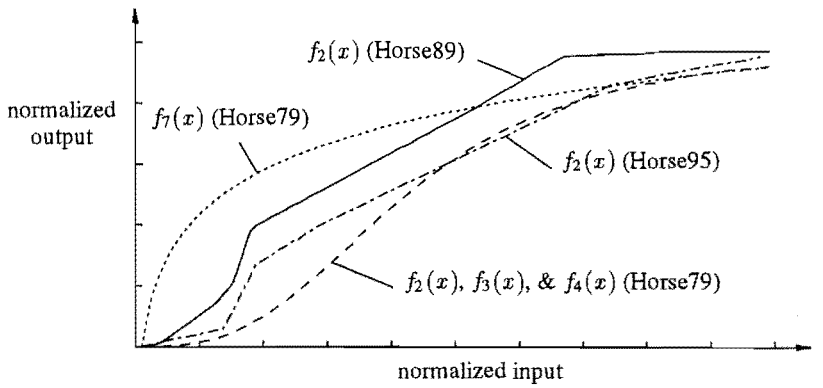

Figure 7.14 Some examples of $f_{1-8}(x)$, as used to predict the ACTH responses shown in figures 7.16-7.18.

realistic mechanism behind the potentiation of the two AVP-stimulated pathways, by the CRH-stimulated pathway. (7.14) is the area of the model most in need of examination, for ACTH synthesis is a slow process, yet here ACTH becomes available quickly. This rapid initiation of input of ACTH into the releasable pool does, however, improve the fit of the model to the data. Perhaps it represents active transport of ACTH secretory vesicles from 'storage' in the interior of the cell, along microtubules, to positions close to the cell membrane where they are available for exocytosis. The ACTH production process is discussed again in section 7.5.4.

7.5.2 Application to *in vitro* data

The model in figure 7.13 was initially tested with some *in vitro* style AVP and CRH concentrations to confirm that it can duplicate *in vitro* results. The results are shown in figure 7.15 where the dynamics of the predicted ACTH appear identical to those actually measured *in vitro* (not shown) [Oki *et al.*, 1991; Oki *et al.*, 1990; Watanabe and Orth, 1987; Won and Orth, 1990; Won *et al.*, 1990].

7.5.3 Application to *in vivo* data

A much more severe test of the model's usefulness is its ability to explain *in vivo* data. The results of fitting the model to the only PES data sets with ACTH, AVP, CRH and cortisol all assayed for a suffucient number of consecutive samples are shown in figures 7.16-7.18. These three data sets are not representative of the entire set of PES experiments, since one of the reasons that they are 'complete' is that ACTH appears to be more closely related to AVP and CRH in these experiments than in others. Nevertheless, the close correspondence between actual ACTH, and that predicted by the model, suggests that ACTH regulation is quite well understood in some *in vitro* and *in vivo* situations.

To be sucessful, a modeling analysis requires accurate estimates of the AVP, CRH and cortisol concentrations at the corticotropes. Following the discussion in section 6.3.1,

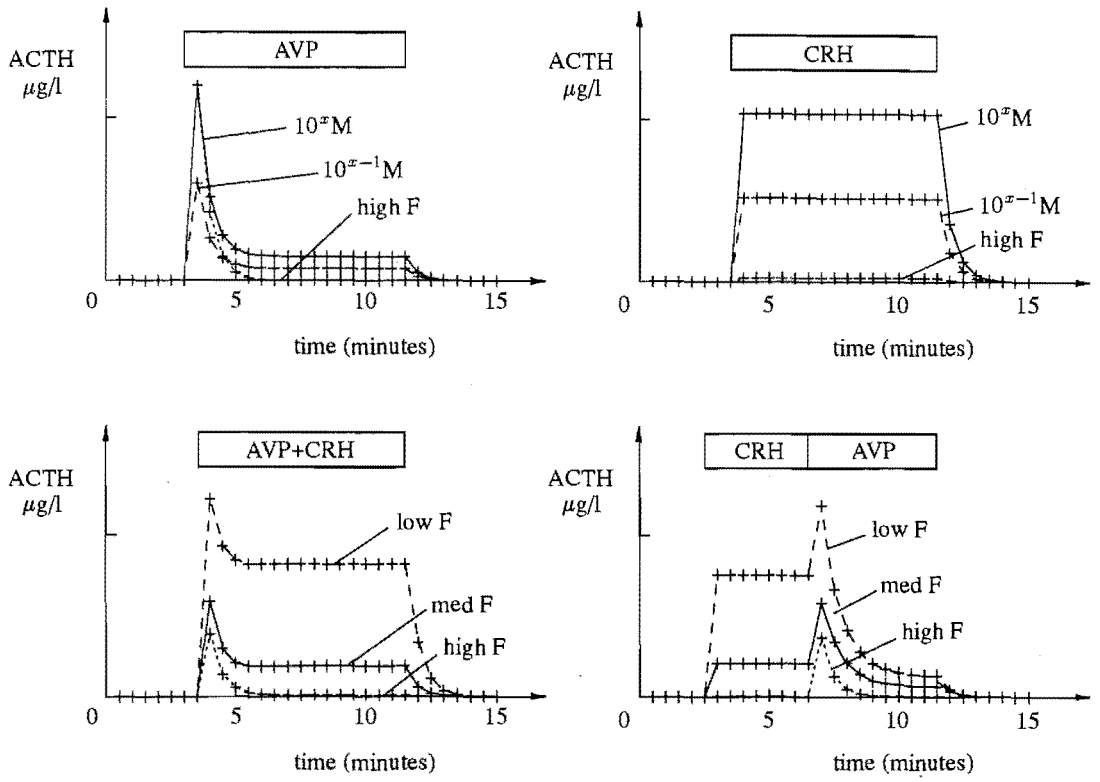

Figure 7.15 Predictions of ACTH by the model in figure 7.13 for various *in vitro* style AVP and CRH presentations. The box indicates the duration of presentation of a constant concentration of AVP or CRH, and is labelled with the secretagogue used. Relative molar (M) concentrations are indicated on the top two graphs.

it appears that PES accurately estimates adenohypophysial AVP concentrations, but a substantial proportion of CRH measured by PES will be the circulating level. Adenohypophysial CRH concentrations were therefore estimated as

$$\mathrm{CRH}(t) \approx 3[\mathrm{CRH}_{\mathrm{ICS}}(t) - \mathrm{CRH}_{\mathrm{jug}}(t)] + \mathrm{CRH}_{\mathrm{jug}}(t) \tag{7.16}$$

where subscripts $_{\mathrm{ICS}}$ and $_{\mathrm{jug}}$ refer to where the measurements were made. The coefficient 3 represents the dilution (range 2-10) in traveling from the adenohypophysis to the ICS. While a coefficient of 5 or 6 might initially appear to be a better 'average' choice, the bracketed term in (7.16) is the difference of similar concentrations which include considerable assay noise. A coefficient of 3 is therefore a compromise between realism and noise sensitivity. $\mathrm{CRH}_{\mathrm{jug}}(t)$ was determined by linear interpolation between (usually 5 min) samples. Where $\mathrm{CRH}_{\mathrm{jug}}(t)$ was greater than $\mathrm{CRH}_{\mathrm{ICS}}(t)$ it was set equal to $\mathrm{CRH}_{\mathrm{ICS}}(t)$. Also, use of different CRH assays appears to have had a significant effect in experiment Horse95 (see figure 6.4) [Alexander, personal communication]. To compensate for this effect CRH concentrations after 109 minutes were reduced by 0.4pmol/l. Adenohypophysial cortisol concentrations were determined by linear interpolation of peripheral concentrations.

The fit of the model to the data from experiment Horse79 (see figure 6.2) is shown in figure 7.16. Most of the variation in ACTH can be explained by AVP, with CRH playing

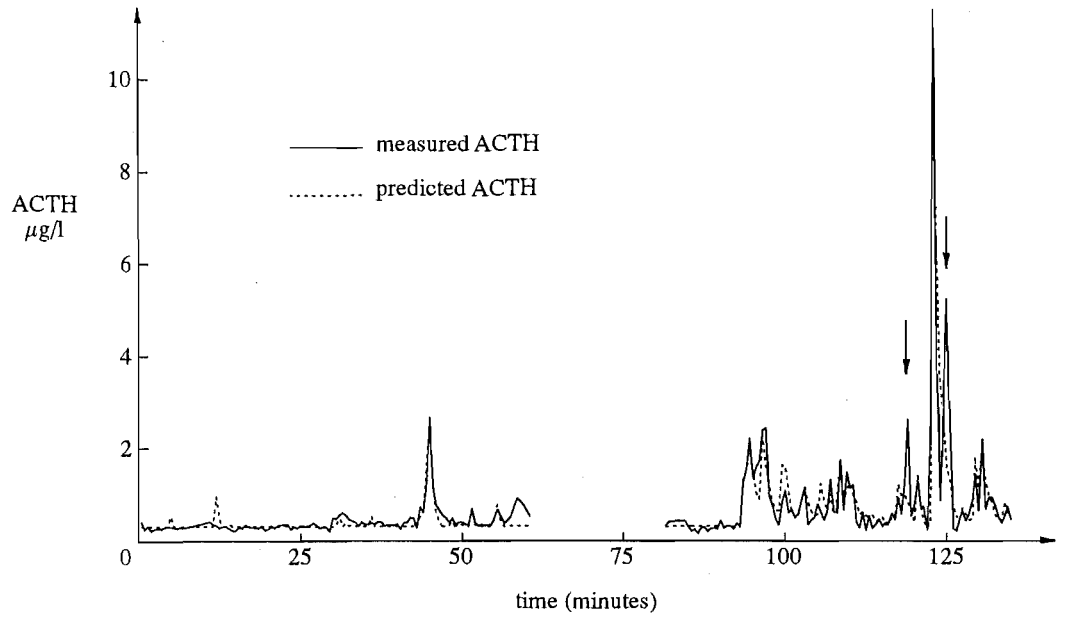

Figure 7.16 Model predictions of ACTH for experiment Horse79. As a result of the discussion in section 7.2.4, the model responses to boluses of AVP and CRH have been delayed slightly to produce the best alignment with the actual ACTH response. The middle section of the data is not shown, as the sampling interval was 5 minutes. Arrows indicate where actual and predicted ACTH disagree. Note that these data are the same as that used to test Schwartz' model in figure 7.12.

only a minor direct role, as expressed by the ratio of AVP-derived to CRH-derived ACTH, i.e. (from (7.13))

$$\frac{\int(k_2\mathrm{PKC}(t)[1+M_1^I(t)][1-f_7(\mathrm{F}(t))]+\mathrm{IP}_3(t)[1+M_2^I(t)])dt}{\int(\mathrm{PKA}(t)[1-f_7(\mathrm{F}(t))])dt} \approx 3$$

even with very high CRH concentrations, and

$$\frac{\max(k_2\mathrm{PKC}(t)[1+M_1^I(t)][1-f_7(\mathrm{F}(t))]+\mathrm{IP}_3(t)[1+M_2^I(t)])}{\max(\mathrm{PKA}(t)[1-f_7(\mathrm{F}(t))])} \approx 8$$

where $\max(x)$ is the maximum value of x. Other quantities come directly from (7.13). The $\approx$ sign indicates that the model fit is usually not critically dependent on the value of any one parameter. CRH appears to have an important indirect influence on ACTH release through potentiation of the effects of PKC and IP_3, with $\bar{M}_1^I(t) \approx 0.6$ and $\bar{M}_2^I(t) \approx 1$. AVP also has an indirect influence on ACTH release by potentiating PKA activation, with $\bar{f}_1(\mathrm{PKC}(t))/k_1 \approx 0.5$. Changes in cortisol concentration seem to be quite important, with $0.2 \leq f_7(F(t)) \leq 0.5$. Interestingly, ACTH depletion is not required to explain any of the observed declines in ACTH, i.e. $f_{10}(x) = 1$, suggesting that the unphysiological AVP and CRH administration scheme used provided insufficient stimulus to markedly reduce ACTH reserves in corticotropes.

The two most significant discrepancies between predicted and actual ACTH in figure 7.16 are indicated by arrows. The first may be a result of the finite sampling interval

which has smoothed out a quite large, but short, AVP pulse. The second provides more reason for concern since there is very little in the AVP/CRH/F data that can explain it. One possible explanation is that there is an additional factor stimulating ACTH secretion. Another, which is equally plausible, uses the fact that concentrations of endogenously produced hormones 'seen' by corticotropes are higher than those measured by PES, while exogenously administered hormone concentrations will be more accurately measured. This effect has been observed to alter the ratio of endogenous/exogenous hormone concentration by factors of 2-10 (see section 6.3.1). Consequently, there may have been a pulse of AVP in the adenohypophysis to stimulate the marked ACTH pulse, although such a pulse would not appear very significant when measured by PES in the presence of exogenously administered AVP. In line with such an explanation, the concentration of AVP, which decreased exponentially following the AVP bolus administration, deviates from exponential decline at the time of the unexplained ACTH pulse.

The fit of the model to the data from experiment Horse89 (see figure 6.3) is shown in figure 7.17. Most of the variation in ACTH is explained by CRH, with AVP playing only a minor role, as indicated by the ratio of CRH- to AVP-derived ACTH, i.e.

$$\frac{\int(\mathrm{PKA}(t)[1 - f_7(\mathrm{F}(t))])dt}{\int(k_2\mathrm{PKC}(t)[1 + M_1^I(t)][1 - f_7(\mathrm{F}(t))] + \mathrm{IP}_3(t)[1 + M_2^I(t)])dt} \approx 48 \qquad (7.17)$$

$$\frac{\max(\mathrm{PKA}(t)[1 - f_7(\mathrm{F}(t))])}{\max(k_2\mathrm{PKC}(t)[1 + M_1^I(t)][1 - f_7(\mathrm{F}(t))] + \mathrm{IP}_3(t)[1 + M_2^I(t)])} \approx 5$$

These two ratios indicate that CRH is enormously more effective at stimulating ACTH release in this experiment than in experiment Horse79, or even an average experiment

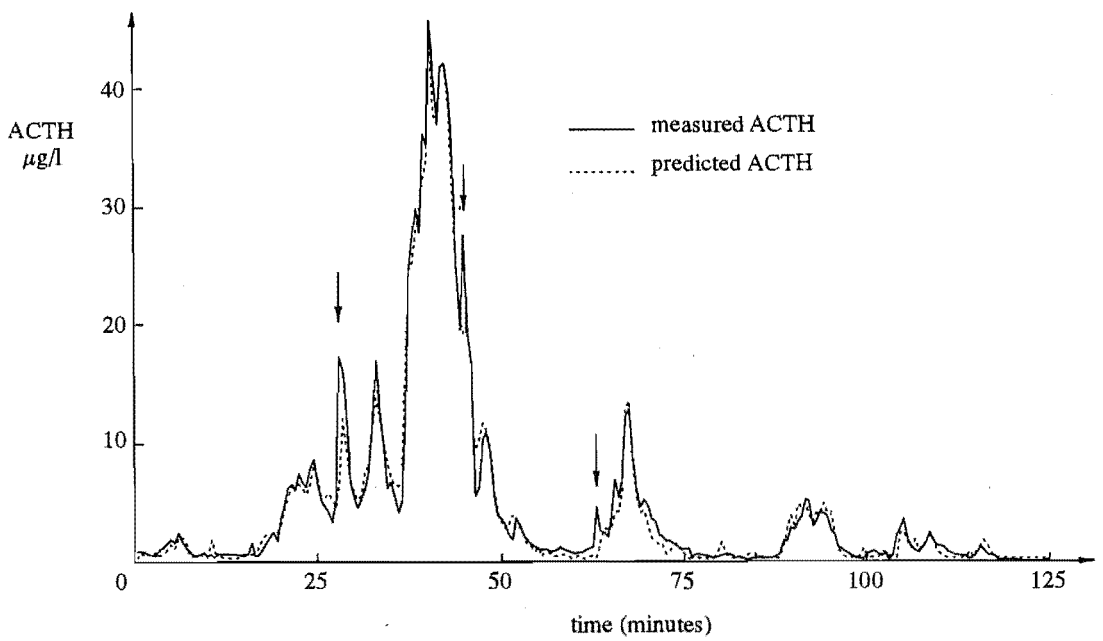

Figure 7.17 Model predictions of ACTH for experiment Horse89. Arrows indicate disagreement between actual and predicted ACTH.

(see section 7.1.2). The effects of CRH are potentiated by AVP with $\bar{f}_1(\text{PKC}(t))/k_1 \approx 0.5$, while those of AVP are potentiated by CRH with

$$\max(M_2^I(t)) \approx 0.7 \quad \text{and} \quad \bar{M}_2^I(t) \approx 0.1$$

The PKC pathway seems to have little direct effect on ACTH regulation, i.e. $k_2 = 0$. Variations in cortisol concentration do not appear to have an effect during the section of the experiment shown in figure 7.17 since $f_7(\text{F}(t)) = 0$, although the low level of cortisol throughout has a dramatic influence on the effectiveness of CRH in releasing ACTH. It also seems that ACTH release has been sufficiently stimulated to reduce the ACTH available for release from corticotropes to quite low levels by the end of the major pulse where $f_8(\text{ACTH}_{\text{avail}}(t)) \approx 0.4$.

Overall, the model provides a very satisfactory explanation for ACTH variations in this experiment. The three situations where it is least satisfactory are indicated by arrows in figure 7.17. The first and second of these may be explained by the temporary $60s$ sampling interval underestimating a CRH pulse, as the predicted ACTH pulses are too small. The third situation is unexplained by the measured hormones, and is evidence for an additional factor.

The fit of the model to the data from experiment Horse95 (see figure 6.4) is shown in figure 7.18. All of the variation in ACTH is explained by CRH along with ACTH depletion, while AVP is seemingly ineffectual in directly stimulating ACTH release, i.e.

$$f_4(x) = k_4 = k_2 = 0$$

although the effects of CRH are still potentiated by AVP with $\bar{f}_1(\text{PKC}(t))/k_1 \approx 0.5$. This dependence on CRH causes some problems, since in this experiment only every

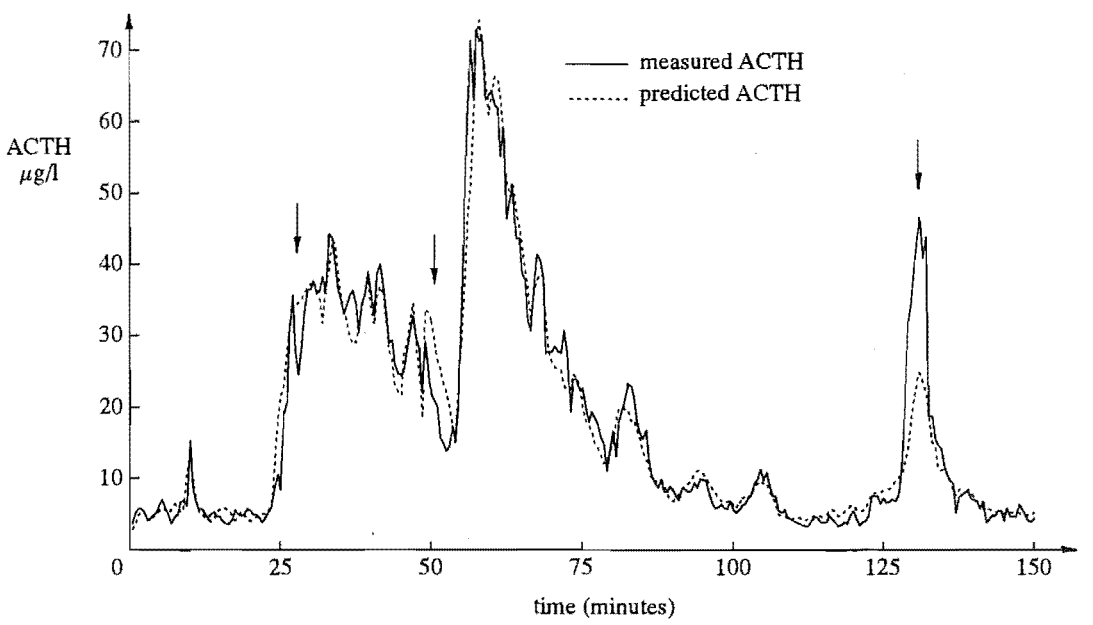

Figure 7.18 Model predictions of ACTH for experiment Horse95. Arrows indicate disagreement between actual and predicted ACTH.

second sample was assayed for CRH. As a result, the CRH signal is not as well defined as those from experiments Horse79 and Horse89 (see section 6.3.4), so less information is available from the model. Once again, the low level of cortisol throughout the experiment has a dramatic influence on the effectiveness of CRH in releasing ACTH, but variations in cortisol during the section of the experiment shown do not appear to be important since $f_7(\mathrm{F}(t)) = 0$. Also, as for experiment Horse89, it seems that ACTH release has been sufficiently stimulated that ACTH levels in the corticotrope become substantially depleted by the end of the major ACTH pulse where $f_{10}(\mathrm{ACTH}_{\mathrm{avail}}(t)) \approx 0.2$.

Correspondence between model output and measured ACTH is less satisfactory than in figure 7.17, although at least part of the difference can be attributed to the unsatisfactory way in which CRH was measured in experiment Horse95. In this context it is important to appreciate that the model in figure 7.13 would not be applicable to PES data with a sampling interval of more than two minutes. This may be the best evidence presently available to demonstrate that rapid sampling is essential to uncover details about the operation of the pituitary. Given the apparent noise on the CRH signal in experiment Horse95, it is perhaps surprising that measured and predicted ACTH agree so well in most parts of the experiment. The three instances where agreement can not be claimed are indicated by arrows. The first of these can possibly be explained by a temporary two minute sampling interval which may have smoothed out a significant CRH pulse. The second cannot be explained by the model, and must be attributed to assay error or an unknown inhibitory factor. The third instance is cause for concern about the model because there is a substantial CRH pulse corresponding to the ACTH pulse, but it does not release enough ACTH. One possible explanation is that the CRH assay is unreliable in the final part of this experiment. Perhaps a more realistic explanation is that the model does not include all the necessary mechanisms to explain the data. The mechanism most likely to correct this discrepancy is desensitization of the corticotropes to CRH. Such a mechanism would mean that the high concentrations of CRH after 70 minutes (see figure 6.4) stimulate less free Ca^{2+}. The amount of releasable ACTH could then increase, while still only allowing the same amount of ACTH to actually be released. The CRH pulse at 130 minutes, which presumably drives the final ACTH pulse, would then be able to release considerably more ACTH. This explanation is supported by *in vitro* evidence for desensitization [Evans *et al.*, 1988]. Note that desensitization seems to occur only when cortisol is low since it is not apparent with physiological cortisol levels, even when CRH is administered, i.e in experiment Horse79 or elsewhere [Schopohl *et al.*, 1986]. Recent results by Childs and Unabia [1990], who demonstrated effects of corticosterone on CRH, but not AVP receptors, suggest that this effect could occur due to modification of receptor function. It is also possible that desensitization could occur due to depletion of an intracellular messenger. Whatever the mechanism, its effect is to reduce the ACTH response to low and medium concentrations of CRH. The model in figure 7.13 does not include desensitization to CRH because this requires $f_1(x)$ in (7.8) to be dependent on all past CRH concentrations, and the form of the dependency was not previously available. An alternative explanation for the discrepancies between actual and predicted ACTH in experiment Horse95 is, as always, that there are additional ACTH regulators involved.

Modeling results for more data sets would be very helpful to substantiate the conclusions that can be drawn from just experiments Horse79, Horse89 and Horse95, but

these are the only experiments to date with good canulations, continuous rapid sampling and all relevant assays completed reliably.

7.5.4 Discussion

Convincing conclusions can be drawn from a modeling analysis only when the model accurately describes some, or all of the processes being modeled. The two tests of a model's validity are that it is based on realistic mechanisms which have been independently established, and that it is able to explain the data sufficiently well. The mechanisms which make up the model in figure 7.13 are clearly set out and justified in section 7.5.1. They are further discussed below. The many different sized and shaped ACTH pulses in the modeled experiments present a very demanding challenge for any model. For this reason, the close correspondence between model output and measured ACTH in figures 7.16-7.18 is good evidence that the model is accurate. Furthermore, the constraints placed on the model by the ACTH signal allow many more conclusions to be drawn, regarding effects of ACTH regulators and mechanisms behind ACTH regulation, than could normally be justified from fitting just three experiments. Nevertheless, the model has been applied to only three experiments and further experimental data are urgently required to challenge these conclusions (see section 8.3).

The most important new conclusions which can be drawn from section 7.5.3 involve the possible effect of cortisol. CRH, with range 0-2.8 pmol/l (Horse95) and 0-5.4 pmol/l (Horse89), is the important signal for ACTH release in experiments Horse89 and Horse95 where cortisol is low (<100nmol/l). Yet CRH, with range 0-14 pmol/l, has limited effect in experiment Horse79, where cortisol levels are in the physiological

experiment	cortisol	CRH (pmol/l)	AVP (pmol/l)	main secretagogue
Horse79	physiological	<14	<160	AVP
Horse89	very low	<5.4	<11000	CRH
Horse95	very low	<2.8	<5000	CRH

Table 7.5 AVP and CRH concentrations in modeling experiments, along with the important ACTH secretagogue.

experiment	cortisol	$\frac{\max(\text{CRH}\rightarrow\text{ACTH})}{\max(\text{AVP}\rightarrow\text{ACTH})}$	$\frac{\max(\text{CRH})}{\max(\text{AVP})}$	CRH effectiveness
Horse79	physiological	0.12	86×10^{-3}	1.4
Horse89	very low	5	0.5×10^{-3}	1.0×10^{4}
Horse95	very low	>10	0.6×10^{-3}	$> 1.8 \times 10^{4}$

Table 7.6 Relative adenohypophysial AVP and CRH concentrations, and their effectiveness at releasing ACTH from corticotropes. AVP(CRH)→ACTH represents the ACTH derived from the AVP(CRH) stimulated pathway. CRH effectiveness is relative to AVP effectiveness and is simply the third column divided by the fourth column. It perhaps best indicates cortisol's effect in the pituitary. Note that all quantities are independent of adenohypophysis to ICS dilution because ratios are used.

range. Similarly, when cortisol concentrations are reduced in experiments Horse89 and Horse95, the CRH and AVP levels are stimulated, respectively, to ≈5 (inter-experiment range 2-20) and ≈100 (inter-experiment range 10-200) times the normal levels (see figures 6.3-6.4). However, such massive levels of AVP are little, if any better at releasing ACTH than those in the physiological range. The above information is also presented in table 7.5, which, along with table 7.6, shows that the principal effect of cortisol is to inhibit ACTH response to CRH. More important is the magnitude of this inhibition, which is calculated in table 7.6 on the basis of information in table 7.5 and from the modeling experiments. Comparison of the magnitude of cortisol's effect in the brain, i.e. ≈ 100 (possible range 2-200), with the size of its pituitary effects given in table 7.6, i.e. $\approx 10^4$ (possible range $3 \times 10^3 - 10^5$), then demonstrates that the important site of cortisol's action is the pituitary, and not the brain as is currently believed. Note that these magnitudes all assume the system is linear, since no other assumptions are available. This does not affect the above conclusions, but realize that cortisol is not said to have a 10^4 fold physiological effect in the pituitary, although the effect is obviously very large. On the other hand, the effectiveness of CRH is conservative in that it is determined relative to that of AVP which may also increase with cortisol suppression. Note also that experiments Horse79, 89 and 95 all support the current understanding of the effects of cortisol on AVP and CRH release from the hypothalamus (see section 5.2.4).

The best understood mechanism behind the synergism between AVP and CRH is the reduction in cAMP degradation associated with PKC activation (see section 5.2.3). This mechanism alone is adequate to fit the model to experiments Horse89 and Horse95, but not to experiment Horse79, which requires the addition of interactions between PKA and PKC+IP_3. It therefore appears that there may be a potentiation effect of PKA on the AVP-stimulated pathways, and furthermore, that this may be the more physiologically important mechanism. In this context, PKA has much less effect on Ca^{2+}influx in experiment Horse79, relative to that in experiments Horse89 and Horse95, even though its potentiating effects appear undiminished. This suggests that the important effects of cortisol occur between PKA activation and Ca^{2+}influx, and also that the effect of cortisol on cAMP accumulation (indicated with a dotted line in figure 7.13) can be neglected. In addition, the lack of direct influence of PKC on Ca^{2+}influx in experiments Horse89 and Horse95, even though cortisol is low, suggests that the effect of cortisol on PKC mediated Ca^{2+}influx can also be neglected. Interestingly, the modeling analysis of experiment Horse79 does not show a requirement for medium and long term effects of cortisol. Perhaps the important physiological effects of cortisol occur over a similar time scale to those of AVP and CRH. This is certainly intuitively reasonable, since delays in feedback loops are destabilizing [Nagrath and Gopal, 1982].

The reason for making the available ACTH in (7.14) dependent on AVP and CRH is to reduce the amount of ACTH released following big peaks of CRH. This was earlier mentioned as the only dubious mechanism in the model. Desensitization to CRH, which the modeling results for experiment Horse95 indicate is required to explain the data, will have the same effect. This mechanism now needs to be included in the model. Tests using experiments Horse79, 89 and 95 may well then allow removal of the dependence of available ACTH on AVP and CRH, making all mechanisms in the model completely substantiated by existing *in vitro* results.

CHAPTER 8

Conclusions and Suggestions for Further ACTH Research

The aim of Part II of this thesis has been to investigate ACTH regulation and the novel pituitary effluent sampling (PES) strategy described in section 6.1.1. This chapter summarizes the results on PES which are contained in Chapter 6, and draws some conclusions about ACTH regulation based on the results in Chapter 7. It finishes with some suggestions for further research.

8.1 Pituitary Effluent Sampling (PES)

PES has revealed that pituitary and hypothalamic hormone concentrations individually vary in an apparently random manner. Other *in vivo* experimental methods are unable to reveal the rich character of these variations, due to problems with access to the hypothalamo-pituitary region, chronic stress levels, deconvolution and sampling rate. All of these problems have been discussed in Chapter 6, the sampling rate and access ones in particular, since they also affect PES data.

The sampling rate limits the accuracy with which variations in hormone concentration can be estimated. This relationship is quantified for the first time in section 6.3.4 and clearly indicates the value of rapid sampling. The results on the value of rapid sampling are supplemented by the small delay between AVP or CRH and ACTH found in section 7.2, along with the observation that the modeling analysis in section 7.5 requires rapidly sampled data. Note that the results in section 6.3.4 are also applicable to other *in vivo* experimental situations. Since experimental cost and information obtained by sampling both increase with increasing sampling rate, a compromise is necessary. Given the way interpretation of hormone concentrations determined by PES is currently lagging their measurement, a $30s$ sampling interval seems appropriate for ACTH and AVP measurement, at least for the present. Where CRH concentrations are expected to be high CRH should also be sampled every $30s$. However, in physiological experiments, advantage can be gained by pooling adjacent $30s$ CRH samples, so that CRH is in reality only assayed once every $60s$.

Section 6.3.5 provides the first quantitative assessment of the size and effect of intercavernous sinus (ICS) blood flow variations. Although the relationships between hormones are not well enough understood to allow the size of the variations to be accurately determined, a 5% ($p<0.05$) upper limit can be placed on the average coefficient

of variation (COV) of blood flow. This limit then indicates that the error in adenohypophysial hormone concentrations measured by PES and caused by blood flow variation may have COV<1%. Thus, blood flow variations are likely to have essentially negligible effect on measurement (by PES) of CRH, AVP and ACTH concentrations at the corticotropes.

8.2 ACTH Regulation

The complication of ACTH regulation is becoming increasingly apparent, with many recent *in vivo* results from other groups indicating a looser association between ACTH and AVP, CRH and cortisol than had been previously proposed, along with a requirement for additional secretagogues with as yet unknown effects. This idea is supported to some degree by the pulse analysis in section 7.2.3 where only ≈76% of ACTH pulses are associated with AVP or CRH pulses. Conversely, section 7.5 shows that a mechanistic model of ACTH regulation, with inputs of measured AVP, CRH and cortisol concentrations, is able to accurately duplicate measured ACTH concentrations when cortisol concentrations are low. When cortisol concentrations are in the physiological range, the same model can still duplicate ACTH concentrations satisfactorily. This work gives fresh hope that in some situations, one of which is when cortisol concentrations are low, AVP, CRH and cortisol are sufficient to explain almost all ACTH secretion. Certainly, until a lot more experiments have been analysed, and the model in figure 7.13 has been suitably refined, incorporation of additional secretagogues into the model seems premature.

Of the three major ACTH regulators, cortisol has the greatest impact on ACTH secretion. The modeling analysis demonstrates that, contrary to current thinking, this negative feedback effect occurs primarily in the pituitary, despite obvious effects in the hypothalamus and hippocampus. Furthermore, it demonstrates that in the pituitary cortisol primarily acts to reduce CRH stimulated ACTH release. Results from the crosscorrelation analysis, pulse analysis and modeling analysis all indicate that AVP is the important physiological signal for ACTH secretion. The modeling analysis also demonstrates that CRH, not AVP, is the important signal for ACTH secretion when cortisol is low. Based on these results it is possible that AVP, with a background of CRH, drives acute changes in ACTH while CRH regulates circulating cortisol concentrations.

The model of ACTH regulation used in the modeling analysis is an advance on one based on static cell culture results [Schwartz, 1990], which, when tested on PES data, could not explain measured ACTH concentrations.

The pulse analysis in section 7.2 suggests that the delay between AVP or CRH and ACTH release is 0-30 seconds, and possibly dependent on the amount of ACTH released.

8.3 Suggestions for Further Research

Results and comments in Chapters 6 and 7, along with results from other workers [Alexander *et al.*, 1991], indicate the detailed information contained in PES data. In particular, the complication of the model in section 7.5 demonstrates the intricate detail that PES can provide, detail which has been previously unavailable to Endocrinologists working *in vivo*. While section 6.3.4 indicates that more rapid PES sampling would

provide even more information, what seems to be much more urgently required is a concerted effort to make use of the intricate detail already apparent with $30s$ sampling. Such an effort will require increasingly sophisticated approaches to analysing PES data, along with greater attention to experimental design, i.e. value and variability of sampling rate, missing samples, choice of stimulus, assay accuracy etc. In the context of both possible approaches and the data, modeling of two metapyrone administration experiments and one AVP and CRH administration experiment has revealed new information about the effects of cortisol on ACTH regulation, and enabled *in vivo* testing of the mechanisms behind ACTH secretion. The AVP and CRH administration experiment was less useful in this regard, because differences between the model output and the measured ACTH could be attributed to errors in the model, or the relative uncertainty in adenohypophysial AVP and CRH concentrations. Therefore, what now appears to be most urgently needed are further physiological experiments, with samples taken as recommended in section 6.3.4. Modeling these experiments will certainly challenge the conclusions made above regarding physiological ACTH regulation, and will also allow further study of the detailed mechanisms behind ACTH release. As with all data analysis, the more experiments available for modeling, the more precise the conclusions that can be drawn from them become.

Until the arrival of good physiological data, the modeling analysis can best be extended by incorporating the changes suggested in section 7.5.4 into the model in figure 7.13. The important mechanisms in the new model will then be IP_3 and protein kinase C (PKC) mediated AVP-stimulated ACTH release, protein kinase A (PKA) mediated CRH-stimulated ACTH release, PKA and PKC mediated potentiation, cortisol dependent inhibition of PKA mediated Ca^{2+} influx, ACTH depletion and desensitization to CRH. This improved model then needs to be fitted to experiments Horse79, 89 and 95, to confirm that it can perform as expected. Having confirmed this, the model, with all parameters fixed, should be fitted to the data from both metapyrone administration experiments, and its performance assessed. Using more than one experiment dramatically increases the constraints on the model, while keeping the experimental 'situation' the same is a necessary simplification at the current stage of model development. This work will undoubtedly suggest further modifications to the model and experiments to test these modifications.

Other suggested investigations based on the results and comments in Chapters 6 and 7, but which are not directly relevant to understanding ACTH regulation, are: (a) *in vivo* validation of the deconvolution model using PES and concurrent peripheral data; (b) a study of whether the spectral content (i.e. rate of variation) of adrenal axis hormones changes with stress, and in particular, exercise; (c) comparison of the pulse analysis results presented in this thesis with those obtained using the Cluster (or any other 'recognized') pulse identification algorithm [Veldhuis and Johnson, 1986]; and (d), with regard to (c), an investigation of data smoothing to reduce the number of falsely detected pulses at sub-10 minute sampling intervals.

References

Abou-Samra A., Catt K.J. and Aguilera G. (1987a), 'Calcium-dependent control of corticotropin release in rat anterior pituitary cell cultures', *Endocrinology* **121**, pp. 965–971.

Abou-Samra A., Catt K.J. and Aguilera G. (1987b), 'Involvement of protein kinase C in the regulation of adrenocorticotropin release from rat anterior pituitary cells', *Endocrinology* **118**, pp. 212–217.

Abou-Samra A., Harwood J.P., Manganiello V.C., Catt K.J. and Aguilera G. (1987c), 'Phorbol 12-myristate 13-acetate and vasopressin potentiate the effect of corticotropin-releasing factor on cyclic AMP production in rat anterior pituitary cells', *Journal of Biological Chemistry* **262**, pp. 1129–1136.

Abramowitz M. and Stegun I.A. (1965), *Handbook of Mathematical Functions*, Dover Publications, New York.

Aguilera G., Wynn P.C., Harwood J.P., Hauger R.L., Millan M.A., Grewe C. and Catt K.J. (1986), 'Receptor mediated actions of corticotropin releasing factor in pituitary gland and nervous system', *Neuroendocrinology* **43**, pp. 79–88.

Aguilera G., Millan M.A., Hauger R.L. and Catt K.J. (1987), 'Corticotropin-releasing factor receptors: distribution and regulation in brain, pituitary, and peripheral tissues', in *[Ganong et al., 1987]*, pp. 48–66.

Ahn A. and Jordan A.K. (1976), 'Profile inversion of simple plasmas and non-uniform regions: three-pole reflection coefficient', *IEEE Transactions on Antennas and Propagation* **AP-24** (6), December, pp. 879–882.

Aki K. and Richards P.G. (1980), *Quantitative Seismology: Theory and Methods*, Vol. 1-2, Freeman, San Francisco.

Al-Dujaili E.A., Hope S.J., Estivariz F.E., Lowry P.J. and Edwards C.R.W. (1981), 'Circulating human pituitary pro-γ-melanotrophin enhances the adrenal response to ACTH', *Nature London* **291**, pp. 156–159.

Alexander S.L., Irvine C.H.G., Livesey J.H. and Donald R.A. (1988), 'Effect of isolation stress on concentrations of arginine vasopressin, α-melanocyte-stimulating hormone and ACTH in the pituitary venous effluent of the normal horse', *Journal of Endocrinology* **116**, pp. 325–334.

Alexander S.L., Irvine C.H.G., Ellis M.J. and Donald R.A. (1991), 'The effect of acute exercise on the secretion of corticotropin-releasing factor, arginine vasopressin, and adrenocorticotropin as measured in pituitary venous blood from the horse', *Endocrinology* **128** (1), pp. 65–72.

Andersen A.H. and Kak A.C. (1982), 'Digital ray tracing in two-dimensional refractive fields', *Journal of the Acoustical Society of America* **72** (5), November, pp. 1593–1606.

Antoni F.A. (1986), 'Hypothalamic control of adrenocorticotropin secretion: advances since the discovery of 41-residue corticotropin-releasing factor', *Endocrine Reviews* **7** (4), pp. 351–378.

Antoni F.A. and Dayanithi G. (1990), 'Secretion of ACTH by perifused isolated rat anterior pituitary cells: pulses of secretagogue enhance the secretory response and modify the effect of atriopeptin', *Journal of Endocrinology* **125**, pp. 365–373.

Antoni F.A., Fink G. and Sheward W.J. (1990), 'Corticotrophin-releasing peptides in rat hypophysial portal blood after paraventricular lesions: a marked reduction in the concentration of corticotrophin-releasing factor-41, but no change in vasopressin', *Journal of Endocrinology* **125**, pp. 175–183.

Arfken G. (1985), *Mathematical Methods for Physicists*, Academic Press, New York, third edition.

Autelitano D.J., Blum M., Lopingo M., Allen R.G. and Roberts J.L. (1990), 'Corticotropin-releasing factor differentially regulates anterior and intermediate pituitary lobe proopiomelanocortin gene transcription, nuclear precursor RNA and mature mRNA in vivo', *Neuroendocrinology* **51**, pp. 123–130.

Axelrod J. and Reisine T.D. (1984), 'Stress hormones: their interaction and regulation', *Science Washington DC* **224** (4648), pp. 452–459.

Azimi M. and Kak A.C. (1983), 'Distortion in diffraction tomography caused by multiple scattering', *IEEE Transactions on Medical Imaging* **MI-2** (4), December, pp. 176–195.

Baltes H.P. (Ed.) (1980), *Inverse Scattering Problems in Optics*, Springer-Verlag, Berlin.

Barnes A. and Solomon L.P. (1973), 'Some curious analytical ray paths for some interesting velocity profiles in geometrical acoustics', *Journal of the Acoustical Society of America* **53**, pp. 147–155.

Bates R.H.T. (1982), 'Astronomical speckle imaging', *Physics Reports* **90** (4), October, pp. 203–297.

Bates R.H.T. (1988), 'JWKB/ Rayleigh-Gans(Born) inverse scattering approximation and reconstruction algorithm', *Inverse Problems* **4** (4), pp. 129–132.

Bates R.H.T. and Cady F.M. (1980), 'Towards true imaging by wideband speckle interferometry', *Optics Communications* **32** (3), March, pp. 365–369.

Bates R.H.T. and McDonnell M.J. (1989), *Image Restoration and Reconstruction*, Clarendon Press, Oxford.

Bates R.H.T. and McKinnon G.C. (1979), 'Towards improving images in ultrasonic transmission tomography', *Australasian Physical and Engineering Sciences in Medicine* **2**, pp. 134–220.

Bates R.H.T. and Minard R.A. (1983), 'Some new approaches to inverse scattering', in Devaney A.J. (Ed.), *Proceedings of SPIE* **413** *(Inverse Optics)*, pp. 56–60.

Bates R.H.T. and Minard R.A. (1984), 'Compensation for multiple reflection', *IEEE Transactions on Sonics and Ultrasonics* **SU-31** (4), July, pp. 330–336.

Bates R.H.T. and Ng F.L. (1972), 'Polarisation-source formulation of electromagnetism and dielectric-loaded waveguides', *IEE Proceedings* **119** (11), November, pp. 1568–1574.

Bates R.H.T. and Robinson B.S. (1981), 'Ultrasonic transmission speckle imaging', *Ultrasonic Imaging* **3** (4), October, pp. 378–394.

Bates R.H.T. and Robinson B.S. (1982), 'A stochastical imaging procedure', in Ash E.E. and Hill C.R. (Eds.), *Acoustical Imaging* **12**, Plenum Press, New York, pp. 185–191.

Bates R.H.T., Garden K.L. and Peters T.M. (1983), 'Overview of computerized tomography with emphasis on future developments', *IEEE Proceedings* **71** (3), March, pp. 356–372.

Bates R.H.T., Smith V.A. and Murch R.D. (1991), 'Managable multidimensional inverse scattering theory', *Physics Reports* **201** (4), April, pp. 185–277.

Bednor J.B., Redner R., Robinson E. and Weglein A. (Eds.) (1983), *Conference on Inverse Scattering Theory: Theory and Application*, SIAM, Philadelphia.

Bergland R.M. and Page R.B. (1978), 'Can the pituitary secrete directly to the brain? (Affirmative anatomical evidence)', *Endocrinology* **102**, pp. 1325–1338.

Bergland R.M. and Page R.B. (1979), 'Pituitary-brain vascular relations: a new paradigm', *Science* **204**, pp. 18–24.

Berntsen S., Andersen J.B. and Gross E. (1990), 'A general formulation of applied potential tomography', *Radio Science* **26** (2), pp. 535–540.

Berryman J.G. (1990), 'Stable iterative reconstruction algorithm for non-linear traveltime tomography', *Inverse Problems* **6** (1), pp. 21–42.

Bertero M. and de Mol C. (1981), 'Stability problems in inverse diffraction', *IEEE Transactions on Antennas and Propagation* **AP-29** (2), March, pp. 368–372.

Bertero M., Brianzi P., Pike E.R. and Rebolia L. (1988a), 'Linear regularizing algorithms for positive solutions of linear inverse problems', *Proceedings of the Royal Society of London A: Mathematical and Physical Sciences* **415**, pp. 257–275.

Bertero M., de Mol C. and Pike E.R. (1988b), 'Linear inverse problems with discrete data, II: Stability and regularisation', *Inverse Problems* **4** (3), pp. 573–594.

Beylkin G. (1985a), 'Imaging of discontinuities in the inverse scattering problem by inversion of a causal generalized Radon transform', *Journal of Mathematical Physics* **26** (1), January, pp. 99–108.

Beylkin G. (1985b), 'Reconstructing discontinuities in multidimensional inverse scattering problems: Smooth errors vs small errors', *Applied Optics* **24** (23), December, pp. 4086–4088.

Bilezikjian L.M. and Vale W.W. (1987), 'Regulation of ACTH secretion from corticotropes: the interaction of vasopressin and CRF', in *[Ganong et al., 1987]*, pp. 85–96.

Blackledge J.M., Burge R.E., Hopcraft K.I. and Wombell R.J. (1987), 'Quantitative diffraction tomography: I. Pulsed acoustic fields', *Journal of Physics D : Applied Physics* **20** (1), January, pp. 1–10.

Blank L. (1982), *Statistical Proceedures for Engineering, Management, and Science*, McGraw-Hill, Tokyo.

Bleistein N., Cohen J.K., DeSonata J.A. and Hagin F.G. (1984), *Inverse Problems of Acoustic and Elastic Wave Profile Inversion*, SIAM, Philadelphia, Chap. Project review of geophysical and ocean sound speed profile inversion, pp. 236–249.

Bolomey J.C., Pichot C. and Gaboriaud G. (1991), 'Planar microwave camera tomography for biomedical applications: critical and prospective analysis of reconstruction algorithms', *Radio Science* **26** (2), March–April, pp. 541–549.

Bond L.J. and Reynolds W.N. (Eds.) (1987), 'Special issue on non-destructive testing', *IEE Proceedings Part A*, **A134** (3), March, pp. 237–306.

Born M. and Wolf E. (1980), *Principles of Optics*, Pergamon Press, Oxford, sixth edition.

Bowman J.J., Senior T.B.A. and Uslenghi P.L.E. (Eds.) (1969), *Electromagnetic and Acoustic Scattering by Simple Shapes*, North-Holland, Amsterdam.

Boyse W.E. and Keller J.B. (1986), 'Inverse elastic scattering in three dimensions', *Journal of the Acoustical Society of America* **79** (2), February, pp. 215–218.

Bracewell R.N. (1978), *The Fourier Transform and its Applications*, McGraw-Hill, New York, second edition.

Brieseman N.P., Thorpe C.W. and Bates R.H.T. (1987), 'Nontactile estimation of glottal excitation characteristics of voiced speech', *IEE Proceedings Pt. A* **134** (10), pp. 807–813.

Brooks V.L. (1989), 'Vasopressin and ANG II in the control of ACTH secretion and arterial and atrial pressure', *American Journal of Physiology* **256**, pp. R339–R347.

Broquetas A., Romeu J., Rius J.M., Elias-Fuste A.R., Cardanna A. and Jofre L. (1991), 'Cylindrical geometry: a further step in active microwave tomography', *IEEE Transactions on Microwave Theory and Techniques* **39** (5), May, pp. 836–844.

Brown B.H. and Barber D. (Eds.) (1988), 'Special issue on electrical impedance tomography – applied potential tomography', *Clinical Physics and Physiological Measurement, Supplement A*, **9**.

Bruckstein A.M. and Kailath T. (1987), 'Inverse scattering for discrete transmission-line models', *SIAM Review* **29** (3), September, pp. 359–389.

Bruhn T.O., Plotsky P.M. and Vale W.W. (1984a), 'Effect of paraventricular lesions on corticotropin-releasing factor (CRF)-like immunoreactivity in the stalk-median eminence: studies on the adrenocorticotropin response to ether stress and exogenous CRF', *Endocrinology* **114**, pp. 57–62.

Bruhn T.O., Sutton R.E., Rivier C.L. and Vale W.W. (1984b), 'Corticotropin-releasing factor regulates proopiomelanocortin messenger ribonucleic acid levels *in vivo*', *Neuroendocrinology* **39** (2), pp. 170–175.

Buckingham J.C. (1985), 'Two distinct corticotrophin releasing activities of vasopressin', *British Journal of Pharmacology* **84**, pp. 213–219.

Budden K.G. (1985), *The Propagation of Radio Waves: The Theory of Radio Waves of Low Power in the Ionosphere and Magnetosphere*, Cambridge University Press, Cambridge.

Budreck D.E. and Rose J.H. (1990), 'Three-dimensional inverse scattering in anisotropic media', *Inverse Problems* **6** (3), pp. 331–348.

Canny B.J. (1990), 'Hippocampal glucocorticoid receptors and the regulation of ACTH secretion', *Molecular and Cellular Endocrinology* **71**, pp. C35–C38.

Canny B.J., Funder J.W. and Clarke I.J. (1989), 'Glucocorticoids regulate ovine hypophysial portal levels of corticotropin-releasing factor and arginine vasopressin in a stress-specific manner', *Endocrinology* **125** (5), pp. 2532–2539.

Caorsi S., Gragnani G.L. and Pastorino M. (1990), 'Microwave imaging by three-dimensional Born linearization of electromagnetic scattering', *Radio Science* **25** (6), November-December, pp. 1221–1229.

Caorsi S., Gragnani G.L. and Pastorino M. (1991), 'An approach to microwave imaging using a multiview moment method solution for a two-dimensional infinite cylinder', *IEEE Transactions on Microwave Theory and Techniques* **39** (6), June, pp. 1062–1067.

Caraty A., Grino M., Locatelli A., Guillaume V., Boudouresque F., Conte-Devoix B. and Oliver C. (1990), 'Insulin-induced hypoglycemia stimulates corticotropin-releasing factor and arginine vasopressin secretion into hypophysial portal blood of conscious, unrestrained rams', *Journal of Clinical Investigation* **85**, pp. 1716–1721.

Carnes M., Goodman B.M. and Lent S.J. (1991), 'High resolution spectral analysis of plasma adrenocorticotropin reveals a multifactorial frequency structure', *Endocrinology* **128** (2), pp. 902–910.

Cha S. and Vest C.M. (1981), 'Tomographic reconstruction of strongly refracting fields and its application to interferometric measurement of boundary layers', *Applied Optics* **20** (16), August, pp. 2787–2794.

Chard T. (1982), *An Introduction to Radioimmunoassay and Related Techniques*, Elsevier Biomedical Press, Amsterdam, second edition.

Chew W.C. and Wang Y.M. (1990), 'Reconstruction of two-dimensional permittivity distribution using the distorted Born iterative method', *IEEE Transactions on Medical Imaging* **9** (2), pp. 218–225.

Childs G.V. (1987), 'Cytochemical studies of the regulation of ACTH secretion', in *[Ganong et al., 1987]*, pp. 248–274.

Childs G.V. and Unabia G. (1989), 'Activation of protein kinase C and L calcium channels enhances binding of biotinylated corticotropin releasing hormone by anterior pituitary corticotropes', *Molecular Endocrinology* **3**, pp. 117–126.

Childs G.V. and Unabia G. (1990), 'Rapid corticosterone inhibition of corticotropin-releasing hormone binding and adrenocorticotropin release by enriched populations of corticotropes: counteractions by arginine vasopressin and its second messengers', *Endocrinology* **126** (4), pp. 1967–1975.

Childs G.V., Unabia G. and Marchetti C. (1987), 'Secretion from corticotropes after avidin-fluorescein stains for biotinylated ligands (CRF or AVP)', *American Journal of Physiology* **252**, pp. E347–E356.

Clayton R.W. and Stolt R.H. (1981), 'A Born-WKBJ inversion method for acoustic reflection data', *Geophysics* **46** (11), November, pp. 1559–1567.

Coates R.T. and Chapman C.H. (1990), 'Ray perturbation theory and the Born approximation', *Geophysics Journal International* **100** (3), pp. 379–392.

Connolly T.J. and Wall D.J.N. (1990), 'On frećhet differentiability of some non-linear operators occuring in inverse problems; an implicit function theorem approach', *Inverse Problems* **6** (5), pp. 949–966.

Cowley J.M. (1975), *Diffraction Physics*, North-Holland, Amsterdam.

Craig I.J.D. and Brown J.C. (1986), *Inverse Problems in Astronomy*, Adam Hilger, Bristol.

Crawford C.R. and Kak A.C. (1979), 'Aliasing artifacts in computerized tomography', *Applied Optics* **18**, pp. 3704–3711.

Daily W.D. (Ed.) (1986), 'Special section on geotomography', *IEEE Proceedings*, **74** (2), February, pp. 243–361.

Dallas W.J. and Wagner R.F. (Eds.) (1987), 'Special issue on medical imaging', *Journal of the Optical Society of America A*, **A4** (5), May, pp. 891–992.

Dallman M.F., Akana S.F., Cascio C.S., Darlington D.N., Jacobson L. and Levin N. (1987a), 'Regulation of ACTH secretion: variations on a theme of B', *Recent Progress in Hormone Research* **43**, pp. 113–173.

Dallman M.F., Akana S.F., Jacobson L., Levin N., Cascio C.S. and Shinsako J. (1987b), 'Characterization of corticosterone feedback regulation of ACTH secretion', in *[Ganong et al., 1987]*, pp. 402–414.

Davey B.L.K. (1989), *Advances in Blind Deconvolution*, Ph.D. thesis, Department of Electrical and Electronic Engineering, University of Canterbury, Christchurch, New Zealand.

Dayanithi G. and Antoni F.A. (1989), 'Rapid as well as delayed inhibitory effects of glucocorticoid hormones on pituitary adrenocorticotropic hormone release are mediated by type II glucocorticoid receptors and require newly synthesized messenger ribonucleic acid as well as protein', *Endocrinology* **125**, pp. 308–313.

DeBold C.R., Sheldon W.R., DeCherney G.S., Jackson R.V., Alexander A.N., Vale W.W., Rivier J. and Orth D.N. (1984), 'Arginine vasopressin potentiates adrenocorticotropin release induced by ovine corticotropin-releasing factor', *Journal of Clinical Investigation* **73**, pp. 533–538.

Defendi R. and Zimmerman E.A. (1978), 'The magnocellular neurosecretory system of the mammalian hypothalamus', in Reichlin *et al.* (Eds.), *The Hypothalamus*, Raven Press, New York, pp. 137–152.

Deschamps G.A. (1972), 'Ray techniques in electromagnetics', *IEEE Proceedings* **60**, pp. 1022–1035.

Devaney A.J. (1982), 'A filtered backpropagation algorithm for diffraction tomography', *Ultrasonic Imaging* **4** (4), October, pp. 336–350.

Devaney A.J. (1983), 'A computer simulation study of diffraction tomography', *IEEE Transactions on Biomedical Engineering* **BME-30** (7), July, pp. 377–386.

Devaney A.J. (1984), 'Geophysical diffraction tomography', *IEEE Transactions on Geoscience and Remote Sensing* **GE-22** (1), January, pp. 3–13.

Devaney A.J. (1985a), 'Diffraction tomography', in Boerner W.M. *et al.* (Eds.), *Inverse Methods in Electromagnetic Imaging*, Reidel, Dordrecht, Holland, pp. 1107–1135.

Devaney A.J. (1985b), 'Generalized projection-slice theorem for fan beam diffraction tomography', *Ultrasonic Imaging* **7** (3), July, pp. 264–275.

Devaney A.J. (1986), 'Reconstructive tomography with diffracting wavefields', *Inverse Problems* **2** (2), May, pp. 161–183.

Devaney A.J. (1987), 'Linearised inverse scattering in attenuating media', *Inverse Problems* **3** (3), pp. 389–397.

Devaney A.J. (1989), 'The limited-view problem in diffraction tomography', *Inverse Problems* **5**, pp. 501–521.

Devaney A.J. and Oristaglio M.L. (1983), 'Inversion procedure for inverse scattering within the distorted-wave Born approximation', *Physical Review Letters* **51** (4), July, pp. 237–240.

Dines K.A. and Lytle R.J. (1979a), 'Computerized geophysical tomography', *IEEE Proceedings* **67** (7), July, pp. 1065–1073, see [Wait, 1979; Dines and Lytle, 1979b].

Dines K.A. and Lytle R.J. (1979b), 'Correction to 'Computerized geophysical tomography'', *IEEE Proceedings* **67** (12), December, p. 1679, see [Dines and Lytle, 1979a].

Du Pasquier D., Dreifuss J.J., Dubois-Dauphin M. and Tribollet E. (1991), 'An autoradiographical study of binding sites for vasopressin located in rat and sheep pituitary glands', *Journal of Endocrinology* **129**, pp. 197–203.

Dubovikova E.A. and Dubovikov M.S. (1987), 'Regularization, experimental errors, and accuracy estimation in tomography and interferometry', *Journal of the Optical Society of America A* **A4** (11), November, pp. 2033–2038.

Duchêne B., Lesselier D. and Tabbara W. (1985), 'Diffraction tomography approach to acoustical imaging and media characterization', *Journal of the Optical Society of America A* **2** (11), pp. 1943–1953.

Ellis M.J., Schmidli R.S., Donald R.A., Livesey J.H. and Espiner E.A. (1990), 'Plasma corticotropin-releasing factor and vasopressin responses to hypoglycaemia in normal men', *Clinical Endocrinology* **32**, pp. 93–100.

Emeric-Sauval E. (1986), 'Corticotropin-releasing factor (CRF)- a review', *Psychoneuroendocrinology* **11** (3), pp. 277–294.

Engler D., Pham T., Fullerton M.J., Funder J.W. and Clarke I.J. (1988), 'Studies of the regulation of the hypothalamic-pituitary-adrenal axis in sheep with hypothalamic-pituitary disconnection I. Effect of an audiovisual stimulus and insulin-induced hypoglycemia', *Neuroendocrinology* **48**, pp. 551–560.

Engler D., Pham T., Fullerton M.J., Ooi G., Funder J.W. and Clarke I.J. (1989), 'Studies of the secretion of corticotropin-releasing factor and arginine vasopressin into the hypophysial-portal circulation of the conscious sheep', *Neuroendocrinology* **49**, pp. 367–381.

Esmersoy C. and Levy B.C. (1986), 'Multidimensional Born inversion with a wide-band plane wave-source', *IEEE Proceedings* **74**, pp. 466–475.

Esmersoy C., Oristaglio M.L. and Levy B.C. (1985), 'Multidimensional Born velocity inversion: Single wideband point source', *Journal of the Acoustical Society of America* **78** (3), September, pp. 1052–1057.

Evans M.J., Brett J.T., McIntosh R.P., McIntosh J.E.A., McLay J.L., Livesey J.H. and Donald R.A. (1988), 'Characteristics of the ACTH response to repeated pulses of corticotropin-releasing factor and arginine vasopressin *in vitro*', *Journal of Endocrinology* **117**, pp. 387–395.

Evans M.J., Marshall A.G., Kitson N.E., Summers K. and Donald R.A. (1992), 'Methods of anterior pituitary cell preparation for in vitro studies: ACTH response to corticotrophin releasing factor and arginine vasopressin', in preparation.

Familari M., Smith A.I., Smith R. and Funder J.W. (1989), 'Arginine vasopressin is a much more potent stimulus to ACTH release from ovine anterior pituitary cells than ovine corticotropin-releasing factor', *Neuroendocrinology* **50**, pp. 152–157.

Fawcett J. and Keller H.B. (1985), 'Three-dimensional ray tracing and geophysical inversion in layered media', *SIAM Journal of Applied Mathematics* **45** (3), June, pp. 492–501.

Felsen L.B. and Marcuvitz N. (1973), *Radiation and Scattering of Waves*, Prentice Hall, Englewood Cliffs, New Jersey.

Fink G., Dow R.C., Casle D., Johnston C.I., Lim A.T., Copolov D.L., Benny J., Carroll S. and Dick H. (1991), 'Atrial natriuretic peptide is a physiological inhibitor of ACTH release: evidence from immunoneutralization *in vivo*', *Journal of Endocrinology* **131**, pp. R9–R12.

Florey E. (1966), *An Introduction to General and Comparative Animal Physiology*, W.B. Sanders, Philadelphia.

Fradkin L.J. (1989), 'Limits of validity of geometrical optics in weakly irregular media', *Journal of the Optical Society of America A* **A6** (9), pp. 1315–1319.

Fritsch P.C. (Ed.) (1965), 'Special issue on radar reflectivity', *IEEE Proceedings*, **53** (8), August, pp. 770–1137.

Ganong W.F. and Murakami K. (1987), 'The role of angiotensin II in the regulation of ACTH secretion', in *[Ganong et al., 1987]*, pp. 176–186.

Ganong W.F., Dallman M.F. and Roberts J.L. (Eds.) (1987), *The hypothalamo-pituitary-adrenal axis revisited*, Vol. 512, Annals of the New York Academy of Sciences.

Garabedian P.R. (1964), *Partial Differential Equations*, Wiley, New York.

Garden K.L., Bones P.J. and Bates R.H.T. (1989), 'From living being to medical image - bridging the dimensionality gap', *Australasian Physical and Engineering Sciences in Medicine* **12** (4), December, pp. 186–204.

Garnero L., Franchois A., Hugonin J., Pichot C. and Joachimowicz N. (1991), 'Microwave imaging - complex permittivity reconstruction by simulated annealing', *IEEE Transactions on Microwave Theory and Techniques* **39** (11), November, pp. 1801–1807.

Gehlbach S. and Sommer F. (1987), 'Frequency diversity speckle processing', *Ultrasonic Imaging* 9, pp. 92–105.

Genazzani A.D. and Rodbard D. (1991), 'Use of the receiver operating characteristic curve to evaluate sensitivity, specificity, and accuracy of methods for detection of peaks in hormone time series', *Acta Endocrinologica* **124** (2), pp. 295–306.

Gertz B.J., Contreras L.N., McComb D.J., Kovacs K., Tyrrell J.B. and Dallman M.F. (1987), 'Chronic administration of corticotropin-releasing factor increases pituitary corticotroph number', *Endocrinology* **120** (1), pp. 381–388.

Gibbs D.M. (1986), 'Vasopressin and oxytocin - hypothalamic modulators of the stress response: a review', *Psychoneuroendocrinology* **11** (2), pp. 131–140.

Gillies G.E., Linton E.A. and Lowry P.J. (1982), 'Corticotropin releasing activity of the new CRF is potentiated several times by vasopressin', *Nature* **299**, pp. 355–357.

Gillies G.E., Puri A., Linton E.A. and Lowry P.J. (1984), 'Comparative chromatography of hypothalamic corticotropin-releasing factors', *Neuroendocrinology* **38** (1), pp. 17–24.

Gjessing D.T. (1978), *Remote Surveilance by Electromagnetic Waves for Air, Water, Land*, Ann Arbor, Michigan.

Griffin J.F.T. (1989), 'Stress and immunity: a unifying concept', *Veterinary Immunology and Immunopathology* **20**, pp. 263–312.

Grossman A. and Tsagarakis S. (1989), 'The hunt for the CIA-factors which demonstrate corticotrophin-inhibitory activity', *Journal of Endocrinology* **123** (2), pp. 169–172.

Guardabasso V., Genazzani A.D., Veldhuis J.D. and Rodbard D. (1991), 'Objective assessment of concordance of secretory events in two endocrine time series', *Acta Endocrinologica* **124**, pp. 208–218.

Guérineau N., Corcuff J., Tabarin A. and Mollard P. (1991), 'Spontaneous and corticotropin-releasing factor-induced cytosolic calcium transients in corticotropes', *Endocrinology* **129** (1), pp. 409–420.

Guillemin R. and Rosenberg B. (1955), 'Humoral hypothalamic control of anterior pituitary: a study with combined tissue cultures', *Endocrinology* **57**, pp. 599–607.

Habashy T.M. (1991), 'A generalized Gel'fand-Levitan-Marchenko integral equation', *Inverse Problems* **7** (5), October, pp. 703–712.

Habashy T.M. and Mittra R. (1987), 'Review of some inverse methods in electromagnetics', *Journal of the Optical Society of America A* **A4** (1), January, pp. 281–291.

Harris F.J. (1978), 'On the use of windows for harmonic analysis with the discrete Fourier transform', *IEEE Proceedings* **66** (1), pp. 51–83.

Haykin S. (1983), *Communication Systems*, Wiley, New York, second edition.

Herman G.T. (Ed.) (1983), 'Special issue on computerized tomography', *IEEE Proceedings*, **71** (3), March, pp. 291–435.

Herrmann G.F. (1987), 'Numerical computation of diffraction coefficients', *IEEE Transactions on Antennas and Propagation* **AP-35** (1), January, pp. 53–61.

Hindmarsh P.C., Matthews D.R., Brain C., Pringle P.J. and Brook C.G. (1990), 'The application of deconvolution analysis to elucidate the pulsatile nature of growth hormone secretion using a variable half-life of growth hormone', *Clinical Endocrinology* **32** (6), pp. 739–747.

Holmes R.L. and Ball J.N. (1974), *The Pituitary Gland*, Cambridge University Press, Cambridge.

Holmes M.C., Antoni F.A. and Szentendrei T. (1984), 'Pituitary receptors for corticotropin-releasing factor: no effect of vasopressin on binding or activation of adenylate cyclase', *Neuroendocrinology* **39**, pp. 162–169.

Howard A.Q., Chew W.C. and Moldoveanu M.C. (1990), 'A new correction to the Born approximation', *IEEE Transactions on Geoscience and Remote Sensing* **28** (3), pp. 394–399.

Iranmanesh A., Lizarralde G., Short D. and Veldhuis J.D. (1990), 'Intensive venous sampling paradigms disclose high frequency adrenocorticotropin release episodes in normal men', *Journal of Clinical Endocrinology and Metabolism* **71** (5), pp. 1276–1283.

Irvine C.H.G. and Alexander S.L. (1987), 'A novel technique for measuring the hypothalamic and pituitary hormone rates from collection of pituitary venous effluent in the normal horse', *Journal of Endocrinology* **113**, pp. 183–192.

Irvine C.H.G., Alexander S.L. and Donald R.A. (1989), 'Effect of osmotic stimulus on the secretion of arginine vasopressin and adrenocorticotropin in the horse', *Endocrinology* **124** (6), pp. 3102–3108.

Jackson D.F. (1988), 'Review of physical diagnostic techniques in medicine and biology: Technical progress and future requirements', *IEE Proceedings Part A* **A135** (6), July, pp. 375–384.

James G.L. (1986), *Geometrical Theory of Diffraction for Electromagnetic Waves*, Peter Peringrus, Stevenage, England, third edition.

James V.H.T., Horner M.W., Moss M.S. and Rippon A.E. (1970), 'Adrenocortical function in the horse', *Journal of Endocrinology* **48**, pp. 319–335.

Jia L., Canny B., Orth D.N. and Leong D.A. (1991), 'Distinct classes of corticotrope mediate corticotropin-releasing hormone- and arginine vasopressin- stimulated adrenocorticotropin release', *Endocrinology* **128** (1), pp. 197–203.

Jin J. and Liepa V.V. (1989), 'Simple moment method program for computing scattering from complex cylindrical obstacles', *IEE Proceedings, Pt H* **136** (4), pp. 321–329.

Joachimowicz N., Pichot C. and Hugonin J. (1991), 'Inverse scattering: an iterative numerical method for electromagnetic imaging', *IEEE Transactions on Antennas and Propagation* **39** (12), December, pp. 1742–1752.

Johnson S.A. and Tracy M.L. (1983), 'Inverse scattering solutions by a sinc basis, multiple source, moment method — Part I: Theory', *Ultrasonic Imaging* **5** (4), October, pp. 361–375.

Jones D.S. (1964), *The Theory of Electromagnetism*, Pergamon Press, New York.

Jones D.S. (1986), *Acoustic and Electromagnetic Waves*, Clarendon Press, Oxford.

Jones M.T. and Gillham B. (1988), 'Factors involved in the regulation of adrenocorticotropic hormone/β-lipotropic hormone', *Physiological Reviews* **68** (3), pp. 743–818.

Kaveh M., Soumekh M. and Mueller R.K. (1982), 'Tomographic imaging via wave equation inversion', *International Conference on Acoustics, Speech, and Signal Processing* **ICASSP 82**, pp. 1553–1556.

Keller J.B. (1959), 'The inverse scattering problem in geometrical optics and the design of reflectors', *IRE Transactions on Antennas and Propagation* **AP-6**, April, pp. 146–149.

Keller J.B. (1969), 'Accuracy and validity of the Born and Rytov approximations', *Journal of the Optical Society of America* **59** (8), August, pp. 1003–1004.

Keller-Wood M.E. and Dallman M.F. (1984), 'Corticosteroid inhibition of ACTH secretion', *Endocrine Reviews* **5** (1), pp. 1–24.

Keller-Wood M.E., Shinsako J. and Dallman M.F. (1984), 'Interaction between stimulus-intensity and corticosteroid feedback in control of ACTH', *American Journal of Physiology* **247** (4), pp. E489–E494.

King M.S. and Baertschi A.J. (1990), 'The role of intracellular messengers in adrenocorticotropin secretion in vitro', *Experientia* **46**, pp. 26–40.

Kinsler L.E., Frey A.R., Coppens A.B. and Sanders J.V. (1982), *Fundamentals of Acoustics*, John Wiley & Sons, New York, third edition.

Kiss J.Z., Mezey E. and Skirboll L. (1984), 'Corticotropin-releasing factor immunoreactive neurons of the paraventricular nucleus become vasopressin positive after adrenalectomy', *Proceedings of the National Academy of Science USA* **81**, pp. 1148–1158.

Kleinman R.E., Roach G.F. and van den Berg P.M. (1990), 'Convergent Born series for large refractive indices', *Journal of the Optical Society of America A* **7** (5), May, pp. 890–897.

Kline M. and Kay I.W. (1965), *Electromagnetic Theory and Geometrical Optics*, Wiley-Interscience, New York.

Knobil E. (1981), 'Patterns of hypophysiotropic signals and gonadotropin secretion in the Rhesus monkey', *Biology of Reproduction* **24** (1), pp. 44–50.

Koch B. and Lutz-Bucher B. (1991), 'Inhibition of protein kinase C activity in cultured pituitary cells attenuates both cyclic AMP-independent and -dependent secretion of ACTH', *Molecular and Cellular Endocrinology* **77** (1-3), pp. 57–65.

Kristensson G. and Krueger R.J. (1987), 'Direct and inverse scattering in the time domain for a dissipative wave equation. III: Scattering operators in the presence of a phase velocity mismatch', *Journal of Mathematical Physics* **28** (2), February, pp. 360–370.

Kushler R.H. and Brown M.B. (1991), 'A model for the identification of hormone pulses', *Statistics in Medicine* **10**, pp. 329–340.

Labrie F., Giguère V., Meunier H., Simard J., Gossard F. and Raymond V. (1987), 'Multiple factors controlling ACTH secretion at the anterior pituitary level', in *[Ganong et al., 1987]*, pp. 97–114.

Lauson H.D. (1974), 'Metabolism of the neurohypophysial hormones', in Knobil E. and Sawyer W.H. (Eds.), *Handbook of Physiology*, Vol. 4, sec. 7, American Physiological Society, Washington, D.C., pp. 287–393.

Leong D.A. (1988), 'A complex mechanism of facilitation in pituitary ACTH cells: Recent single-cell studies', *Journal of Experimental Biology* **139**, pp. 151–168.

Leviatan Y. and Boag A. (1987), 'Analysis of electromagnetic scattering from dielectric cylinders using a multifilament current model', *IEEE Transactions on Antennas and Propagation* **AP-35** (10), pp. 1119–1127.

Levin N., Shinsako J. and Dallman M. (1988), 'Corticosterone acts on the brain to inhibit adrenalectomy-induced adrenocorticotropin secretion', *Endocrinology* **122**, pp. 694–701.

Levy B.C. and Esmersoy C. (1988), 'Variable background Born inversion by wavefield backpropagation', *SIAM Journal of Applied Mathematics* **48** (4), August, pp. 952–972.

Lines L.R. (Ed.) (1986), 'Special issue on seismic inversion', *IEEE Proceedings*, **74** (3), March, pp. 387–509.

Linton E.A., Tilders F.J.H., Hodgekinson S., Berkenbosch F., Vermes I. and Lowry P.J. (1985), 'Stress-induced secretion of adrenocorticotropin in rats is inhibited by administration of antisera to ovine corticotropin-releasing factor and vasopressin', *Endocrinology* **116**, pp. 966–970.

Linton E.A., Behan D.P., Saphier P.W. and Lowry P.J. (1990), 'Corticotropin-releasing hormone (CRH)-binding protein: reduction in the adrenocorticotropin-releasing activity of placental but not hypothalamic CRH', *Journal of Clinical Endocrinology and Metabolism* **70** (6), pp. 1574–1580.

Little G.W., Island D., Lance E.M. and Harris A.P. (1958), 'Alterations of adrenal steroid patterns in man resulting from treatment with a chemical inhibitor of 11 β-hydroxylation', *Journal of Clinical Endocrinology* **18**, pp. 906–912.

Liu J.H., Muse K., Contreras P., Gibbs D., Vale W.W., Rivier J. and Yen S.S.C. (1983), 'Augmentation of ACTH-releasing activity of synthetic corticotropin releasing factor (CRF) by vasopressin in women', *Journal of Clinical Endocrinology and Metabolism* **57**, pp. 1087–1089.

Liu J., Robinson P.J., Funder J.W. and Engler D. (1990), 'The biosynthesis and secretion of adrenocorticotropin by the ovine anterior pituitary is predominantly regulated by arginine vasopressin (AVP)', *The Journal of Biological Chemistry* **265** (24), pp. 14136–14142.

Livesey J.H., Donald R.A., Irvine C.H.G., Redekopp C. and Alexander S.L. (1988), 'The effects of cortisol, vasopressin (AVP), and corticotropin-releasing factor administration on pulsatile adrenocorticotropin, α-melanocyte-stimulating hormone, and AVP secretion in the pituitary venous effluent of the horse', *Endocrinology* **123** (2), pp. 713–720.

Livesey J.H., Carne A., Irvine C.G.H., Ellis M.J., Evans M.J., Smith R. and Donald R.A. (1991), 'Structure of equine corticotropin releasing factor', *Peptides* **12**, pp. 1437–1440.

Lockshin R.A. and Zakeri Z.F. (1990), 'Programmed cell death: new thoughts and relevance to aging', *Journal of Gerontology* **45**, pp. B135–140.

López F.J. and Negro-Vilar A. (1988), 'Estimation of endogenous adrenocorticotropin half-life using pulsatility patterns: a physiological approach to the evaluation of secretory episodes', *Endocrinology* **123** (2), pp. 740–746.

Lowry P.J., Estivariz F.E., Gillies G.E., Kruseman A.C.N. and Linton E.A. (1986), 'CRF: its regulation of ACTH and pro-opiomelanocortin peptide release and extra-hypothalamic occurrence', *Acta Endocrinologica Supplementum* **276**, pp. 56–61.

Lundblad J.R. and Roberts J.L. (1988), 'Regulation of proopiomelanocortin gene expression in pituitary', *Endocrine Reviews* **9** (1), pp. 135–158.

Lutz-Bucher B.G., Jeandel L., Heisler S., Roberts J.L. and Koch B. (1987), 'Evidence that AVP receptors in AtT-20 corticotropes are not coupled to secretion of POMC-derived peptides', *Molecular and Cellular Endocrinology* **53**, pp. 161–167.

Lytle R.J. and Dines K.A. (1980), 'Iterative ray tracing between boreholes for underground image reconstruction', *IEEE Transactions on Geoscience and Remote Sensing* **GE-18** (3), July, pp. 234–240.

Magnin P.A., von Ramm O.T. and Thurstone F.L. (1982), 'Frequency compounding for speckle contrast reduction in phased array images', *Ultrasonic Imaging* **4**, pp. 267–281.

Makara G.B., Antoni F.A., Stark E. and Karteszi M. (1984), 'Hypothalamic organization of CRF-containing structures', in Muller E.E. and Macleod R.M. (Eds.), *Neuroendocrine Perspectives*, Elsevier, Amsterdam, pp. 71–119.

Marshall A.G., Evans M.J., Livesey J.H. and Donald R.A. (1991), 'Continuous physiological concentrations of CRF potentiate the ACTH response to pulses of AVP in perifused equine pituitary cells', in *Proceedings of the New Zealand Society of Endocrinology*, p. 190.

Martin C. (1985), *Endocrine Physiology*, Oxford University Press, New York.

Mason D.R. (1988), 'The effect of vasopressin, phorbol ester and a calcium ionophore on ACTH release from ovine pituitary cells', *Proceedings of the Endocrine Society of Australia* **31**, abstract S32.

McEwen B.S., De Kloet E.R. and Rostene W. (1986), 'Adrenal steroid receptors and actions in the nervous system', *Physiological Reviews* **66**, pp. 1121–1188.

McFarland L.Z., Clegg M.T. and Ganong W.F. (1960), 'Concentration of ACTH in cavernous sinus and peripheral blood collected from unanethetized sheep', *Proceedings of the Society for Experimental Biology and Medicine* **103**, pp. 538–539.

McIntosh R.P. and McIntosh J.E.A. (1985), 'Dynamic characteristics of luteinizing hormone release from perifused sheep anterior pituitary cells stimulated by combined pulsatile and continuous gonadatropin-releasing hormone', *Endocrinology* **117** (1), pp. 169–179.

McKinnon G.C. and Bates R.H.T. (1980), 'A limitation on ultrasonic transmission tomography', *Ultrasonic Imaging* **2**, pp. 48–54.

Merchenthaler I., Hynes M.A., Vigh S., Shally A.V. and Petrusz P. (1984), 'Corticotropin-releasing factor (CRF)- origin and course of afferent pathways to the median eminence (ME) of the rat hypothalamus', *Neuroendocrinology* **39** (4), pp. 296–306.

Milsom S.R., Conaglen J.V., Donald R.A., Espiner E.A., Nicholls M.G. and Livesey J.H. (1985), 'Aumentation of the response to CRF in man: relative contributions of endogenous angiotensin and vasopressin', *Clinical Endocrinology* **22**, pp. 623–628.

Milsom S.R., Donald R.A., Espiner E.A., Nicholls M.G. and Livesey J.H. (1986), 'The effect of peripheral catecholamine concentrations on the pituitary-adrenal response to corticotropin releasing factor in man', *Clinical Endocrinology* **25**, pp. 241–246.

Minard R.A. (1985), *Imaging in a Distorting Medium*, Ph.D. thesis, Department of Electrical and Electronic Engineering, University of Canterbury, Christchurch, New Zealand.

Minard R.A., Robinson B.S. and Bates R.H.T. (1985), 'Full-wave computed tomography. Part 3: Coherent shift-and-add imaging', *IEE Proceedings Part A* **132** (1), January, pp. 50–58.

Misell D.L. (1978), 'The phase problem in electron microscopy', in Cosslett V.E. and Barer R. (Eds.), *Advances in Optical and Electron Microscopy, Vol. 7*, Academic Press, London, pp. 185–279.

Morris P.G. (1986), *Nuclear Magnetic Resonance Imaging in Medicine and Biology*, Clarendon Press, Oxford.

Morse P.M. and Feshbach H. (1953), *Methods of Theoretical Physics*, McGraw-Hill, New York, Vol. 1&2.

Murakami K., Hashimoto K. and Ota Z. (1984), 'Interaction of synthetic ovine corticotropin releasing factor and arginine vasopressin on in vitro ACTH release by the anterior pituitary of rats', *Neuroendocrinology* **39**, pp. 49–53.

Murch R.D. (1990), *Inverse Scattering and Shape Reconstruction*, Ph.D. thesis, Department of Electrical and Electronic Engineering, University of Canterbury, Christchurch, New Zealand.

Murch R.D. (1992), 'An extended Born approximation', *Inverse Problems*, accepted as a letter.

Murch R.D., Tan D.G.H. and Wall D.J.N. (1988), 'Newton-Kantorovich method applied to the two-dimensional inverse scattering for an exterior Helmholtz problem', *Inverse Problems* **4** (4), pp. 1117–1128.

Nagrath I.J. and Gopal M. (1982), *Control Systems Engineering*, Wiley, New Delhi.

Nashed M.Z. (1981), 'Operator-theoretic and computational approaches to ill-posed problems with applications to antenna theory', *IEEE Transactions on Antennas and Propagation* **AP-29** (2), March, pp. 220–231.

Negro-Vilar A., Johnston C., Spinedi E., Valenca M. and Lopez F. (1987), 'Physiological role of peptides and amines on the regulation of ACTH secretion', in *[Ganong et al., 1987]*, pp. 218–236.

Neill J.D., Dailey R.A., Tsou R.C. and Tindall G.T. (1977), 'Secretion of luteinizing hormone releasing hormone (LHRH) in monkeys', *Advances in Experimental Medicine and Biology* **87**, pp. 203–224.

Newton R.G. (1966), *Scattering Theory of Waves and Particles*, McGraw-Hill, New York.

Newton R.G. (1980), 'Inverse scattering II: Three dimensions', *Journal of Mathematical Physics* **21** (7), July, pp. 1698–1715, see [Newton, 1981a].

Newton R.G. (1981a), 'Erratum to 'Inverse scattering II: Three dimensions", *Journal of Mathematical Physics* **22** (3), March, p. 631.

Newton R.G. (1981b), 'Inversion of reflection data for layered media: A review of exact methods', *Geophysical Journal of the Royal Astronomical Society* **65** (1), April, pp. 191–215.

Newton R.G. (1981c), 'Inverse scattering III: Three dimensions, continued', *Journal of Mathematical Physics* **22** (10), October, pp. 2191–2200, see [Newton, 1982].

Newton R.G. (1982), 'Erratum to 'Inverse scattering III: Three dimensions, continued", *Journal of Mathematical Physics* **23** (5), May, p. 693.

Ng T.B., Chung D. and Li C.H. (1981), 'Isolation and properties of β-endorphin-(1-27), N-acetyl-β-endorphin, corticotropin, γ-lipotropin and neurophysin from equine pituitary glands', *International Journal on Peptide and Protein Research* **18**, pp. 164–169.

Nicholson S.A. and Gillham B. (1989), 'Glucocorticoids act rapidly *in vitro* to attenuate second messenger responses to ACTH secretagogues in rats', *Journal of Endocrinology* **122**, pp. 545–551.

Norton S.J. and Linzer M. (1982), 'Correcting for ray refraction in velocity and attenuation tomography: a perturbation approach', *Ultrasonic Imaging* **3** (2), July, pp. 201–233.

Oki Y., Nicholson W.E. and Orth D.N. (1990), 'Role of protein kinase-C in the adrenocorticotropin secretory response to arginine vasopressin (AVP) and the synergistic response to AVP and corticotropin releasing factor by perifused rat anterior pituitary cells', *Endocrinology* **127** (1), pp. 350–357.

Oki Y., Peatman T.W., Qu Z. and Orth D.N. (1991), 'Effects of intracellular Ca^{2+} depletion and glucocorticoid on stimulated adrenocorticotropin release by rat anterior pituitary cells in a microperifusion system', *Endocrinology* **128** (3), pp. 1589–1596.

Oliver C., Mical R.S. and Porter J.C. (1977), 'Hypothalamic-pituitary vasculature: evidence for retrograde blood flow in the pituitary stalk', *Endocrinology* **101**, pp. 598–604.

O'Sullivan F. and O'Sullivan J. (1988), 'Deconvolution of episodic hormone data: an analysis of the role of season on the onset of puberty in cows', *Biometrics* **44**, pp. 339–353.

Palkovits M. (1987), 'Anatomy of neural pathways affecting CRH secretion', in *[Ganong et al., 1987]*, pp. 139–150.

Pan S.X. and Kak A.C. (1983), 'A computational study of reconstruction algorithms for diffraction tomography: Interpolation vs filtered-backpropagation', *IEEE Transactions on Acoustics, Speech, and Signal Processing* **ASSP-31**, pp. 1262–1275.

Paoloni F.J. (1986), 'The effects of attenuation on the Born reconstruction procedure for microwave diffraction tomography', *IEEE Transactions on Microwave Theory and Techniques* **MTT-34** (3), March, pp. 366–368.

Paoloni F.J. (1987), 'Implementation of microwave diffraction tomography for measurement of dielectric constant distribution', *IEE Proceedings Part H* **H134** (1), February, pp. 25–29.

Parasnis D.S. (1979), *Principles of Applied Geophysics*, Chapman and Hall, London, third edition.

Perrin M.H., Haas Y., Rivier J.E. and Vale W.W. (1986), 'Corticotropin-releasing factor binding to the anterior pituitary receptor is modulated by divalent-cations and guanyl', *Endocrinology* **118**, pp. 1171–1179.

Plotsky P.M. (1991), 'Pathways to the secretion of adrenocorticotropin: a view from the portal', *Journal of Neuroendocrinology* **3** (1), pp. 1–9.

Plotsky P.M. and Sawchenko P.E. (1987), 'Hypophysial-portal plasma levels, median eminence content, and immunohistochemical staining of corticotropin-releasing factor, arginine vasopressin, and oxytocin after pharmacological adrenalectomy', *Endocrinology* **120**, pp. 1361–1369.

Plotsky P.M. and Vale W.W. (1984), 'Hemorrhage induced secretion of corticotropin releasing-like immunoreactivity into the rat hypophysial portal circulation and its inhibition by glucocorticoids', *Endocrinology* **119**, pp. 2393–2396.

Plotsky P.M., Bruhn T.O. and Vale W.W. (1985), 'Evidence for multifactor regulation of the adrenocorticotropin secretory response to hemodynamic stimuli', *Endocrinology* **116** (2), pp. 633–639.

Plotsky P.M., Cunningham E.T., Jr. and Widmaier E.P. (1989), 'Catecholaminergic modulation of corticotropin-releasing factor and adrenocorticotropin secretion', *Endocrine Reviews* **10** (4), pp. 437–458.

Porter J.C., Mical R.S., Kamberi I.A. and Grazia Y.R. (1970), 'A procedure for the cannulation of a pituitary stalk portal vessel and perfusion of the pars distalis in the rat', *Endocrinology* **87**, pp. 197–201.

Porter J.C., Ondo J.G. and Cramer O.M. (1974), 'Nervous and vascular supply of the pituitary gland', in Knobil E. and Sawyer W.H. (Eds.), *Handbook of Physiology*, Vol. 4, sec. 7, American Physiological Society, Washington, D.C., pp. 33–43.

Pratt R.G. and Worthington M.H. (1988), 'The application of diffraction tomography to cross-hole seismic data', *Geophysics* **53** (10), October, pp. 1284–1294.

Ramachandran G.N. and Srinivasan R. (1970), *Fourier Methods in Crystallography*, Wiley-Interscience, New York.

Ramm A.G. (1990), 'Is the Born approximation good for solving the inverse problem when the potential is small?', *Journal of Mathematical Analysis and Applications* **147** (2), pp. 480–485.

Rea D.G. (Ed.) (1984), 'Special issue on the 1984 International Geoscience and Remote Sensing Symposium (IGARSS 1983): Remote Sensing: Extending Man's Horizon', *IEEE Transactions on Geoscience and Remote Sensing*, **GE-22** (6), November, pp. 469–727.

Recht L.D., Hoffman D.L., Haldar J., Silverman A. and Zimmerman E.A. (1981), 'Vasopressin concentrations in hypophysial portal plasma: insignificant reduction following removal of the posterior pituitary gland', *Neuroendocrinology* **33**, pp. 88–90.

Redei E. and Evans C.J. (1989), 'Dual control of corticotropin secretion: isolation of corticotropin-inhibiting factor', in Tache Y., Morley J.E. and Brown M.R. (Eds.), *Neuropeptides and Stress*, Spinger-Verlag, New York, pp. 61–72.

Redekopp C., Livesey J.H., Toth A. and Donald R.A. (1985), 'Effect of ovine corticotropin releasing factor and arginine vasopressin on ACTH and aldosterone secretion in sheep', *Hormone and Metabolic Research* **17**, pp. 428–429.

Redekopp C., Irvine C.H.G., Donald R.A., Liversy J.H., Sadler W., Nicholls M.G., Alexander S.L. and Evans M.J. (1986), 'Spontaneous and stimulated adrenocorticotropin and vasopressin pulsatile secretion in the pituitary venous effluent of the horse', *Endocrinology* **118** (4), pp. 1410–1416.

Reisine T. and Affolter H. (1987), 'Hormone receptor regulated proopiomelanocortin gene-expression', *Biochemical Pharmacology* **36** (2), pp. 191–195.

Riley V. (1981), 'Psychoneuroendocrine influences on immunocompetence and neoplasia', *Science* **212**, pp. 1100–1109.

Rittmaster R.S., Cutler J.B., Jr., Gold P.W., Brandon D.D., Tomai T., Loriaux D.L. and Chrousos G.P. (1987), 'The relationship of saline-induced changes in vasopressin secretion to basal and corticotropin-releasing hormone-stimulated adrenocorticotropin and cortisol secretion in man', *Journal of Clinical Endocrinology and Metabolism* **64** (2), pp. 371–376.

Rivier C.L. and Plotsky P.M. (1986), 'Mediation by corticotropin releasing factor (CRF) of adenohypophysial hormone secretion', *Annual Review of Physiology* **48**, pp. 475–494.

Rivier C.L. and Vale W.W. (1983a), 'Interaction of corticotropin-releasing factor and arginine vasopressin on adrenocorticotropin secretion *in vivo*', *Endocrinology* **113** (3), pp. 939–942.

Rivier C.L. and Vale W.W. (1983b), 'Modulation of stress-induced ACTH release by corticotropin-releasing factor, catecholamines and vasopressin', *Nature* **305** (5932), pp. 325–327.

Rivier C.L. and Vale W.W. (1985), 'Neuroendocrine interaction between corticotropin releasing factor and vasopressin on adrenocorticotropic hormone secretion in the rat', in Schrier R.W. (Ed.), *Vasopressin*, Raven Press, New York, pp. 181–188.

Rivier J., Spiess J. and Vale W.W. (1983), 'Characterization of rat hypothalamic corticotropin-releasing factor', *Proceedings of the National Academy of Science USA* **80**, pp. 4851–4855.

Roberts J.L., Lundblad J.R., Eberwine J.H., Fremeau R.T., Salton S.R.J. and Blum M. (1987), 'Hormonal regulation of POMC gene expression in pituitary', in *[Ganong et al., 1987]*, pp. 275–285.

Robinson B.S. (1982), *Speckle Processing for Ultrasonic Imaging*, Ph.D. thesis, Department of Electrical Engineering, University of Canterbury, Christchurch, New Zealand.

Robinson B.S. and Bates R.H.T. (1980), 'Wideband ultrasonic diffraction measurements', *Australasian Physical and Engineering Sciences in Medicine* **3** (6), pp. 233–238.

Robinson B.S. and Greenleaf J.F. (1986), 'The scattering of ultrasound by cylinders: Implications for diffraction tomography', *Journal of the Acoustical Society of America* **80** (1), July, pp. 40–49.

Royston J.P. (1989), 'The statistical analysis of pulsatile hormone secretion data', *Clinical Endocrinology* **30**, pp. 201–210.

Sabatier P.C. (1983), 'Theoretical considerations for inverse scattering', *Radio Science* **18** (1), pp. 1–18.

Sabatier P.C. (1987), *Basic Methods of Tomography and Inverse Problems*, Malvern Physics Series, Adam Hilger, Bristol, Chap. Basic Concepts and Methods of Inverse Problems, pp. 471–635.

Saffran M. and Schally A.V. (1955), 'The release of corticotropin by anterior pituitary tissues *in vitro*', *Canadian Journal of Physiology* **33**, pp. 408–415.

Sapolsky R.M., Armanini M.P., Packan D.R., Sutton S.W. and Plotsky P.M. (1990), 'Glucocorticoid feedback inhibition of adrenocorticotropic hormone secretagogue release', *Neuroendocrinology* **51**, pp. 328–336.

Sawchenko P.E. (1989), 'Neuropeptides, the paraventricular nucleus, and the integration of hypothalamic neuroendocrine and autonomic function', in Taché Y., Morley J.E. and Brown M.R. (Eds.), *Neuropeptides and Stress*, Springer-Verlag, New York, pp. 73–91.

Sawchenko P.E., Swanson L.W. and Vale W.W. (1984), 'Corticotropin-releasing factor: co-expression within distinct subsets of oxytocin-, vasopressin-, and neurotensin-immunoreactive neurons in the hypothalamus of the male rat', *Journal of Neuroscience* **4**, pp. 1118–1129.

Scaccianoce S., Muscolo L.A.A., Cigliana G., Navarra D. and Angelucci L. (1991), 'Evidence for a specific role of vasopressin in sustaining pituitary-adrenocortical stress response in the rat', *Endocrinology* **128** (6), pp. 3138–3143.

Scales J.A. and Gersztenkorn A. (1988), 'Robust methods in inverse theory', *Inverse Problems* **4**, pp. 1071–1091.

Schoenberger M. (1984), 'Special issue on seismic signal processing', *IEEE Proceedings* **72** (10), October, pp. 1235–1412.

Schomberg H. (1978), 'An improved approach to reconstructive ultrasound tomography', *Journal of Physics D: Applied Physics* **11**, pp. L181–L185.

Schopohl J., Hauer A., Kaliebe T., Stalla G.K., von Werder K. and Müller O.A. (1986), 'Repetitive and continuous administration of human corticotropin releasing factor to human subjects', *Acta Endocrinologica* **112**, pp. 157–165.

Schultz K.I. and Jaggard D.L. (1987), 'Microwave projection imaging for refractive objects: A new method', *Journal of the Optical Society of America A* **A4** (9), September, pp. 1773–1782.

Schwartz J. (1990), 'Evidence for intrapituitary intercellular control of adrenocorticotropin secretion', *Molecular and Cellular Endocrinology* **68**, pp. 77–83.

Schwartz J. and Vale W.W. (1988), 'Dissociation of the adrenocorticotropin secretory responses to corticotropin-releasing factor (CRF) and vasopressin or oxytocin by using a specific cytotoxic analog of CRF', *Endocrinology* **122** (4), pp. 1695–1700.

Schwartz J., Billestrup N., Perrin M., Rivier J. and Vale W.W. (1986), 'Identification of corticotropin-releasing factor (CRF) target-cells and effects of dexamethasone on binding in anterior pituitary using a fluorescent analog of CRF', *Endocrinology* **119** (5), pp. 2376–2382.

Schwartz J., Canny B., Vale W.W. and Funder J.W. (1989a), 'Intrapituitary cell-cell communication regulates ACTH secretion', *Neuroendocrinology* **50**, pp. 716–722.

Schwartz J., Familari M., Wallace C. and Funder J.W. (1989b), 'Dissociation of ACTH-secretory mechanisms in rat pituitary cells: evidence that basal and vasopressin-stimulated secretion act via a mechanism distinct from that of corticotrophin-releasing factor', *Journal of Neuroendocrinology* **1** (2), pp. 117–120.

Schwartz J., Pham T., Rao A. and Funder J.W. (1991), 'Effect of AVP on susceptability of ovine pituitary-cells to a cytotoxic analog of CRF', *American Journal of Physiology* **260** (6), pp. E905–E909.

Seagar A.D. and Bates R.H.T. (1985), 'Full-wave computed tomography IV: Low-frequency electric current CT', *IEE Proceedings Part A* **A132** (7), November, pp. 455–466.

Sengbush R.L. (1983), *Seismic Exploration Methods*, International Human Resources Development Corporation, Boston.

Share L. (1988), 'Role of vasopressin in cardiovascular regulation', *Physiological Reviews* **68** (4), pp. 1248–1276.

Shen P.J., Clarke I.J., Canny B.J., Funder J.W. and Smith A.I. (1990), 'Arginine vasopressin and corticotropin releasing factor: binding to ovine anterior pituitary membranes', *Endocrinology* **127** (5), pp. 2085–2089.

Shimizu H., Chubachi N. and Kushibiki J. (Eds.) (1989), *Acoustical Imaging* **17**, Plenum Press, New York.

Shipston M.J. and Antoni F.A. (1991), 'Early glucocorticoid feedback in anterior pituitary corticotropes: differential inhibition of hormone release induced by vasopressin and corticotrophin-releasing factor *in vitro*', *Journal of Endocrinology* **129**, pp. 261–268.

Sieber A.J. (Ed.) (1983), 'Special issue on the 1983 International Geoscience and Remote Sensing Symposium (IGARSS 1982): Remote Sensing: The promise of Remote Sensing', *IEEE Transactions on Geoscience and Remote Sensing*, **GE-21** (3), July, pp. 228–405.

Silver S. (Ed.) (1949), *Microwave antenna theory and design*, McGraw-Hill Book Company Inc., Republished in 1965 by Dover Publications Inc., New York.

Silverman A., Hou-Yu A. and Kelly D.D. (1989), 'Modification of hypothalamic neurons by behavioral stress', in Tache Y., Morley J.E. and Brown M.R. (Eds.), *Neuropeptides and Stress*, Spinger-Verlag, New York, pp. 23–38.

Sisson S. (1914), *The Anatomy of the Domestic Animals*, W. B. Saunders Co., Philadelphia.

Skolnik M.I. (Ed.) (1970), *Radar handbook*, McGraw-Hill, New York.

Slaney M. and Kak A.C. (1985), 'Imaging with diffraction tomography', Technical Report. School of Electrical Engineering, Purdue University, West Lafayette, Indiana 47907.

Slaney M., Kak A.C. and Larsen L.E. (1984), 'Limitations of imaging with first-order diffraction tomography', *IEEE Transactions on Microwave Theory and Techniques* **MTT-32** (8), August, pp. 860–874.

Sleeman B.D. (1982), 'The inverse problem of acoustic scattering', *IMA Journal of Applied Mathematics* **29**, pp. 113–142.

Smith K.A. (1990), 'Immunological and endocrinological parameters of stress in deer', B. Pharm (Hons) Thesis, Otago.

Smith A.M., Goldberg M. and Lim E.S.K. (1980), 'Numerical ray tracing in media involving continuous and discrete boundaries', *Ultrasonic Imaging* **2** (4), October, pp. 291–301.

Smith V.A., Murch A.R. and Dingle A.A. (1988), 'Non-random noise mechanisms', *Proceedings of the National Electronics Conference* **25**, Sept, pp. 188–193.

Sneidman T.I. and Vogel C.R. (1989), 'Well posedness and convergence of some regularisation methods for non-linear ill posed problems', *Inverse Problems* **5** (2), pp. 227–238.

Soumekh M. and Kaveh M. (1986), 'A theoretical study of model approximation errors in diffraction tomography', *IEEE Transactions on Ultrasonics, Ferroelectrics, and Frequency Control* **UFFC-33** (1), January, pp. 10–20.

Soumekh M., Kaveh M. and Mueller R.K. (1983), 'Fourier domain reconstruction methods with application to diffraction tomography', *Acoustical Imaging* **13**, pp. 17–30.

Spencer A.J.M. (1980), *Continuum Mechanics*, Longman, London.

Spiesberger J.L. (1985), 'Ocean acoustic tomography', *Journal of the Acoustical Society of America* **77** (1), January, pp. 83–100.

Spinedi E., Giacomini M., Jacquier M. and Gaillard R.C. (1991), 'Changes in the hypothalamo-corticotrope axis after bilateral adrenalectomy: evidence for a median eminence site of glucocorticoid action', *Neuroendocrinology* **53**, pp. 160–170.

Statistics (1991), *Key Statistics*, Department of Statistics, Wellington, January/February.

Stratton J.A. (1941), *Electromagnetic Theory*, McGraw-Hill, New York.

Tabbara W., Duchene B., Pichot C., Lesselier D., Chommeloux L. and Joachimawicz N. (1988), 'Diffraction tomography: contribution to the analysis of some applications in microwaves and ultrasonics', *Inverse Problems* **4**, pp. 305–331.

Tan D.G.H. (1988), *Implementable Multi-dimensional Inverse Scattering Theory*, Ph.D. thesis, Department of Electrical and Electronic Engineering, University of Canterbury, Christchurch, New Zealand.

Thomson D.O. and Chimenti D.E. (Eds.) (1986), *Review of progress in Quantitative Nondestructive Evaluation*, Vol. 5A, Plenum, New York.

Thomson M. and Smith R. (1989), 'The action of hypothalamic and placental corticotropin releasing factor on the corticotrope', *Molecular and Cellular Endocrinology* **62**, pp. 1–12.

Tijhus A.G. (1987), *Electromagnetic Inverse Profiling: Theory and Numerical Implementation*, VNU Science Press, Utrechet.

Truesdell C.A. (1977), *A First Course in Rational Continuum Mechanics, volume 1: General Concepts*, Academic Press, New York.

Urban R.J., Evans W.S., Rogol A.D., Kaiser D.L., Johnson M.L. and Veldhuis J.D. (1988a), 'Contemporary assessments of objective peak-detection algorithms. I. The paradigm of the luteinizing hormone pulse signal in men', *Endocrine Reviews* **9**, pp. 3–39.

Urban R.J., Kaiser D.L., van Cauter E., Johnson M.L. and Veldhuis J.D. (1988b), 'Contempory assessments of objective peak-detection algorithms. II. Studies in men', *American Journal of Physiology* **254**, pp. E113–E119.

Urban R.J., Johnson M.L. and Veldhuis J.D. (1989), '*In vivo* biological validation and biophysical modeling of the sensitivity and positive accuracy of endocrine peak detection. I. The LH pulse signal', *Endocrinology* **124** (5), pp. 2541–2547.

Urban R.J., Johnson M.J. and Veldhuis J.D. (1991), '*In vivo* biological validation and biophysical modeling of the sensitivity and positive accuracy of endocrine peak detection. II. The follicle-stimulating hormone pulse signal.', *Endocrinology* **128** (4), pp. 2008–2014.

Urick R.J. (1975), *Underwater Sound for Engineers*, McGraw-Hill, New York.

Veldhuis J.D. (1991), 'Temporal architecture of in vivo endocrine glandular signaling: obtaining a secretory blueprint by deconvolution analysis', *Molecular and Cellular Endocrinology* **77** (1-3), pp. C63–C71.

Veldhuis J.D. and Johnson M.L. (1986), 'Cluster analysis: a simple, versatile and robust algorithm for endocrine pulse detection', *American Journal of Physiology* **250**, pp. E486–E493.

Veldhuis J.D. and Johnson M.L. (1990a), 'An overview of computer algorithms for deconvolution-based assessment of *in vivo* neuroendocrine secretory events', *Biotechniques* **8** (6), pp. 634–639.

Veldhuis J.D. and Johnson M.L. (1990b), 'Editorial: returning to the roots of endocrinology: the challenge of evaluating *in vivo* glandular secretory activity', *Endocrinology* **127** (6), pp. 2611–2617.

Veldhuis J.D., Iranmanesh A., Johnson M.L. and Lizarralde G. (1990a), 'Amplitude, but not frequency, modulation of adrenocorticotropin secretory bursts gives rise to the nyctohemeral rhythm of the corticotropic axis in man', *Journal of Clinical Endocrinology and Metabolism* **71** (2), pp. 452–463.

Veldhuis J.D., Iranmanesh A., Johnson M.L. and Lizarralde G. (1990b), 'Twenty-four-hour rhythms in plasma concentrations of adenohypophysial hormones are generated by distinct amplitude and/or frequency modulation of underlying pituitary secretory bursts', *Journal of Clinical Endocrinology and Metabolism* **71** (6), pp. 1616–1623.

Wait J.R. (Ed.) (1979), 'Special issue on applications of electromagnetic theory to geophysical exploration', *IEEE Proceedings*, **67** (7), July, pp. 979–1076.

Wang Y.M. and Chew W.C. (1989), 'An iterative solution of the two-dimensional electromagnetic inverse scattering problem', *International Journal of Imaging Systems and Technology* **1** (1), pp. 100–108.

Watanabe T. and Orth D.N. (1987), 'Detailed kinetic analysis of adrenocorticotropin secretion by dispersed rat anterior pituitary cells in a microperifusion system: Effects of ovine corticotropin releasing factor and arginine vasopressin', *Endocrinology* **121** (3), pp. 1133–1145.

Watanabe T. and Orth D.N. (1988), 'Effects of several *in vitro* systems on the potencies of putative adrenocorticotropin secretagogues on rat anterior pituitary cells', *Endocrinology* **122** (5), pp. 2299–2308.

Watanabe T., Oki Y. and Orth D.N. (1989), 'Kinetic actions and interactions of arginine vasopressin, angiotensin-II, and oxytocin on adrenocorticotropin secretion by rat anterior pituitary cells in the microperifusion system', *Endocrinology* **125** (4), pp. 1921–1931.

Watson G.N. (1966), *A Treatise on the Theory of Bessel Functions*, Cambridge University Press, Cambridge, second edition.

Webb S. (Ed.) (1988), *The Physics of Medical Imaging*, Medical Science Series, Adam Hilger, Bristol.

Wells P.N.T. (1977), *Biomedical Ultrasonics*, Academic Press, London.

Wells P.N.T. (Ed.) (1987), 'Special issue on medical imaging', *IEE Proceedings Part A*, **134** (2), February, pp. 97–236.

Westcott B.S. (1983), *Shaped Reflector Antenna Design*, Research Studies Press, England.

Weston V.H. (1989), 'Splitting and the reflection operator for the wave equation in R^3', *Journal of Mathematical Physics* **30** (11), pp. 2545–2562.

Whitnall M.H. (1989), 'Stress selectivity activates the vasopressin-containing subset of corticotropin-releasing hormone neurons', *Neuroendocrinology* **50**, pp. 702–707.

Whitnall M.H. and Gainer H. (1988), 'Major pro-vasopressin-expressing and pro-vasopressin-deficient subpopulations of corticotropin-releasing hormone neurons in normal rats', *Neuroendocrinology* **47**, pp. 176–180.

Whitnall M.H., Mezey E. and Gainer H. (1985), 'Co-localization of corticotropin-releasing factor and vasopressin in median eminence neurosecretory vesicles', *Nature* **317**, pp. 248–250.

Wilcox C.H. (1984), *Sound Propagation in Stratified Fluids*, Springer-Verlag, New York.

Wittert G.A., Stewart D.E., Graves M.P., Ellis M.J., Evans M.J., Wells J.E., Donald R.A. and Espiner E.A. (1991), 'Plasma corticotrophin releasing factor and vasopressin responses to exercise in normal man', *Clinical Endocrinology* **35** (4), pp. 311–317.

Wittert G.A., Livesey J.H., Or H.K., Donald R.A. and Espiner E.A. (1992), 'Raised corticotrophin levels in Addison's disease are not associated with increased arginine vasopressin and corticotrophin releasing factor concentrations in peripheral plasma', *Journal of Clinical Endocrinology*, in revision.

Wolfson B., Manning R.W., Davis L.G. and Arentzen R. (1985), 'Co-localization of corticotropin releasing factor and vasopressin mRNA in neurons after adrenalectomy', *Nature* **315** (6014), pp. 59–61.

Wombell R.J. and Fiddy M.A. (1987), 'Acoustical imaging beyond Born and Rytov', *Acoustical Imaging* **16**, pp. 373–381.

Wombell R.J. and Fiddy M.A. (1988), 'Inverse scattering within the distorted-wave born approximation', *Inverse Problems* **4** (3), pp. 123–127.

Won J.G.S. and Orth D.N. (1990), 'Roles of intracellular and extracellular calcium in the kinetic profile of adrenocorticotropin secretion by perifused rat anterior pituitary cells. I. Corticotropin releasing factor stimulation', *Endocrinology* **126** (2), pp. 849–857.

Won J.G.S., Oki Y. and Orth D.N. (1990), 'Roles of intracellular and extracellular calcium in the kinetic profile of adrenocorticotropin secretion by perifused rat anterior pituitary cells. II. Arginine vasopresson, oxytocin, and angiotensin-II stimulation', *Endocrinology* **126** (2), pp. 858–868.

Wu R. and Toksöz M.N. (1987), 'Diffraction tomography and multisource holography applied to seismic imaging', *Geophysics* **52** (1), January, pp. 11–25.

Xue H. and Wei Y. (1987), 'A fast reconstruction algorithm for diffraction tomography', *Acoustical Imaging* **16**, pp. 415–419.

Yokota M., Takenaka T. and Fukumitsu O. (1986), 'Scattering of a hermite-gaussian beam mode by parallel dielectric cylinders', *Journal of the Optical Society of America A* **3** (4), pp. 580–586.

Zimmerman E.A. and Silverman A. (1983), 'Vasopressin and adrenal cortical interactions', in Cross B.A. and Leng G. (Eds.), *The Neurohypophysis: Structure, Function and Control*, Elsevier, Amsterdam.